

## 16. SITE 823<sup>1</sup>

### Shipboard Scientific Party<sup>2</sup>

#### HOLE 823A

**Date occupied:** 21 September 1990  
**Date departed:** 21 September 1990  
**Time on hole:** 11 hr, 22 min  
**Position:** 16°36.981'S, 146°47.037'E  
**Bottom felt (rig floor; m; drill-pipe measurement):** 1649.7  
**Distance between rig floor and sea level (m):** 11.32  
**Water depth (drill-pipe measurement from sea level, m):** 1638.4  
**Total depth (rig floor; m)** 1769.50  
**Penetration (m)** 119.80  
**Number of cores (including cores with no recovery):** 13  
**Total length of cored section (m):** 119.80  
**Total core recovered (m):** 123.73  
**Core recovery (%):** 103.3  
**Oldest sediment cored:**  
Depth (mbsf): 119.80  
Nature: nannofossil claystone  
Earliest age: Pleistocene

#### HOLE 823B

**Date occupied:** 21 September 1990  
**Date departed:** 26 September 1990  
**Time on hole:** 4 days, 9 hr, 22 min  
**Position:** 16°36.982'S, 146°47.053'E  
**Bottom felt (rig floor; m; drill-pipe measurement):** 1649.2  
**Distance between rig floor and sea level (m):** 11.32  
**Water depth (drill-pipe measurement from sea level, m):** 1637.9  
**Total depth (rig floor; m):** 2454.60  
**Penetration (m):** 805.40  
**Number of cores (including cores with no recovery):** 84  
**Total length of cored section (m):** 805.40  
**Total core recovered (m):** 754.85  
**Core recovery (%):** 93.7  
**Oldest sediment cored:**  
Depth (mbsf): 805.40  
Nature: nannofossil chalk  
Earliest age: late Miocene

#### HOLE 823C

**Date occupied:** 26 September 1990  
**Date departed:** 30 September 1990

**Time on hole:** 4 days, 22 hr, 50 min  
**Position:** 16°36.983'E, 146°47.066'E  
**Bottom felt (rig floor; m; drill-pipe measurement):** 1649.2  
**Distance between rig floor and sea level (m):** 11.41  
**Water depth (drill-pipe measurement from sea level, m):** 1637.8  
**Total depth (rig floor; m):** 2660.20  
**Penetration (m):** 1011.00  
**Number of cores (including cores with no recovery):** 24  
**Total length of cored section (m):** 227.00  
**Total core recovered (m):** 186.04  
**Core recovery (%):** 82.0  
**Oldest sediment cored:**  
Depth (mbsf): 1011.00  
Nature: quartz foraminifer packstone  
Earliest age: middle Miocene

**Principal results:** Site 823 is located in the central-western Queensland Trough, toward the deepest part of the basin. This location was selected to recover a basinal section that would provide material for paleoceanographic studies, as well as a record of basin-fill sediments to correlate with other drill sites on a transect from the Australian continental margin to the Queensland Plateau. An excellent total recovery of 92% with APC/XCB/RCB drilling was achieved by penetrating a 1011.0-m-thick sequence of uppermost middle Miocene to Pleistocene hemipelagic to pelagic sediments. These sediments are interbedded with numerous gravity-flow deposits that have been interpreted as turbidites, debris flows, and slumps. Benthic foraminifer assemblages indicate that the depositional environment remained at lower bathyal paleodepths (1000–2000 m) during this period. Although more than 1800 gravity-flow deposits were recognized, chronological integrity of the microfossil biostratigraphy was maintained throughout the sequence, indicating that nearly contemporaneous deposition of the redeposited material took place.

Seven major sedimentary units were recovered between the seafloor and 1011.0 mbsf. These lithologic units have been distinguished as follows:

1. *Unit I:* depth, 0–120.7 mbsf; age, Pleistocene. Unit I contains pelagic to hemipelagic sediments interbedded with redeposited layers that have been interpreted as turbidites and debris flows. This unit is divided into two subunits on the basis of differences in clay contents and presence of debris flows.

*Subunit IA:* depth, 0–85.4 mbsf; age, Pleistocene. Subunit IA consists of light greenish-gray to gray nannofossil micrite ooze with clay, foraminifers, and bioclasts; clayey nannofossil mixed sediments with micrite, foraminifers, and bioclasts; nannofossil ooze with micrite and clay; and clayey nannofossil ooze. These sediments are interbedded with lithoclastic floatstone and rudstone and often contain mud clasts, which have been interpreted as debris flows, and bioclastic packstone and grainstone that often show normal grading; these also have been interpreted as turbidites.

*Subunit IB:* depth, 85.4–120.7 mbsf; age, Pleistocene. Subunit IB consists of dark greenish-gray claystone with nannofossils and, in some cases, quartz and micrite; dark gray nannofossil clayey to clayey nannofossil mixed sediments; clayey nannofossil ooze; and nannofossil clay mixed sediments with quartz. Interbedded layers

<sup>1</sup> Davies, P. J., McKenzie, J. A., Palmer-Julson, A., et al., 1991. *Proc. ODP, Init. Repts.*, 133: College Station, TX (Ocean Drilling Program).

<sup>2</sup> Shipboard Scientific Party is as given in list of participants preceding the contents.

of gray sandy packstone with foraminifers, quartz, and nannofossils and bioclastic packstone with quartz, micrite, and nannofossils were interpreted as turbidites.

2. *Unit II*: depth, 120.7–352.75 mbsf; age, late Pliocene. Unit II contains gray to greenish-gray nannofossil ooze with clay and bioclasts interbedded with gray to dark gray lithoclastic rudstone (interpreted as debris flows) and gray to greenish-gray bioclastic and skeletal packstones that exhibit normal grading and abrupt basal contacts, sedimentary features indicative of turbidites. At 305 mbsf, a distinct transition from nannofossil ooze to chalk can be seen.

3. *Unit III*: depth, 352.75–535.7 mbsf; age, early Pliocene. Unit III is distinguished by a subunit containing pelagic to hemipelagic sediments, enclosed between two subunits composed of massive debris flows and slumps.

*Subunit IIIA*: depth, 352.75–440.3; age, early Pliocene. Subunit IIIA consists of dark gray to gray nannofossil chalk with bioclasts and foraminifers or quartz; clayey nannofossil mixed sediments and dolomitic nannofossil chalk with clay intermixed with dark greenish-gray lithoclastic rudstone, conglomerate, and mixed sediments that were interpreted as debris flows and slumps. One of these debris flows is 30 m thick. Deformation of soft sediments occurs below these debris flows.

*Subunit IIIB*: depth, 440.3–516.8 mbsf; age, early Pliocene. Subunit IIIB contains nannofossil siltstone with bioclasts, calcite, and pyrite; light greenish-gray to greenish-gray nannofossil chalk; nannofossil chalk with micrite; and mixed sediments. In contrast, common dark greenish-gray gravity-flow deposits and a few light greenish-gray, carbonate-rich bioclastic packstones (interpreted as turbidites) indicate increased influence of a carbonate platform source for this detrital influx.

*Subunit IIIC*: depth, 516.8–535.7 mbsf; age, early Pliocene. In Subunit IIIC, two debris flows composed of mud clasts in a matrix of greenish-gray to dark greenish-gray mixed sediments with micrite have been separated by an interval of relatively undeformed, light greenish-gray nannofossil chalk.

4. *Unit IV*: depth, 535.7–715.0 mbsf; age, early Pliocene to late Miocene. Unit IV is characterized by larger-scale slump features. Compared with the overlying Unit III, its sediments show variable clay contents with accompanying color changes from light greenish-gray to dark greenish-gray. These are foraminifer nannofossil chalk; nannofossil mixed sediment to chalk with foraminifers and bioclasts, becoming clayey nannofossil chalk with foraminifers, bioclasts, and/or quartz; and nannofossil chalk with clay or foraminifer nannofossil clayey chalk with depth. Dark greenish-gray bioclastic foraminifer packstone layers, exhibiting graded bedding indicative of turbidites, sometimes were found inverted within slumps. Microfaults are associated with some slumps. Clasts and matrix in greenish-gray lithoclast rudstones, interpreted as debris flows, have been cut by *Chondrites* and *Zoophycos*, indicating post-depositional bioturbation. The base of Unit IV is a debris flow.

5. *Unit V*: depth, 715.0–795.7 mbsf; age, early Pliocene to late Miocene. Unit V has a higher clay content in the dark gray nannofossil mixed sediment to nannofossil claystone. Greenish-gray nannofossil chalk is present, although it is less abundant than in the overlying Unit IV. Unit V contains a few foraminifer skeletal packstone layers that have been interpreted as turbidites. Laminations occur in the transitions from darker- to lighter-colored mixed sediments.

6. *Unit VI*: depth, 795.7–899.1 mbsf; age, late Miocene. Unit VI is distinguished by distinctive color oscillations produced by alternations of white to light gray, strongly bioturbated nannofossil chalk to mixed sediments and limestone and clayey nannofossil chalk with dark greenish-gray nannofossil mixed sediments and claystone. Interbedded layers of partially graded lithified calcareous grainstone with siliciclastics and traces of glauconite and skeletal packstone, both interpreted as turbidites, are dark greenish-gray. Multiple generations of microfaults and large-scale slump folds are present. Lithoclastic rudstone and floatstone, interpreted as debris flows, are common. In fact, Unit VI together with Unit VII contain about 50% of the total number of debris flows observed in the entire Site 823 sequence.

7. *Unit VII*: depth, 899.1–1011.0 mbsf; age, late Miocene to middle Miocene. Unit VII is defined by the occurrence of shallow-

water, platform-derived pebbles and clasts within lithoclastic rudstones, interpreted as debris flows. The pebbles and clasts contain coralline algae, large benthic foraminifers, coral fragments, and dolostone fragments. These sediments include nannofossil chalk with clay, foraminifers, and bioclasts; clayey nannofossil mixed sediments; and nannofossil claystone. Increases in the amount of clay, siliciclastics, and traces of glauconite give these sediments a dark gray color. Medium sand- to silt-sized, gray bioclastic packstone and quartz foraminifer packstone layers having well-defined upward-fining sequences have been interpreted as turbidites.

Measurements of bulk density, grain density, porosity, and water content define six physical property units that correlate well with both lithologic changes and downhole logs. The numerous gravity-flow deposits of varying compositions significantly influence and alter the normal compaction trend with depth. An excellent inverse correlation between the velocity and calcium logs indicates that in addition to normal compaction and cementation processes, the calcium carbonate vs. clay contents are controlling porosity variations in the sequence.

Carbonate contents of sediments range between 18% and 80%. Because Queensland Trough receives redeposited material from both Queensland Plateau and the Australian continental margin, this large variability may reflect dilution of the pelagic carbonate component by terrigenous influxes from the margin and by a fluctuating influx of shallow-water carbonate sediments from the adjacent carbonate platforms. Changes in the relative contribution of gravity-flow deposits and suspended material from each source to the basin sequence should contribute to changes in overall sedimentation rates. Between 0 and 3.5 Ma, the sedimentation rate was 11 cm/k.y.; while between 3.5 and 5.9 Ma, it increased to 16.6 cm/k.y. A 10-fold decrease to 1 cm/k.y. occurred between 8.2 and 10.4 Ma. The upper Miocene to lower Pliocene sediments tend to have higher clay contents; this is particularly the case for the lowermost upper Miocene sediments. Between 3.5 and 5.9 Ma, the combination of high sedimentation rates and increasing clay contents with depth points to an increased influx of terrigenous material that was manifested in the core as an increased number of debris flows and large slumps. In contrast, the low sedimentation rates and very high clay contents between 8.2 and 9.4 Ma might imply a significant decrease in the influx of fine-grained, plateau-derived carbonate, although the presence of debris flows with shallow-water pebbles and clasts indicates that material was being eroded from the platform margin. The quartz content remains comparatively constant throughout the sequence.

Carbonate mineralogy of the sediments deposited during the last approximately 2.6 Ma shows up to 50% aragonite, with up to 30% high Mg-calcite (HMC). Below 200 mbsf, the HMC disappears from the sediments, while aragonite disappears below 300 mbsf. The high concentration of metastable carbonates in the upper Pliocene to Pleistocene sediments provides definitive evidence for the contribution of shallow-water material to the basin during this interval. In fact, micrite is rare to absent in sediments below lithologic Unit III, but appears again in lithologic Unit VI, implying that production and transport of fine-grained carbonate from shallow-water environments bordering Queensland Trough to deeper waters diminished dramatically between the latest late Miocene and early Pliocene, approximately 6.0 to 4.2 Ma.

Interstitial water chemistry succinctly reflects diagenetic reactions occurring within these sediments. With the dissolution of metastable carbonates, aragonite and HMC, the concentrations of  $\text{Sr}^{2+}$  increase steadily and reach high values at depth because of the absence of  $\text{SO}_4^{2-}$  to precipitate celestite. Concentrations of  $\text{SO}_4^{2-}$  are totally depleted between about 50 and 550 mbsf as a result of sulfate reduction. A downward trend toward increasing concentrations of  $\text{Ca}^{2+}$  and decreasing concentrations of  $\text{Mg}^{2+}$  relative to concentrations of chloride apparently has been controlled by the formation of authigenic calcite and dolomite. Concentrations of chloride tend to increase with depth. As at other Leg 133 sites, interstitial water chemistry indicates the presence of a source of water having elevated salinity at depth below the sampled section.

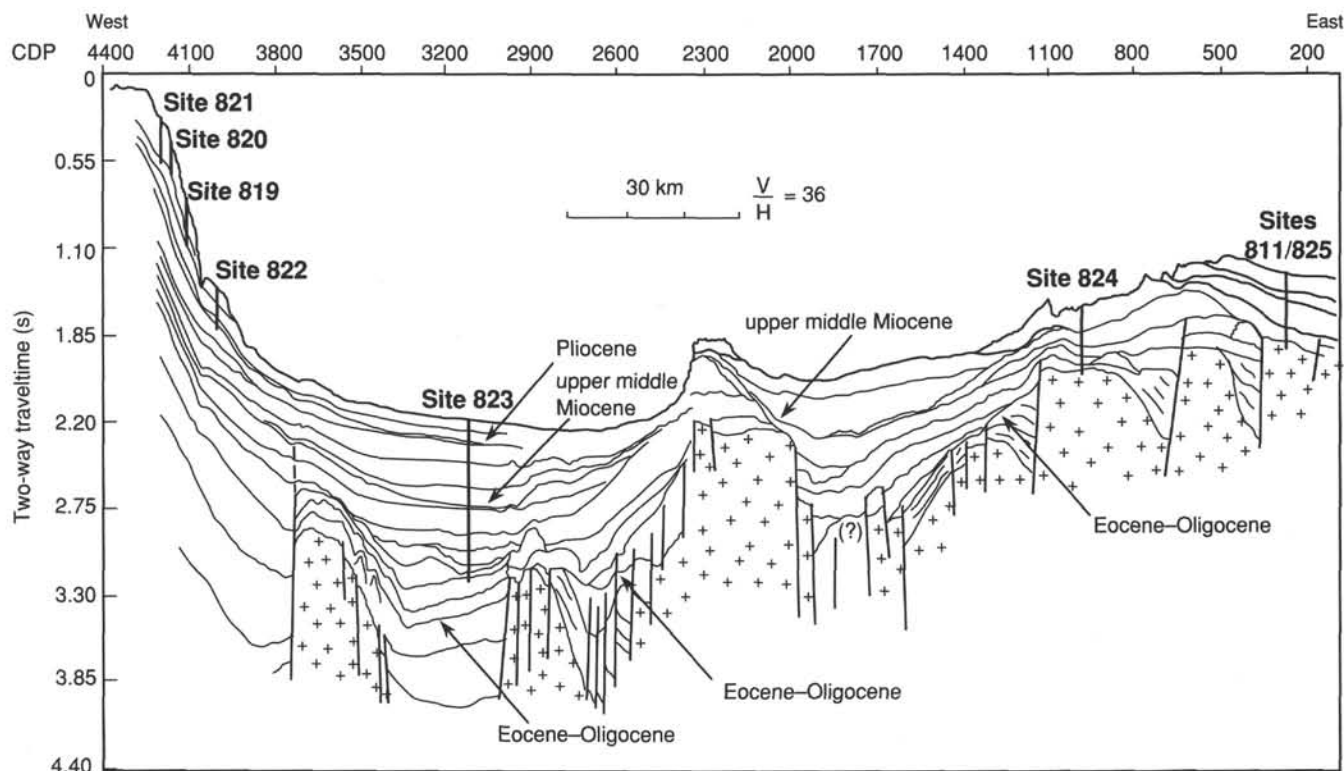


Figure 1. Schematic section of Site 823 across Queensland Trough.

Total organic carbon contents of the sediments were mostly low, often 0%, but never exceeding 0.55%. This organic matter has a mixed marine and terrestrial origin. High concentrations of methane were recorded, but presented no safety and/or pollution problems, because evolution of methane to ethane ratio with depth was normal. Concentrations of methane increased significantly below the sulfate-reduction zone beginning at 50 mbsf, indicating a bacterial origin for the gas. We observed mixing of upward-migrating, thermogenic free hydrocarbons with biogenic gases below 400 mbsf.

## BACKGROUND AND SCIENTIFIC OBJECTIVES

### The Queensland Trough Transect

Current knowledge of the evolution of carbonate platforms associated with passive margins is based almost exclusively on studies in the Caribbean, particularly on the Blake Plateau and the Bahama Banks. Studies of these platforms along with comparative studies off the eastern coast of the U.S. have provided a frequently applied model for the evolution of passive-margin carbonate platforms. ODP studies off northeastern Australia were intended to define new models and to provide a new perspective for old models.

The Queensland Trough transect (see "Introduction" chapter, this volume) through Sites 819 to 824 includes the slope of the Great Barrier Reef, the basin infill in the Queensland Trough, and the slope along the western margin of the Queensland Plateau. Thus, in addition to specific objectives defined for each site or sets of sites, this transect should help to define the interaction and development of the basin and its adjacent platforms, focusing on slope and basin infill processes. Further, basin sequences should define a record of corresponding oceanographic changes.

Site 823 is located in the central-western Queensland Trough, toward the deepest part of the basin. A schematic section tying east-west seismic profiles across Queensland

Trough from the Great Barrier Reef slope to the western flank of the Queensland Plateau is shown in Figure 1, while the pre-drilling prognosis at the site is shown in Figure 2. The section illustrates the general structural style of shallow portions of the trough and its margins. Shallow (1.7 s TWT) planated basement tilt blocks occur beneath western Queensland Plateau (CDPs, 200–1100) and are bounded by relatively steep, westerly dipping rotational normal faults. Half-grabens formed by these blocks contain an easterly dipping (?) Upper Cretaceous synrift section that is up to about 800 m thick. These tilt blocks, and in some places the synrift section, eroded during the formation of the Paleocene "breakup" unconformity, correspond to the beginning of seafloor spreading in the Coral Sea Basin to the northeast. Beneath the eastern flank of the Queensland Trough (CDPs, 1400–1700), the dip of the faults bounding the tilt blocks switches to the east, and the corresponding synrift and pre-rift sections dip to the west. Complex faulting beneath the eastern part of the trough (CDPs, 1700–2000) may be related to wrenching, which indicates that strike-slip movement probably was important in the development of the trough. A large, planated basement block in the center of the trough (CDPs, 200–2300) may be bounded by a major, near-vertical fault on its eastern flank and by a series of smaller, high-angle normal faults on its western flank, which progressively downstep basement to the west. This high can be identified from seismic data both north and south along the strike of the trough. West of this high, sediment thickness might be as much as 3000 m. In the center of the trough (CDPs, 2600–2900), another major half-graben containing (?) Cretaceous pre-rift and synrift sections occurs at a depth of 3.1 s TWT. Both this section and the underlying basement tilt block have been planated by the Paleocene "breakup" unconformity. The western flank of the high was formed by a complex vertical fault system. Another planated basement high occurs beneath the western flank of the trough (CDPs, 3600–3800) at a

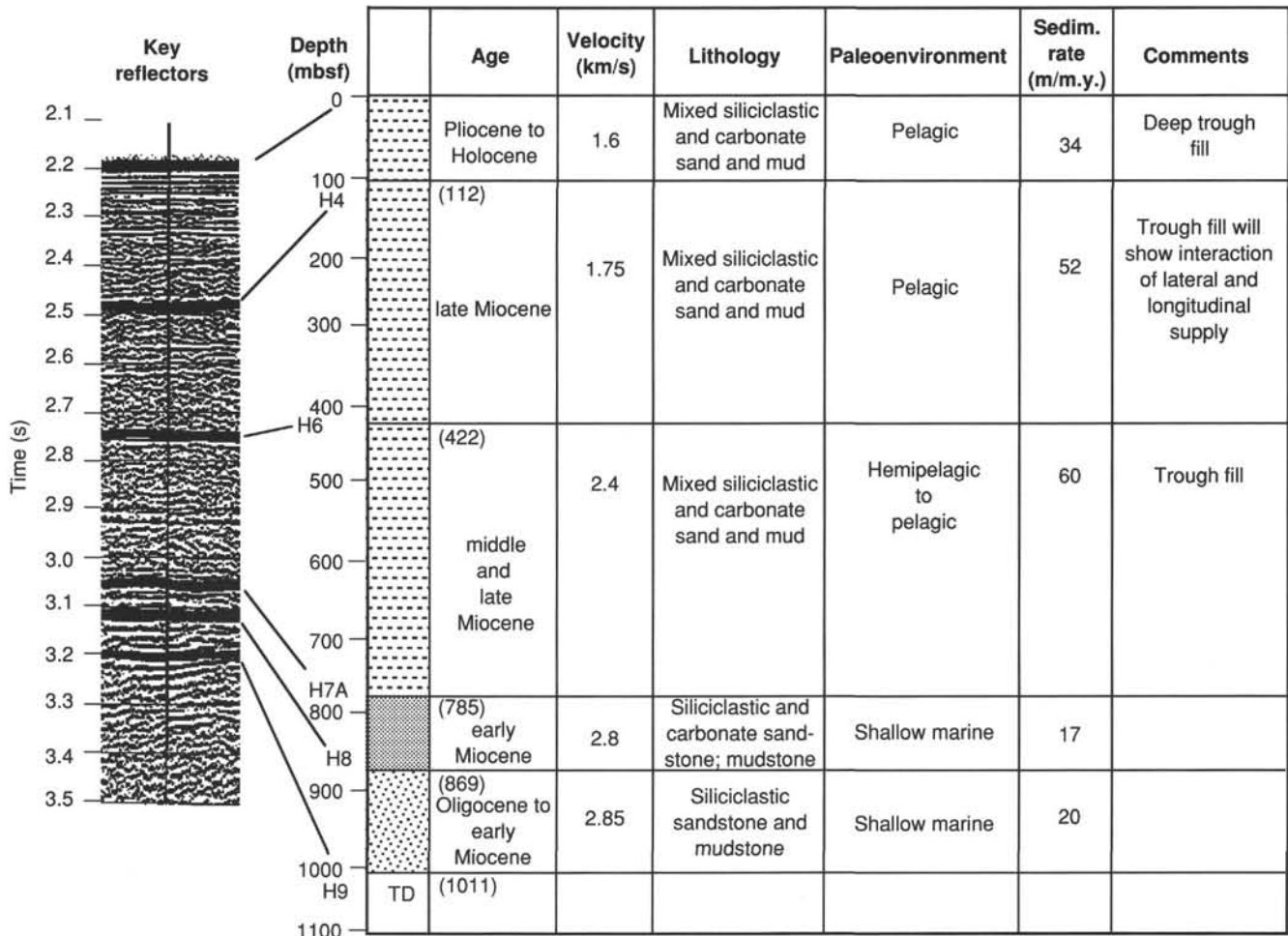


Figure 2. Graphic pre-cruise drilling prognosis for Site 823.

depth of 2.9 s TWT and is bounded by high-angle faults. A broad anticline formed by flexural and compaction drape over this block extends to high levels within the section. The thickest sedimentary section within the trough occurs beneath its western flank, where it may be more than 4000 m thick.

Pre-Oligocene mounds or build-ups occur on the flanks of these highs beneath the western part of Queensland Trough and have been draped by the overlying Miocene section. Similar build-ups also occur on basement highs on the western margin of Queensland Plateau, between Sites 824 and 811. A major lower-middle Miocene(?) build-up occurs on top of the large basement high in the center of the trough (CDPs, 2000–2300), associated with a substantial debris apron that extends westward into the deeper part of the trough. A marked change in depositional style takes place across the unconformity: from essentially conformable sequences to onlapping basin-fill sequences. On the western flank of the trough, the Pliocene-Pleistocene section displays strong downlapping character and thins eastward.

Site 823 was positioned to recover a basinal section that would provide material for paleoceanographic studies, as well as a record of basin fill and basin/platform interactions. Specific objectives of drilling at Site 823 were as follows:

1. To determine the age and facies of basinal sediments.
2. To derive a sea-level signature in a deep basin setting and to relate this signature to that obtained from the shelf-margin setting at Sites 819 through 822.

3. To derive a high-resolution paleoceanographic record reflecting late Cenozoic variations in climate.

## OPERATIONS

### Transit to Site 823

The sea voyage to Site 823 (proposed Site NEA-5) began at 2200L (all times given in local time, or L) 20 September and covered 27 nmi in 2.7 hr at an average speed of 10.0 kt. A seismic survey was run over Site 823 that covered 13 nmi in 2.3 hr at an average speed of 5.6 kt. A Datasonics beacon was dropped at 0350L, September 21.

### Hole 823A

Hole 823A was located at 16°36.981'S, 146°47.037'E; the PDR predicted a water depth of 1637.2 m from sea level. The bit was lowered to a water depth of 1638.4 m from sea level for the first shot. Hole 823A was spudded at 0739L, 21 September. From Core 133-823A-1H, we recovered 5.82 m of sediments, indicating that the mud line was at a water depth of 1649.7 m from sea level. Continuous APC cores (Cores 133-823A-1H through -11H) were taken from 0 to 119.8 mbsf, with 119.8 m cored and 123.73 m recovered (103.3% recovery; high recovery rates are result of gas expansion). APC coring ended when overpull reached 120,000 lb. The hole was displaced with heavy mud as a precaution because methane concentrations reached 100,000 ppm.

### Hole 823B

Hole 823B was located at 16°36.982'S, 146°47.053'E. The bit was lowered to a water depth of 1636.7 m from sea level for the first shot. Hole 823B was spudded at 1618L, 21 September. From Core 133-823B-1H, we recovered 8.28 m of sediment, indicating that the mud line was at a water depth of 1637.9 m from sea level. Continuous APC cores (Cores 133-823B-1H through -12H) were taken from 0 to 112.8 mbsf, with 112.8 m cored and 117.6 m recovered (104.3% recovery; high recovery rates result from gas expansion). WSTP water samples were taken and temperatures were measured at 55.8 and 103.3 mbsf, but we recovered only seawater in these samples.

Cores 133-823B-13X through -84X were taken from 112.8 to 805.4 mbsf, with 692.6 m cored and 637.1 m recovered (92.0% recovery). XCB coring ended when recovery decreased to as little as 1.2 m per each 9.5-m cored interval. Poor recovery in the last four cores was a result of jamming; our rotating time increased to 100 min/core, and some of the cores were burned by the resulting friction. The hole was displaced with heavy mud as a precaution because values of methane reached 50,000 ppm; ethane, 14 ppm; and propane, 10 ppm. The  $C_1/C_2$  ratio was subnormal, indicating no hydrocarbon migration at the 57°C/km geothermal gradient. Scattered  $C_4$  and  $C_5$  levels as high as 12 ppm were detected from 718 to 776 mbsf.

### Hole 823C

A used 9-7/8-in. RBI C-7 four-cone insert bit and mechanical bit release (MBR) were run with an RCB outer core barrel, nine 8-1/4-in. drill collars, and hydrolex jars with two drill collars above. Hole 823C was spudded at 0405L, 26 September, at 16°36.983'S, 146°47.066'E. We washed the hole down with a wash barrel in place from 0 to 573.0 mbsf, and then discarded the wash barrel material. We then removed the wash barrel and used a center bit to drill from 573.0 to 784.0 mbsf.

Cores 133-823C-1R to -24R were taken from 784.0 to 1011.0 mbsf, with 227.0 m cored and 186.1 m recovered (82.0% recovery). A short trip was made up to 108.0 mbsf and back, when we encountered a 20,000-lb drag and 15 m of fill at the bottom of the hole. We released the RCB bit with the MBR and then shifted the sleeve. An open BHA was pulled with no drag to 107.7 mbsf for logging. Logs were run as follows:

1. The induction/density/sonic/caliper/gamma-ray (DITE/HLDT/SDT/MCDG/NGT) logging tool was placed into the hole at 2235L, 28 September, but the tool could go no deeper than 344.7 mbsf. We logged the hole up to 88 mbsf. A new conical side-entry sub (CSES) was rigged up in 3-1/2 hr, and we installed the logging tool in it. Drill pipe was run to 779.4 mbsf—the top of the hard formation—with scattered 20,000-lb drag. The logging tool encountered 28.4 m of fill at the bottom of the hole; we pulled the drill pipe out of the hole during logging, with scattered drag to 20,000 lb. Our logs indicated that scattered tight sections in the hole were closing back to a diameter of 7 in. as soon as the 8-1/4-in. drill string passed through. The tool was back out of the hole at 1240L, 29 September.

2. The geochemical/aluminum clay tool/gamma-ray (GST/ACT/CNTG/NGT/TCC) logging tool was installed in the CSES at 1432L, when we ran the drill string to 779.4 mbsf, with occasional drag to 20,000 lb. The tool reached 34.3 m off the bottom and was pulled back out of the hole at 0050L, 30 September.

3. The formation microscanner/gamma-ray/temperature (FMS/NGT/TCC) logging tool was placed in the CSES at

0340L, 30 September; We ran pipe into the hole to 943.3 mbsf, with scattered 20,000-lb drag. The logging tool reached bottom 55.8 m above the total depth of the hole. We pulled the drill pipe out of the hole during logging, with scattered drag of up to 20,000 lb. The logs indicated that tight sections in the hole were closing back to a diameter of 4-1/2-in. as soon as the 8-1/4-in. drill string passed through. We pulled out the top of the CSES to the moonpool. The logging tool was out of the hole at 1200L, 30 September.

Our first use of the new CSES was successful in all respects. In the future, the CSES should permit logging in troublesome holes, but this will increase the risk to the BHA and logging tools. Some minor operational problems were encountered, such as our having to remove a flapper valve because logging tools hung up in it when being removed from the CSES, which damaged the logging tool heads. We ran drill pipe into the hole and then displaced the hole with heavy mud, per PPSP guidelines as a precaution because values of  $C_1$  gas reached 70,000 ppm;  $C_2$ , 35 ppm; and scattered readings of  $C_3$  to  $C_5$  to 12 ppm were detected below 976 mbsf. The  $C_1/C_2$  ratio was subnormal, indicating no hydrocarbon migration at the 57°C/km geothermal gradient.

Table 1 contains the coring summary for Site 823.

### SITE GEOPHYSICS

*JOIDES Resolution* separated from the beacon at Hole 822A at 2002L (JD 263/1022UTC), 20 September 1990, and began the 2.7-hr transit to Site 823 (proposed Site NEA-5) at 2200L (JD 263/1200UTC). A magnetometer was towed immediately after departure, and continuous bathymetric and magnetic data were recorded during the Line 8 transit, heading about 115° across Queensland Trough. The ship arrived at a position of 16°36.980'S and 146°39.300'E, about 7.3 nmi west of Site 823, at 0042L (JD 263/1442UTC), ready to start the site-location survey.

Site 823 lies in about 1638 m of water, just west of the axis of Queensland Trough, and about 110 km east-northeast of the town of Cairns (Fig. 3). It is about 59 km east of the edge of the Great Barrier Reef, 100 km west of Holmes Reef on the western edge of Queensland Plateau, about 50 km east of Sites 819 through 821, and 65 km east-southeast of Site 822. The site lies about 65 km west of a significant bathymetric high (at a water depth of about 1220 m) within the eastern flank of Queensland Trough. Site 823 forms part of a transect of Leg 133 drilling sites that extends east from the Great Barrier Reef across Queensland Trough to western Queensland Plateau, in the vicinity of Holmes Reef. The site was selected with the intention of obtaining a complete basin section for a paleo-oceanographic history and to correlate basin-fill responses with sites on the adjacent Great Barrier Reef and Queensland Plateau margins.

The area was first recognized as a potential ODP drilling target from 1982 Geophysical Services International (GSI) air-gun data from the Queensland Trough (GSI Lines 7 and 11; Fig. 3). In 1987, the BMR vessel *Rig Seismic* was used to conduct a site survey at this location (Symonds and Davies, 1988; Feary et al., 1990), and about 95 km of 24-channel, 80-in.<sup>3</sup> water-gun seismic, magnetic, and bathymetric data were collected on a grid of north-south and east-west lines (BMR Line 75/41; Figs. 3 and 4). The site lies at the intersection of two lines within this grid (Feary et al., 1990)—one located using the global positioning system (GPS) and the other using a transit satellite/dead-reckoning (DR) system.

An important requirement of Leg 133 site-location surveys was that any seismic records obtained on board the *JOIDES Resolution* resemble as much as possible in appearance those

Table 1. Coring summary, Site 823.

Core no.	Date (Sept. 1990)	Time (UTC)	Depth (mbsf)	Length cored (m)	Length recovered (m)	Recovery (%)
<i>Hole 823A</i>						
1H	20	2150	0-5.8	5.8	5.82	100.0
2H	20	2210	5.8-15.3	9.5	9.61	101.0
3H	20	2240	15.3-24.8	9.5	9.81	103.0
4H	20	2310	24.8-34.3	9.5	9.56	100.0
5H	20	2340	34.3-43.8	9.5	9.80	103.0
6H	20	0010	43.8-53.3	9.5	9.97	105.0
7H	21	0035	53.3-62.8	9.5	9.96	105.0
8H	21	0110	62.8-72.3	9.5	9.86	104.0
9H	21	0155	72.3-81.8	9.5	9.91	104.0
10H	21	0225	81.8-91.3	9.5	9.93	104.0
11H	21	0300	91.3-100.8	9.5	9.87	104.0
12H	21	0340	100.8-110.3	9.5	9.69	102.0
13H	21	0415	110.3-119.8	9.5	9.94	104.0
Coring totals				119.8	123.73	103.3
<i>Hole 823B</i>						
1H	21	0625	0-8.3	8.3	8.28	99.7
2H	21	0650	8.3-17.8	9.5	9.85	103.0
3H	21	0715	17.8-27.3	9.5	9.74	102.0
4H	21	0745	27.3-36.8	9.5	9.86	104.0
5H	21	0820	36.8-46.3	9.5	9.83	103.0
6H	21	0855	46.3-55.8	9.5	10.05	105.8
7H	21	1040	55.8-65.3	9.5	9.88	104.0
8H	21	1115	65.3-74.8	9.5	10.00	105.2
9H	21	1145	74.8-84.3	9.5	10.00	105.2
10H	21	1220	84.3-93.8	9.5	9.96	105.0
11H	21	1250	93.8-103.3	9.5	10.06	105.9
12H	21	1430	103.3-112.8	9.5	10.12	106.5
13X	21	1530	112.8-122.4	9.6	8.27	86.1
14X	21	1555	122.4-132.1	9.7	9.69	99.9
15X	21	1625	132.1-141.7	9.6	9.49	98.8
16X	21	1655	141.7-151.4	9.7	9.86	101.0
17X	21	1835	151.4-161.1	9.7	8.10	83.5
18X	21	1905	161.1-170.8	9.7	9.16	94.4
19X	21	1940	170.8-180.5	9.7	9.36	96.5
20X	21	2015	180.5-190.2	9.7	6.41	66.1
21X	21	2045	190.2-199.8	9.6	10.02	104.4
22X	21	2225	199.8-209.1	9.3	9.95	107.0
23X	21	2300	209.1-218.7	9.6	9.28	96.6
24X	21	2335	218.7-228.0	9.3	7.49	80.5
25X	21	2359	228.0-237.7	9.7	9.83	101.0
26X	22	0025	237.7-247.3	9.6	9.76	101.0
27X	22	0210	247.3-257.0	9.7	9.77	101.0
28X	22	0245	257.0-266.7	9.7	9.20	94.8
29X	22	0315	266.7-276.3	9.6	9.29	96.8
30X	22	0355	276.3-286.0	9.7	8.47	87.3
31X	22	0425	286.0-295.6	9.6	9.71	101.0
32X	22	0630	295.6-305.3	9.7	8.78	90.5
33X	22	0700	305.3-314.9	9.6	8.91	92.8
34X	22	0740	314.9-324.6	9.7	8.80	90.7
35X	22	0815	324.6-334.2	9.6	9.83	102.0
36X	22	0850	334.2-343.9	9.7	10.08	103.9
37X	22	0930	343.9-353.4	9.5	10.03	105.6
38X	22	1020	353.4-363.0	9.6	10.11	105.3
39X	22	1130	363.0-372.7	9.7	9.53	98.2
40X	22	1235	372.7-382.4	9.7	9.87	102.0
41X	22	1340	382.4-392.0	9.6	9.84	102.0
42X	22	1450	392.0-401.6	9.6	10.03	104.5
43X	22	1555	401.6-411.3	9.7	9.97	103.0
44X	22	1720	411.3-420.9	9.6	9.71	101.0
45X	22	1815	420.9-430.6	9.7	10.06	103.7
46X	22	1915	430.6-440.3	9.7	9.93	102.0
47X	22	2020	440.3-449.9	9.6	8.23	85.7
48X	22	2115	449.9-459.6	9.7	6.96	71.7

Table 1 (continued).

Core no.	Date (Sept. 1990)	Time (UTC)	Depth (mbsf)	Length cored (m)	Length recovered (m)	Recovery (%)
49X	22	2230	459.6-478.1	9.6	9.10	94.8
50X	22	2335	469.2-478.1	8.9	4.70	52.8
51X	23	0050	478.9-487.8	8.9	0.01	0.1
52X	23	0200	487.8-497.5	9.7	7.02	72.4
53X	23	0320	497.5-507.1	9.6	9.90	103.0
54X	23	0450	507.1-516.8	9.7	8.30	85.5
55X	23	0600	516.8-526.4	9.6	9.67	101.0
56X	23	0735	526.4-535.7	9.3	10.11	108.7
57X	23	0930	535.7-545.4	9.7	8.52	87.8
58X	23	1130	545.4-555.0	9.6	9.94	103.0
59X	23	1305	555.0-564.7	9.7	7.33	75.5
60X	23	1550	564.7-574.3	9.6	10.15	105.7
61X	23	1715	574.3-583.9	9.6	9.87	103.0
62X	23	1825	583.9-593.6	9.7	9.51	98.0
63X	23	1945	593.6-603.2	9.6	9.32	97.1
64X	23	2105	603.2-612.8	9.6	7.37	76.8
65X	23	2225	612.8-622.5	9.7	8.64	89.1
66X	23	2340	622.5-632.2	9.7	9.73	100.0
67X	24	0055	632.2-641.6	9.4	9.67	103.0
68X	24	0215	641.6-650.9	9.3	9.96	107.0
69X	24	0345	650.9-660.6	9.7	9.76	100.0
70X	24	0515	660.6-670.3	9.7	9.91	102.0
71X	24	0640	670.3-679.9	9.6	9.57	99.7
72X	24	0830	679.9-689.6	9.7	9.94	102.0
73X	24	1010	689.6-699.3	9.7	9.89	102.0
74X	24	1150	699.3-708.9	9.6	10.00	104.1
75X	24	1320	708.9-718.6	9.7	9.78	101.0
76X	24	1500	718.6-728.2	9.6	9.89	103.0
77X	24	1640	728.2-737.9	9.7	9.86	101.0
78X	24	1845	737.9-747.6	9.7	5.83	60.1
79X	24	2040	747.6-757.3	9.7	9.91	102.0
80X	24	2230	757.3-767.0	9.7	9.75	100.0
81X	25	0040	767.0-776.7	9.7	7.77	80.1
82X	25	0305	776.7-786.4	9.7	6.42	66.2
83X	25	0635	786.4-795.7	9.3	5.12	55.0
84X	25	0900	795.7-805.4	9.7	1.20	12.4
Coring totals				805.4	754.85	93.7
<i>Hole 823C</i>						
1R	26	1310	784.0-793.6	9.6	6.87	71.5
2R	26	1415	793.6-802.9	9.3	6.18	66.4
3R	26	1525	802.9-812.6	9.7	6.32	65.1
4R	26	1655	812.6-822.3	9.7	6.36	65.5
5R	26	1820	822.3-832.0	9.7	8.63	88.9
6R	26	1935	832.0-841.7	9.7	2.55	26.3
7R	26	2110	841.7-851.4	9.7	8.50	87.6
8R	26	2300	851.4-861.1	9.7	1.64	16.9
9R	26	0045	861.1-870.8	9.7	8.84	91.1
10R	26	0215	870.8-880.4	9.6	9.06	94.4
11R	26	0410	880.4-890.1	9.7	8.44	87.0
12R	26	0620	890.1-899.7	9.6	9.15	95.3
13R	26	0805	899.7-909.4	9.7	9.95	102.0
14R	26	0940	909.4-919.1	9.7	8.16	84.1
15R	26	1140	919.1-928.8	9.7	9.78	101.0
16R	26	1310	928.8-938.4	9.6	7.83	81.5
17R	26	1440	938.4-948.0	9.6	9.65	100.0
18R	26	1615	948.0-957.3	9.3	8.57	92.1
19R	26	1800	957.3-966.9	9.6	7.43	77.4
20R	26	1940	966.9-976.6	9.7	9.53	98.2
21R	27	2125	976.6-986.2	9.6	8.75	91.1
22R	27	2245	986.2-995.9	9.7	9.55	98.4
23R	28	0030	995.9-1005.6	9.7	8.90	91.7
24R	28	0125	1005.6-1011.0	5.4	5.40	100.0
Coring totals				227.0	186.04	82.0

collected during the 1987 site surveys by *Rig Seismic*, thus reducing ambiguity when defining sites and when comparing the seismic stratigraphy of the two data sets. Accordingly, we modified parts of the *JOIDES Resolution* seismic deployment systems.

The site-location survey was designed simply to confirm the seismic character and position of Site 823 along the east-west *Rig Seismic* line that crossed it. Following the survey, we expected to relocate the site using the confirmed GPS coordinates and the beacon dropped while maneuvering onto the location using the *Resolution's* dynamic positioning system. The distribution of regional seismic data in the area around the site is shown in Figure 3, while the tracks of the original *Rig Seismic* site survey and the *JOIDES Resolution* site-location survey are shown in Figure 4. Following a reduction in ship's speed to 5 kt, the *JOIDES Resolution's* single-channel seismic profiling system was deployed, and seismic recording began at JD 263/1500UTC, 20 September 1990, in rough seas (Beaufort Scale force of 4 to 5), with swells of 2 m. The *JOIDES Resolution* sailed east across Site 823 (Fig. 4), and we stopped acquiring seismic data and retrieved our equipment at JD 263/1635UTC, 20 September 1990, after recording about 15 km of seismic and magnetic data. We used GPS navigation throughout the survey, and we consider the ship's track to be positioned accurately. In general, our seismic equipment operated well, and we obtained fair quality analog monitor records (Fig. 5), although these are noisy because of the rough seas. Reasonable correlation at the site existed between *Rig Seismic* and *JOIDES Resolution* seismic profiles (Fig. 5); however, because of the compressed nature of the *Resolution's* seismic records and the absence of definitive seismic characteristics in the area, reliable site confirmation using only seismic data was difficult.

Following the survey, *JOIDES Resolution* returned to the confirmed GPS position of Site 823 at JD 263/1700UTC, 20 September 1990. Thrusters were lowered and we achieved final positioning of the ship over the site using dynamic positioning. A beacon was dropped at JD 263/1750UTC; final coordinates of Hole 823A are 16°36.981'S and 146°47.037'E, with a water depth of 1638.4 m (drill-pipe measurement from sea level).

Basement cannot be seen in either the *JOIDES Resolution* or *Rig Seismic* water-gun data across the site; however, in normal resolution air-gun data near the site area (GSI Lines 7 and 111; Fig. 3), the site lies about 2.3 s TWT below seafloor. The upper 0.82 s TWT (~845 m) of sediments at the site have been subdivided into six units by thin zones of high-amplitude, flat-lying reflectors (Fig. 5). All these units have a chaotic or reflection-free configuration. They have been underlain by a 0.09 s TWT (~130 m) thick unit composed of high-amplitude, parallel reflectors, which onlap the basal unit at the site. This basal unit is about 0.09 s TWT (~120 m) thick and extends to just beyond TD. The unit has a variable thickness in the site area and contains subparallel reflectors that exhibit gentle folding and small-throw faulting. This folding and faulting appear to intensify in the section beneath this unit.

To provide some predictive capability during drilling at Site 823, we estimated the TWT/depth relationship below the seafloor by using stacking-derived interval velocities from BMR site-survey seismic lines across the site (Fig. 6).

## LITHOSTRATIGRAPHY

### Introduction

Site 823 is located in the central-western part of the Queensland Trough, toward the deepest part of the basin in a

water depth of 1638 m. During APC drilling in Holes 823A and 823B, XCB drilling in Hole 823B, and RCB drilling in Hole 823C, we recovered 103.3% (Hole 823A), 93.9% (Hole 823B), and 82% (Hole 823C) of the section, respectively. The Miocene to Pleistocene sequence that we encountered at Site 823 consists of hemipelagic sediments interbedded with turbidites, debris flows, and slump deposits. The fine-grained "background" sediments (referred to hereafter as hemipelagic sediments) contain varying amounts of clay and carbonate and range from clayey and sandy mixed sediments to more pelagic nanofossil ooze and chalk with varying amounts of foraminifers, clay, quartz, and micrite. More than 1860 sediment gravity-flow deposits, interpreted as turbidites, debris flows, and slumps, occur throughout the more than 1000 m of sediment cored at Site 823.

Thickness and composition of redeposited sediments and mineralogical changes in hemipelagic sediments were used to define seven lithologic units (Figs. 7, 8, 9, and 10). Hemipelagic sediments in Subunit IA, Unit II, Subunit IIIC, and Units IV and VI are nanofossil ooze to chalk, with small amounts of clay, whereas Subunits IB, IIIA, and IIIB and Units V and VII have greater amounts of noncarbonate components. The addition of considerable terrigenous sediments can be seen in the variability in composition of these sediments and in fluctuation of clay contents. Increases in noncarbonate minerals in hemipelagic sediments exhibit a good correlation with increased occurrence of thick sediment gravity flows, mainly debris flows (Fig. 8).

The nature and relative abundance of sediment gravity flows also vary among different lithologic units (Figs. 8 and 9). Unit I contains a variety of different sediment gravity flows, whereas Unit II contains numerous thin turbidites. Unit III is dominated by thick debris flows and slumps, but Unit IV has the most slumped intervals. Unit V has the least sediment gravity-flow deposits, and Unit VI indicates an increase in turbidites and debris flows. Unit VII has numerous debris flows and turbidites that contain carbonate clasts derived from neritic sources. More than 50% of all the debris flows occur in Units VI and VII (Fig. 9).

Because many of the redeposited sediments are composed of grains derived from both terrigenous and neritic carbonate sources, it is difficult to establish a satisfactory lithologic nomenclature. Ideally, the terms floatstone, rudstone, packstone, and grainstone have been used to describe neritic-carbonate sediments (see "Explanatory Notes" chapter, this volume). At Site 823, these terms were used to describe variations in texture of coarse-grained, redeposited sediments containing carbonate grains derived from neritic sources. In many cases, coarse siliciclastic sediments are major or minor components in mixed sediments and have been described using this terminology. To clarify discussions, general interpretative names have been used to describe redeposited sediments, but descriptions of each lithologic unit provide information about sedimentary structures and compositions, which substantiate these interpretations. Intervals showing evidence of deformation of soft sediments, including folding and sheared-out folds, are simply referred to as slumped intervals. Debris-flow deposits typically are conglomerates containing clasts of cohesive mud that had eroded from the slope and trough. These conglomeratic clasts either have been supported by a muddy matrix (floatstones) or have clast-supported fabrics (rudstones) surrounded by muds. In places, debris-flow conglomerates are closely associated with (and merge with) slumped intervals and contain clasts composed of folded muddy sediments compositionally similar to slumped intervals. Most of these conglomerates are debris flows, but those that have been graded represent coarse-grained tur-

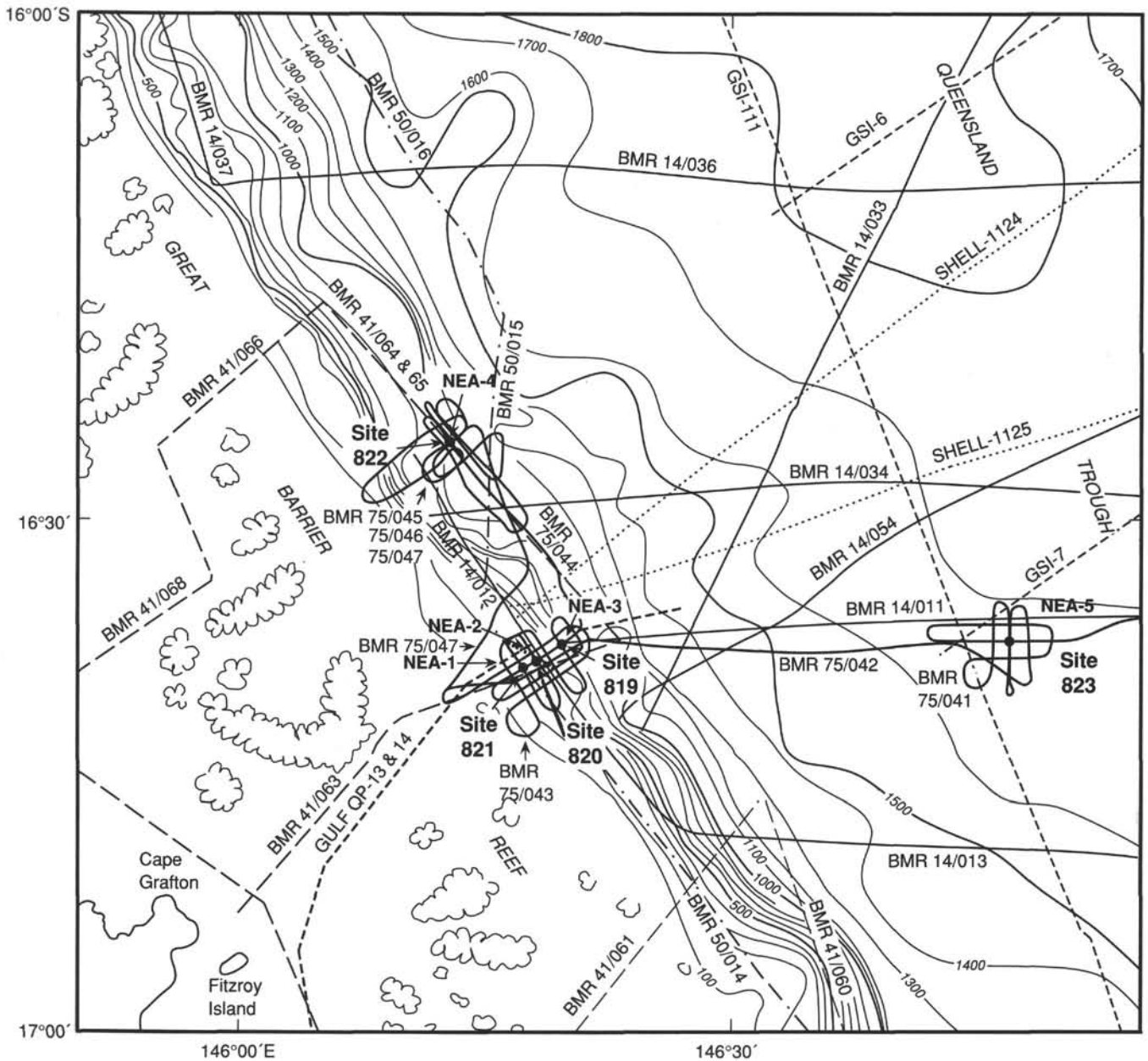


Figure 3. Track chart showing distribution of regional seismic data in the area around Site 823. Also shows locations of Sites 819, 820, 821, and 822, and simplified bathymetry in meters.

bidites. Redeposited sediments, including grainstone, packstone, terrigenous sandstone, and sandy mixed sediments, which show all or parts of the Bouma sequence ( $T_a$  = A grading;  $T_b$  = B-plane lamination;  $T_c$  = cross lamination and ripples;  $T_d$  = laminated silts;  $T_e$  = muddy fine fraction of the gravity flow), generally have been referred to as turbidites. A continuum exists from slumps to debris flows to turbidites.

#### Lithologic Units

**Unit I (Cores 133-823A-1H to -13H and Cores 133-823B-1H to -13X-6; depth, 0–119.8 mbsf [Hole 823A] and 0–120.7 mbsf [Hole 823B]; thickness, 119.8 m [Hole 823A] and 120.7 m [Hole 823B]; age, Pleistocene)**

Unit I contains numerous turbidites, debris flows, and slump deposits that are regularly interbedded with hemipelagic sediments.

Within this unit, clay contents increase downward. Hemipelagic sediments are light greenish-gray nannofossil ooze with micrite; light gray to gray nannofossil micritic ooze with clay, foraminifers, and bioclasts; passing downward into more clay-rich, olive gray nannofossil clayey mixed sediments with micrite to dark gray claystone with quartz, nannofossils, and micrite. Slumping occurs in several cores in the unit, but is most abundant in Subunit IA. The Subunit IA/Subunit IB boundary is associated with an increase in clay contents within sediments, shown by darker colors. Subunit IA contains thin turbidites and thick debris flows and slumps, whereas Subunit IB has thicker turbidites and debris flows that decrease in thickness at about 85 mbsf (Fig. 10). The hemipelagic sediments of Subunit IB are dominated by dark greenish-gray nannofossil claystone and dark gray clayey mixed sediments.

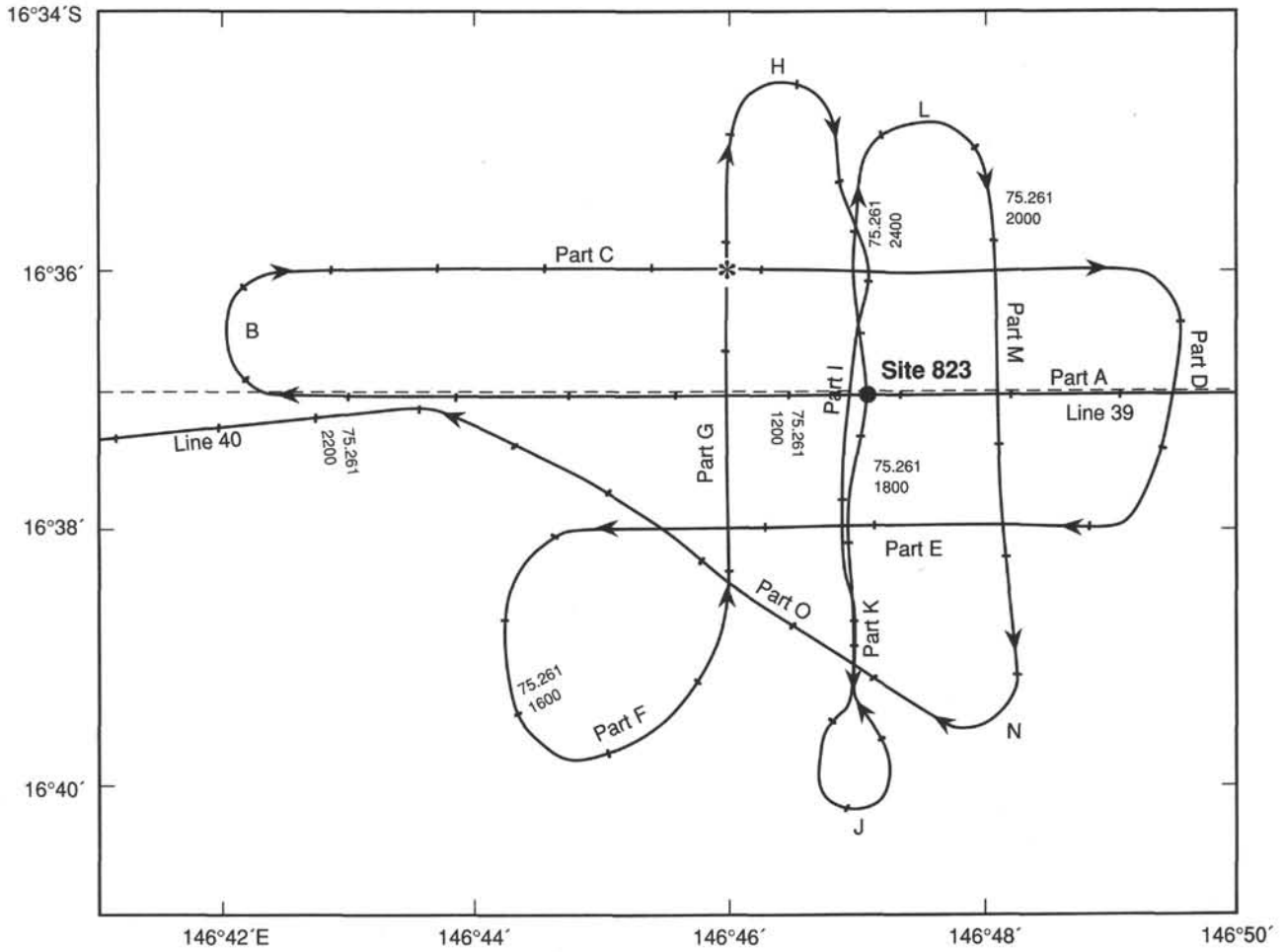


Figure 4. JOIDES Resolution Leg 133 site-location tracks (dotted line) and Rig Seismic 1987 site-survey tracks (solid line) around Site 823.

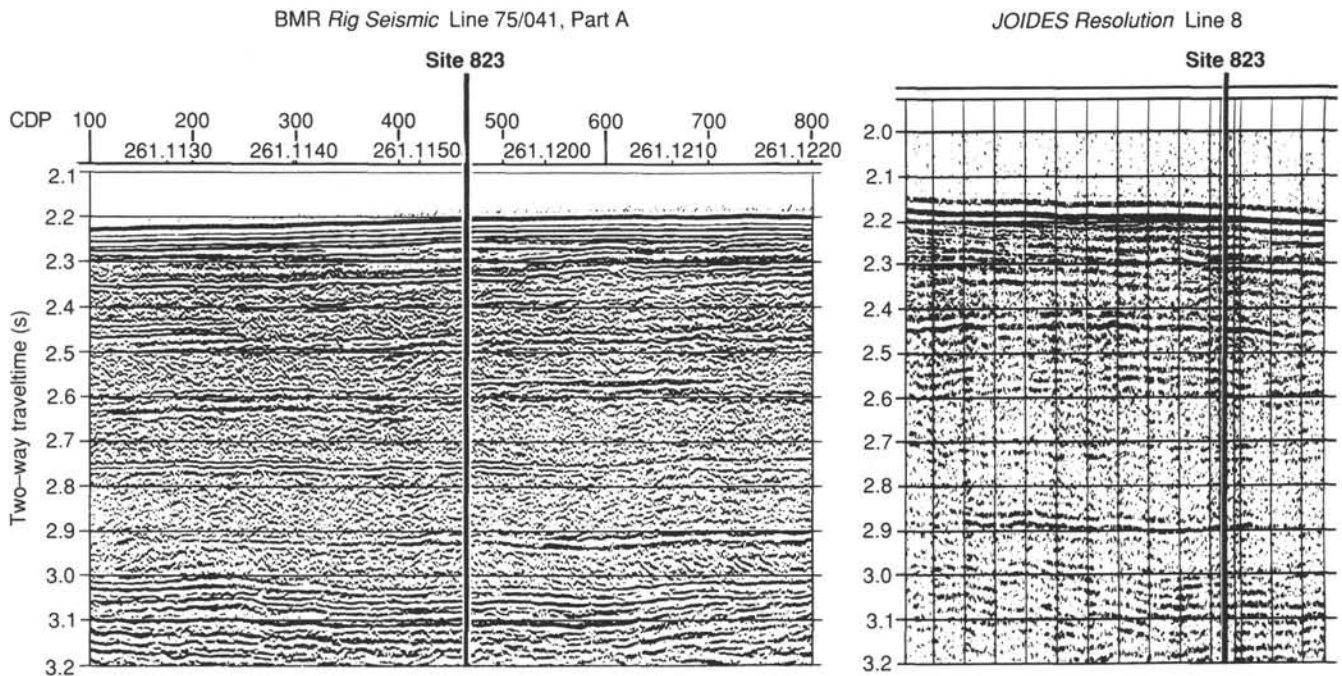


Figure 5. Comparison of JOIDES Resolution and Rig Seismic 80-in.<sup>3</sup> water-gun seismic profiles across Site 823.

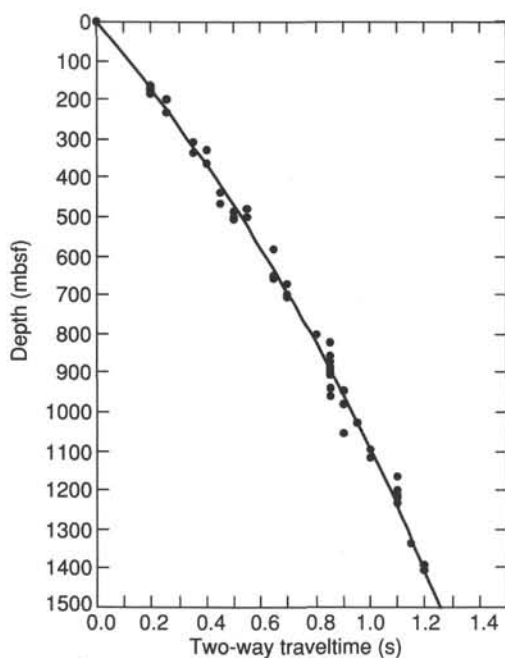


Figure 6. Two-way traveltime (TWT)/depth curve for Site 823, computed using stacking-derived interval velocities from BMR site-survey seismic data.

Sediment gravity-flow deposits make up 46% of this unit. The bioclastic packstones (turbidites) are greenish-gray to gray with silt- to sand-sized grains (Fig. 11). A typical turbiditic packstone has a sharp basal contact, is gray (brownish), and consists of unlithified coarse to fine sand-size bioclasts with foraminifers and siliciclastic sand. A turbidite packstone typically grades upward into light olive-gray, bioturbated clayey nannofossil mixed sediment with quartz or nannofossil ooze with foraminifers, bioclasts and siliciclastic sand. The turbidites are overlain by and interbedded with light greenish-gray nannofossil ooze, which are the hemipelagic or pelagic background sediments. The upper part of the turbidite is dark-colored due to an admixture of the background pelagic sediment with reworked hemipelagic sediments. Burrows are commonly filled with the fine-grained bioclastic packstone. Beds of foraminifer-rich fine-grained packstone are usually well-sorted and homogeneous and do not always show grading. The lack of grading could point to a source material pre-sorted by strong bottom water currents along the slope or could be an artifact of the drilling, where the finer silty material was redistributed.

**Subunit IA** (Cores 133-823A-1H to -10H-3, 60 cm, and Cores 133-823B-1H to -10H-2, 30 cm; depth, 0–85.4 mbsf [Hole 823A] and 0–86.1 mbsf [Hole 823B]; thickness, 85.4 m [Hole 823A] and 86.1 m [Hole 823B]; age, Pleistocene)

Subunit IA begins at the sediment/water interface, while the bottom of Subunit IA is immediately above a slump that consists of dark greenish-gray nannofossil claystone in Core 133-823A-10H-3, 60 cm, and Core 133-823B-10H-2, 30 cm, at 85.4 and 86.1 mbsf, respectively. This boundary coincides with a sharp decrease in carbonate contents as well as a decrease in bulk density (Fig. 8; see “Physical Properties” section, this chapter). The hemipelagic sediments of Subunit IA include (1) light greenish-gray, light gray, or gray nannofossil ooze with either micrite and clay, bioclasts, or foraminifers and clay; and (2) clayey nannofossil ooze. Pteropods occur in Sections 133-823A-1H-1 and -1H-2.

Redeposited sediments in Subunit IA are dominated by slumped intervals showing deformation of soft sediments and thick intervals of rudstone and floatstone, which have been interpreted as debris flows. Debris flows occur in Cores 133-823A-1H, -3H, and -6H, and in Cores 133-823B-3H and -6H. Large slumps typically consist of contorted and folded, greenish-gray to gray, locally laminated nannofossil ooze and occur in Cores 133-823A-3H and -8H. Beds of bioclastic packstone (up to 90 cm thick), interpreted as turbidites, are common. Most of these bioclastic packstones are thin (<5 cm) between 0 and 34 mbsf (Cores 133-823A-1 H to -4H). The bioclastic particles are pteropods, ostracods, benthic and planktonic foraminifers, *Halimeda* plates, echinoid spines, and sponge spicules. Thickness of both the packstone beds and the slumps increases between 34 and 85 mbsf (Cores 133-823A-4H to -10H). Two unusual light gray to pale yellow turbidite layers with no siliciclastic sediments but enriched in bioclasts occur in Sections 133-823A-4H-7 and -5H-3 to -5H-4 (Fig. 12). No evidence of erosion of hemipelagic ooze was seen beneath the turbidites. However, erosion must have occurred farther upslope, as indicated by mud clasts contained within a debris flow in Section 133-823A-5H-6.

An unusual debris flow in Core 133-823A-1H contains gravel-sized clasts of volcanic lithic fragments, feldspar, quartz, bioclasts, foraminifers, and biotite, in addition to redeposited mud clasts. A cobble of semilithified/firm mud in this debris flow yielded an age of 300 k.y., clearly older than the ooze of the core-catcher sample (<275 k.y.; see “Biostratigraphy” section, this chapter).

**Subunit IB** (Cores 133-823A-10H-3, 60 cm, to -13H-CC, and Cores 133-823B-10H-2, 30 cm, to -13X-6; depth, 85.4–119.8 mbsf [Hole 823A] and 86.1–120.7 mbsf [Hole 823B]; thickness, 34.4 m [Hole 823A] and 34.6 m [Hole 823B]; age, Pleistocene)

The contact between Subunits IA and IB has been defined as the top of a slump consisting of contorted, dark greenish-gray nannofossil claystone. The hemipelagic sediments of this subunit include dark greenish-gray claystone with nannofossils and nannofossil clayey mixed sediments and greenish-gray nannofossil ooze. Quartz is a minor component (10%–25%) in and below Core 133-823A-13H. Maximum thicknesses of turbidite beds increase down the core, whereas debris flows are rare and thin (Fig. 10).

Very thin beds of well-sorted, medium sand- to silt-sized bioclastic packstone (turbidites) are locally common. In Core 133-823A-11H, centimeter-thick packstone turbidites alternate with greenish-gray nannofossil clayey mixed sediments. The number of turbidites and their frequency increase toward the bottom of the subunit. Foraminifers commonly are pyritic and are minor components in the bioclastic packstone beds and burrow infills. The abundance and thickness of slumps clearly decrease downward within this subunit. However, the amount and thickness of the turbidites are as great as those in the lower part of Subunit IA. The base of Subunit IA was defined by the last thick turbiditic packstone above a color change to lighter greenish-gray hemipelagic sediments in Unit II, associated with a decrease in clay content.

**Unit II** (Cores 133-823B-13X-6 to -37X-6; depth, 120.7–352.75 mbsf; thickness, 232.05 m; age, late Pliocene)

Unit II consists of numerous beds of turbiditic packstone that are thinly interbedded with hemipelagic nannofossil ooze to chalk. Thicknesses of these turbidite interbeds change at the Unit I/Unit II boundary (Fig. 8). Although individual turbidite beds are relatively thin (typically <10–20 cm), the total proportion of turbidites is greater in Unit II than in all other units (Fig. 9). Clay contents gradually decrease down-

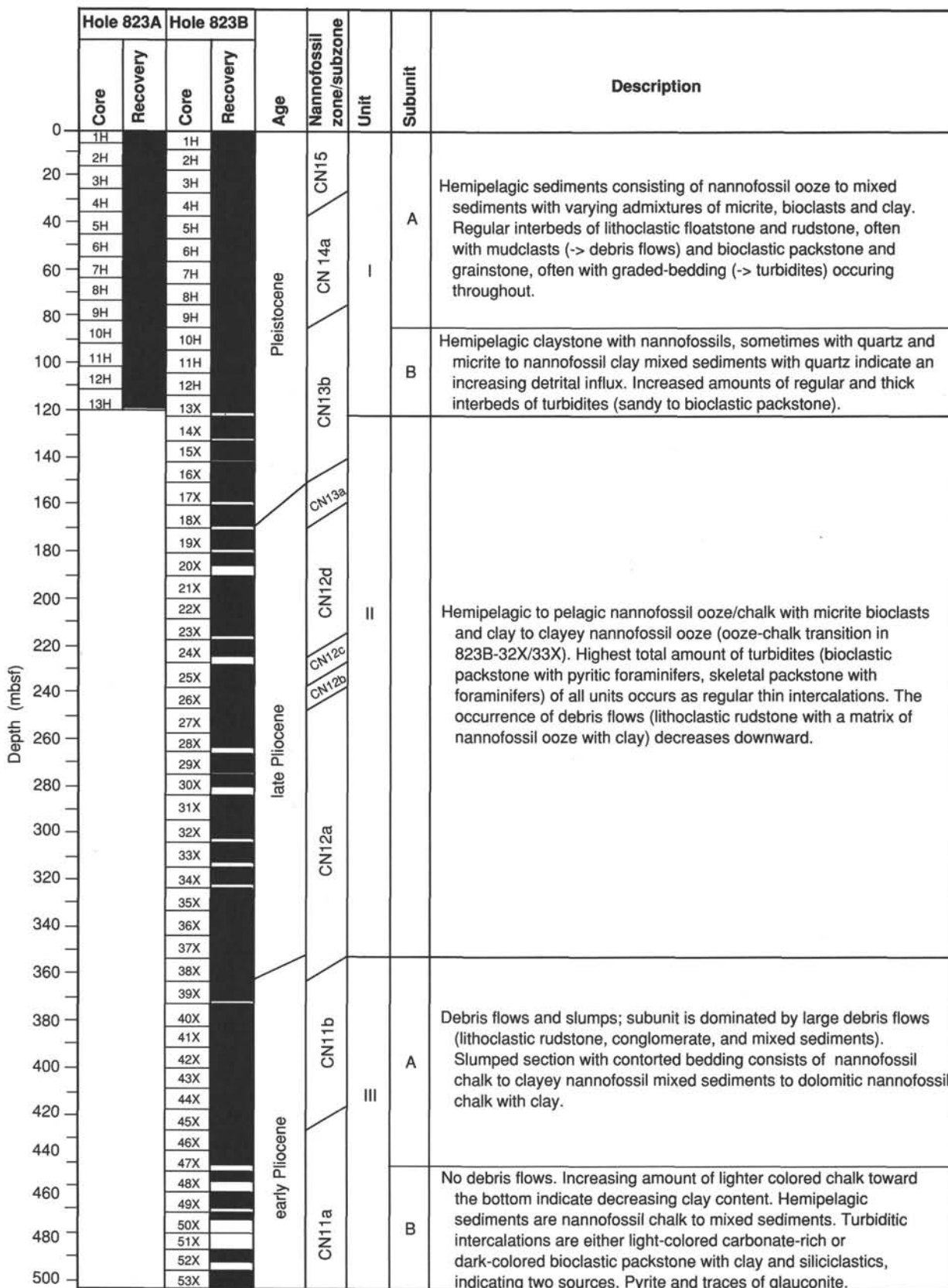


Figure 7. Chart showing division of seven lithologic units of Site 823 with respect to cores. Note excellent recovery throughout cored intervals.

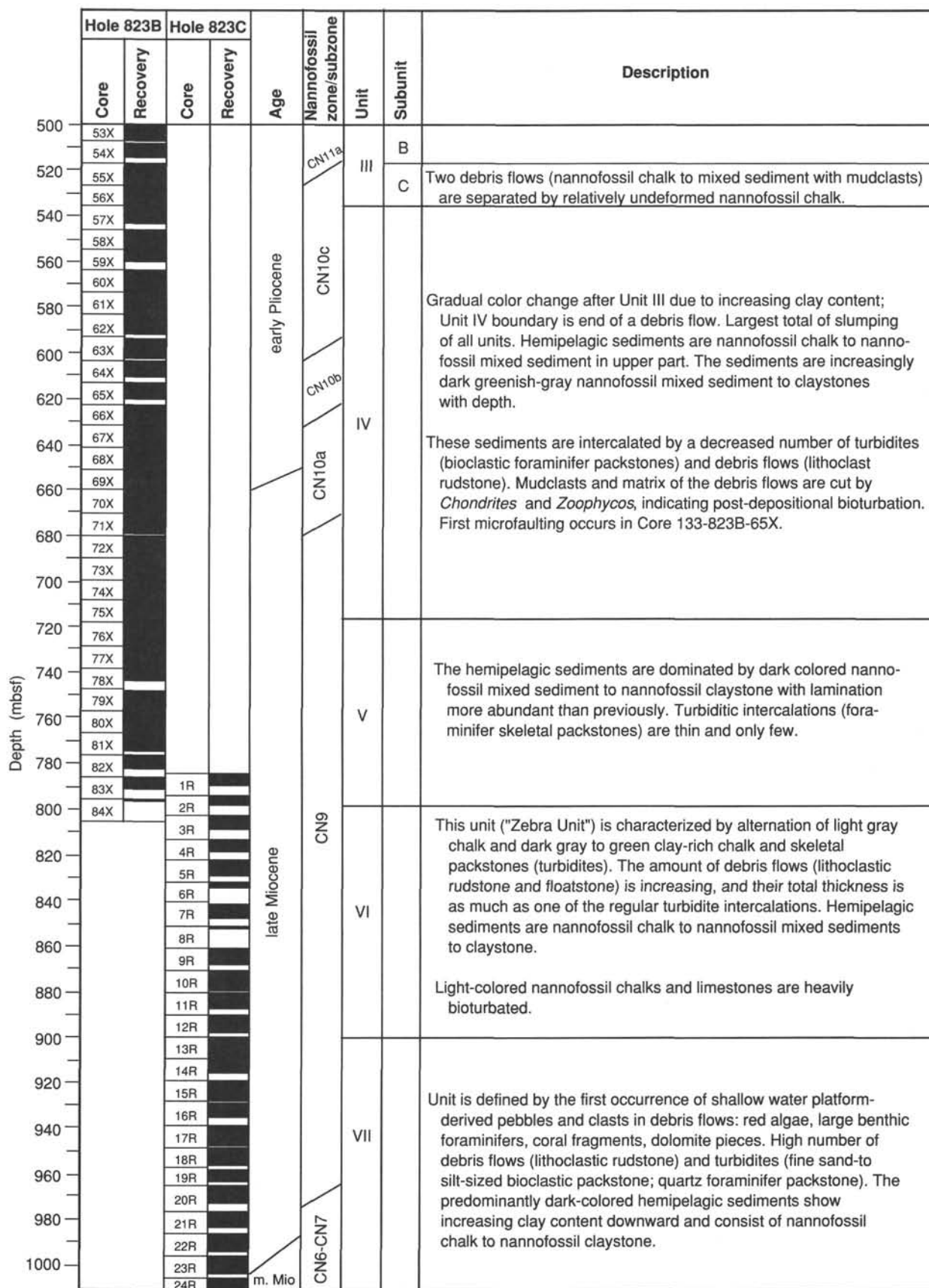


Figure 7 (continued).

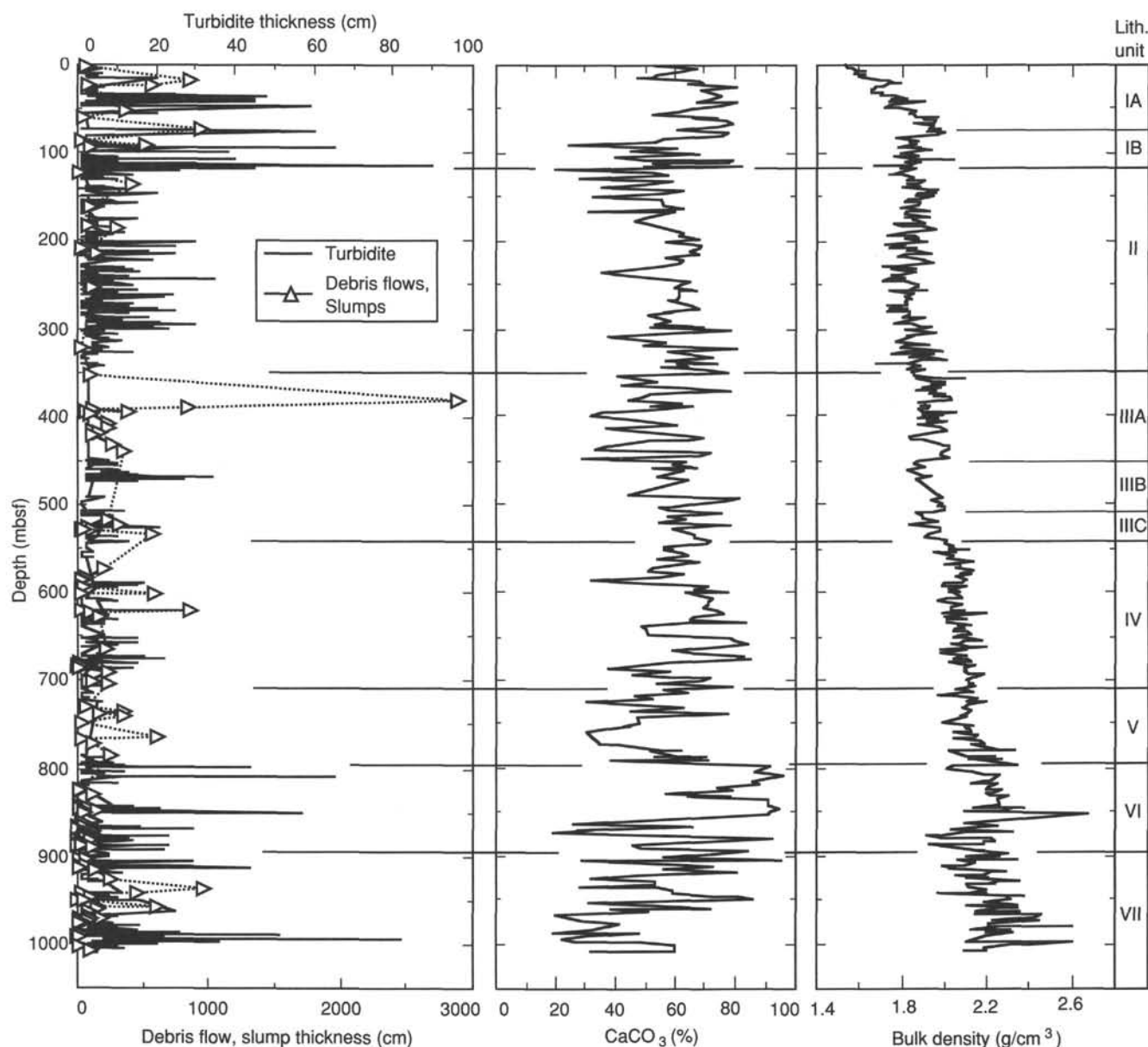


Figure 8. Distribution of thickness of sediment gravity-flow deposits (turbidites, debris flows, and slumps) combined for all three holes at Site 823 was one criterion used to define sedimentary units. These are compared to percentage of calcium carbonate (see "Inorganic" section, this chapter) and bulk density (see "Physical Properties" section, this chapter).

ward with a color change from greenish-gray to light gray. Unit II contains a few thick debris flows and slumps (Fig. 13).

The hemipelagic sediments are a relatively uniform light greenish-gray nanofossil ooze to chalk with variable amounts of clay, bioclasts, foraminifers, and micrite. These hemipelagic sediments are regularly intercalated with dark greenish-gray bioclastic packstones (turbidites). Intervals of gray to light gray clayey nanofossil ooze may contain micrite. Gray foraminifer nanofossil ooze has been intercalated with dark gray clayey nanofossil ooze with micrite in Cores 133-823B-31X and -32X. This is immediately above the ooze-to-chalk transition, which is gradational between Cores 133-823B-32X and -33X (305.3 mbsf). Gray nodules of dolomitic nanofossil chalk were recovered in Section 133-823B-32X-4 to -32X-6. The lowest 15 m of the unit (Cores 133-823B-36X and -37X) are highly bioturbated, light

greenish-gray nanofossil chalk and has the highest carbonate values of the unit (up to 77%  $\text{CaCO}_3$ ).

The thickness of the medium sand- to silt-sized turbiditic bioclastic packstone interbeds does not exceed 40 cm and averages approximately 10 cm. Turbidites are graded with sharp basal contacts and gradational tops. The composition of the turbidites is similar to that in Unit I and contains bioclasts, foraminifers, and siliciclastic grains that grade upward into silt-sized, clay-enriched mixed sediments that have been overlain by nanofossil ooze. Turbidites in Core 133-823B-35X have scoured bases. Pyritic grains and foraminifers filled with pyrite and minor siliciclastics are common. Debris-flow deposits (lithoclastic rudstone to floatstone) occur in Cores 133-823B-15X, -20X, and -22X. The mud clasts and matrix are nanofossil ooze with variable amounts of clay, having colors

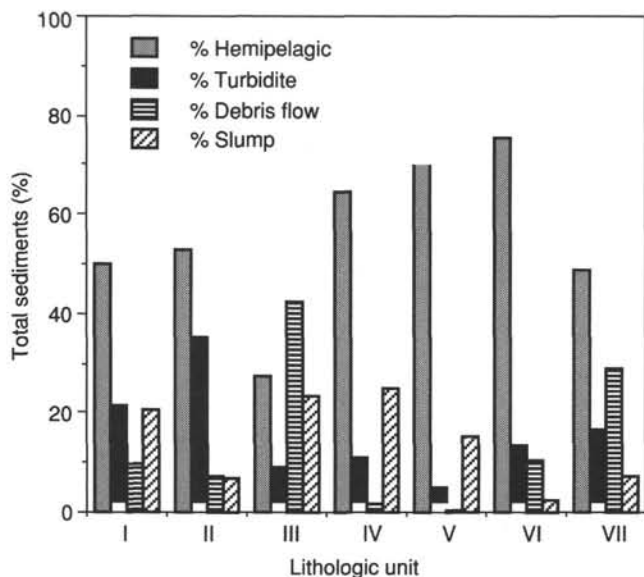


Figure 9. Percentage of redeposited sediments and hemipelagic sediments relative to thickness of total sediments in each lithologic unit at Site 823.

in different hues of gray. The thickness of debris-flow deposits and slumped intervals decreases with depth.

**Unit III (Cores 133-823B-37X-6, 135 cm, to -56X-CC; depth, 352.75–535.7 mbsf; thickness, 182.95 m; age, early Pliocene)**

Debris flows and slump deposits are most abundant in Unit III. Unit III is characterized by the downward increase in debris flows that contain chalky and mixed sediments in both clasts and matrix having different colors resulting from varying clay contents (Fig. 9). The top and bottom of this unit are marked by debris flows (Fig. 13). The top occurs in Section 133-823B-37X-6, where light gray nanofossil chalk of Unit II is underlain by a gray lithoclastic rudstone with clasts of laminated nanofossil chalk, including folded clasts that originated as slump folds (Fig. 14). The increased clay contents result in a lower carbonate content (Fig. 8). Our division into three subunits (IIIA through IIIC) is based on the occurrence of a less disturbed interval (IIIB) between the other two subunits, which are dominated by debris flows and slump deposits. Subunit IIIB also is lighter colored and is composed of carbonate-enriched chalks and mixed sediments. Turbidites occurring in Subunits IIIA and IIIC were not considered as separate beds, but are parts of slumped intervals having a high degree of soft-sediment deformation. However, Subunit IIIB contains numerous undisturbed turbidites (Figs. 8 and 15).

Large slumps and debris flows can be distinguished in the seismic profile as chaotic reflectors (see "Seismic Stratigraphy" section, this chapter) and are characterized in physical-property data by higher bulk density and lower water content and porosity (see "Physical Properties" section, this chapter).

**Subunit IIIA (Cores 133-823B-37X-6 to -46X-CC; depth, 352–440.3 mbsf; thickness, 88.3 m; age, early Pliocene)**

Debris flows comprising Subunit IIIA consist of gray lithoclastic rudstone with clasts and matrix of similar composition (mixed sediments). The lithoclastic floatstone intervals have been interpreted as matrix-supported debris flows with pebble-sized clasts of nanofossil to clayey nanofossil chalk and a matrix of nanofossil chalk with foraminifers (Fig. 14). Lithoclastic rudstones having a clast-supported fabric with clasts of nanofossil mixed sediments occur in Sections 133-

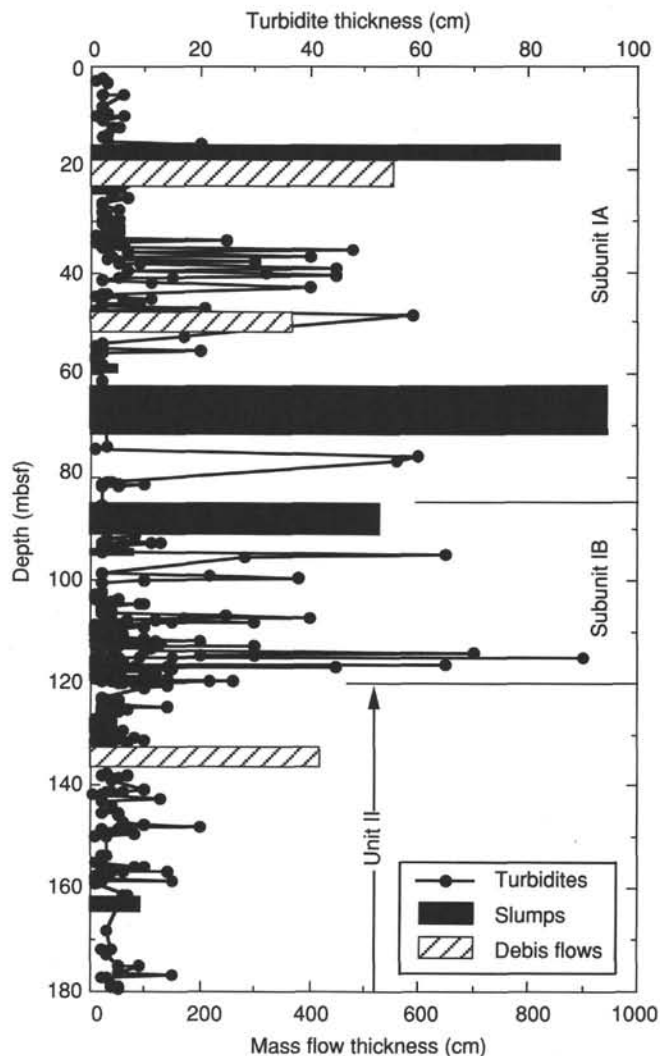


Figure 10. Distribution of sediment gravity flows (turbidites, slumps, and debris flows) in lithologic Unit I and upper part of Unit II of Hole 823A. Frequency and thickness of these deposits were used to define Subunits IA and IB as well as the Unit I/Unit II contact.

823B-42X-3 and -42X-5. Slumped intervals are common throughout this unit and typically occur below debris-flow deposits. The slumped intervals are folded (soft-sediment deformation) and consist of gray bioturbated to laminated nanofossil chalk with foraminifers and bioclasts, light to dark gray nanofossil mixed sediments, and dark gray clayey nanofossil chalk with quartz. Pyrite is a minor component in dark greenish-gray sandstones/siltstones with bioclasts and calcite (Core 133-823B-46X). Most of the sediments in this subunit show soft-sediment deformation features, such as contorted bedding and folding. A foraminifer bioclastic packstone is intensively slump-folded in Core 133-823B-42X, implying that the coarser-grained, possibly turbiditic bed was deposited and was later folded as the slump moved downslope. The slumping involved mass movement of a thick interval of bedded sediments. Bioturbation is locally very intense (e.g., Core 133-823B-44X). In several debris-flow deposits, bioturbation crosscuts and post-dates the deposition. This is shown by *Chondrites* (?) burrows that cut through mud clasts as well as the matrix (Fig. 16). This observation also suggests that these mud clasts, in most cases, were still

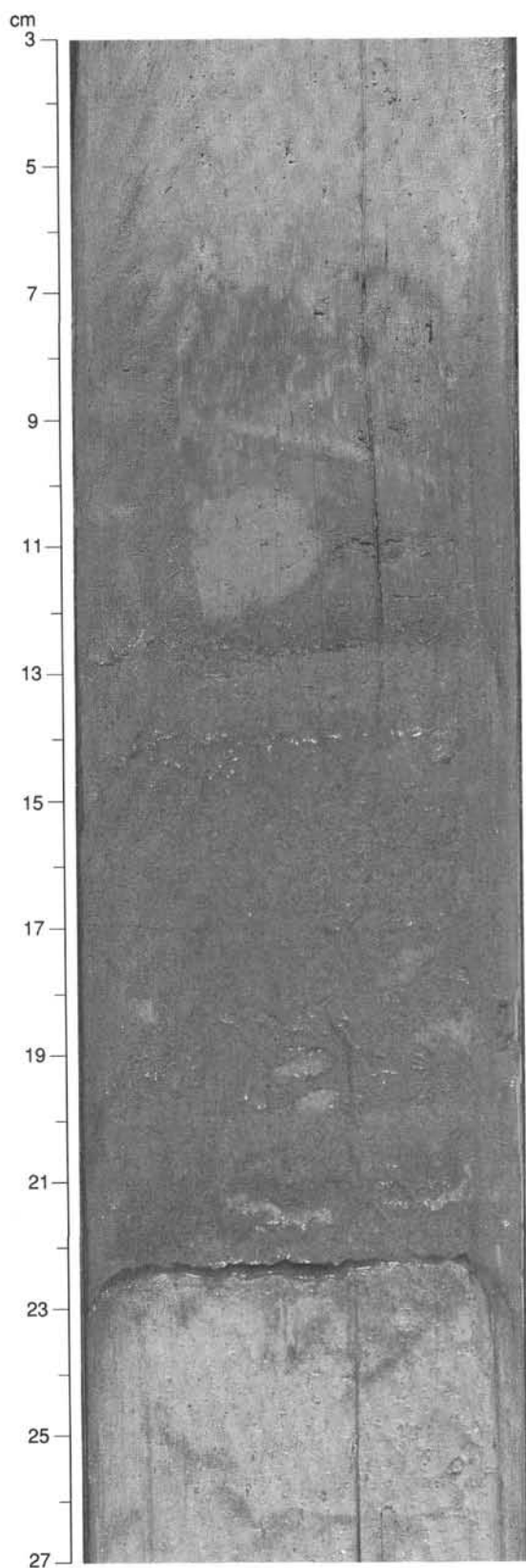


Figure 11. Gray bioclastic packstone (turbidite) with a sharp bottom and graded bedding in interval 133-823A-5H-6, 3–27 cm, Subunit IA. Note the darker-colored ooze at the transitional interval on top of the turbidite, both of which are bioturbated.

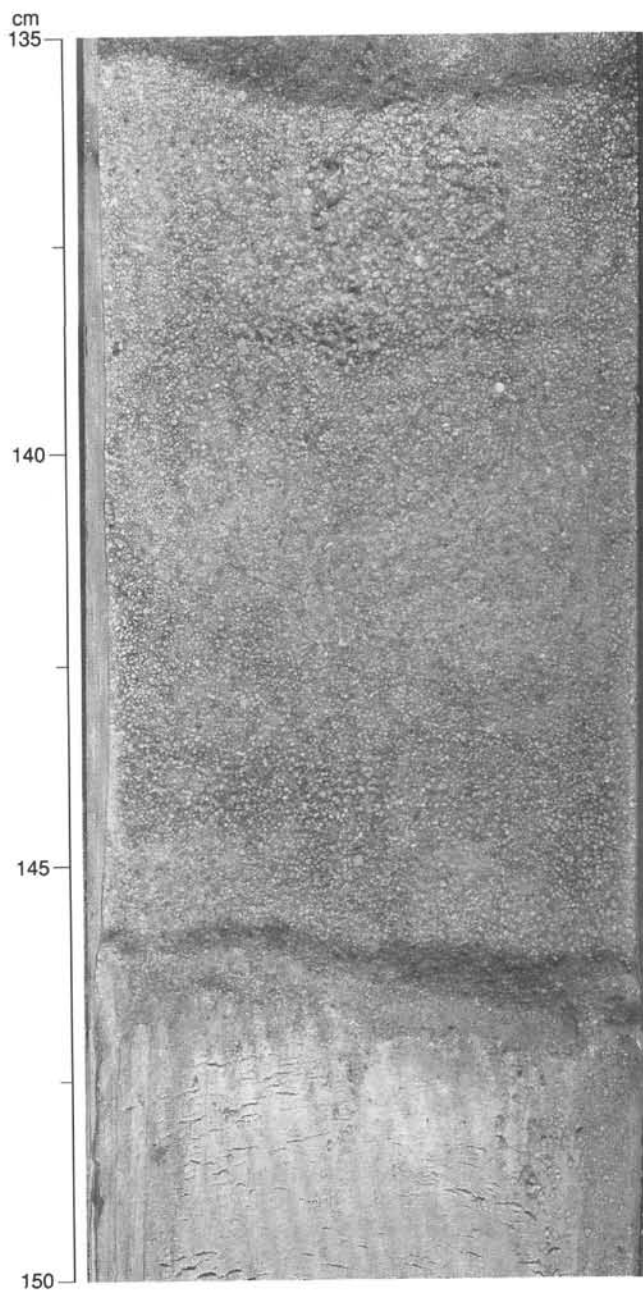


Figure 12. Light gray to pale yellow turbidite layer ( $T_A$ ) without siliciclastics and enriched in bioclastics in interval 133-823A-5H-3, 135–150 cm, Subunit IA. More than one event might be amalgamated, as indicated by two superimposed coarser-grained intervals.

soft and able to be burrowed, in addition to being easily abraded and deformed, as indicated by their well-rounded shapes and the presence of folded clasts. The folded clasts indicate that the debris flow was initiated as a slump and evolved into a debris flow having continued downslope movement.

*Subunit IIIB (Cores 133-823B-47X to -54X-CC; depth, 440.3–516.8 mbsf; thickness, 76.5 m; age, early Pliocene)*

Debris flows are absent in this subunit, which consists of interbedded hemipelagic sediments and thin turbidites. Lighter-colored sediments toward the bottom indicate decreasing clay contents. The top of the subunit consists of gray nanno-

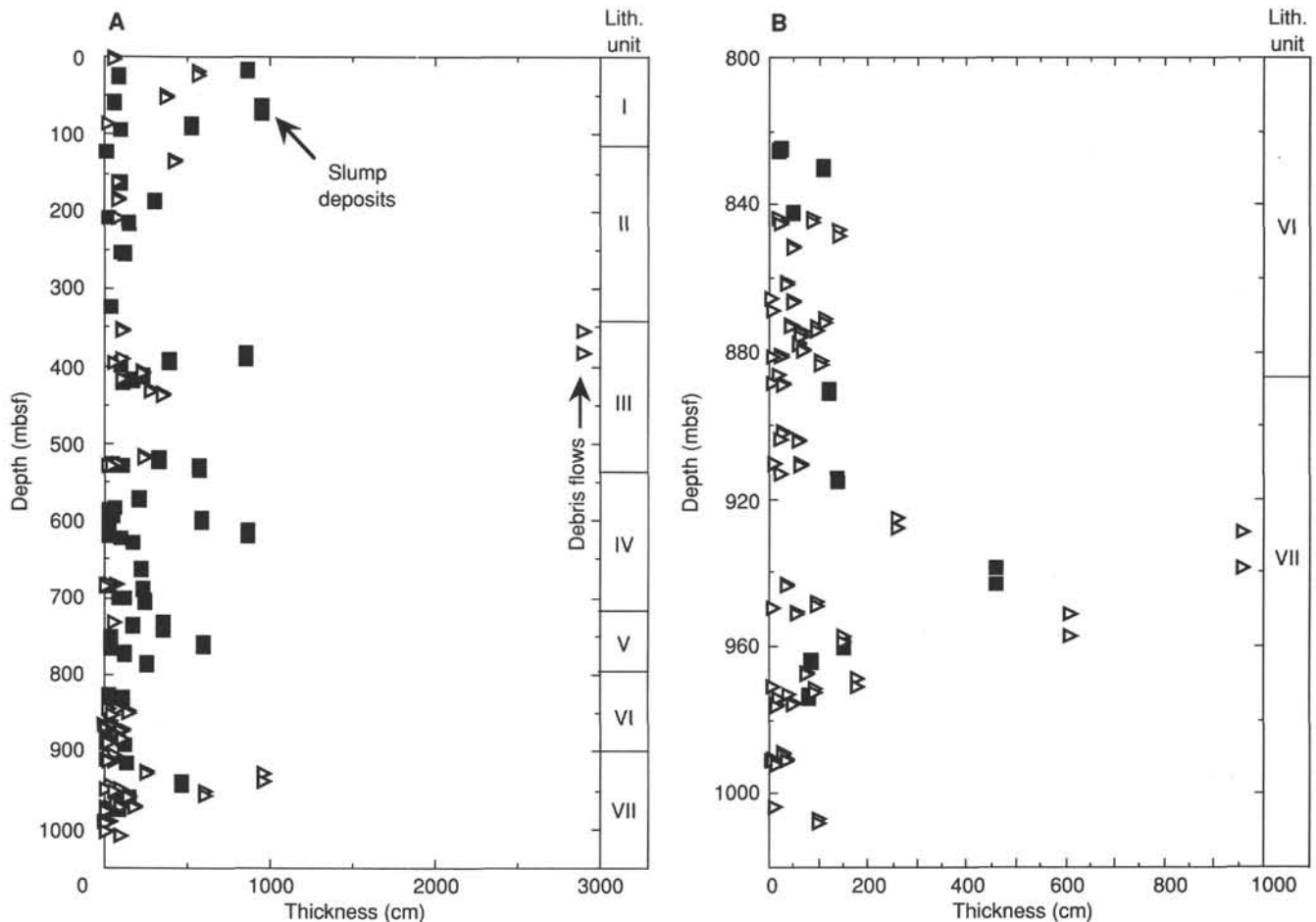


Figure 13. A. Plot of all slumped intervals and debris-flow deposits of Site 823 with their basal depths. Thick debris flows occur in Units I, III, and VII. B. Debris flows and slumps of two lowermost Units VI and VII, which contain 50% of all described debris flows.

fossil chalk to mixed sediments with bioclasts and micrite, intercalated with a dark greenish-gray claystone. Glauconite appears as a trace mineral. A gradual downward transition occurs into lighter greenish-gray nanofossil chalk to mixed sediments with foraminifers and bioclasts. These hemipelagic sediments have been interbedded with turbidites that consist of dark greenish-gray, laminated, medium- to fine-grained, very thinly bedded (mostly <10 cm) bioclastic foraminifer packstones with clay and quartz (turbidites; Fig. 15). An unusual bed of light greenish-gray bioclastic packstone with dolomite rhombs in Core 133-823B-50X most likely is a turbidite derived from a carbonate source area.

**Subunit IIIC (Cores 133-823B-55X to -56X-CC; depth, 516.8–535.7 mbsf thickness, 18.9 m; age, early Pliocene)**

This interval is highly deformed, suggesting that the entire unit represents slumps and debris flows. The deformed sediments consist of greenish-gray to dark greenish-gray bioturbated or finely laminated nanofossil chalk, laminated nanofossil chalk with foraminifers and bioclasts, and mixed sediments with micrite. The upper debris flow (516.8–522.4 mbsf) has contorted lamination and mud clasts of from a few millimeters up to 6 cm in size, whereas the lower debris flow (526.4–531.4 mbsf) has horizons of isolated, well-rounded, discoidal chalk pebbles. The light greenish-gray nanofossil chalk between the two debris flows is strongly bioturbated.

Deformation of soft sediments (slumping) occurs in Core 133-823B-56X toward the bottom of the unit.

**Unit IV (Cores 133-823B-57X to -75X-5, 40 cm; depth, 535.7–715 mbsf [Hole 823B]; thickness, 179.3 m; age, early Pliocene to late Miocene)**

Unit IV consists of hemipelagic and pelagic sediments with abundant slumped intervals and lesser turbidites and debris-flow deposits. The upper boundary of this unit is at the base of the overlying debris flow. The sediments of Unit IV exhibit a large-scale cyclic variation between hemipelagic clay-rich sediments and dominant pelagic chalks. Light greenish-gray to greenish-gray, finely laminated nanofossil chalk with foraminifers or clay alternates with gray bioturbated nanofossil chalk and dark gray clayey nanofossil mixed sediments with foraminifers and bioclasts. Intervals having gray to dark grayish-green, clay and quartz-enriched nanofossil chalk, mixed sediments, and claystone occur in Cores 133-823B-58X to -63X and Cores 133-823B-67X to -68X. Pyrite occurs in burrows or has been dispersed in these sediments (e.g., in Core 133-823B-68X) and is generally restricted to the dark clay-rich sediments.

Bioturbated sediments alternate with planar-laminated intervals. In Core 133-823B-58X, the lamination locally exhibits low-angle wedges. In the same core, variations in the amount of foraminifers, bioclasts, and clay give the sediment a rhythmic

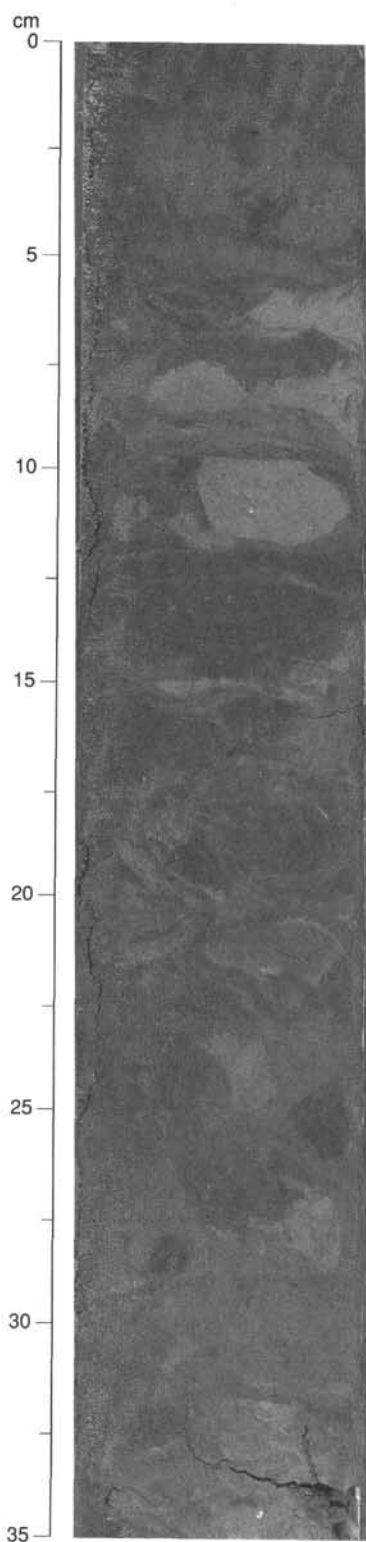


Figure 14. Lithoclastic rudstone interval from upper boundary of Unit III. Darker-colored pebble-sized nanofossil to clayey nanofossil chalk clasts are suspended in this debris flow in a matrix of nanofossil chalk with foraminifers (interval 133-823B-37X-7, 0–35 cm).

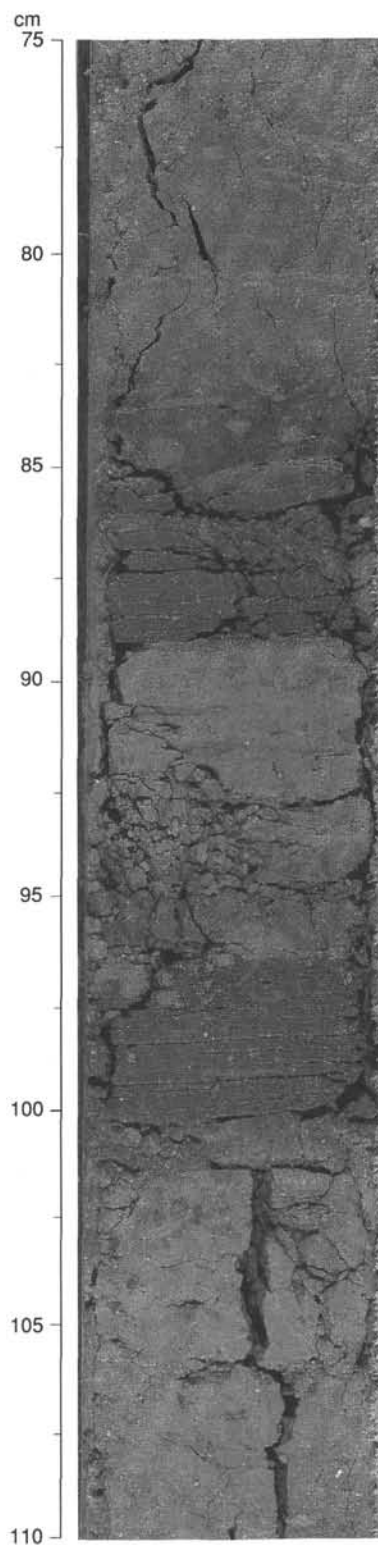


Figure 15. Medium-grained, dark-gray, bioclastic packstones (turbidite) with a thin graded base ( $T_a$ ) overlain by a laminated ( $T_b$ ) interval in Subunit IIIB, interval 133-823B-48X-4, 75–110 cm. Note bioturbation and alteration with light-colored nanofossil chalk.

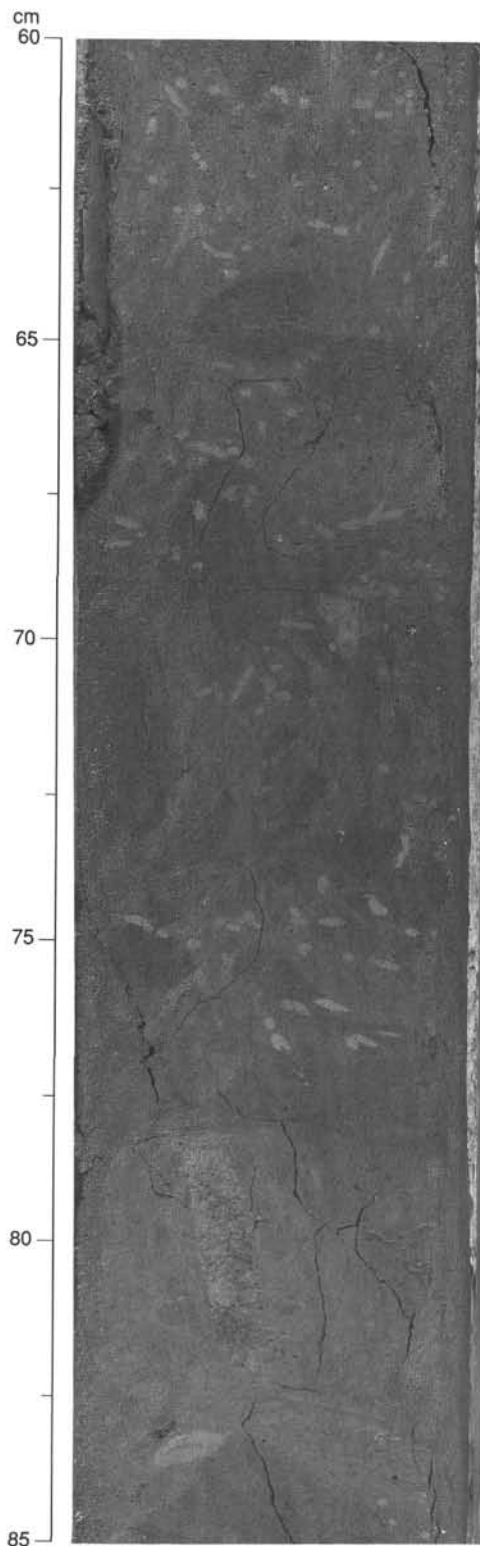


Figure 16. Burrows cut across both mud clasts and matrix of a debris flow, indicating post-depositional bioturbation (interval 133-823B-44X-4, 60–85 cm).

mic color banding on a 10-cm scale. Strong lamination occurs in the silty, fine-grained nannofossil chalk to mixed sediment in Core 133-823B-73X.

Unit IV has the greatest abundance of slumped intervals at Site 823 (Fig. 9). Slumping may have been associated with large debris flows. Bioturbation (*Zoophycos* and *Chondrites*) in Unit III in a lithoclastic rudstone crosscuts clasts and matrix, post-dating the deposition of the debris flow in Core 133-823B-65X. Slumped intervals having contorted or overturned beds are more than 2 m thick in Cores 133-823B-63X, -65X, -66X, -73X, and -74X.

Thickness of the turbidite beds does not exceed 20 cm. In Cores 133-823B-59X and -71X, quartz is a minor component in the dark greenish-gray to olive foraminifer packstones (turbidites). Quartz grains are more abundant at the base of upward-fining sequences.

**Unit V (Cores 133-823B-75X-5, 40 cm, to -83X-CC [Hole 823B] and Cores 133-823C-1R to -2R-3, 110 cm; depth, 715–795.7 mbsf [Hole 823B] and 784.0–797.7 mbsf [Hole 823C]; thickness, 80.7 m [Hole 823B] and 13.7 m [Hole 823C]; age, early Pliocene to late Miocene)**

Unit V is dominated by relatively clay-rich hemipelagic sediments and contains the lowest number of debris flows and turbidites at Site 823 (Fig. 9). Slumps occur in Cores 133-823B-77X, -78X, and -80X. The top of the unit is defined by a sharp downward change from light greenish-gray nannofossil chalk to a dark greenish-gray structureless and homogeneous nannofossil siliciclastic claystone in Core 133-823B-76X. This transition also was seen in a decrease of carbonate contents, which remain below 60% in Unit IV with a few exceptions (see "Organic Geochemistry" section, this chapter). Below a 1.5-m interval of greenish-gray nannofossil chalk in Section 133-823B-75X-6, the clay content increases, as reflected by the abundance of claystones. Fine laminations generally have been restricted to the lighter-colored nannofossil chalk and mixed sediments, whereas the dark gray claystones are structureless and often contain dispersed iron sulfide nodules. The bottom of Unit V has been defined by the occurrence of a nearly white nannofossil chalk in Unit VI, indicating a change in the amount of fine terrigenous sediments brought into the vicinity of Site 823.

**Unit VI (Cores 133-823C-2R-3, 110 cm, to -12R-CC and Core 133-823B-84X [Hole 823B]; depth, 797.7–899.1 mbsf [Hole 823C] and 795.7–796.9 mbsf [Hole 823B]; thickness, 101.4 m [Hole 823C] and 1.2 m [Hole 823B]; age, late Miocene)**

Unit VI is a distinct unit characterized by alternating dark- and light-colored beds and that has been informally termed the "Zebra Unit." The upper boundary of Unit VI was placed at the top of a white nannofossil chalk with micrite, marking the onset of dominantly pelagic background sedimentation. Dark greenish-gray laminated packstones (turbidites) have been regularly interbedded with light-colored pelagic sediments, such as white nannofossil chalk to light greenish-gray highly bioturbated nannofossil chalk with clay. The sediment gravity-flow deposits are common in this unit, while single turbidites are up to up to 60 cm thick (Figs. 8 and 9).

Intense bioturbation commonly occurs in light to dark greenish-gray, relatively pure nannofossil chalk with foraminifers. This lithology may also be laminated and lack bioturbation. Another interval of white nannofossil chalk with dolomite and clay occurs in Section 133-823C-2R-4, 110–150 cm.

Microfaults in chalky limestone are common in the unit. They are most prominent in laminated nannofossil limestones and produce offsets in lamination in more competent chalk layers. At least two different stress fields may have existed

(Figs. 17, 18, and 19). Mud clasts in a debris-flow deposit also show offsets, indicating syn-sedimentary movements (in Section 133-823C-5R-2). All of these features suggest brittle deformation. Faulting does not affect the entire section, but seems to affect discrete intervals, which suggests either deformation in more competent horizons and/or displacements during specific time intervals or that the faults were spaced so that we would encounter them in the borehole at only a few intervals. Slickensides with concentrations of chlorite were found along small fault planes.

Graded packstones (turbidites) have sharp lower boundaries and gradational tops and contain glauconite as a minor constituent. The turbidites are coarser-grained, with well-developed Bouma sequences. Locally, they have erosional bases (scours) that grade into the lower part ( $T_a$ ), fine planar laminations ( $T_b$ ), and grade into cross-laminated ( $T_c$ ) intervals. Several amalgamated turbiditic events were recognized in the well-lithified grainstones to packstones. The fine silty to muddy top of the turbidites ( $T_d$  and  $T_e$ ) consisting of clayey nanofossil chalk typically are heavily bioturbated (Fig. 20). The darker interbeds are more clay-rich and often display wispy laminations.

A debris-flow deposit contains contorted mud clasts composed of white nanofossil limestone and dark greenish-gray nanofossil clayey chalk and is overlain by several pebbly turbidites (Fig. 21). The clasts must have been deformed during their transport within the gravity flow. They represent the pelagic sediment that eroded because of the debris flow. Several turbidites (foraminifer grainstone with siliciclastics) having an accumulation of fairly well-rounded nanofossil chalk clasts at the base occur in Section 133-823C-7R-6 (Fig. 22). Thick slumped intervals occur in Cores 133-823C-1R, -5R, and -12R; debris flows thicker than 1 m occur in Cores 133-823C-7R, -10R, and -11R. These clasts are up to boulder size and consist of nanofossil chalk. These large clasts float in a silty to very fine sandy calcareous mudstone matrix.

**Unit VII (Cores 133-823C-12R-CC to -24R; depth, 899.1–1011 mbsf; thickness, 111.9 m; age, late Miocene to middle Miocene)**

The top of Unit VII is defined by the first occurrence of clasts that were derived from shallow-water carbonate platform sources in debris flows and in poorly sorted bioclastic packstones with foraminifers (turbidites; Fig. 23). Besides abundant locally pyritized planktonic foraminifers, well-rounded intraclasts of nanofossil chalk with foraminifers occur in the gravity-flow deposits. Shallow-water particles include fragments of columnar corallinaceans, large benthic foraminifers, and thick mollusk shells. A gradual increase downward in clay-rich intervals and the disappearance of the light greenish-gray nanofossil chalks occur in Cores 133-823C-13R to -17R. The darker sediments are gray to dark gray clayey nanofossil mixed sediments to clayey mixed sediments and have been interbedded with lighter-colored nanofossil chalks. In Core 133-823C-18R, sediments are dominated by gray to dark gray clayey foraminifer mixed sediments, with local occurrences of claystone. A higher abundance of terrigenous and shallow water-derived sediments occurs between Cores 133-823C-17R and -24R. These hemipelagic sediments are clayey foraminifer mixed sediments to claystones with siliciclastics and nanofossils.

Turbidites (skeletal packstones) and debris flows (lithoclastic rudstones) are common and thick (Figs. 8 and 9). A bioclastic packstone (turbidite) in interval 133-823C-14R-3, 0–20 cm, has a grain-size range from medium sand to silt, shows grading at the base ( $T_a$ ), followed by planar lamination ( $T_b$ ) and low-angle cross lamination ( $T_c$ ), overlain by an increasingly bioturbated top ( $T_d$ ; Fig. 24). The bases of some

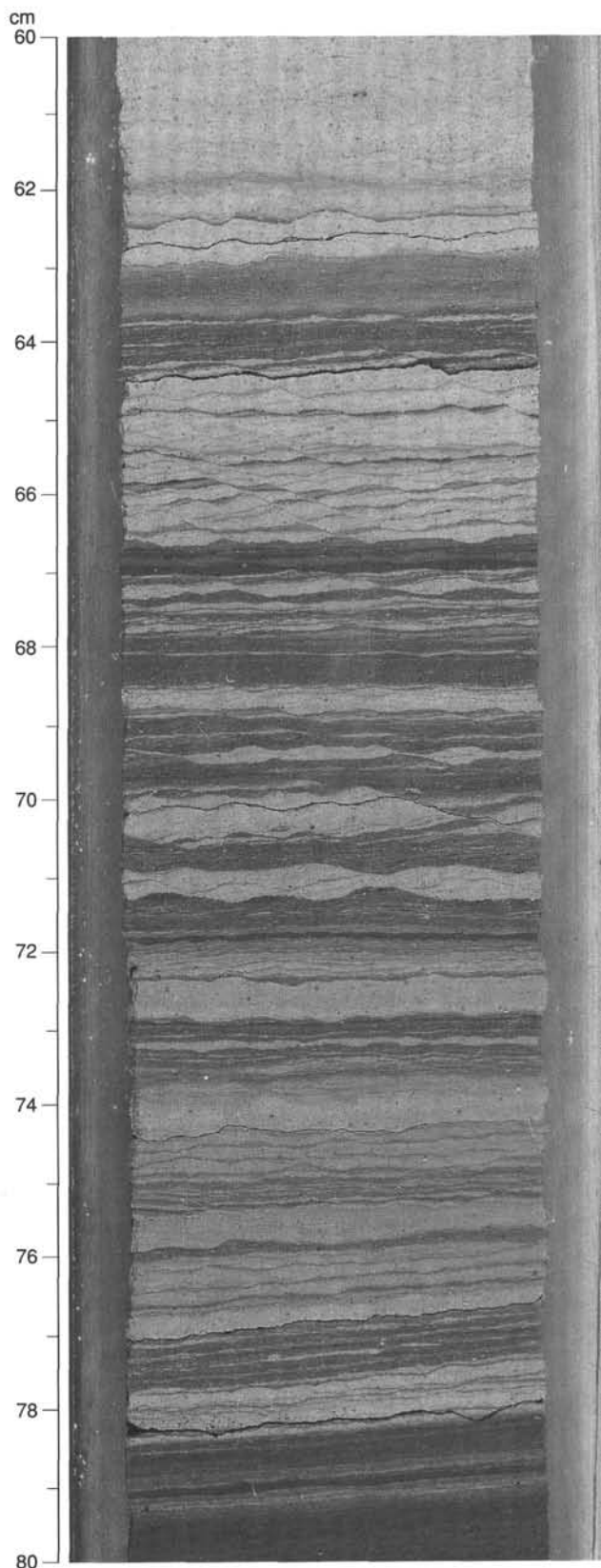


Figure 17. Microfaults that cut a finely laminated nanofossil chalk to produce "wavy" lamination in Unit VI, interval 133-823C-11R-4, 60–80 cm.

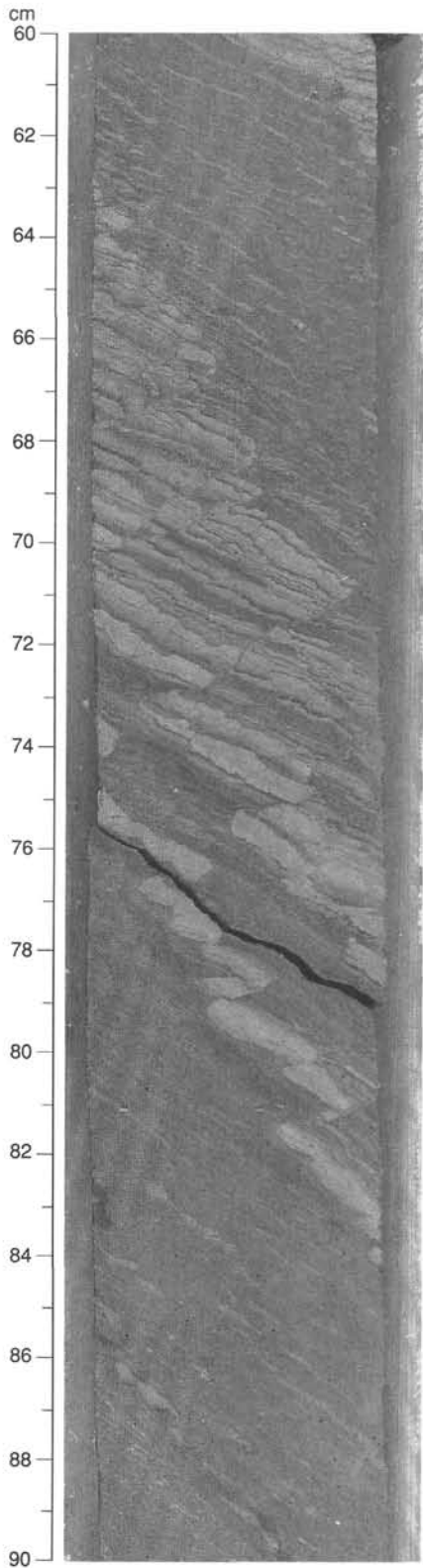


Figure 18. Microfaults that produce an offset of more competent calcareous layers within a slumped sequence may result from axial planar cleavage of large slump fold in Unit VI, interval 133-823C-5R-3, 60–90 cm.

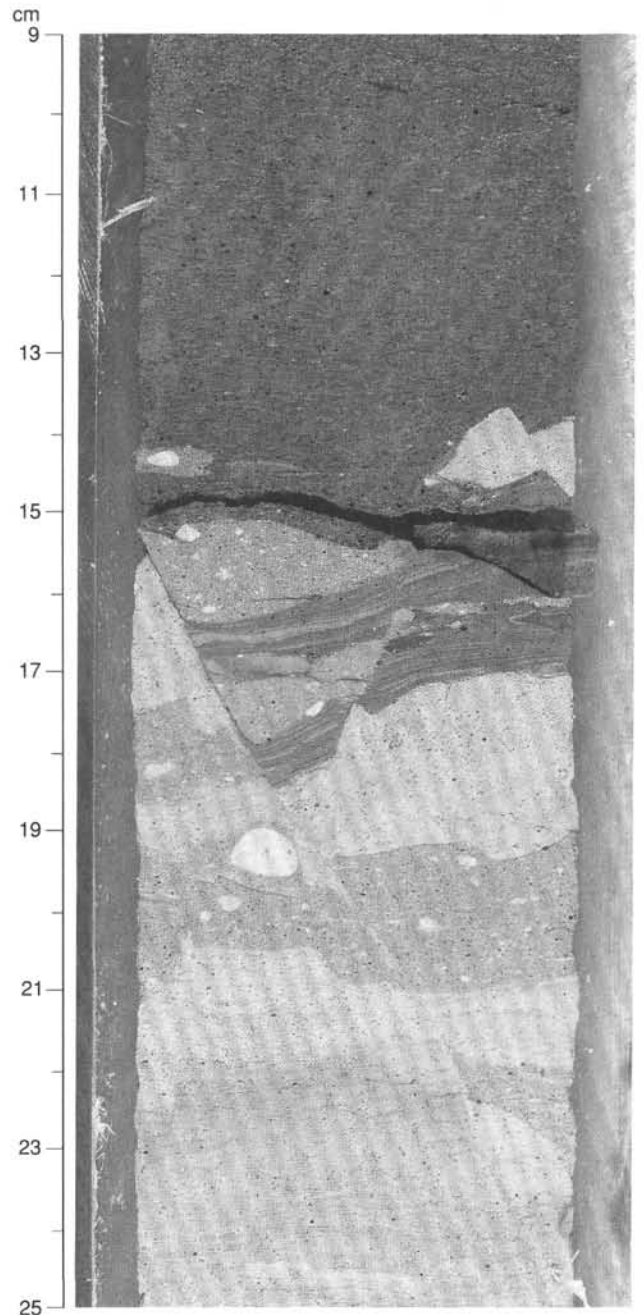


Figure 19. Two microfault systems caused by two stress fields applied during two deformational events, Unit VI, interval 133-823C-3R-CC, 9–25 cm.

of these turbidites have been enriched in quartz grains (Fig. 25). Rudstones contain angular fragments of corals, coralline algae, and other neritic carbonate debris that was seen in intervals 133-823C-13R-1, 93–96 cm; -17R-4, 33–70 cm; -18R-1, 85 cm; -18R-2, 94–105 cm; -19R-5, 50 cm; -20R-1, 65–75 cm (with branching coral); -20R-3 to -20R-5; and -22R-4, 0–35 cm. Core 133-823-20R has a high concentration of debris-flow deposits with neritic carbonate components. In Cores 133-823-21R and -22R, we recovered a high number of more distal turbidites with Bouma intervals  $T_c$  and  $T_d$ . The planar-laminated cycle  $T_b$  is represented in only a few sandy mixed sediments with foraminifers and quartz. Gravity flows containing carbonate components derived

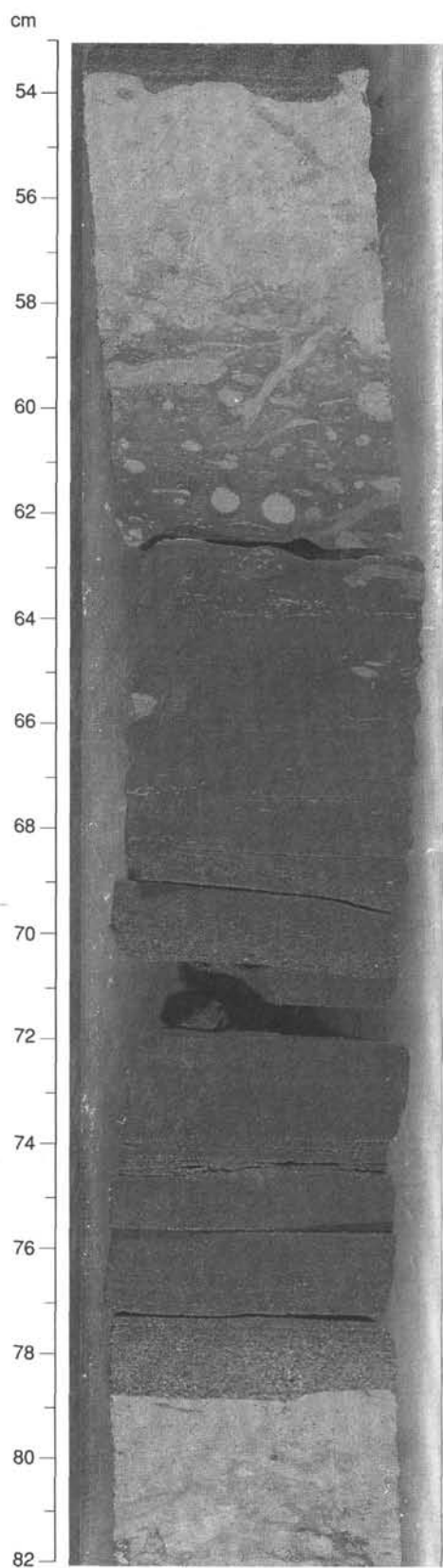


Figure 20. Turbidites with coarse-grained grading base ( $T_a$ ), planar lamination ( $T_b$ ), and cross lamination ( $T_c$ ). At least two turbiditic events are evidenced by coarse-grained layers. Muddy to silty top ( $T_d$ ) is heavily bioturbated with burrows filled with lighter-colored nannofossil chalk. Overlying turbidite shows scouring at the base, Unit VI, interval 133-823C-2R-1, 53–82 cm.

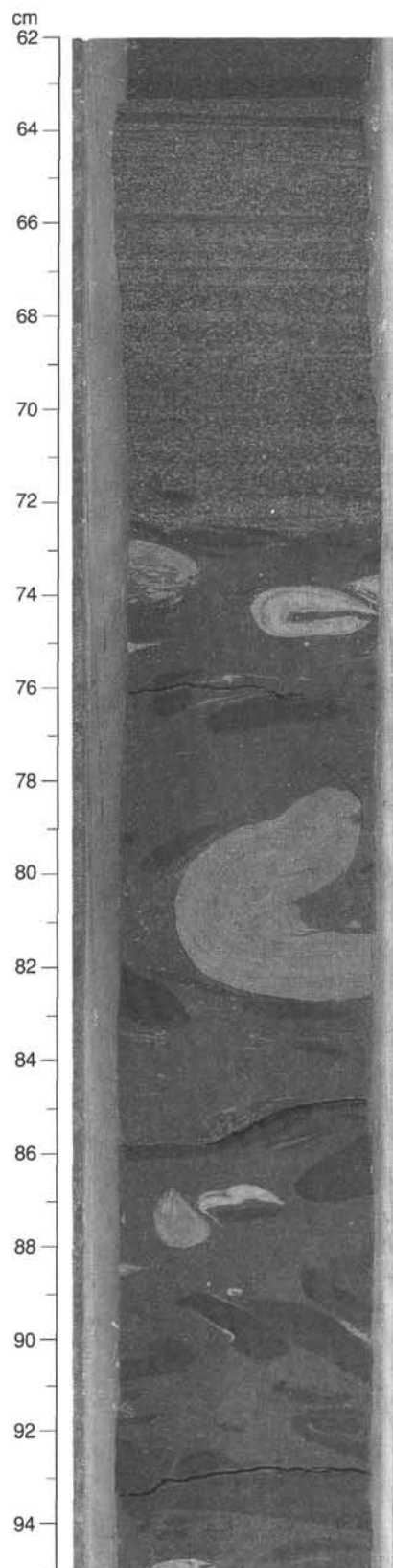


Figure 21. Debris flow (matrix is silty to fine sandy packstone) with contorted clasts of white nannofossil limestone or dark greenish-gray nannofossil clayey chalk from Unit VI, interval 133-823C-7R-4, 62–95 cm. Top is cut by turbidites ( $T_a$ ) having well-developed planar laminations ( $T_b$ ).

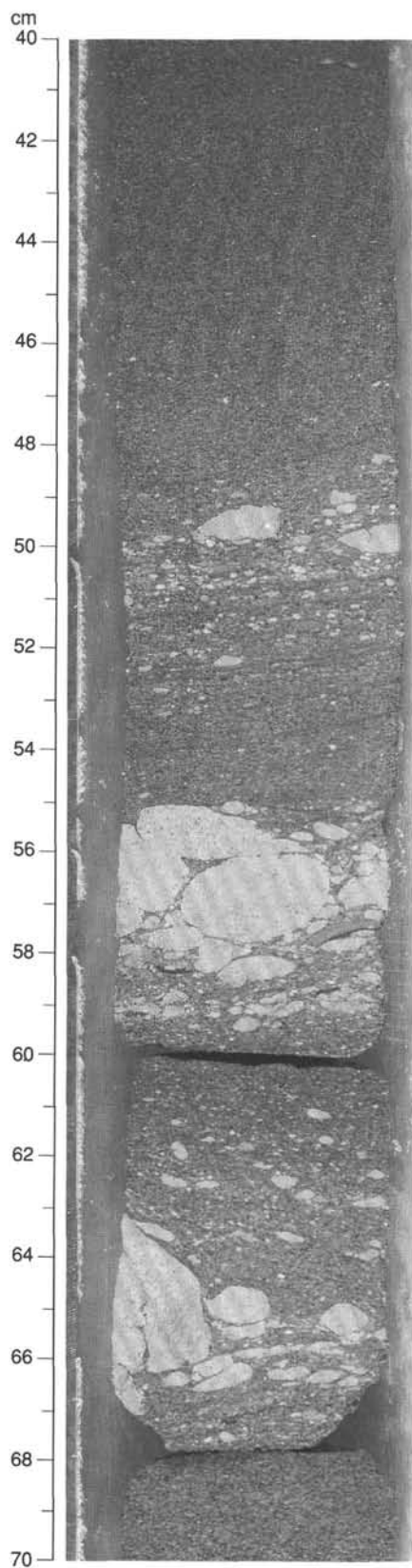


Figure 22. A micritic foraminifer grainstone to rudstone with siliciclastic sand that contains rounded gravel-sized clasts of limestone at the base, from Unit VI, interval 133-823C-7R-6, 40–70 cm. Several graded intervals having conglomeratic bases indicate amalgamation of several turbidites.

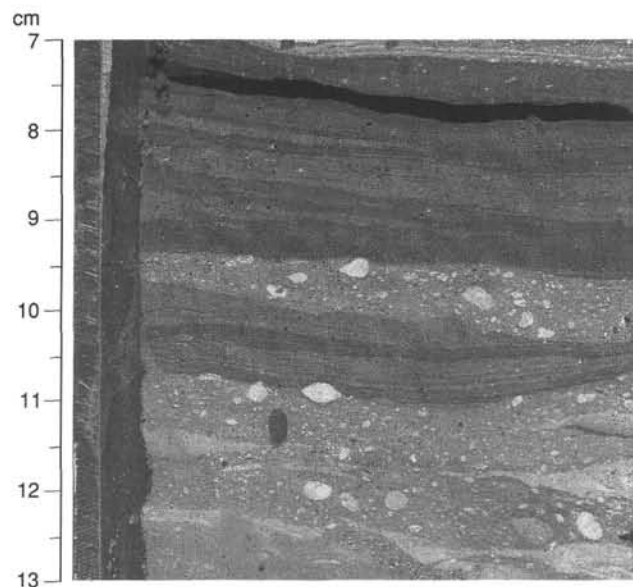


Figure 23. Skeletal packstone with large benthic foraminifers, poorly sorted, at top of Unit VII, Section 133-823C-12R-CC at 10 cm.

from neritic sources are present mainly in Core 133-823C-20R. The abundance of gravity-flow deposits that consist of light-gray, poorly sorted, pebbly sandy wackestone with pebbles of shelf-derived(?) dolomitic nodules and randomly dispersed benthic foraminifers increases downward. In Section 133-823C-15R-2, 130–134 cm, a *Zoophycos* trace fossil is offset by a microfault, indicating that faulting followed deposition and bioturbation (Fig. 26).

#### Age Distribution of Gravity-Flow Deposits

The biostratigraphic age control for the sediments of Site 823 is good. Linear interpolation between the time markers assumes a relatively constant sedimentation rate (see “Biostratigraphy” section, this chapter). This suggests a regular influx of gravity-flow deposits. The rare occurrence of reworked microfossils, the absence of major erosive features, and the high frequency of thin (<10 cm) turbidites support this assumption. However, mudstone clasts contained in debris flows suggest erosion of older material farther up the slope. By subtracting the thickness of the redeposited sediments within the depth intervals from 0 to 350 mbsf (Units I and II; 0–3.5 Ma; total of 108.1 m of sediment gravity flows) and 354 to 762 mbsf (Units III to V; 3.5–5.9 Ma; total of 133 m of sediment gravity flows), we estimated hemipelagic sedimentation rates of 6.9 and 11.4 cm/k.y., respectively. These calculations indicate an increased rate of hemipelagic sedimentation between 3.5 and 5.9 Ma, comparable to overall sedimentation rates (see “Sedimentation Rates” section, this volume). These rates are very high for a purely pelagic environment and suggest a high, constant influx of fine sediments, mainly terrigenous and fine carbonate periplatform clays. The interval between approximately 680 and 970 mbsf lacks age datums, but the interval between approximately 972 and 1011 mbsf has relatively low sedimentation rates (1 cm/k.y.).

Linear interpolation of the thickness of individual sediment gravity-flows vs. known ages allows one to estimate ages of the intervening sediments, particularly the sediment gravity-flow deposits (Fig. 27). Thick turbidites and debris flows occurred between 0 and 1.25 Ma (Unit I), with larger debris flows and slumps occurring at about 0.025, 0.32, 0.65, 0.9, and 1.05 Ma. Between 1.25 and 3.5 Ma (Unit II),

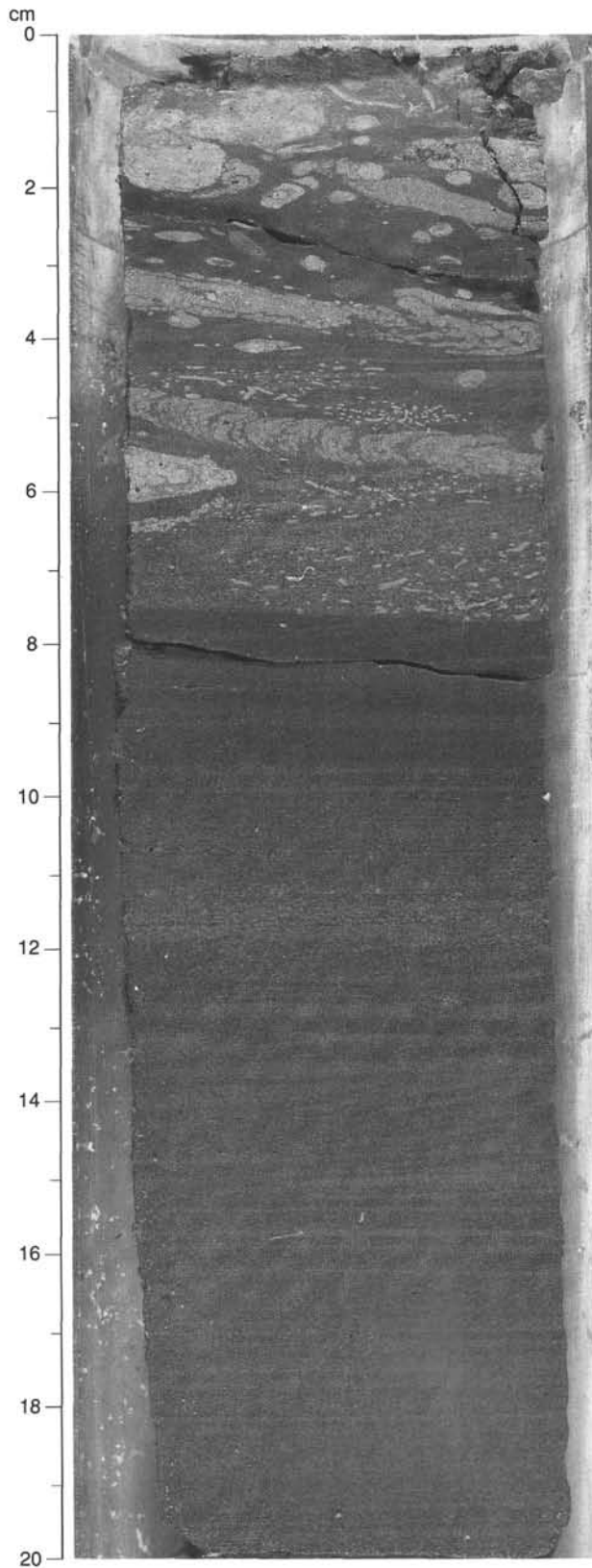


Figure 24. A bioclastic packstone (turbidite) in interval 133-823C-14R-3, 0–20 cm ranges in grain size from medium sand to silt, shows grading at the base ( $T_a$ ) that is followed by planar lamination ( $T_b$ ) and low-angle cross lamination ( $T_c$ ), and has an increasingly bioturbated top ( $T_d$ ).

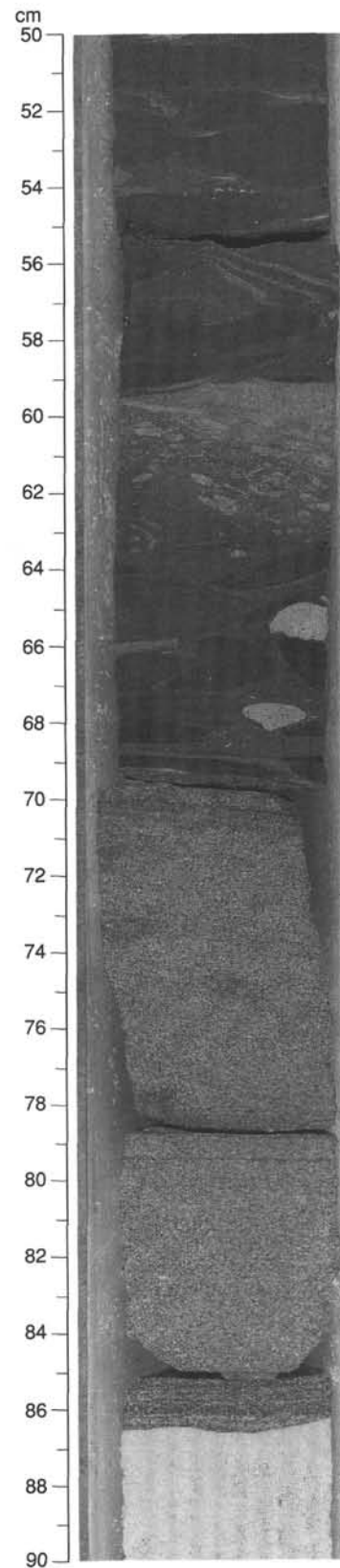


Figure 25. Gray bioclastic packstone (turbidite), parallel laminated, upward-fining from coarse sand-sized to fine sand-sized. This turbidite is overlain by a gray lithoclastic rudstone (debris flow). Ellipsoidal to flattened clasts are suspended in a clayey nannofossil chalk matrix, Unit VII, interval 133-823C-14R-3, 50–90 cm.

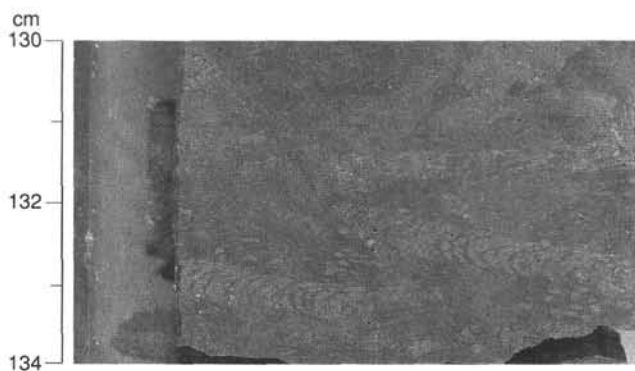


Figure 26. *Zoophycos* trace fossils in a bioturbated contorted foraminifer nannofossil chalk exhibiting post-date contortion and pre-date reverse microfaulting, Unit VII, Sample 133-823C-15R-2, 130–134 cm.

frequency of turbidites is higher, but the thickness of turbidite beds clearly is lower than that in Unit I. A large debris-flow and slump interval (Subunit IIIA) occurred between 3.5 and 3.9 Ma. The time between 4.3 and 6 Ma was dominated by hemipelagic sediments with slumping. The thickness and frequency of turbidites and debris flows increase toward 10 Ma, between 6 and 10.4 Ma (Units VI and VII). However, only a few biostratigraphic datums were available in this time interval. Because sediment gravity flows were deposited very rapidly, compared to the intervening hemipelagic sediments, variations in abundances of sediment gravity flows might result in nonlinear sedimentation rates and additional age data obtained in post-cruise studies after estimating ages.

### Summary and Conclusions

The background sedimentation in Site 823 is pelagic to hemipelagic nannofossil ooze to chalk and mixed sediment to claystone with variable amounts of terrigenous clay. The clay content varies throughout the stratigraphic sequence and is directly related to the color of the sediments. The influx of fine-grained and coarse-grained redeposited sediments derived from terrigenous and carbonate platform sources in addition to pelagic sedimentation resulted in high sedimentation rates for Site 823 (up to 16.6 cm/k.y.; see "Biostratigraphy" section, this chapter). The nannofossil ooze/chalk contains micrite in the first three lithologic units, between 0 and 535 mbsf (0 to 4.2 Ma). Increased influx of terrigenous clay occurred in Subunits IA, IIIA and IIIB, V and VII. The position of the site at the basin margin, close to the slope east of the Queensland Plateau, resulted in the frequent deposition of sediment gravity flows, interpreted as turbidites, debris flows, and slumps. A cumulative thickness of 332 m of redeposited sediments was recorded. Their thickness distribution shows a high and increasing occurrence of turbidites in Units I and II, between 0 and 3.5 Ma (Fig. 27). Unit III (3.5–4.2 Ma) is dominated by thick debris-flow and slump deposits, whereas Unit IV (4.2–5.5 Ma) has the highest cumulative percentage of slump deposits. Unit V (5.5–6.3 Ma) has the smallest amount of turbidites and debris flows. The number of gravity-flow deposits increases again in the lowermost two Unit VI (6.3–7.5 Ma) and VII (7.5–10.4 Ma), indicating an increased influx of relatively coarse-grained continental and platform-derived sediments between 6.3 and 10.4 Ma.

The sedimentary structures and composition of the gravity-flow deposits change in the different lithologic units. Well-sorted bioclastic packstones in Units I and II typically contain

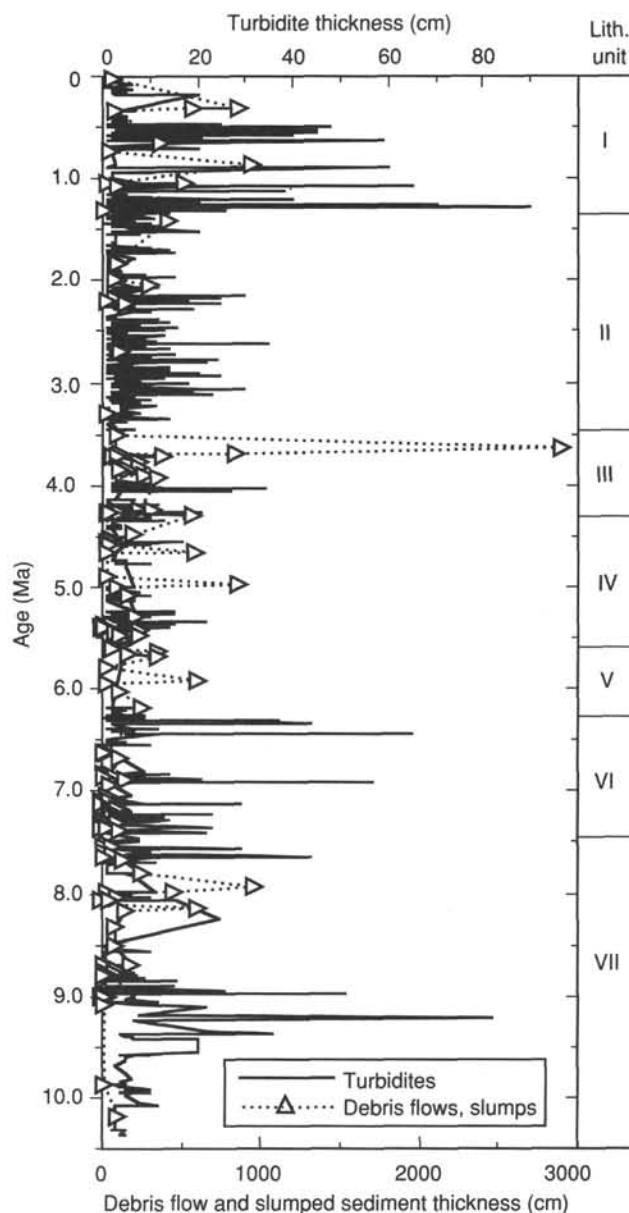


Figure 27. Linear interpolation of sediment gravity-flow thicknesses vs. known biostratigraphic ages permits first approximation of their distribution relative to time.

abundant foraminifers at the base. These distal turbidites were not erosive and were deposited frequently. They have been incorporated in less-frequent slumping events. The turbidites in Units III to VII are coarser-grained and have a higher abundance of coarse-grained quartz. Bouma sequences (in some cases showing  $T_a$ ,  $T_b$ ,  $T_c$ ,  $T_d$ , and  $T_e$  intervals) having local erosive bases (scours) occur in Units VI and VII. The greater degree of lithification enhanced the excellent preservation of the sedimentary structures within these turbiditic intervals. Pure carbonate turbidites are very rare. Coarser-grained, shallow-water carbonate debris was found only in turbidites and debris flows of Subunit IA and Unit VII. The debris in Unit VII was derived from older (middle Miocene[?]) build-up in close proximity east of Site 823.

All observed sedimentary features indicate a mixing of material from two or three major sources: the northeastern

Australian shelf, isolated build-ups west of Queensland Plateau, and a mixing of those sources with transport down the axis of Queensland Trough. The dark greenish-gray, clay-rich mud clasts in debris flows are similar to sediments recovered in Sites 819 through 822. Channels cut into the slope of the northeastern Australian margin, such as those seen at Site 822, were conduits for large-scale gravity flows. Post-depositional bioturbation affecting both matrix and mud clasts and the soft-sediment deformation in mud clasts indicate that slope-failure affected unconsolidated sediments and resulted in redeposition of large amounts of unlithified slope sediments. Miocene tectonic movements are indicated by micro-faulting, which caused brittle faulting of the limestones in Units VI and VII. This indicates a post-depositional faulting of relatively well-lithified sediments. However, bioturbation locally cuts across microfaults and offset burrows, which indicates syn-sedimentary deformation and may imply several deformation phases. This brittle deformation may have been caused by late tectonic phases resulting from intraplate stresses, whereas an earlier deformation may have resulted from downslope movement and is associated with gravitation stresses resulting in axial-planar cleavage in slump folds. Seismic reflection profiles also indicate that vertical faults affected the lowermost upper Miocene sediments. A major compressional tectonic phase with intraplate-type magmatism at about 6 Ma in Papua New Guinea may also have resulted in transfer of stress across a broad region during the late Miocene-early Pliocene and resulted in extensional stress and accelerated subsidence of Queensland Trough.

Effects of changes in sea level on sedimentation are most likely expressed in the occurrence of thick debris-flow deposits. The large debris flow in Unit III between 3.9 and 3.5 Ma may have been related to a decline in sea level at 3.8 Ma, whereas decreases in sea level at 3.0, 1.86, 1.4, 1.0, and 0.8 Ma may have caused a higher frequency of turbidite deposition at these times as well as the large-scale slump deposits of Unit I. The interpolated ages of the debris flows in Unit VII, based on a linear sedimentation rate, are not reliable; therefore, it is possible that part of these debris flows that contained shallow-water carbonate components might have been caused by the lowstand in sea level at 10.4 Ma or the shedding of shallow components into the trough may coincide with a period of successive lowstands.

Variable clay contents and the presence of micrite in sediments deposited between 0 and 3.5 Ma indicate the mixing of sediments derived from continental and carbonate-bank sources. The absence of micrite between 4.2 and 6.2 Ma may have climatic, paleoceanographic, and tectonic implications, suggesting that carbonate production on the banks was drastically reduced, possibly as a result of the incursion of colder surface water during the latest late Miocene (6–5 Ma) and increased subsidence of the platforms. The high sedimentation rate and the increased clay contents of the sediments, as well as the occurrence of slumps and debris flows between 5.9 and 3.5 Ma, point to an increased influx of terrigenous material. The high clay contents and low sedimentation rate (<1 cm/k.y.) between 7.5 and 10.4 Ma suggest an absence of shallow-water carbonate production of fine-grained periplatform sediments, but coarse-grained carbonates were eroded and redeposited at this time, perhaps because of a presumed lowstand of sea level.

## BIOSTRATIGRAPHY

### Introduction

At Site 823, 1011 m of Pleistocene to middle Miocene sediments was recovered. Calcareous nannofossil and plank-

tonic foraminifers generally were abundant at this site, and preservation of microfossils is good. A biostratigraphic overview with preliminary calcareous nannofossil and planktonic foraminiferal zones is shown in Figure 28. High abundances of certain planktonic foraminiferal species suggest that tropical conditions persisted throughout the time interval represented.

The Pleistocene/Pliocene boundary at Site 823 lies between the core-catcher samples of Cores 133-823B-13X and 133-823B-16X. The early/late Pliocene boundary is in Core 133-823B-38X. The top of the late Miocene, defined by the highest occurrence of *Discoaster quinqueramus*, is seen in Sample 133-823B-69X-CC. Uppermost middle Miocene sediments are represented in Samples 133-823C-23R-CC and -24R-CC and have been delineated by the presence of abundant *Globorotilia siakensis*.

Benthic foraminifers are present throughout the whole succession, but preservation deteriorates down the hole. Benthic foraminiferal assemblages point to a bathyal setting, with an influx of neritic faunal elements in the turbidite layers.

### Calcareous Nannofossils

At Site 823, we recovered generally abundant and well-preserved Holocene through upper Miocene calcareous nannofossils. Virtually all the conventional nannofossil markers for the time interval were found, and we have established a fairly fine-resolution biostratigraphy (Fig. 28). Three holes were drilled at this site. Hole 823B duplicates Hole 823A for the upper 120-m sequence and extends to 786 mbsf. Nannofossil stratigraphy of Hole 823A is consistent with that of Hole 823B, thus results from Hole 823A have been omitted in the following discussion.

The lowest occurrence of *Emiliania huxleyi* is in Sample 133-823B-3H-CC; the first three cores have been assigned to the *Emiliania huxleyi* Zone (CN15) and are younger than 0.275 Ma. The highest occurrence of *Pseudoemiliania lacunosa* (0.465 Ma) is in Sample 133-823B-4H-CC. The CN14a/CN14b boundary (0.465 Ma), therefore, is within Core 133-823B-4H. This indicates a hiatus or low sedimentation rate within this core. The next biohorizon recognized is the top of the interval of dominance of small *Gephyrocapsa* (0.93 Ma) in Sample 133-823B-9H-CC. The *Helicosphaera sellii* highest occurrence datum (1.27 Ma) was not identified in Hole 823B, but was documented in Hole 823A in the core-catcher sample of Core 133-823A-13H. The *Calcidiscus tropicus* highest occurrence datum (1.48 Ma) is in Sample 133-823B-16X-CC.

*Discoaster brouweri* was found first in Sample 133-823B-18X-CC, and the Pliocene/Pleistocene boundary was placed at this biohorizon. A succession of highest occurrences of *Discoaster pentaradiatus* (2.29 Ma), *D. surculus* (2.42 Ma), and *D. tamalis* (2.6 Ma) occurs in Samples 133-823B-24X-CC, -25X-CC, and -26X-CC, respectively. The highest occurrence of *Reticulofenestra pseudumbilica* (3.51 Ma) is in Sample 133-823B-38X-CC. This biohorizon defines the CN11/CN12 zonal boundary, which corresponds to the lower Pliocene/upper Pliocene transition.

The beginning of the acme of *Discoaster asymmetricus* (3.88 Ma) occurs in Sample 133-823B-45X-CC; this biohorizon further divides Zone CN11 into Subzones CN11a and CN11b. The highest occurrence of *Amaurolithus tricorniculatus* (4.24 Ma) is in Sample 133-823B-55X-CC. *Ceratolithus armatus* occurs from Samples 133-823B-63X-CC to -66X-CC; an age of 4.6 Ma and 5.06 Ma, respectively, was assigned to these two samples.

The highest occurrence of *Discoaster quinqueramus* (5.26 Ma) is in Sample 133-823B-69X-CC. This biohorizon delimits the Miocene/Pliocene boundary. *Amarulithus amplificus* occurs in Samples 133-823B-77X-CC and -80X-CC and suggests

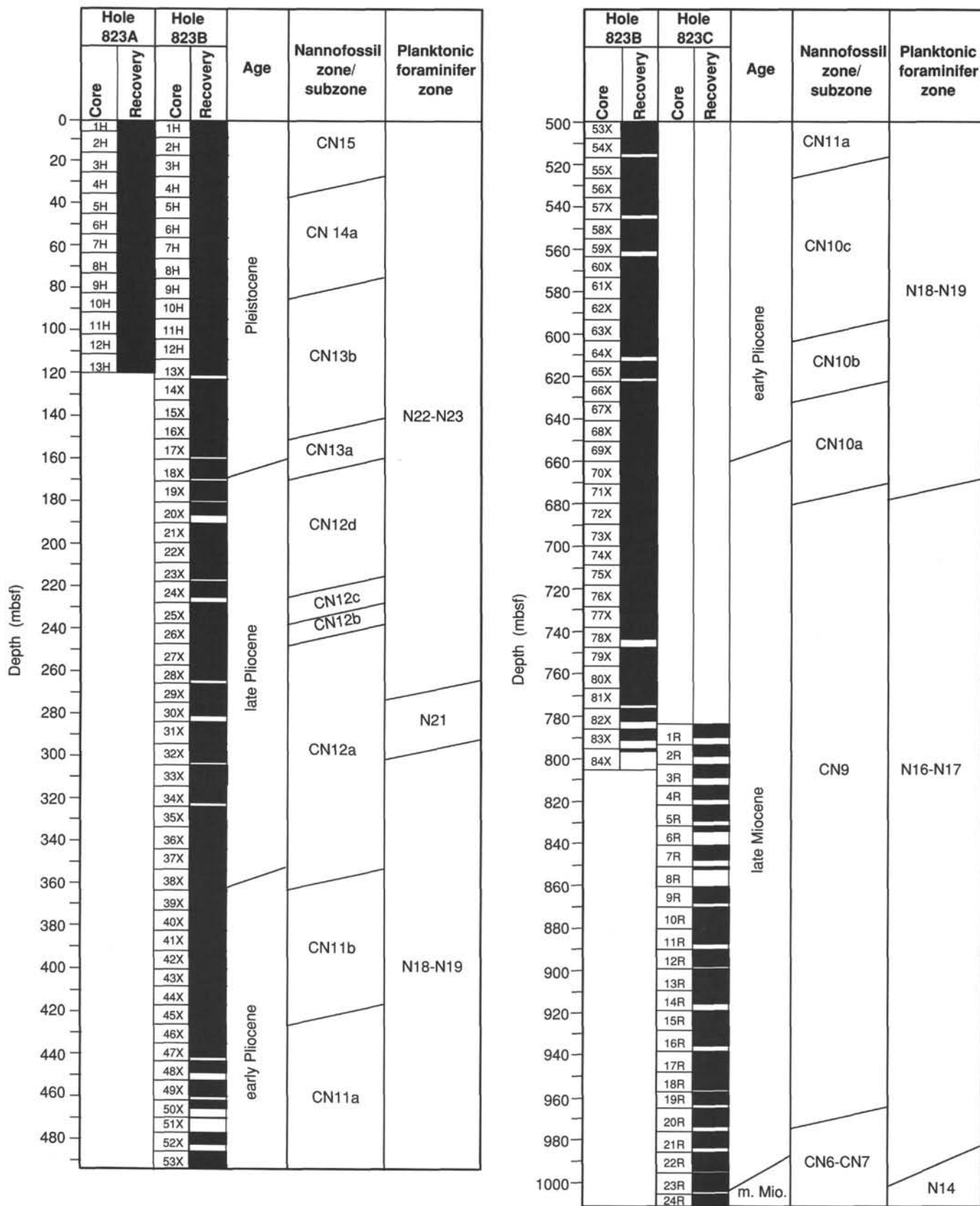


Figure 28. Preliminary nannofossil and foraminifer biostratigraphy, Site 823.

an age range between 5.6 and 5.9 Ma for this stratigraphic interval. No further biohorizons were encountered in the additional core-catcher samples from Hole 823B, but *Discoaster quinquerramus* is consistently present to the bottom of this hole. This indicates an age range of 5.9 to 8.2 Ma for these samples.

The first two cores from Hole 823C overlap with the lowest interval cored in Hole 823B. Samples 133-823C-1R-CC through -19R-CC have been dated as 5.9 to 8.2 Ma by the presence of *Discoaster berggrenii*. *D. quinquerramus* in this stratigraphic interval. Two biohorizons were encountered lower down in the core-catcher samples of the hole: the highest occurrence of *Catinaster calyculus* (8.75 Ma) in Sample 133-823C-20R-CC and the highest occurrence of *Catinaster coalitus* (9.0 Ma) in Sample 133-823C-22R-CC. Sample 133-823C-23R-CC yielded few nannofossils, including rare specimens of *Catinaster coalitus*, and has an age range of 9.0 to 10.8 Ma. The lowest core-catcher sample (133-823C-24R-CC) contains a few poorly preserved nannofossils and is probably younger than 11.6 Ma, based on the absence of *Cyclicargolithus floridanus*, a common species in middle Miocene marine sediments.

### Planktonic Foraminifers

Hole 823A contains highly diverse, tropical Pleistocene planktonic foraminiferal assemblages (Zone N22–N23). Preservation of tests is good, and all samples yielded abundant specimens. The following successive Pleistocene biohorizons were recognized: the latest occurrence of *Globigerinoides ruber* pink in Core 133-823A-2H (0.12 Ma); the first occurrences of *Bolliella adamsi* and *Globorotalia fimbriata* in Core 133-823A-3H; the highest occurrences of *Globorotalia tumida flexuosa* and *Globorotalia crassaformis hessi* in Core 133-823A-4H; the first occurrence of *Globigerina rubescens* pink in Core 133-823A-5H; the first occurrence of *Bolliella prae-adamsi* in Core 133-823A-6H; and the highest occurrence of *Globorotalia tosaensis* in Core 133-823A-7H (0.6 Ma).

From Hole 823B, we recovered upper Miocene to Pleistocene sediments. Most core-catcher samples contain well-preserved, abundant tropical planktonic foraminifers, except for those samples that contain redeposited material (Samples 133-823B-19X-CC and -38X-CC through -40X-CC). For a discussion of the Pleistocene, see previous discussion.

The highest occurrences of *Globigerinoides fistulosus* (1.6 Ma) and *Globigerinoides obliquus* (1.8 Ma) were found in Samples 133-823B-17X-CC and -22X-CC, respectively. In the latter sample, additional bioevents are the highest occurrences of *Globorotalia limbata*, *Neogloboquadrina humerosa*, and *Globigerina decoraperta*. The lowest occurrence of *Globorotalia truncatulinoides*, marking the lower limit of Zone N22–N23, is in Sample 133-823B-29X-CC.

The lowest occurrence of *Globigerinoides fistulosus* (2.9 Ma) is located in Sample 133-823B-30X-CC, whereas the highest occurrence of *Globoquadrina altispira* (2.9 Ma) is found in Sample 133-823B-31X-CC. In the next lower sample, the top of the *Sphaeroidinellopsis* lineage is present (3.0 Ma). In addition, in Core 133-823B-32X, the lowest appearance of *Globorotalia tosaensis* occurs, indicating the lower limit of Zone N21. The earliest Pleistocene and late Pliocene faunas have been dominated by species of a tropical nature, such as *Globigerinoides sacculifer*, *Globigerinoides ruber*, *Globigerinella aequilateralis*, *Globigerinoides conglobatus*, and *Globorotalia tumida tumida*.

The highest occurrence of *Globigerinoides nepenthes* (3.9 Ma) is located in Sample 133-823B-52X-CC. The lower boundary of Zone N18–N19 occurs in Sample 133-823B-70X-CC, as defined by the first appearance of *Globorotalia tumida*

*tumida*. Abundant-to-common planktonic foraminifers in this zone include *Globigerinoides sacculifer*, *Globigerinoides ruber*, *Globigerinoides obliquus*, *Globigerinoides altispira*, *Neogloboquadrina acostaensis*; less frequent are *Pulleniatina primalis*, *Globigerina woodi*, *Globigerina nepenthes*, *Globorotalia margaritae*, and *Sphaeroidinellopsis seminulina*. In the lower part of this zone (around 5.0 Ma), *Neogloboquadrina pachyderma* specimens (left- and right-coiled varieties) occur, which indicates some colder water influence, although more than 95% of the fauna is tropical. This species disappears from the record around 6.0 Ma.

Hole 823C yielded abundant late-to-middle Miocene planktonic foraminiferal faunas. The foraminiferal assemblages in late Miocene Zone N16–N17 are dominated by species from the tropical belt, such as *Globigerinoides sacculifer*, *Globoquadrina altispira*, *Globorotalia tumida plesiotumida*, and *Sphaeroidinellopsis seminulina*. *Globorotalia siakensis* (highest occurrence at 10.4 Ma) is present in Samples 133-823C-23R-CC and -24R-CC, which led us to assign the lowest part of the hole to Zone N14, corresponding to the uppermost middle Miocene.

### Benthic Foraminifers

Selected core-catcher samples from Holes 823A, 823B, and 823C were examined for benthic foraminiferal assemblages. Benthic foraminifers are well-preserved in Hole 823A, whereas preservation deteriorated in Hole 823B below Core-133-823B-50X. Benthic foraminifers have recrystallized in Hole 823C core-catcher samples.

In addition to core-catcher samples, three turbidite layers within Core-133-823A-5H were examined for transported contents of benthic foraminifers. These samples showed a size-sorting of only the smaller than 250- $\mu$ m-size fraction remaining. The samples contain a mixture of neritic, upper bathyal and middle-to-lower bathyal benthic foraminifers. In addition, one of the faunas (Sample 133-823A-5H-4, 15–19 cm) contains reefal benthic foraminifers.

Benthic foraminiferal assemblages contain typical bathyal species associations, including *Bolivinospis cubensis*, *Bulimina aculeata*, *Bulimina alazanensis*, *Bulimina mexicana*, *Cibicidoides bradyi*, *Cibicidoides cicatricosus*, *Cibicidoides mundulus*, *Cibicidoides pachyderma*, *Eggerella bradyi*, *Globocassidulina subglobosa*, *Hoeglundina elegans*, *Laticarinina pauperata*, *Planulina wuellerstorfi*, *Rectuvigerina multcostata*, *Sigmilopsis schlumbergeri*, *Sphaeroidina bulloides*, *Uvigerina hispida*, *Uvigerina peregrina*, *Uvigerina pigmaea*, and *Uvigerina proboscidea* (van Morkhoven et al., 1986). Several taxa place an upper depth limit estimate of the middle bathyal zone or deeper (>600 m), including *Anomalinoidea globulosus*, *Cibicidoides robertsonianus*, and *Pyrgo murrhina* (van Morkhoven et al., 1986). *In-situ* benthic foraminifer faunas contain abundant *Planulina wuellerstorfi* and lack species that generally are restricted to depths shallower than 1000 m, indicating a lower bathyal (1000–2000 m) paleodepth for Site 823. Some samples also contain displaced reefal, neritic, and upper-to-middle bathyal benthic foraminifers, such as *Amphistegina* spp., *Bulimina marginata*, *Buliminella elegantissima*, *Elphidium* spp., *Hanzawaia mantaensis*, *Hyalinea balthica*, *Peneroplis* sp., and *Planorbulina* spp.

### PALEOMAGNETISM

Paleomagnetism in all archive halves of core sections from Holes 823A, 823B, and 823C was measured at 10-cm intervals using the shipboard pass-through cryogenic magnetometer, both before and after AF demagnetization at 15 mT. Whole-core volume magnetic susceptibilities also were measured at

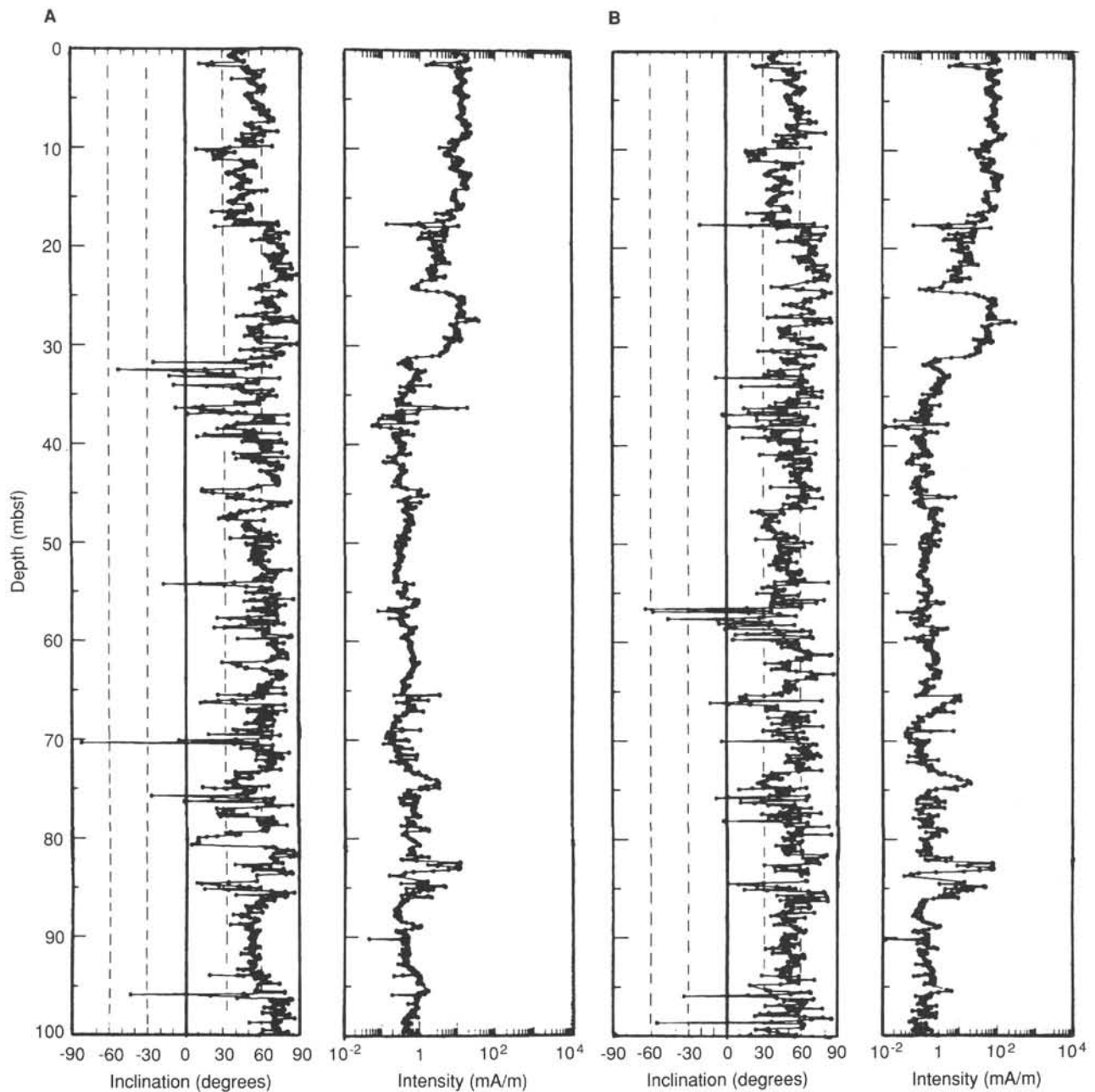


Figure 29. Variations downhole of magnetic inclination and intensity for the interval from 0 to 100 mbsf in Hole 823B. A. Before AF demagnetization at 15 mT. B. After AF demagnetization at 15 mT.

10-cm intervals using a Bartington pass-through susceptibility meter. In general, our demagnetization treatment resulted in a small decrease of remanent intensity and a slight reduction of scatter in inclination data, especially in the upper 100 mbsf in Holes 823A and 823B (Fig. 29) and in rotary cores obtained from the less-disturbed and/or lithified sediments below about 800 mbsf in Hole 823C. However, the persistence of normal polarity throughout the 1011.0-m-thick sequence of these sediments of uppermost Miocene to Pleistocene age (see "Biostratigraphy" section, this chapter) shows that remanent magnetization of the sediments is either pervasively overprinted or has been remagnetized with a normal polarity. If an overprint is the cause, we were unable to remove it with AF demagnetization of 15 mT.

Shipboard paleomagnetic measurements provided little reliable magnetostratigraphic information because of scattered inclinations throughout XCB cored sections. We hope that stepwise thermal and AF demagnetization at >15-mT fields for oriented discrete samples will reveal a reliable magnetostratigraphy. A total 926 discrete samples were collected for shore-based studies.

A whole-core volume susceptibility composite for Site 823 shows several distinct high-susceptibility zones, separated by zones of slightly lower values that contain high-frequency changes (Fig. 30). The cluster of higher susceptibility peaks correlates with zones of increased turbidite deposition (see "Lithostratigraphy" section, this chapter). This general correlation, which was observed in the last four sites, indicates

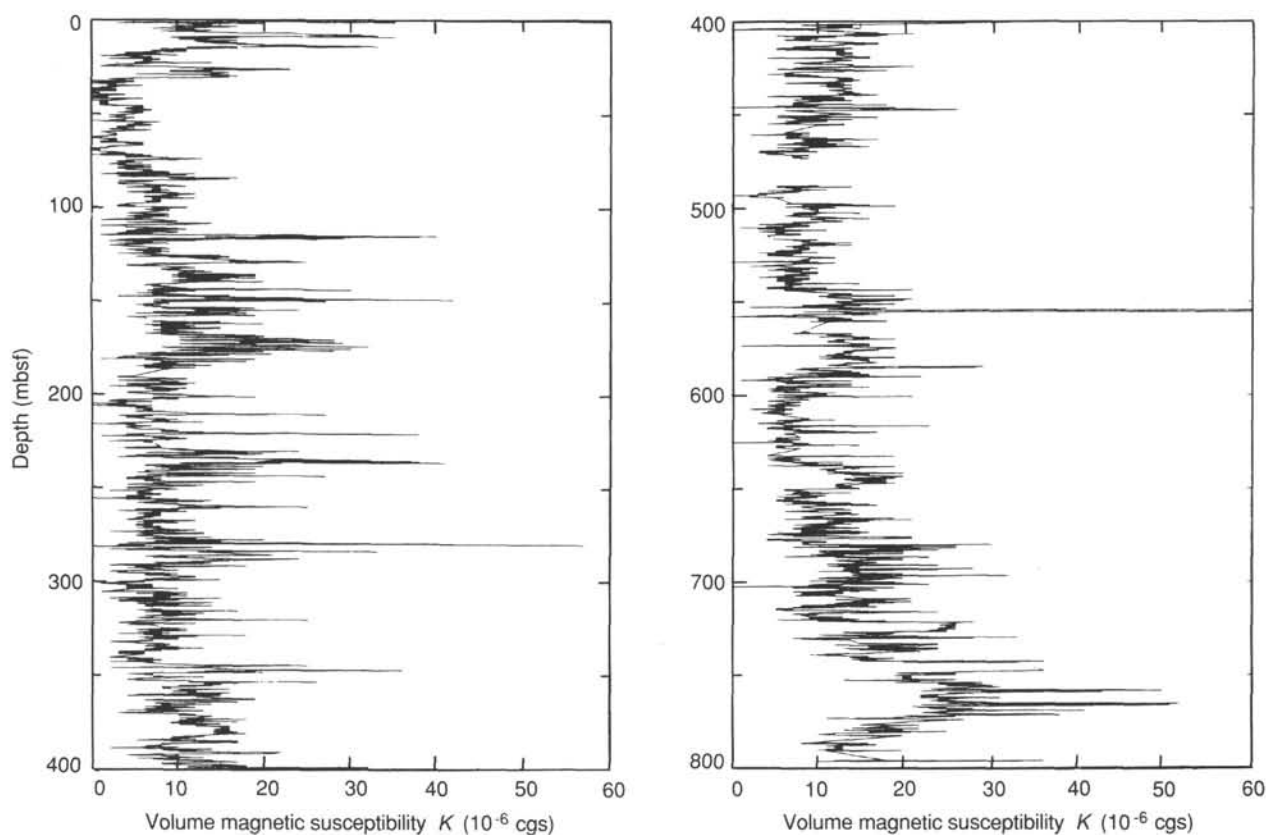


Figure 30. Variation of magnetic susceptibility with depth for the interval from 0 to 800 mbsf, Hole 823B.

that an upslope sediment influx, perhaps from a fluviodeltaic setting and/or a later reworking of these deposits, controls the magnetic susceptibility signal. Various peaks in susceptibility data correlate well with peaks in natural remanent magnetization intensity.

### SEDIMENTATION RATES

Sediments at Site 823 yielded a large number of biohorizons, both calcareous nannofossils and planktonic foraminifers, all of which appeared in proper order, which is remarkable given that the sediment section is laced with turbidites. More remarkable yet is that in an age-depth plot (Fig. 31), these biohorizons form a nearly straight line from the Holocene to the mid-Pliocene, another from the mid-Pliocene into the late Miocene, and possibly a third in the earliest late Miocene(?) and the late middle Miocene. The first interval extends from the seafloor to approximately 435 mbsf (0–3.51 Ma) for a sedimentation rate of just over 11 cm/k.y. Changes in sedimentation rates are abrupt in the mid-Pliocene, and the interval from about 435 to 771 mbsf (3.51–5.9 Ma) identifies a second trend with a significantly higher sedimentation rate of 16.6 cm/k.y. The third trend has been defined by four biohorizons near the bottom of the cored section, in the interval from 972 to 991 mbsf (8.2–10.4 Ma). The sedimentation rate for this interval is less than 1 cm/k.y.

Biohorizons that are significantly off a straight-line trend may contain a real signal; however, given the sample spacing, the inherent error is too large to attach any significance to potential short-term variations in sedimentation.

## INORGANIC GEOCHEMISTRY

### Interstitial Waters

Interstitial water samples were taken from cores listed in Table 2. In addition, the “Barnes” downhole water sampler (WSTP) was deployed before Cores 133-823B-12H, -17X, -22X, -22X, and -32X. Samples were squeezed and analyzed according to the methods outlined in the “Explanatory Notes” chapter (this volume).

#### Calcium, Magnesium, Potassium, and Strontium

Concentrations of calcium, magnesium, and potassium all decrease from that of seawater (10.47, 53.56, and 10.31 mM, respectively) within the top 100 mbsf to minimum values of 3.13, 12.99, and 1.69 mM, respectively (Fig. 32 and Table 2). In contrast to Sites 819 to 822, the depth of the minimum  $\text{Ca}^{2+}$  value (32.35 mbsf) is shallower than that for  $\text{Mg}^{2+}$  (524.2 mbsf) and  $\text{K}^{+}$  (552.8 mbsf). Below these depths, values increase toward the bottom of the hole. Concentrations of  $\text{Ca}^{2+}$  increase to nearly 20 mM;  $\text{Mg}^{2+}$  to 22 mM; and  $\text{K}^{+}$  to 3.7 mM. An increase in concentration at the base of the core is similar to the trend seen at Site 815, although the magnitude of this increase is less.

Concentrations of strontium in pore waters increase steadily from surface-water values of 102 to 2877  $\mu\text{M}$  at 990.5 mbsf (Fig. 32 and Table 2). The large increase in interstitial-water  $\text{Sr}^{2+}$  is a combination of (1) the result of recrystallization of biogenic calcite and aragonite to low-Mg calcite and (2) the absence of sulfate in pore fluids. The absolute concentration

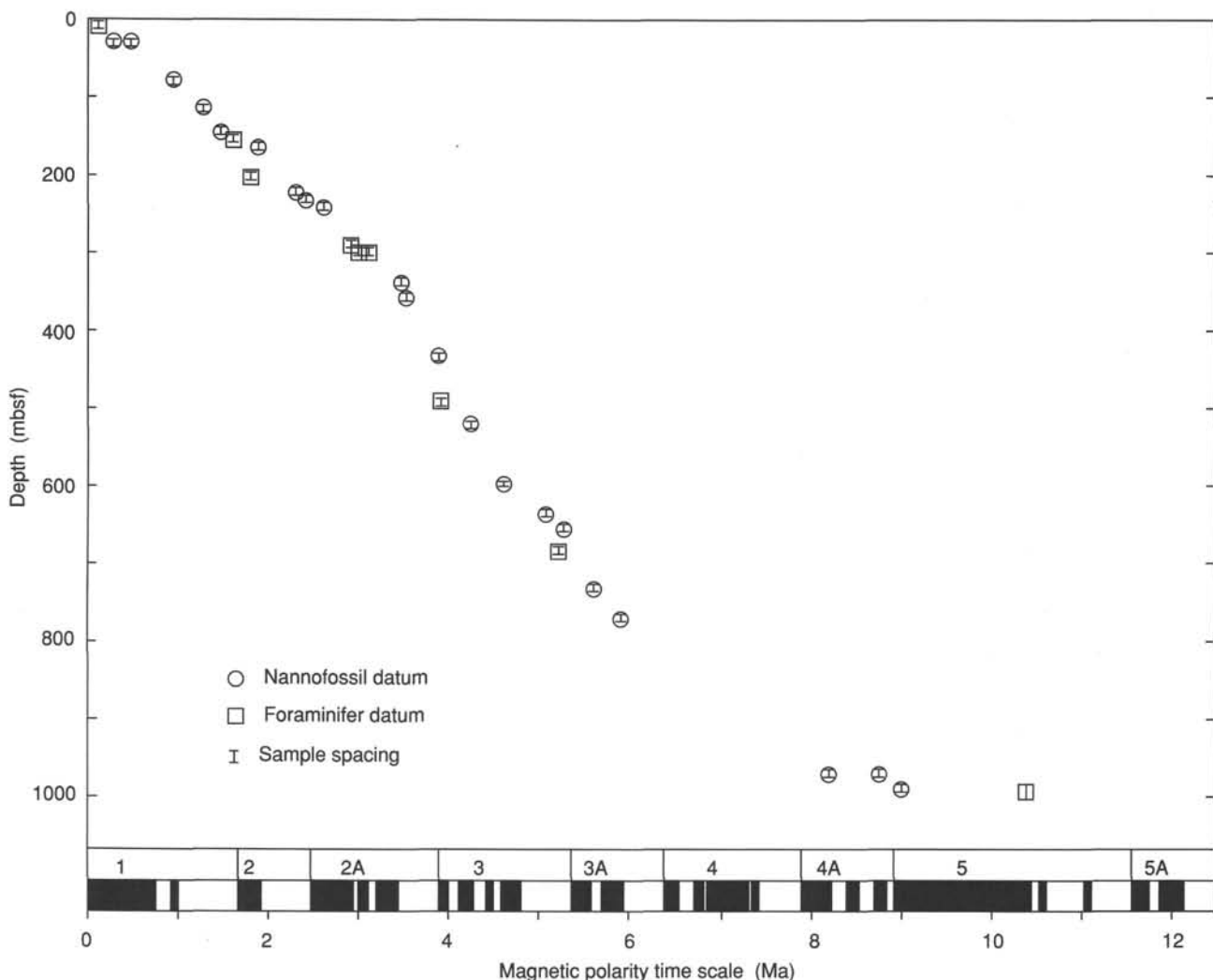


Figure 31. Plot of age vs. depth for Site 823.

of  $\text{Sr}^{2+}$  attained is one of the highest values ever recorded in DSDP and ODP sites. Employing a distribution coefficient of 0.05 for incorporating  $\text{Sr}^{2+}$  into LMC, one can calculate the equilibrium concentration of Sr in diagenetic LMC. These calculations (shown in Fig. 33) indicate that it is possible to form LMC with values of strontium of more than 3000 ppm.

When concentrations of  $\text{Ca}^{2+}$ ,  $\text{Mg}^{2+}$ ,  $\text{K}^+$ , and  $\text{Sr}^{2+}$  are normalized to surface-water salinity, a maximum loss of 7.33 mM of  $\text{Ca}^{2+}$  and 40.86 mM of  $\text{Mg}^{2+}$  occurs. Calcium probably is being used to form authigenic calcite, whereas magnesium is being consumed during the formation of dolomite. Potassium also is being depleted in the pore waters, with a net loss of 8.67 mM (Fig. 34). The loss of  $\text{K}^+$  and some of the  $\text{Mg}^{2+}$  probably results from formation of illite from kaolinite (see "Inorganic Geochemistry" section, "Site 822" chapter, this volume).

#### Sodium and Chloride

As at Sites 819 to 822, salinity of pore fluids decreases rapidly with depth as a result of the removal of  $\text{SO}_4^{2-}$  and  $\text{HCO}_3^-$ . Chloride concentrations are close to that of modern seawater in the upper 300 mbsf (Fig. 34). Below this depth, Cl<sup>-</sup> concentrations increase to 570 mM at a depth of 990.5 mbsf. An increase in Cl<sup>-</sup> may be a common feature in sediments of late Miocene to early Pliocene age at the sites drilled in Queensland Trough; increases in Cl<sup>-</sup> were observed at Sites 815, 817, 818, 822, and 823. Such a common trend suggests

that perhaps the evaporitic unit postulated to underlie Site 815 may be an extensive feature of Queensland Trough.

Concentrations of  $\text{Na}^+$  increase to 519 mM at 64.0 mbsf, suggesting the addition of  $\text{Na}^+$  from the reaction of feldspar to form kaolinite (see "Inorganic Geochemistry" section, "Site 822" chapter, this volume). This trend can be observed in the increasing Na/Cl ratio, which reaches maximum values coincident with a maximum in  $\text{Na}^+$  concentration. Values of Na/Cl ratios return to those of seawater at the bottom of the cored interval (Fig. 34).

#### Alkalinity, Ammonia, Phosphate, and Sulfate

Concentrations of alkalinity, ammonia, and sulfate at Site 823 have been affected by sulfate reduction of organic matter in sediments. Alkalinity rapidly increases from a seawater value of 2.46 to 12.55 mM at 55.8 mbsf (Fig. 35 and Table 2). Below this maximum, alkalinity decreases to 1.836 mM at 639.55 mbsf. High alkalinity values occur at the same depth, where sulfate decreases to zero from a seawater value of 28.54 mM. Sulfate is absent between 51.25 and 552.8 mbsf. The small amounts of sulfate measured in some samples in this interval represent either contamination from surface seawater or the diffusion of sulfate from an underlying source. Concentrations of ammonia increase to approximately 3743  $\mu\text{M}$  and decrease to approximately 3000  $\mu\text{M}$  at the bottom of the hole (Fig. 35 and Table 2). As a result of the low amounts of water

Table 2. Interstitial water data for Site 823.

Core, section, interval (cm)	Depth (mbsf)	pH	Alk. (mM)	Sal. (g/kg)	Cl <sup>-</sup> (mM)	Mg <sup>2+</sup> (mM)	Ca <sup>2+</sup> (mM)	SO <sub>4</sub> <sup>2-</sup> (mM)	NH <sub>4</sub> <sup>+</sup> (μM)	Si (μM)	K <sup>+</sup> (mM)	Sr <sup>2+</sup> (μM)	Na <sup>+</sup> (mM)
Seawater	0.00	7.93	2.456	35.0	544.84	53.56	10.47	30.22	0	5	10.31	105	469.16
133-823A-													
1H-3, 145-150	4.45	7.51	4.421	35.0	542.92	52.11	9.31	26.80	91	250	11.42	133	466.33
2H-5, 145-150	13.25	7.35	4.635	35.0	545.80	50.94	8.81	26.96	131	202	11.94	148	472.49
3H-5, 145-150	22.75	7.40	7.759	33.8	546.76	47.22	5.32	15.72	733	210	12.07	157	467.76
4H-5, 145-150	32.25	7.50	9.881	32.5	542.92	39.00	3.13	6.93	1616	149	11.43	190	468.97
5H-5, 145-150	41.75	7.43	12.196	31.8	549.65	33.03	3.72	0.67	232	284	10.06	202	479.00
6H-5, 145-150	51.25	7.43	12.011	32.2	549.65	31.36	4.10	0.00	1095	310	9.74	218	479.47
7H-1, 0-7	55.80	8.01	12.550	31.8	544.84	31.55	4.12	0.00	2178	274	8.24	241	475.15
7H-5, 145-150	60.75	7.39	11.421	31.8	543.88	29.67	4.36	0.00	2198	316	9.84	220	474.76
8H-5, 145-150	70.25	7.43	10.354	31.8	556.37	28.10	4.12	0.00	2579	314	12.67	221	486.60
9H-5, 145-150	79.75	7.52	9.538	32.0	546.76	28.18	3.52	0.00	2820	238	10.05	201	479.63
10H-5, 145-150	89.25	7.78	8.922	31.8	546.76	27.61	3.39	0.00	2981	135	9.95	196	480.37
12H-1, 0-7	103.30	8.33	9.912	31.8	541.96	28.42	4.83	0.43	2519	212	5.50	212	477.80
12H-5, 140-150	110.70	7.82	7.745	32.2	541.96	25.91	3.97	0.00	2961	133	8.11	197	478.48
13H-5, 145-150	117.75	7.87	7.929	31.8	544.84	25.18	3.97	0.00	2901	151	8.24	216	482.90
133-823B													
15X-5, 140-150	139.50	7.82	7.668	31.8	546.76	26.15	3.77	0.20	3121	183	7.25	234	484.15
17X-1, 0-7	151.40	7.70	4.450	34.0	547.72	44.72	7.73	20.38	2680	101	7.56	211	477.38
18X-3, 140-150	165.50	7.66	7.651	31.5	552.53	25.98	4.05	0.65	3021	183	6.44	282	491.40
21X-3, 140-150	194.60	7.92	6.824	32.0	548.69	23.74	4.14	0.00	3222	183	8.21	374	487.57
22X-1, 0-7	199.80	7.59	7.914	32.2	546.76	25.94	4.74	0.50	3101	183	5.58	409	484.83
24X-2, 140-150	221.60	7.76	6.081	31.8	546.76	20.96	5.14	0.00	3543	202	5.25	477	490.89
26X-1, 0-7	237.70	8.03	6.822	33.8	542.92	27.50	5.20	4.32	2840	169	4.31	505	484.82
27X-6, 140-150	256.20	7.86	5.968	31.8	547.72	21.41	3.81	0.00	3262	133	4.73	432	494.39
30X-2, 140-150	279.20	7.82	4.959	31.8	551.57	21.87	3.80	0.35	3442	137	4.39	619	496.82
32X-1, 0-7	295.60	8.03	5.752	31.8	542.92	23.73	5.96	3.60	2901	173	3.66	662	488.61
33X-4, 140-150	311.20	7.91	3.780	32.0	545.80	20.44	5.21	2.42	2820	129	3.98	687	494.95
36X-5, 140-150	341.60	7.91	3.068	31.8	558.29	18.45	4.82	0.04	3442	129	4.43	703	505.62
39X-5, 140-150	370.40	7.97	3.537	31.8	554.45	19.16	4.64	0.00	3262	75	3.49	654	502.33
42X-4, 140-150	397.90	7.84	3.893	31.8	550.61	18.67	5.73	0.45	3543	181	2.95	742	498.62
45X-5, 140-150	428.30	7.73	3.528	31.8	548.69	17.23	5.67	0.00	3743	167	2.84	825	498.18
48X-4, 140-150	455.80	7.70	2.950	31.8	556.37	15.81	6.16	0.19	3342	161	2.60	1029	507.75
52X-4, 140-150	493.70	7.83	2.838	31.8	560.22	13.26	7.41	0.00	3282	173	2.45	1185	513.61
55X-5, 140-150	524.20			32.0	557.42	12.99	7.91	0.00	3202	145	1.70	1269	508.17
58X-5, 140-150	552.80	7.87	2.431	32.0	560.32	13.12	8.43	0.48	3302	145	1.69	1338	512.95
61X-5, 135-150	581.65	7.72	2.335	32.2									
64X-1, 135-150	604.55	7.91	2.081	32.2	563.22	13.71	9.00	1.08	3282	135	2.27	1515	512.68
67X-5, 135-150	639.55	7.90	1.836	32.2	570.96	14.18	9.29	0.69	3482	117	2.25	1780	518.97
70X-5, 110-125	667.70	7.81	1.897	32.2	568.06	13.42	10.27	1.20	3342	163	2.33	1879	515.44
73X-2, 135-150	692.45	7.87	1.910	32.2	571.93	14.40	10.75	1.14	3282	143	2.44	1913	515.09
76X-4, 135-150	724.45	7.79	2.848	32.2	568.06	14.02	11.90	0.55	2921	179	2.28	2248	510.47
79X-4, 135-150	753.45	7.70	2.680	32.4	571.93	14.54	13.42	1.37	3081	248	2.65	2335	511.02
82X-1, 135-150	778.05	7.56	3.181	32.5	568.06	16.60	12.24	1.96	3081	256	2.13	2410	507.46
133-823C													
1R-3, 130-150	788.30	7.91	2.258	32.5	569.03	17.15	12.25	2.60	3442	105	3.10	2162	506.82
4R-1, 130-150	813.90			33.0	570.96	17.65	13.63	2.79	3009	80	3.73	2023	505.21
7R-2, 130-150	844.50			33.8	566.13	18.95	14.70	2.92	3097	109	3.75	2248	495.32
10R-1, 125-150	872.05			33.8	575.80	17.05	16.16	1.92	3448	72	2.74	2444	504.13
13R-4, 130-150	905.50			35.0	575.80	16.60	17.70	1.78	3387	74	2.34	2785	501.47
16R-4, 130-150	934.60			35.0	570.00	18.57	18.11	2.84	3009	78	2.16	2774	493.61
19R-3, 130-150	961.60			34.0	576.77	20.33	19.77	3.97	2933	78	2.88	2750	495.21
22R-3, 130-150	990.50			33.8	570.00	21.88	18.00	5.63	3061	103	3.68	2877	490.99

recovered below 813.9 mbsf, alkalinities were not measured below this depth.

#### Silica

Concentrations of silica were low at Site 823 because of the absence of siliceous microfossils in the sediments. Concentrations increase from surface-water values of 5 to 310 μM at 51.25 mbsf. Below this depth, concentrations decrease to 100 μM at the base of the sampled interval (Table 2).

#### Results From WSTP Samples

As a result of degree of induration of the sediments at Site 823, the WSTP tool was unable to penetrate successfully into these sediments to acquire representative water samples. As a result, all WSTP samples have been contaminated

with seawater and do not accurately reflect variations in interstitial water chemistry shown by squeezed samples (Figs. 32, 34, and 35).

#### Carbonate Content and X-ray Diffraction Data

Samples for X-ray diffraction (XRD) analyses were taken from interstitial-water squeeze cakes and physical properties samples.

Sediments at Site 823 are predominantly calcite (Fig. 36 and Table 3). High-Mg calcite (HMC) and aragonite are present in the top 300 mbsf of Site 823 in concentrations up to 30% and 53.5%, respectively. HMC and aragonite decrease to 0% below 200 and 300 mbsf, respectively.

When mineral concentrations are calculated as percentages of quartz, carbonate, and clay, we see that clay concentra-

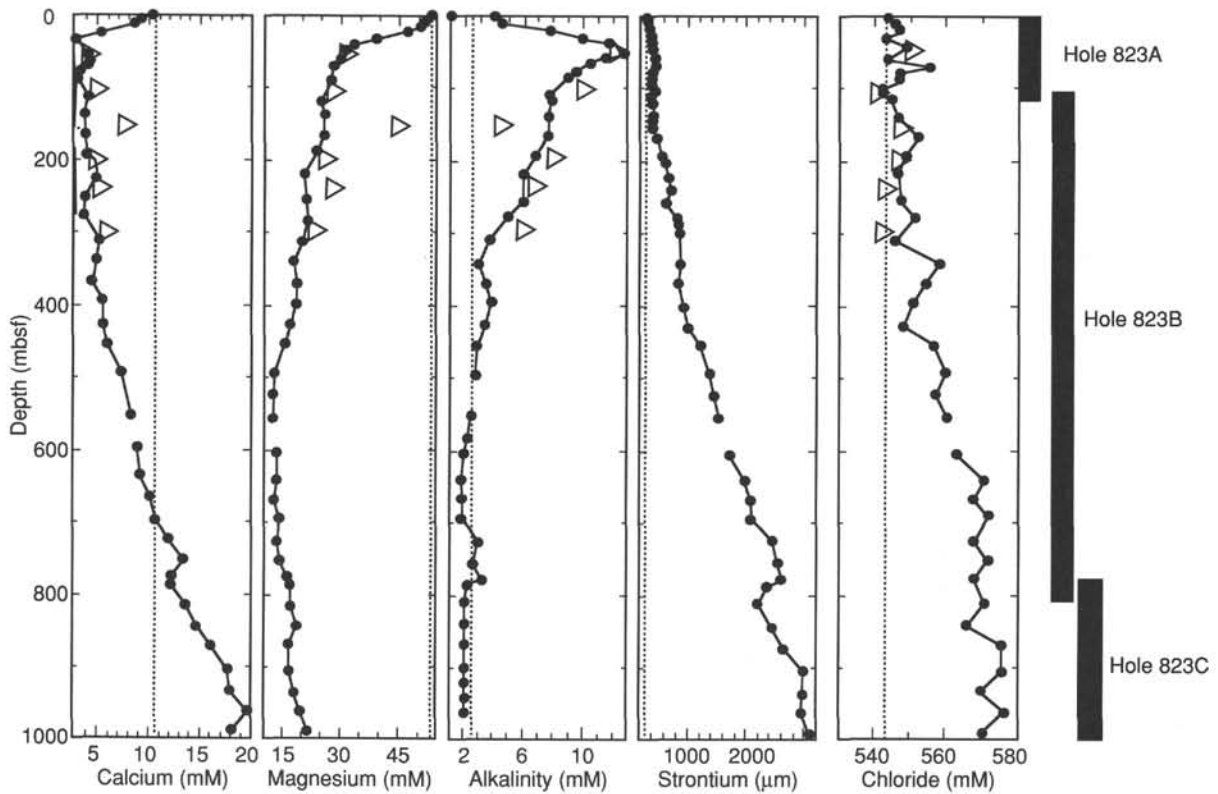


Figure 32. Calcium, magnesium, alkalinity, strontium, and chloride data as a function of depth for Site 823. Open triangles indicate data from WSTP samples. Composition of seawater is indicated by dotted line.

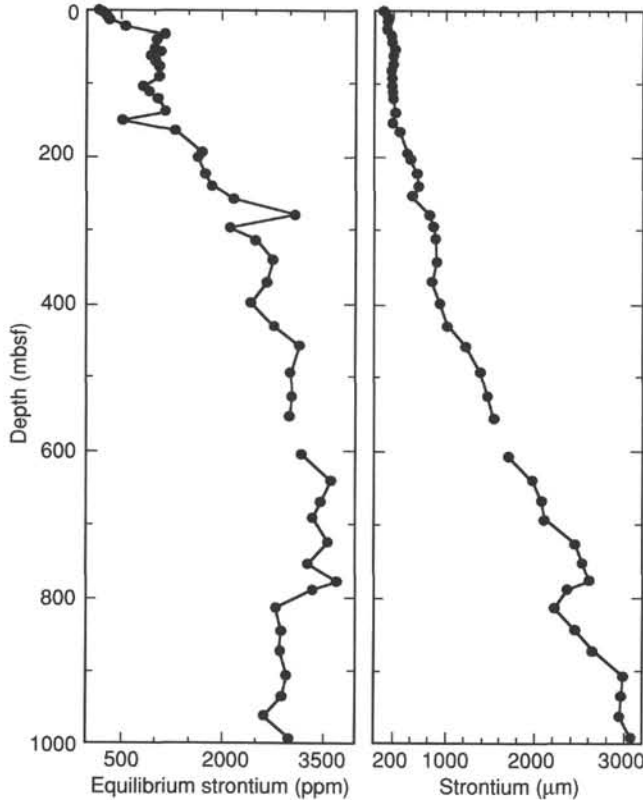


Figure 33. Concentration of Sr<sup>2+</sup> in pore waters at Site 823 and the equilibrium concentration of Sr in LMC precipitated from these pore fluids.

tions increase with increasing depth, whereas quartz remains relatively constant (Fig. 36 and Table 4).

Calcium carbonate values range from 18% to 80% (Fig. 36, 37, and Table 4) and are highly variable. These variations principally result from dilution of the carbonate fraction of the sediment by varying amounts of terrigenous influxes (see "Lithostratigraphy" section, this chapter)

**ORGANIC GEOCHEMISTRY**

In addition to safety monitoring for hydrocarbons, the main purpose of shipboard organic geochemistry studies at Site 823 was to assess the amount and origin of organic matter preserved in Pleistocene to middle Miocene pelagic sediments deposited in western central Queensland Trough. Our second purpose was to characterize the proportions of different light hydrocarbons generated in these sediments through biogenic or thermogenic decay of organic matter.

**Samples**

A total 133 samples were collected from Holes 823A, 823B, and 823C at 10-m intervals over depths ranging from 4 to 1008 mbsf. All sediments were analyzed for their composition of light hydrocarbons (C<sub>1</sub>-C<sub>6</sub>) using headspace analyses. These samples also were analyzed for total nitrogen, sulfur, and carbon, using an NA 1500 Carlo Erba NCS analyzer.

**Volatile Hydrocarbons**

Hydrocarbon gases (C<sub>1</sub>-C<sub>6</sub>) in sediments were analyzed as part of ODP's safety and pollution-prevention monitoring program, using the headspace technique, the vacutainer technique (when gas pockets were observed in the core liner), the Carle gas chromatograph (for determining concentrations of C<sub>1</sub>-C<sub>3</sub>), and the NGA gas chromatograph (mainly for deter-

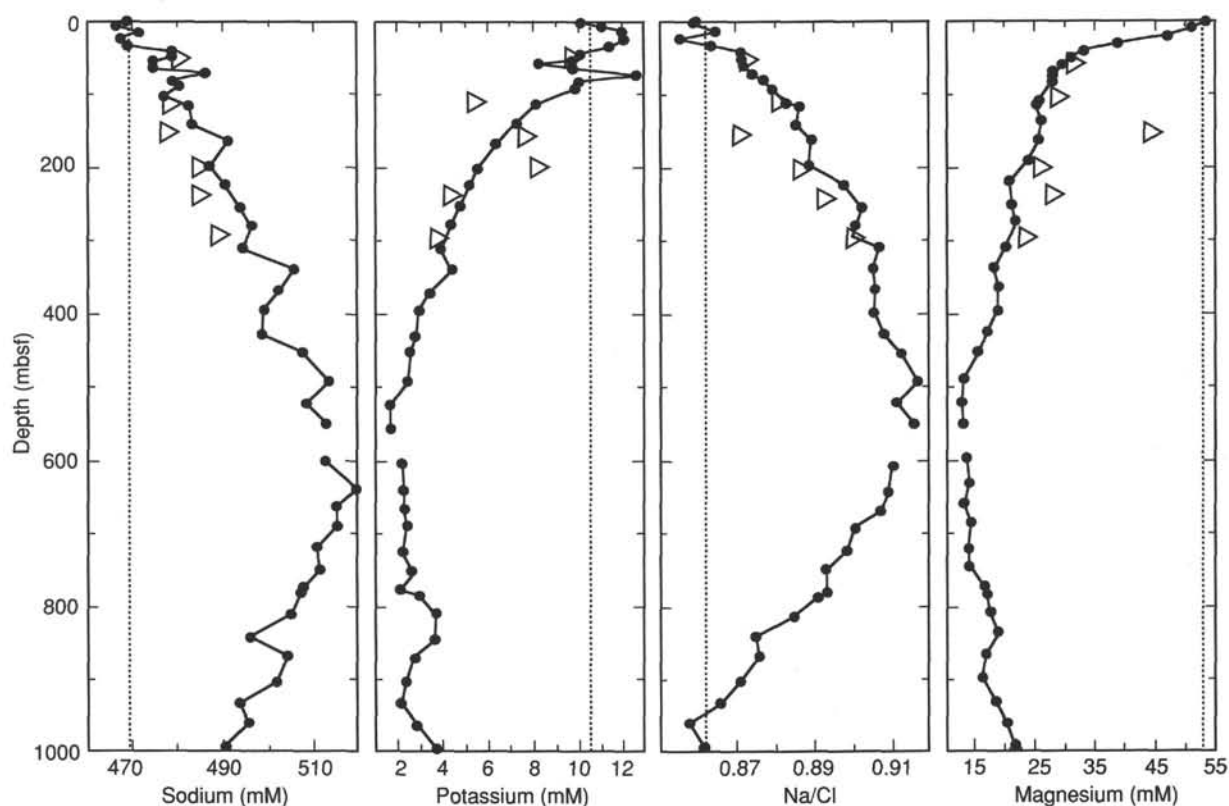


Figure 34. Sodium, potassium, Na/Cl, and magnesium as a function of depth for Site 823; open triangles are WSTP samples. The composition of seawater is indicated by the dotted line.

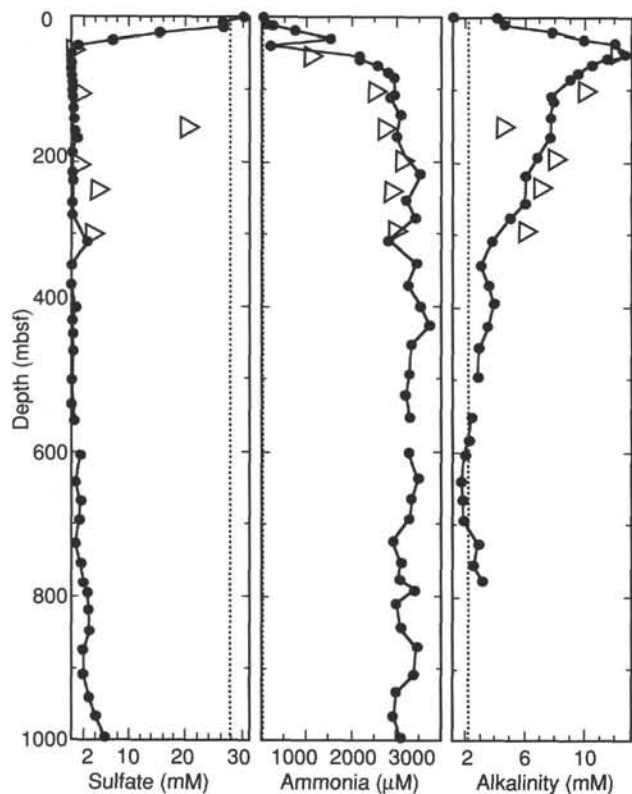


Figure 35. Concentrations of sulfate, ammonia, and alkalinity as a function of depth for Site 823; open triangles indicate WSTP samples. The composition of seawater is indicated by the dotted line.

mining concentrations of  $C_4-C_6$ ). Results of 133 headspace analyses and of 11 vacutainer samples from Site 823 are presented in Tables 5 and 6. Figure 38 shows the WSTP-temperature data from Sites 817, 820, 822, and 823 and the geothermal gradient used at Site 823 for interpreting depth-related evolution of the  $C_1/C_2$  ratio.

Sediments at Site 823 contained high concentrations of methane, which represented no safety and/or pollution hazards. The evolution of the  $C_1/C_2$  ratio with increasing depth and temperature showed no anomalous trend (Fig. 39), and values from headspace analyses ranged between 6,000 and 500 (normal to subnormal trends between 30° and 62°C).

Concentrations of headspace samples of methane were low in the sulfate-reduction zone (Fig. 40, see also "Inorganic Geochemistry" section, Fig. 35, this chapter), but increased rapidly below 50 mbsf. The observed coincidence between low concentrations of sulfate and high amounts of methane (>10,000 ppm) in the sediments suggests a bacterial origin of methane in the sulfate-free section (between 50 and 400 mbsf) of the sediments at Site 823 (Fig. 41).

Below 400 mbsf, the appearance of both ethane and propane (Fig. 40), and the decrease of the  $C_1/(C_2+C_3)$  values below 3000 at shallow depths and low temperatures (Fig. 41), are factors that clearly indicate the beginning of a mixing with thermogenic free hydrocarbons. The presence of the gas components ethane to iso-pentane (Fig. 40) indicates that the influence of thermogenic hydrocarbons was increasing in sediments below 700 mbsf, except in mixed or redeposited sediments (turbidites, slumps, and debris flows) of Unit VI (see also "Lithostratigraphy" section, this chapter).

By contrast, the increase in sulfate concentrations observed below 700 mbsf (see also "Inorganic Geochemistry" section, Fig. 35, this chapter) might have progressively re-

Table 3. Carbonate data for Site 823.

Core, section, interval (cm)	Depth (mbsf)	Carbonate (%)
133-823A-		
1H-1, 44-47	0.44	53.40
1H-3, 91-93	3.91	65.00
1H-3, 145-150	4.45	67.30
2H-1, 90-93	6.70	62.40
2H-3, 90-93	9.70	53.80
2H-5, 90-93	12.70	52.30
2H-5, 145-150	13.25	47.10
3H-1, 91-93	16.21	68.10
3H-3, 91-93	19.21	69.60
3H-5, 91-93	22.21	64.40
3H-5, 145-150	22.75	69.10
4H-1, 90-92	25.70	80.50
4H-3, 90-92	28.70	68.70
4H-5, 90-92	31.70	72.50
4H-5, 145-150	32.25	66.90
5H-1, 90-93	35.20	75.20
5H-3, 90-93	38.20	72.10
5H-5, 90-93	41.20	67.60
5H-5, 145-150	41.75	81.10
6H-1, 91-93	44.71	75.60
6H-3, 91-93	47.71	66.30
6H-5, 91-93	50.71	61.60
6H-5, 145-150	51.25	63.50
7H-1, 90-93	54.20	52.50
7H-3, 90-93	57.20	73.80
7H-5, 90-93	60.20	65.60
7H-5, 145-150	60.75	77.40
8H-1, 90-93	63.70	76.90
8H-3, 90-93	66.70	79.10
8H-5, 90-93	69.70	74.80
8H-5, 145-150	70.25	65.60
9H-1, 91-93	73.21	60.80
9H-3, 91-93	76.21	78.10
9H-5, 91-93	79.21	75.30
9H-5, 145-150	79.75	60.50
10H-1, 90-93	82.70	56.50
10H-3, 90-93	85.70	53.60
10H-5, 90-93	88.70	24.70
10H-5, 145-150	89.25	50.10
11H-1, 91-94	92.21	60.40
11H-3, 91-94	95.21	40.20
11H-5, 91-94	98.21	45.40
12H-1, 90-93	101.70	68.20
12H-1, 90-93	104.20	39.70
12H-3, 90-93	104.70	63.60
12H-3, 90-93	107.20	50.10
12H-5, 90-93	107.70	78.90
12H-5, 93-96	110.23	77.10
12H-5, 140-150	110.70	78.00
133-823B		
13X-1, 91-94	111.21	52.50
12X-7, 70-73	113.00	58.60
13X-1, 90-93	113.70	49.60
13X-3, 91-94	114.21	82.10
13X-3, 86-89	116.66	30.20
13X-5, 91-94	117.21	31.60
13X-5, 145-150	117.75	20.30
13X-5, 90-93	119.70	52.60
14X-1, 90-93	123.30	57.90
14X-3, 90-93	126.30	57.10
14X-5, 90-93	129.30	28.30
15X-1, 90-93	133.00	59.10
15X-3, 90-93	136.00	49.50
15X-5, 90-93	139.00	35.60
15X-5, 140-150	139.50	52.00
16X-1, 90-92	142.60	63.00
16X-3, 90-92	145.60	56.10
16X-5, 90-93	148.60	32.70
17X-1, 90-93	152.30	55.20
17X-3, 90-93	155.30	38.20
17X-5, 90-93	158.30	56.10
18X-1, 85-88	161.95	63.30
18X-3, 85-88	164.95	31.20
18X-3, 140-150	165.50	58.70
18X-5, 85-88	167.95	60.20
19X-1, 90-93	171.70	50.10

Table 3 (continued).

Core, section, interval (cm)	Depth (mbsf)	Carbonate (%)
19X-3, 90-93	174.70	46.10
19X-5, 90-93	177.70	46.70
20X-1, 90-93	181.40	51.30
20X-3, 90-93	184.40	56.40
21X-1, 90-93	191.10	62.90
21X-3, 90-93	194.10	61.30
21X-3, 140-150	194.60	63.60
21X-5, 90-93	197.10	67.80
22X-1, 90-93	200.70	56.80
22X-3, 90-93	203.70	68.80
22X-5, 90-93	206.70	68.50
23X-1, 90-93	210.00	65.10
23X-3, 90-93	213.00	62.30
23X-5, 90-92	216.00	68.10
24X-1, 90-92	219.60	57.10
24X-2, 140-150	221.60	62.80
24X-3, 90-92	222.60	62.90
24X-5, 90-92	225.60	61.30
25X-1, 90-93	228.90	55.60
25X-3, 90-93	231.90	36.80
25X-5, 90-93	234.90	35.90
26X-1, 90-92	238.60	45.50
26X-3, 90-92	241.60	62.10
26X-5, 90-92	244.60	65.10
27X-3, 90-93	250.42	62.20
27X-5, 90-93	253.42	60.10
27X-6, 140-150	255.42	67.50
27X-7, 90-93	256.42	61.60
28X-2, 90-92	259.40	61.80
28X-4, 90-92	262.40	61.60
28X-6, 90-92	265.40	61.10
29X-1, 90-92	267.60	58.10
29X-3, 90-92	270.60	58.10
29X-5, 90-92	273.60	66.20
30X-1, 91-93	277.21	68.10
30X-2, 140-150	279.20	56.50
30X-3, 91-93	280.21	59.10
30X-5, 91-93	283.21	50.90
31X-3, 91-92	288.97	45.90
31X-5, 91-92	291.97	58.40
31X-7, 91-92	294.97	53.20
32X-1, 90-93	296.50	70.00
32X-3, 90-93	299.50	51.60
32X-5, 90-93	302.50	78.40
33X-1, 90-93	306.20	59.40
33X-3, 90-93	309.20	37.50
33X-4, 140-150	311.20	50.00
34X-1, 90-93	315.80	56.70
34X-3, 90-93	318.80	49.90
34X-5, 93-96	321.83	80.40
35X-1, 100-102	325.60	58.10
35X-3, 100-102	328.60	67.40
35X-5, 100-102	331.60	72.60
36X-1, 100-104	335.20	57.00
36X-3, 96-100	338.16	74.30
36X-5, 96-99	341.16	60.70
36X-5, 140-150	341.60	64.80
37X-1, 90-93	344.80	55.50
37X-3, 90-93	347.80	70.30
37X-5, 90-93	350.80	77.50
38X-1, 90-92	354.30	40.90
38X-3, 97-99	356.79	56.70
38X-5, 97-99	359.79	53.90
39X-1, 72-75	363.72	42.10
39X-3, 72-75	366.72	62.80
39X-5, 72-75	369.72	78.40
39X-5, 140-150	370.40	73.70
40X-1, 100-103	373.70	52.20
40X-3, 100-103	376.70	48.80
40X-5, 100-103	379.70	44.50
41X-1, 100-103	383.40	62.10
41X-3, 100-103	386.40	51.50
41X-5, 100-103	389.40	66.00
42X-1, 100-103	393.00	53.50
42X-3, 100-103	396.00	35.50
42X-4, 140-150	397.90	26.20
42X-5, 100-103	399.00	31.60
43X-1, 100-102	402.60	44.40

Table 3 (continued).

Core, section, interval (cm)	Depth (mbsf)	Carbonate (%)
43X-3, 100-102	405.60	47.00
43X-5, 100-102	408.60	60.60
44X-1, 100-102	412.30	37.30
44X-3, 97-99	415.27	63.60
45X-1, 100-102	421.90	69.40
45X-3, 100-102	424.90	64.30
45X-5, 100-102	427.90	51.90
45X-5, 140-150	428.30	67.60
46X-1, 100-102	431.60	37.00
46X-3, 100-102	434.60	45.10
46X-5, 100-102	437.60	33.70
47X-1, 100-102	441.30	71.60
47X-3, 100-102	444.30	68.10
47X-5, 100-102	447.30	28.70
48X-1, 100-102	450.90	63.50
48X-3, 100-102	453.90	59.40
48X-4, 140-150	455.80	67.60
48X-5, 56-58	456.46	52.60
49X-1, 100-103	460.60	62.80
49X-3, 100-103	463.60	62.60
49X-5, 100-103	466.60	54.00
50X-1, 100-103	470.20	64.30
50X-3, 100-103	473.20	58.60
52X-1, 100-103	488.80	44.10
52X-3, 107-109	491.87	75.30
52X-4, 140-150	493.70	81.60
52X-5, 90-93	494.70	77.40
53X-1, 107-109	498.57	66.10
53X-3, 100-102	501.50	59.10
53X-5, 56-57	503.60	54.60
53X-7, 5-6	506.09	58.70
54X-1, 100-103	508.10	75.60
54X-3, 100-103	511.10	63.60
54X-5, 94-96	514.04	58.10
55X-1, 100-103	517.80	63.70
55X-3, 100-103	520.80	55.00
55X-5, 95-97	523.75	78.40
55X-5, 140-150	524.20	73.00
56X-1, 112-114	527.52	59.50
56X-3, 105-107	530.45	63.40
56X-5, 58-60	532.98	66.50
57X-1, 120-122	536.90	66.60
57X-3, 132-133	540.02	71.80
57X-5, 134-135	543.04	70.20
58X-1, 105-107	546.45	56.10
58X-3, 107-108	549.47	59.10
58X-5, 106-108	552.46	56.40
58X-5, 140-150	552.80	54.10
59X-1, 104-106	556.04	62.10
59X-3, 104-106	559.04	64.70
59X-5, 101-103	562.01	54.40
60X-1, 126-128	565.96	68.40
60X-3, 134-135	569.04	60.10
60X-5, 119-120	571.89	52.30
61X-1, 149-150	575.79	50.80
61X-3, 143-145	578.73	62.60
61X-5, 140-150	581.70	53.70
61X-5, 149-150	581.79	54.80
62X-1, 146-149	585.36	32.20
62X-3, 146-149	588.36	50.40
62X-5, 146-149	591.36	71.40
63X-1, 144-149	595.04	66.80
63X-3, 144-149	598.04	77.50
63X-5, 144-149	601.04	64.00
64X-1, 135-150	604.55	66.00
64X-2, 137-140	606.07	72.60
64X-4, 141-144	609.11	70.90
65X-1, 144-147	614.24	71.10
65X-3, 144-147	617.24	69.70
65X-5, 144-147	620.24	74.20
66X-1, 100-102	623.50	76.00
66X-3, 100-102	626.50	67.00
66X-5, 100-102	629.50	65.10
67X-1, 115-118	633.35	83.50
67X-3, 56-58	635.76	65.10
67X-5, 57-59	638.77	48.70
67X-5, 135-150	639.55	60.60
68X-1, 49-52	642.09	50.70

Table 3 (continued).

Core, section, interval (cm)	Depth (mbsf)	Carbonate (%)
68X-3, 63-66	645.23	51.60
68X-5, 81-84	648.41	51.40
69X-1, 57-59	651.47	78.70
69X-3, 109-111	654.99	80.10
69X-5, 72-75	657.62	84.60
70X-1, 146-147	662.06	74.50
70X-3, 146-147	665.11	59.20
70X-5, 135-150	668.00	56.10
70X-6, 146-147	669.61	66.10
71X-1, 84-86	671.14	83.10
71X-3, 86-89	674.16	80.40
71X-5, 81-84	677.11	85.00
72X-1, 87-90	680.77	57.60
72X-3, 114-116	684.04	52.80
72X-5, 79-81	686.69	38.10
73X-1, 124-125	690.84	58.40
73X-3, 70-71	693.30	45.60
73X-4, 135-150	695.45	58.30
73X-5, 53-55	696.13	72.20
74X-1, 93-94	700.23	68.60
74X-3, 82-84	703.12	54.40
74X-5, 59-60	705.89	79.30
75X-1, 80-83	709.70	56.50
75X-3, 80-83	712.70	64.10
75X-5, 80-83	715.70	46.40
76X-1, 125-127	719.85	52.90
76X-3, 125-127	722.85	31.00
76X-4, 135-150	724.45	34.20
76X-5, 125-127	725.85	30.30
77X-1, 142-143	729.62	62.90
77X-3, 133-135	732.53	46.20
77X-5, 140-142	735.60	45.10
78X-1, 129-131	739.19	78.10
78X-2, 129-131	740.69	47.20
78X-3, 129-131	742.19	49.60
79X-1, 148-149	749.08	47.80
79X-2, 146-148	750.56	42.80
79X-3, 142-144	752.02	45.20
79X-4, 135-150	753.45	47.60
79X-5, 136-138	754.96	36.10
80X-1, 143-145	758.73	30.70
80X-3, 142-144	761.72	32.80
80X-5, 138-140	764.68	32.70

Table 3 (continued).

Core, section, interval (cm)	Depth (mbsf)	Carbonate (%)
81X-1, 146-149	768.46	34.30
81X-3, 146-149	771.46	35.10
81X-5, 146-149	774.46	40.70
82X-1, 134-135	778.04	55.60
82X-1, 135-150	778.05	62.10
82X-2, 134-135	779.54	61.80
82X-3, 134-135	781.04	51.90
823C-1R-1, 101-102	785.01	60.90
823C-1R-3, 22-23	787.22	53.40
823B-83X-1, 144-146	787.84	61.10
823C-1R-3, 130-150	788.30	70.60
823B-83X-2, 130-132	789.20	58.00
823C-1R-5, 29-31	790.29	71.10
823B-83X-3, 130-132	790.70	38.70
823C-2R-1, 85-87	794.45	65.80
2R-3, 149-150	798.09	91.90
3R-1, 121-123	804.11	87.00
3R-3, 14-16	806.04	96.60
4R-1, 28-30	812.88	86.20
4R-1, 130-150	813.90	64.60
4R-3, 100-102	816.60	87.90
5R-1, 8-10	822.38	74.10
5R-3, 97-99	826.27	78.90
5R-5, 109-110	829.39	56.70
6R-1, 36-38	832.36	78.50
6R-1, 127-128	833.27	64.40
6R-2, 10-13	833.60	91.30
7R-1, 7-9	841.77	90.80
7R-2, 130-150	844.50	45.30
7R-3, 10-11	844.80	95.10
7R-5, 120-122	848.90	92.00
8R-1, 75-77	852.15	91.00
9R-1, 73-74	861.83	25.80
9R-3, 124-127	865.34	66.00
9R-5, 118-119	868.28	27.60
10R-1, 38-40	871.18	32.30
10R-1, 130-150	872.10	70.40
10R-3, 50-52	874.30	19.30
10R-5, 140-143	878.20	61.10
11R-1, 78-79	881.18	92.60
11R-3, 83-85	884.23	72.60
11R-5, 84-86	887.24	46.10
12R-1, 86-87	890.96	48.60

Table 3 (continued).

Core, section, interval (cm)	Depth (mbsf)	Carbonate (%)
12R-3, 121-123	894.31	84.20
12R-5, 53-56	896.63	72.10
13R-1, 60-62	900.30	56.60
13R-3, 61-63	902.80	95.60
13R-4, 130-150	904.99	62.30
13R-5, 41-43	905.60	28.90
14R-1, 108-110	910.48	72.80
14R-3, 103-105	913.43	56.60
14R-5, 132-134	916.72	80.70
15R-1, 23-25	919.33	76.40
15R-3, 9-10	922.19	48.20
15R-5, 43-44	925.53	32.20
16R-1, 52-54	929.32	53.70
16R-3, 86-88	932.66	53.10
16R-4, 130-150	934.60	27.80
16R-5, 123-124	936.03	54.40
17R-1, 62-64	939.02	59.10
17R-3, 40-42	941.80	59.60
17R-5, 5-6	944.45	72.60
17R-7, 20-22	947.60	81.10
18R-1, 96-98	948.96	85.70
18R-3, 79-81	951.79	31.00
18R-5, 111-113	955.11	52.30
19R-1, 113-115	958.43	71.80
19R-3, 110-111	961.40	38.70
19R-3, 130-150	961.60	28.60
19R-5, 33-34	963.63	51.00
20R-1, 80-81	967.70	19.70
20R-3, 57-58	970.47	45.80
20R-5, 69-70	973.59	28.70
21R-1, 134-136	977.94	41.20
21R-3, 94-95	980.54	66.50
21R-5, 20-21	982.80	32.60
22R-1, 85-86	987.05	19.00
22R-3, 1-3	989.21	48.20
22R-3, 120-136	990.40	30.20
22R-5, 83-84	993.03	22.50
23R-1, 93-94	996.83	27.00
23R-3, 58-60	999.48	47.80
23R-5, 117-119	1003.07	60.10
24R-1, 117-119	1006.77	60.00
24R-3, 38-39	1008.98	31.70

duced the activity of the methane-producing bacteria and the beginning of the decrease in methanogenesis (at approximately 60°C) seem to be indicated by additional factors (Figs. 41, 42, and 43) as follows:

1. A sharp decrease in both the  $C_1/(C_2 + C_3)$  and  $C_2/C_3$  ratios observed below 960 mbsf resulting from a sharp decrease in concentrations of both methane and ethane in sediments.

2. Higher total organic contents observed below 900 mbsf in the clayey sediments of Unit VII, probably the result of better preservation of organic matter from degradation by sulfate-reducing bacteria.

On the basis of gas composition and gas ratios (i.e., predominance of iso-alkanes vs. normal-alkanes, Figs. 40, and 42), we think that the hydrocarbons detected in two major mixing zones (between 700 and 770 mbsf and below 940 mbsf) were generated from kerogens that reached a maturity stage at the onset of the "oil window" (0.5% vitrinite reflectance).

#### Organic Carbon Contents

Total organic carbon (TOC) contents together with total nitrogen and sulfur concentrations recorded in Site 823 are presented in Table 6.

Values of organic carbon at Site 823 were very low to low, not exceeding 0.55% TOC (Fig. 43). In all lithologic units, where bioclastic turbidites have been interbedded

with more pelagic sediments, TOC contents showed short-term variations with relatively high amplitudes (between 0% and 0.55%) that correspond to lithological changes. Higher values for organic contents were observed below 900 mbsf in the clayey-rich sediments of Unit VII (see also "Lithostratigraphy" section, this chapter). The low sedimentation rates observed in this unit (approximately 26 m/m.y., see also "Biostratigraphy" section, this chapter) we think indicates better preservation of organic matter in these sediments, probably the result of a progressive decrease in the activity of sulfate-reducing bacteria with increasing temperatures.

Concentrations of total sulfur in these sediments showed cyclic changes that ranged between 0% and 0.8%. Average values increased in the sulfate-free section below 50 mbsf and decreased below 640 mbsf (Fig. 43).

Concentrations of total nitrogen in these sediments were very low, ranged between 0% and 0.04%, increased with depth, and followed the trend of both organic carbon and clay contents in these sediments (Fig. 43).

On the basis of TOC/nitrogen ratios (Fig. 43), organic matter we encountered at Site 823 may be a mixing of terrestrial with marine organic materials. The coincidence between increasing organic carbon and nitrogen contents in clayey sediments also indicates better preservation of the marine and labile organic fractions in the sediments having the finest grain size. As a consequence of low organic contents,

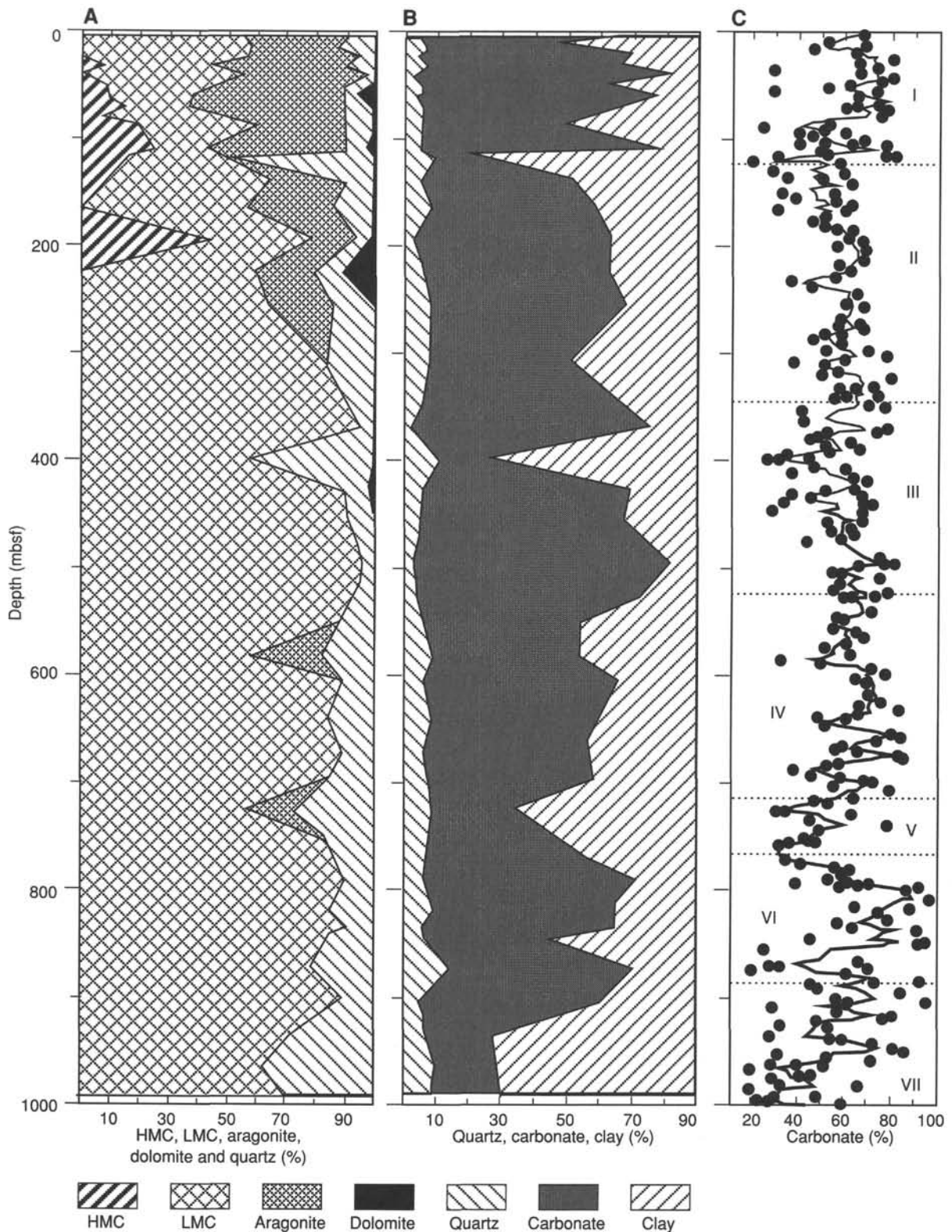


Figure 36. X-ray diffraction and carbonate data for Site 823. In graph (A) it is assumed that the sediment is composed entirely of calcite, aragonite, quartz, and dolomite. Percentages of clay, carbonate, and quartz (B) are then calculated using X-ray diffraction data and percentage of carbonate (C).

Table 4. X-ray diffraction data for Site 823.

Core, section, interval (cm)	Depth (mbsf)	Calcite (%)	Aragonite (%)	Quartz (%)	Dolomite (%)
133-823A-					
1H-3, 145-150	4.45	55.3	36.9	7.3	0.4
2H-5, 145-150	13.25	57.6	27.5	14.9	0.0
3H-5, 145-150	22.75	57.9	35.2	6.9	0.0
4H-5, 145-150	32.25	46.5	43.4	10.1	0.0
5H-5, 145-150	41.75	57.3	40.2	2.6	0.0
6H-5, 145-150	51.25	45.8	43.9	9.5	0.9
7H-5, 145-150	60.75	37.8	52.1	4.5	5.7
8H-5, 140-150	70.20	37.2	53.5	9.3	0.0
9H-5, 140-150	79.70	52.3	38.4	9.3	0.0
10H-5, 140-150	89.20	59.9	28.9	11.1	0.0
823B-12H-5, 140-150	110.70	44.4	46.1	7.0	2.5
823A-13H-5, 90-95	117.20	50.8	0.0	49.2	0.0
823B-15X-5, 140-150	139.20	64.7	25.1	10.2	0.0
823B-18X-3, 140-150	165.50	57.5	27.4	15.0	0.0
823C-21X-3, 140-150	194.60	78.8	15.6	4.9	0.8
133-823B-					
24X-4, 140-150	224.60	59.8	19.8	10.7	9.8
27X-6, 140-150	256.20	64.7	21.4	13.8	0.0
33X-4, 140-150	308.70	83.8	0.0	16.2	0.0
36X-5, 140-150	341.60	90.0	0.0	10.0	0.0
39X-4, 140-150	368.90	96.2	0.0	3.8	0.0
42X-4, 140-150	397.90	58.0	0.0	42.0	0.0
45X-5, 140-150	428.30	90.0	0.0	8.1	1.9
48X-4, 140-150	455.80	91.3	0.0	8.7	0.0
52X-5, 140-150	495.10	96.5	0.0	3.3	0.2
55X-5, 140-150	524.20	93.9	0.0	6.1	0.0
58X-5, 140-150	552.80	87.6	0.0	12.4	0.0
61X-5, 135-150	581.65	59.6	22.1	18.4	0.0
64X-1, 135-150	604.55	90.4	0.0	9.6	0.0
67X-5, 135-150	639.55	84.7	0.0	15.3	0.0
70X-5, 135-150	667.95	89.2	0.0	10.4	0.4
73X-4, 135-150	695.45	85.2	0.0	14.3	0.5
76X-4, 135-150	724.45	57.7	15.3	27.0	0.0
79X-4, 135-150	753.45	83.9	0.0	16.1	0.0
82X-1, 135-150	778.05	89.4	0.0	10.6	0.0
133-823C-					
1R-3, 130-150	788.30	91.3	0.0	8.7	0.0
4R-1, 130-150	813.90	84.8	0.0	15.2	0.0
6R-1, 127-128	833.27	91.1	0.0	8.9	0.0
7R-2, 130-150	844.50	83.9	0.0	16.1	0.0
10R-1, 130-150	872.10	78.2	0.0	21.8	0.0
13R-1, 130-150	901.00	90.5	0.0	9.5	0.0
16R-4, 130-150	934.60	71.5	0.0	27.7	0.8
823C-19R-3, 130-150	961.60	63.2	0.0	36.8	0.0
823C-22R-3, 130-150	990.50	70.4	0.0	29.6	0.0

we were unable to conduct detailed geochemical characterization of kerogen types using the Rock-Eval pyrolysis method as originally planned.

## PHYSICAL PROPERTIES

### Index Properties

Six physical-property units were identified in terms of data from Holes 823A, 823B, and 823C (Tables 7 through 11; Figs. 44 through 50). These units are (1) Unit A (0–80 mbsf), (2) Unit B (80–330 mbsf), (3) Unit C (330–540 mbsf), (4) Unit D (540–750 mbsf), (5) Unit E (750–850 mbsf), and (6) Unit F (850–1000 mbsf). Unit A (0–80 mbsf) consists of nannofossil ooze showing significant changes in index properties. Bulk densities increase with depth from 1.53 to 2.0 g/cm<sup>3</sup> at a rate of 0.18 g/cm<sup>3</sup>/100 m over the top 80-m interval. Grain densities remain relatively constant and have an average value of 2.79 ± 0.09 g/cm<sup>3</sup>. A decrease down the hole in porosity and water contents with normal compaction trends was observed. Earlier porosity values range from 74% near the seafloor to near 50% at 80 mbsf, with a decreasing rate of 12%/100 m. Water

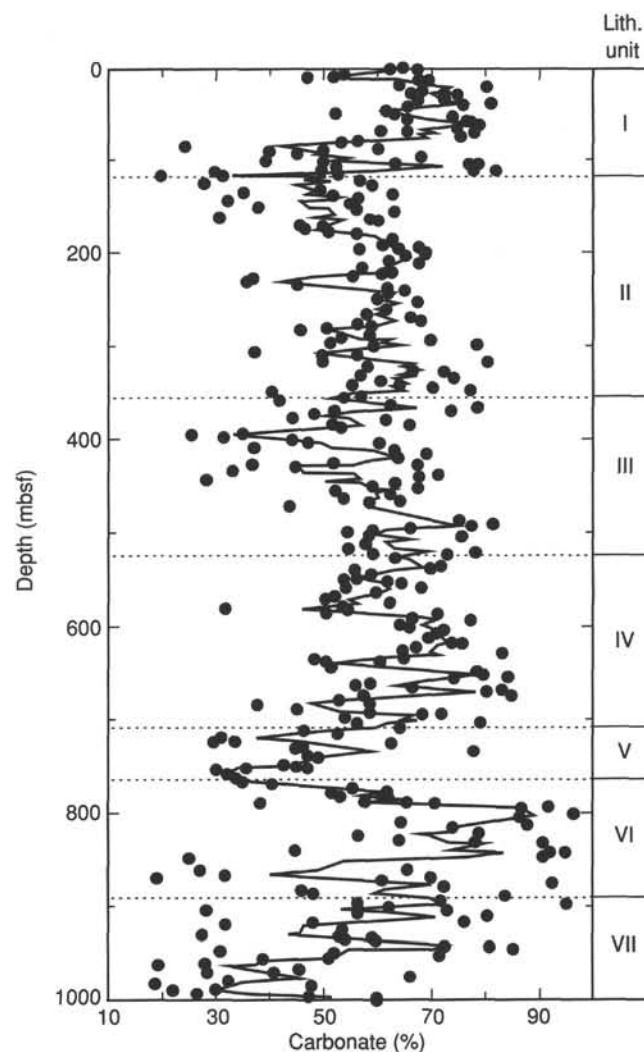


Figure 37. Percent carbonate data for Sites 823. Lithologic units are shown for comparison.

contents range from about 98% to 38%, with a decreasing rate of 28%/100 m for the same interval.

Unit B (80–330 mbsf) consists predominantly of gravity-flow deposits with nannofossil clay mixed sediments to nannofossil micritic ooze. Index property data show considerable variability, but remain relatively constant with depth. Bulk density remains 1.9 ± 0.06 g/cm<sup>3</sup>. Grain densities decrease slightly to 2.76 ± 0.07 g/cm<sup>3</sup> for this unit. In addition, porosity remains at 55.7 ± 3.2%, and water content at 45.1 ± 5.7%.

Unit C (330–540 mbsf) consists predominantly of gravity-flow deposits, with sediments showing a much higher degree of compaction. Gravity-flow deposits alternate with claystone, chalk, and sandstone. Index property data exhibit lesser variability than those in Unit B. The average value of bulk density increases slightly to 1.93 ± 0.07 g/cm<sup>3</sup>. Grain densities decrease slightly to 2.75 ± 0.08 g/cm<sup>3</sup>. General compaction trends again were observed in porosity and water content data, but to a lesser extent than those observed for Unit A. Porosity decreases from approximately 58% to 50%, with a decreasing rate of 4%/100 m. Water contents range

Table 5. Volatile hydrocarbon data from headspace and vacutainer analyses at Site 823.

Core, section, interval (cm)	Depth (mbsf)	Sample	Volume (mL)	Gas chromatograph	C <sub>1</sub> (ppm)	C <sub>2</sub> (ppm)	C <sub>3</sub> (ppm)	C <sub>1</sub> /C <sub>2</sub>	C <sub>1</sub> /(C <sub>2</sub> + C <sub>3</sub> )	C <sub>2</sub> /C <sub>3</sub>
133-823A-										
1H-3, 149-150	4.49	HS	5	CAR132	3	0	0			
2H-5, 149-150	13.29	HS	5	CAR132	3	0	0			
3H-5, 149-150	22.79	HS	5	CAR132	3	0	0			
4H-5, 149-150	32.29	HS	5	CAR132	5	0	0			
5H-5, 149-150	41.79	HS	5	CAR132	62	0	0			
6H-5, 149-150	51.29	HS	5	CAR132	9,756	0	0			
823B-6H-5, 149-150	53.79	HS	5	CAR132	25,403	0	0			
823A-7H-5, 149-150	60.79	HS	5	CAR132	49,709	0	0			
823B-7H-7, 69-70	65.49	HS	5	CAR132	61,157	0	0			
823A-8H-5, 149-150	70.29	HS	5	CAR132	51,757	0	0			
823A-9H-5, 149-150	79.79	HS	5	CAR132	54,472	0	0			
823B-9H-5, 149-150	82.29	HS	5	CAR132	50,776	0	0			
823A-10H-5, 145-146	89.25	HS	5	CAR132	45,328	0	0			
823B-10H-7, 65-66	93.95	HS	5	CAR132	46,893	0	0			
823A-11H-5, 149-150	98.79	HS	5	CAR132	25,445	0	0			
823B-12H-7, 62-63	112.92	HS	5	CAR132	26,454	0	0			
823A-13H-7, 78-80	120.08	HS	5	CAR132	22,490	0	0			
133-823B-										
13X-6, 57-58	120.87	HS	5	CAR132	8,542	0	0			
14X-1, 149-150	123.89	HS	5	CAR132	62,758	0	0			
47X-4, 149-150	446.29	HS	5	CAR132	5,693	3	3	1898	949	1.0
48X-4, 149-150	455.89	HS	5	CAR132	8,325	5	6	1665	757	0.8
49X-4, 149-150	465.59	HS	5	CAR132	38,384	7	7	5483	2742	1.0
50X-2, 149-150	472.19	HS	5	CAR132	57,409	10	7	5741	3377	1.4
52X-4, 149-150	493.79	HS	5	CAR132	33,317	6	5	5553	3029	1.2
53X-3, 149-150	501.99	HS	5	CAR132	32,595	8	8	4074	2037	1.0
54X-2, 149-150	510.09	HS	5	CAR132	6,573	4	4	1643	822	1.0
55X-5, 140-141	524.2	HS	5	CAR132	73,470	17	15	4322	2296	1.1
56X-3, 0-1	529.4	HS	5	CAR132	46,533	14	23	3324	1258	0.6
57X-2, 149-150	538.69	HS	5	CAR132	33,666	7	8	4809	2244	0.9
58X-5, 149-150	552.89	HS	5	CAR132	48,509	11	11	4410	2205	1.0
60X-6, 0-1	572.2	HS	5	CAR132	4,033	5	12	807	237	0.4
61X-5, 149-150	581.79	HS	5	CAR132	50,684	16	29	3168	1126	0.6
62X-3, 149-150	588.39	HS	5	CAR132	9,551	5	6	1910	868	0.8
64X-1, 149-150	604.69	HS	5	CAR132	39,788	10	10	3979	1989	1.0
65X-5, 149-150	620.29	HS	5	CAR132	46,645	12	11	3887	2028	1.1
66X-4, 149-150	628.49	HS	5	CAR132	42,485	11	10	3862	2023	1.1
67X-5, 149-150	639.69	HS	5	CAR132	7,822	8	14	978	356	0.6
68X-1, 0-1	641.6	HS	5	CAR132	2,988	4	8	747	249	0.5
69X-5, 149-150	658.39	HS	5	CAR132	30,271	9	8	3363	1781	1.1
70X-5, 115-116	667.8	HS	5	CAR132	44,850	12	11	3738	1950	1.1
71X-5, 149-150	677.79	HS	5	CAR132	50,458	11	7	4587	2803	1.6
72X-5, 149-150	687.39	HS	5	CAR132	58,046	14	10	4146	2419	1.4
73X-2, 148-149	692.58	HS	5	CAR132	52,370	14	11	3741	2095	1.3
74X-5, 149-150	706.79	HS	5	CAR132	32,665	8	5	4083	2513	1.6
76X-4, 149-150	724.59	HS	5	CAR132	32,545	25	39	1302	509	0.6
77X-3, 148-149	732.68	HS	5	CAR132	58,871	22	17	2676	1510	1.3
77X-7, 41-43	737.61	HS	5	CAR132	8,624	9	9	958	479	1.0
78X-2, 149-150	740.89	HS	5	CAR132	53,253	17	11	3133	1902	1.5
79X-6, 0-1	755.1	HS	5	CAR132	35,236	14	9	2517	1532	1.6
80X-4, 149-150	763.29	HS	5	CAR132	47,133	22	14	2142	1309	1.6
81X-3, 148-149	771.48	HS	5	CAR132	59,091	23	8	2569	1906	2.9
82X-1, 148-149	778.18	HS	5	CAR132	7,118	9	4	791	548	2.3
83X-1, 148-149	787.88	HS	5	CAR132	9,634	10	0	963	963	
133-823C-										
1R-3, 130-131	788.3	HS	5	CAR132	19,775	9	0	2197	2197	
2R-2, 0-1	795.1	HS	5	CAR132	78,703	35	0	2249	2249	
3R-2, 0-1	804.4	HS	5	CAR132	42,289	12	0	3524	3524	
4R-4, 148-149	818.58	HS	5	CAR132	73,808	36	0	2050	2050	
5R-4, 0-1	826.8	HS	5	CAR132	58,257	18	0	3237	3237	
6R-2, 0-1	833.5	HS	5	CAR132	46,734	16	0	2921	2921	
7R-2, 130-131	844.5	HS	5	CAR132	60,103	28	0	2147	2147	
8R-1, 0-2	851.4	HS	5	CAR132	13,313	10	0	1331	1331	
9R-5, 149-150	868.59	HS	5	CAR132	9,808	9	0	1090	1090	
10R-5, 148-150	878.28	HS	5	CAR132	7,380	6	0	1230	1230	
12R-2, 148-150	893.08	HS	5	CAR132	52,384	16	0	3274	3274	
13R-7, 6-10	908.25	HS	5	CAR132	52,644	29	7	1815	1462	4.1
15R-2, 149-150	922.09	HS	5	CAR132	46,061	18	3	2559	2193	6.0
16R-4, 149-150	934.79	HS	5	CAR132	54,922	38	13	1445	1077	2.9
17R-3, 0-1	941.4	HS	5	CAR132	64,369	30	6	2146	1788	5.0
17R-4, 0-1	942.9	HS	5	CAR132	51,218	23	4	2227	1897	5.8
19R-3, 149-150	961.79	HS	5	CAR132	82,373	78	52	1056	634	1.5
20R-1, 0-1	966.9	HS	5	CAR132	26,805	27	29	993	479	0.9
20R-6, 148-149	975.88	HS	5	CAR132	56,956	33	29	1726	919	1.1
21R-3, 1-2	979.61	HS	5	CAR132	29,878	17	17	1758	879	1.0
21R-6, 95-97	985.05	HS	5	CAR132	17,136	18	25	952	399	0.7
22R-3, 133-134	990.53	HS	5	CAR132	45,327	37	57	1225	482	0.6
23R-3, 1-2	998.91	HS	5	CAR132	24,844	16	17	1553	753	0.9
23R-6, 1-2	1003.41	HS	5	CAR132	8,089	10	10	809	404	1.0
24R-1, 0-1	1005.6	HS	5	CAR132	33,064	22	26	1503	689	0.8
24R-2, 148-149	1008.58	HS	5	CAR132	42,666	32	46	1333	547	0.7

HS = headspace sample.

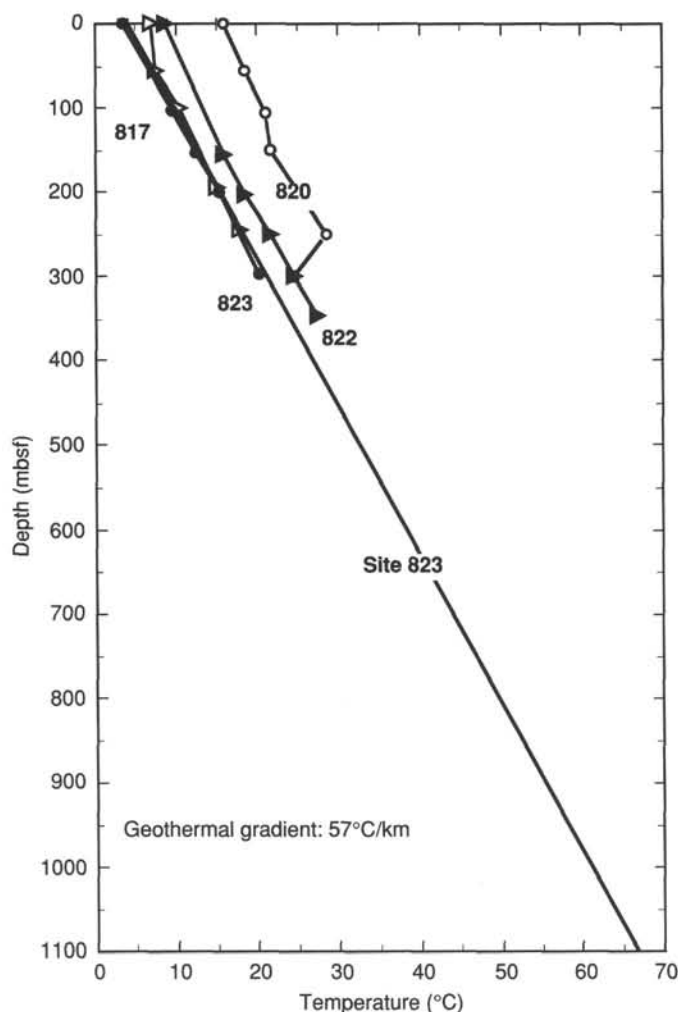


Figure 38. Geothermal gradient and WSTP-temperature data from Sites 817, 820, 822, and 823.

from approximately 45% to 30%, with a decreasing rate of 12%/100 m.

Unit D (540–750 mbsf) consists of gravity-flow deposits and mixed sediments to nannofossil chinks with foraminifers. The common occurrence of coarse-grained quartz results in significant changes in grain density. The same uniform compaction trends as seen in Unit C were still observed. The average value of bulk density increases considerably to  $2.07 \pm 0.05 \text{ g/cm}^3$ . Grain densities decrease distinctively to  $2.7 \pm 0.06 \text{ g/cm}^3$ , probably the result of an increase in quartz contents. Values for porosity and water content remain similar to the decreasing rate in Unit C.

Unit E (750–850 mbsf) consists of nannofossil chinks, calcareous packstones, and floatstones to mudstones, with sediments showing a much higher degree of lithification. The general lithology of this unit is homogeneous nannofossil or micritic ooze deposits intercalated with coarse and cemented terrestrial sand. A distinctly independent compaction trend was observed (i.e., increasing bulk density and corresponding decrease in porosity and water contents). Bulk density increases from approximately 2.1 to a value of  $2.3 \text{ g/cm}^3$ , with an increasing rate of  $0.2 \text{ g/cm}^3/100 \text{ m}$ . Porosity decreases from approximately 40% to 30%, with a decreasing rate of 11%/100 m, which represents almost double that measured in Units C and D. Water contents decrease from approximately 25% to 15%, with a decreasing

rate of 10%/100 m. Grain densities remain around  $2.7 \pm 0.04 \text{ g/cm}^3$ .

Unit F (850–1000 mbsf) has a similar lithology to Unit E, but with increasing clay contents. High clay contents at the top of this unit exhibit relatively low bulk densities and high porosities and water content. Consequently, Unit F exhibits an exaggerated compaction cyclicity compared to Unit E. Grain densities increase slightly to  $2.71 \pm 0.06 \text{ g/cm}^3$ . An increasing trend was observed for bulk density, with values going from approximately 2.0 to  $2.3 \text{ g/cm}^3$ , with a rate of  $0.16 \text{ g/cm}^3/100 \text{ m}$ . Porosities decrease from approximately 40% to 25%, with a decreasing rate of 11%/100 m. In addition, water content values decrease from 40% to 10%, with a decreasing rate of 20%/100 m for the unit.

### P-Wave Velocity

Compressional wave velocity, as determined with the Hamilton frame apparatus, was measured at the top 85 mbsf only. Below 85 mbsf, we could not detect a 500-kHz compressional wave signal because of the occurrence of gas in the sediments. Velocity values exhibit a variation between 1.45 and 1.66 km/s (Fig. 48). A series of high-velocity peaks were observed that are associated with the presence of turbidites.

### Vane Shear Strength

Values of undrained shear strength for Hole 823B were obtained using a four-bladed vane shear apparatus for samples taken from APC and XCB cores. The resulting shear strengths have been plotted relative to depth in Figure 49.

The uppermost 80-m section indicates a gradual increase in shear strength with depth, with an increasing rate of about 0.56 kPa/m. As described above, Unit A consists primarily of a calcareous ooze. Thus, an increasing trend is the result of normal compaction. A series of high shear-strength peaks are associated with these turbidites. From 80 mbsf to the last sample tested at 195.43 mbsf, data show considerable variability. This is because of the presence of turbidite and debris-flow sequences.

### Thermal Conductivity

Values of thermal conductivity indicate a general increasing trend at the top 80-m section, from approximately 0.9 to  $1.3 \text{ W/m} \cdot \text{K}$  (Fig. 50). From 80 to 313 mbsf, thermal conductivities exhibit greater variations, but remain relatively constant with depth, with a mean value about  $1.08 \text{ W/m} \cdot \text{K}$ . A noticeable low value ( $0.61 \text{ W/m} \cdot \text{K}$ ) at 216 mbsf probably is associated with a high water-content zone.

### Conclusions

Sediment index properties, compressional wave velocities, vane shear strengths, and thermal conductivities allow one to characterize sediments at Site 823 into six physical-property units. Unit A extends from the seafloor to 80 mbsf and consists predominantly of calcareous ooze having a high water content. Physical properties change significantly with depth, but are consistent with normal compaction trends. Turbidites and debris flows occur in Units B through F and exhibit significantly different compaction trends related to compositional differences. Physical properties data exhibit considerable variability through most of these units. Bulk densities do not vary with depth in Units B, C, and D, but exhibit a stepped increase. A normal compaction trend reappears again in Units C and D, whereas grain densities are much less in Unit D. Units E and F exhibit independent, normal compaction trends, with average grain density remaining around  $2.7 \text{ g/cm}^3$ . Physical-property unit boundaries among these five units almost correlate with reflectors observed in seismic profiles.

Table 6. Hydrocarbon data from headspace and vacutainer samples, Site 823.

Core, section, interval (cm)	Depth (mbsf)	Sample	Volume (mL)	Gas chromat.	C <sub>1</sub> (ppm)	C <sub>2</sub> (ppm)	C <sub>3</sub> (ppm)	I-C <sub>4</sub> (ppm)	N-C <sub>4</sub> (ppm)	I-C <sub>5</sub> (ppm)	C <sub>1</sub> /C <sub>2</sub>	C <sub>1</sub> /(C <sub>2</sub> +C <sub>3</sub> )	C <sub>2</sub> /C <sub>3</sub>	C <sub>3</sub> /C <sub>4</sub> +	i-C <sub>4</sub> /n-C <sub>4</sub>	C <sub>4</sub> /C <sub>5</sub>
133-823B-																
15X-5, 149-150	139.59	HS	5	GC1	28,539	0	0	0	0	0						
16X-3, 149-150	146.19	HS	5	GC1	16,860	0	0	0	0	0						
17X-1, 149-150	152.89	HS	5	GC1	27,112	0	0	0	0	0						
18X-3, 149-150	165.59	HS	5	GC1	29,142	0	0	0	0	0						
19X-5, 149-150	178.29	HS	5	GC1	42,516	0	0	0	0	0						
20X-4, 149-150	186.49	HS	5	GC1	11,882	0	0	0	0	0						
21X-3, 149-150	194.69	HS	5	GC1	21,107	0	0	0	0	0						
22X-5, 149-150	207.29	HS	5	GC1	31,628	0	0	0	0	0						
23X-5, 149-150	216.59	HS	5	GC1	31,197	0	0	0	0	0						
24X-2, 149-150	221.69	HS	5	GC1	12,912	0	0	0	0	0						
27X-6, 149-150	255.51	HS	5	GC1	4,684	0	0	0	0	0						
28X-5, 0-2	263	HS	5	GC1	33,772	0	0	0	0	0						
29X-5, 149-150	274.19	HS	5	GC1	29,424	0	0	0	0	0						
30X-6, 62-63	284.42	HS	5	GC1	7,178	0	0	0	0	0						
31X-6, 149-150	294.05	HS	5	GC1	21,035	0	0	0	0	0						
32X-2, 149-150	298.59	HS	5	GC1	10,410	0	0	0	0	0						
33X-4, 149-150	311.29	HS	5	GC1	11,188	0	0	0	0	0						
34X-5, 0-2	320.9	HS	5	GC1	9,383	0	0	0	0	0						
35X-4, 149-150	330.59	HS	5	GC1	10,844	0	0	0	0	0						
36X-5, 140-141	341.6	HS	5	GC1	6,654	0	0	0	0	0						
38X-6, 149-150	361.81	HS	5	GC1	16,830	0	8	0	0	0		2104				
39X-5, 140-141	370.4	HS	5	GC1	3,536	0	0	0	0	0						
40X-2, 149-150	375.69	HS	5	GC1	11,656	0	0	0	0	0						
41X-4, 149-150	388.39	HS	5	GC1	16,357	0	4	0	0	0		3271				
42X-4, 149-150	397.99	HS	5	GC1	26,482	0	10	0	0	4	0	2648		2.5		
43X-4, 149-150	407.59	HS	5	GC1	5,675	0	4	0	0	0		1419				
44X-5, 0-2	417.3	HS	5	GC1	13,467	0	9	0	0	0	0	1496				
45X-5, 149-150	428.39	HS	5	GC1	9,340	0	4	0	0	0		2335				
46X-5, 149-150	438.09	HS	5	GC1	21,370	0	12	0	0	0		1781				
68X-4, 1-2	646.11	HS	5	GC1	2,519	0	10	0	0	0		252				
76X-4, 148-149	724.58	HS	5	GC1	20,951	13	42	5	4	14	1612	381	0.3	1.8	1.3	0.6
77X-3, 149-150	732.69	HS	5	GC1	18,661	5	15	0	0	4	3732	933	0.3	3.8		
77X-7, 42-43	737.62	HS	5	GC1	8,751	3	11	0	0	0	2917	625	0.3			
78X-2, 148-149	740.88	HS	5	GC1	33,914	10	20	0	0	5	3391	1130	0.5	4.0		
79X-6, 0-2	755.1	HS	5	GC1	18,615	7	14	0	0	4	2659	886	0.5	3.5		
80X-4, 148-149	763.28	HS	5	GC1	26,614	10	15	0	0	4	2661	1065	0.7	3.8		
81X-3, 149-150	771.49	HS	5	GC1	19,193	7	10	7	0	0	2742	1129	0.7	1.4		
82X-1, 149-150	778.19	HS	5	GC1	6,330	5	5	0	0	0	1266	633	1.0			
83X-1, 149-150	787.89	HS	5	GC1	8,035	3	0	0	0	0	2678	2678				
133-823C-																
1R-3, 131-132	788.31	HS	5	GC1	9,664	4	0	0	0	0	2416	2416				
3R-2, 1-2	804.41	HS	5	GC1	10,501	1	0	0	0	0	5251	5251				
4R-4, 149-150	818.59	HS	5	GC1	33,499	12	0	0	0	0	2792	2792				
5R-4, 1-2	826.81	HS	5	GC1	12,073	2	0	0	0	0	6037	6037				
7R-2, 131-132	844.51	HS	5	GC1	28,240	11	0	0	0	0	2567	2567				
9R-5, 148-149	868.58	HS	5	GC1	17,565	6	0	0	0	0	2928	2928				
20R-1, 1-2	966.91	HS	5	GC1	13,189	25	26	9	0	8	528	259	1.0	1.5		1.1
20R-6, 149-150	975.89	HS	5	GC1	21,026	12	23	3	0	0	1752	601	0.5	7.7		
21R-3, 0-1	979.6	HS	5	GC1	10,361	5	14	0	0	0	2072	545	0.4			
21R-6, 96-97	985.06	HS	5	GC1	14,700	25	35	5	0	3	588	245	0.7	4.4		1.7
22R-3, 134-135	990.54	HS	5	GC1	24,400	22	62	8	4	8	1109	290	0.4	3.1	2.0	1.5
23R-3, 0-1	998.9	HS	5	GC1	6,528	9	12	0	0	0	725	311	0.8			
23R-6, 0-1	1003.4	HS	5	GC1	5,099	0	10	0	0	0		510				
24R-1, 1-2	1005.61	HS	5	GC1	14,603	9	33	2	0	0	1623	348	0.3	16.5		
24R-2, 149-150	1008.59	HS	5	GC1	33,588	28	77	8	4	9	1200	320	0.4	3.7	2.0	1.3
133-823B-																
30X-3, 0-10	279.3	VAC	5	GC1	61,402	0	4	0	0	0		15351				
31X-6, 0-10	292.56	VAC	5	GC1	14,314	0	8	0	0	0		1789				
33X-6, 0-50	312.8	VAC	5	GC1	10,405	0	0	0	0	0						
34X-5, 0-20	320.9	VAC	5	GC1	59,468	0	4	0	11	0		14867				
35X-6, 0-10	332.1	VAC	5	GC1	21,558	0	0	0	0	0						
36X-6, 100-120	342.7	VAC	5	GC1	919,346	0	68	0	0	0		13520				
37X-3, 130-150	348.2	VAC	5	GC1	174,958	0	13	0	3	0		13458				
38X-1, 60-70	354	VAC	5	GC1	39,547	0	4	0	0	0		9887				
39X-6, 0-10	370.5	VAC	5	GC1	187,425	0	20	0	0	0		9371				
40X-2, 130-140	375.5	VAC	5	GC1	214,133	0	21	0	0	0		10197				
41X-5, 0-5	388.4	VAC	5	GC1	210,438	0	23	0	0	0		9149				

HS = headspace; VAC = vacutainer sample.

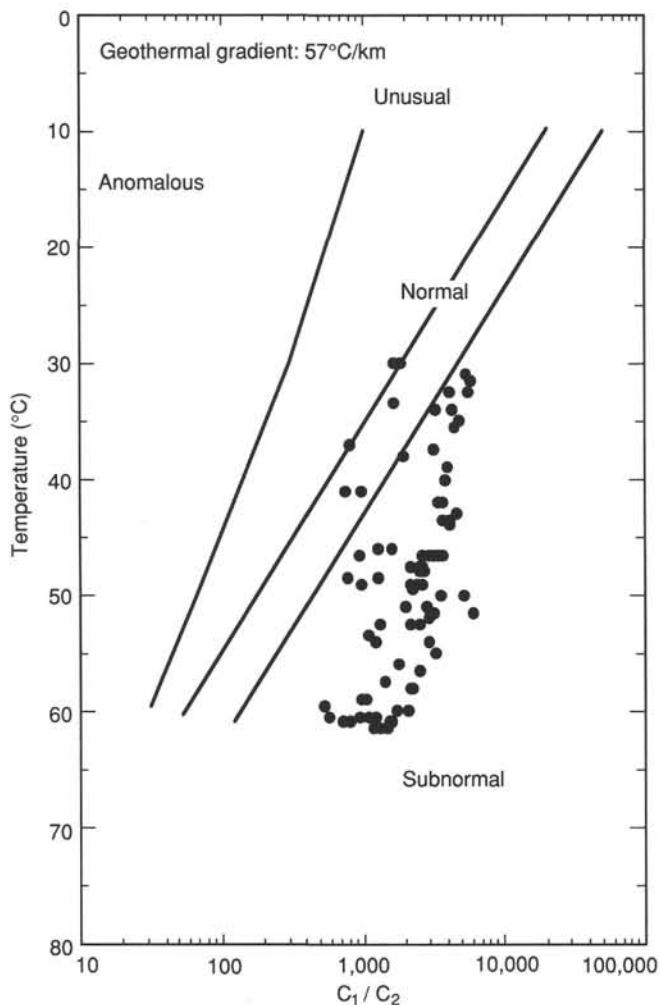


Figure 39. Distribution of the  $C_1/C_2$  ratio from headspace analyses with temperature at Site 823. Diagram was compiled for ODP ship-board safety and pollution-prevention monitoring program.

## DOWNHOLE MEASUREMENTS

### Reliability of Logs

Bridges (i.e., horizons having reduced hole size that were impassible for logging tools) controlled our logging strategy at Site 823. After the first tool string was set down on a bridge only 200 m into the open hole, we inserted a conical side-entry sub (CSES) into the drill string. The CSES allowed us to lower pipe to an arbitrary depth (usually 782 mbsf) while the logging tool was in the pipe, then move the logging tool into the open hole to obtain open-hole logs while pulling the pipe. This first operational trial of the CSES was successful; although minor technical problems were encountered, the CSES permitted open-hole logging using all three strings of virtually the entire hole.

At Site 823, the CSES had a major impact on logging success, but only minor impact on log reliability. The base of the pipe was lowered from 106.8 mbsf, the depth of the first seismic stratigraphic run, to 173.2 mbsf for subsequent runs. Therefore, we merged open-hole seismic stratigraphic logs for the interval from 114.1 to 175.0 mbsf from the first run with deeper logs from our second run. Comparing these two runs showed that the second run, which used the CSES, needed a 3-m downward shift, presumably because of error in our tool

zeroing with the CSES. The geochemical and FMS logging runs required similar shifts. In contrast, previous Leg 133 sites needed only small depth shifts. Logs depicted in Figures 51 to 58 were shifted appropriately.

Hole size was the most important control for accuracy of logs from Leg 133, and hole size at Hole 823C was relatively uniform below 450 mbsf, but irregular above 450 mbsf. Three types of caliper log were obtained (1) an apparent caliper calculated from the sonic log (see "Explanatory Notes" chapter, this volume), (2) a caliper (Fig. 51) from the mechanical caliper device (MCD), and (3) a two-axis caliper (Fig. 58) from the FMS. The lithodensity tool caliper was not operational at this site. The FMS caliper is much more reliable than either the sonic or MCD calipers. Based on correlation of the largest caliper values with anomalously low density values (Fig. 51), we suspect that numerous highest-porosity portions of the lithodensity run above 450 mbsf were obtained with only marginal pad contact against the wall of the borehole. As discussed later, this pattern implies that porosity and Archie component,  $m$ , calculations will be in error in these zones (Fig. 53). Most other logs do not require pad contact and thus are relatively insensitive to minor changes in borehole size. However, changes in hole size above 450 mbsf are so large and numerous that post-cruise correction of borehole size will be required for virtually all log types.

As is often the case with ODP holes, our initial sonic logs from Hole 823C exhibited a few zones with cycle skipping and, consequently, with unreliable swings in apparent velocity. Reprocessing (see "Explanatory Notes" chapter, this volume) appears to have removed virtually all unreliable data, and we consider the reprocessed velocity log in Figure 51 to be of good quality. However, occasional swings to low velocity above 450 mbsf should be treated with caution because of possible borehole effects. For the short interval from 971.6 to 987.2 mbsf at the bottom of the hole, resistivity logs (but not sonic logs) are available because the resistivity tool is much lower on the tool string. A pseudosonic log was generated and used for this interval, based on regression of sonic transit time on logarithm of shallow resistivity for the overlying interval from 932.5 to 971.5 mbsf ( $R = -0.55$ ).

The spectral gamma-ray logging tool is the only tool on the seismic stratigraphic combination that can provide useful electrical resistivity formation factor data even through pipe. On the geochemical tool string, useful through-pipe data were obtained using spectral gamma-ray, aluminum clay, and gamma-ray spectroscopy tools. At Hole 823C, through-pipe spectral gamma-ray logs were obtained for the intervals from 0 to 173.2 and from 0 to 178.2 mbsf during two runs of the geochemical combination; open-hole spectral gamma-ray logs were obtained for the lower part of this interval during the first run of our seismic stratigraphic combination. Through-pipe aluminum clay and gamma-ray spectroscopy logs were obtained during the same two passes of the geochemical string, although pipe was moved 5 m between the two passes to permit discrimination of changes in pipe thickness from changes in the formation. Subjective examination of through-pipe geochemical logs for Hole 823C indicates that with these one can detect geochemical changes in the formation. However, we have not yet corrected for pipe size in these logs.

With a repeat pass of the geochemical combination we also obtained a short interval of open-hole logs. As expected, our second runs of the spectral gamma-ray and aluminum clay logs were offset by irradiation effects in zones where the tool string paused or slowed for calibration before beginning the second run. However, the two passes generally exhibit high correlation of log character (Fig. 52). The potassium log is an exception that appears to have fair to poor replicability and the small-scale (<2 m) character of most of the logs. Repeat

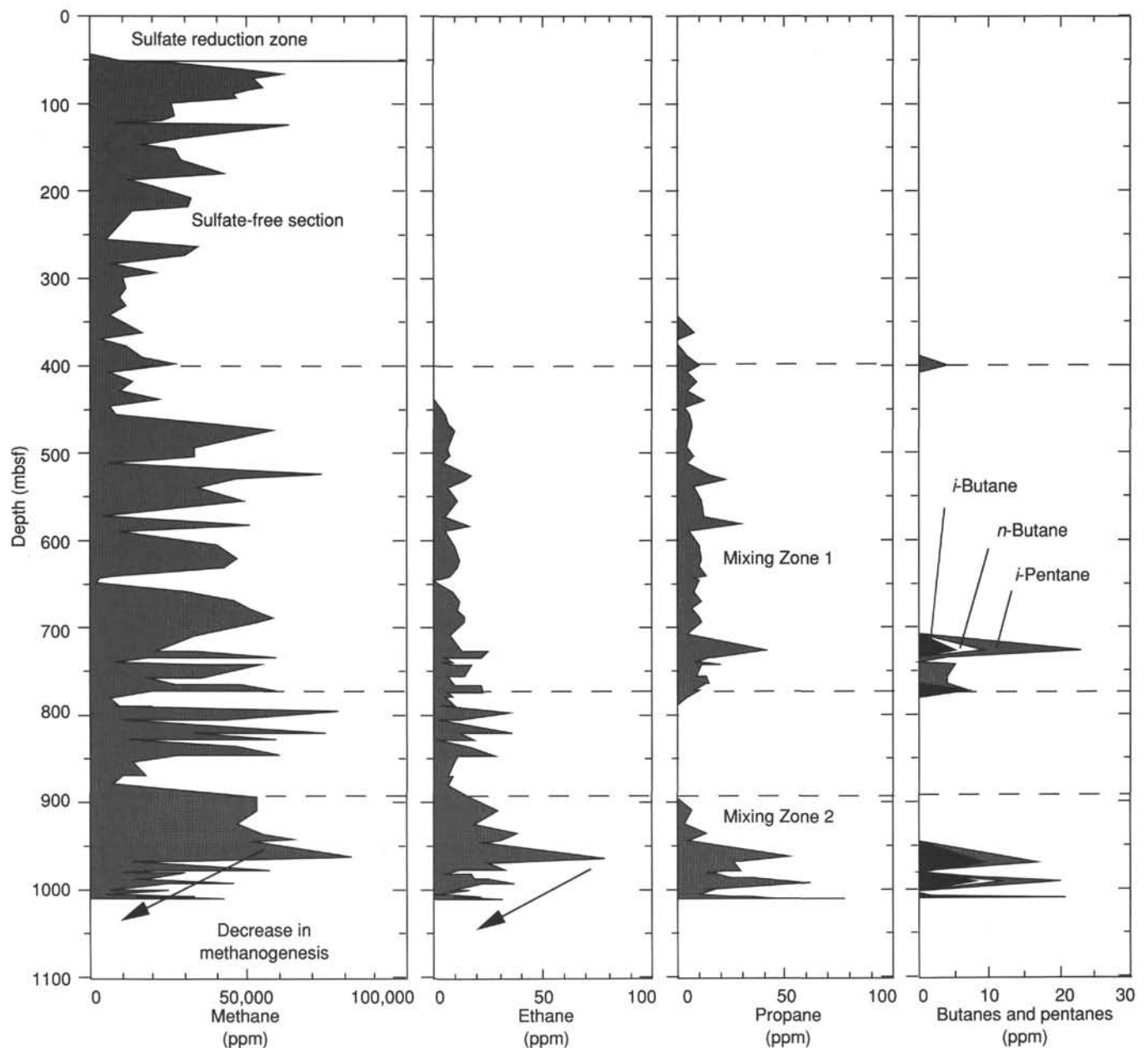


Figure 40. Distribution with depth of amounts of hydrocarbon gas in headspace samples at Site 823.

passes of resistivity and sonic logs also indicated good replicability (Fig. 52).

Logging with the FMS was successful. Because logging with the side-entry sub precluded use of the wireline heave compensator, raw FMS logs show substantial degradation from the ship's heave. However, the amount of residual ship's heave is comparable to that we observed for some FMS data from previous legs, particularly those in rough seas. We successfully removed this residual ship's heave from these previous data using an accelerometer log obtained simultaneously with FMS logging; thus, we anticipate no problem when removing ship's heave from the Site 823 FMS data during post-cruise reprocessing. Particularly high quality logs were obtained from below 450 mbsf, where hole size was almost constant, but the large variations in hole size above 450 mbsf probably degraded the quality of pad contact in that interval.

Post-cruise reprocessing will be required to assess the extent of possible degradation in this upper portion of the log.

#### Velocity, Resistivity, and Density Relationships

Velocity, resistivity, and density strongly correlate throughout almost all of the logged interval at Hole 823C (Fig. 51). This correlation arises from dominance of porosity in all three logs. Two additional porosity logs were obtained using the geochemical tool string, but are not shown (neutron and hydrogen). An uncalibrated neutron porosity log was generated by the aluminum clay tool; because the californium source was much stronger than the americium/beryllium sources used in conventional neutron porosity tools, apparent porosities are much higher and uncalibrated. The gamma-ray spectrometry tool (GST) detects variations in amounts of hydrogen relative to several other elements (see "Explanatory

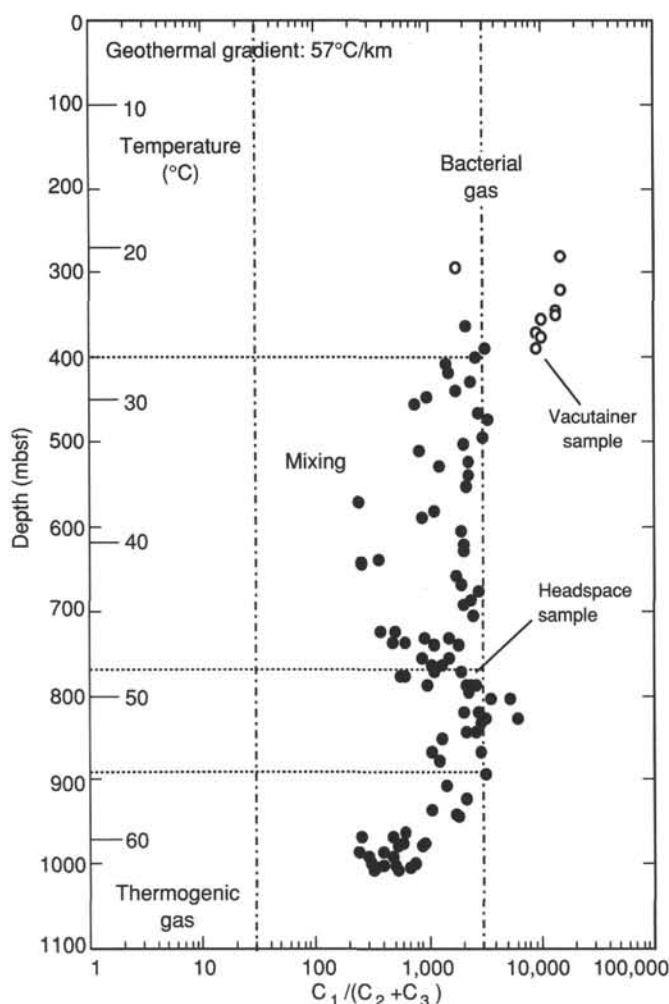


Figure 41. Evolution with depth and temperature of the  $C_1/(C_2+C_3)$  ratio at Site 823.

Notes" chapter, this volume); again, the values are uncalibrated, but potentially useful as a relative measure. For both neutron porosities and GST hydrogen counts, total hydrogen was detected without distinguishing whether hydrogen occurs in free water in pores or bound water in clay minerals. Thus, these two logs may overestimate porosity in clay-rich intervals.

Changes in velocity and density with depth (Fig. 51) generally follow a gradual compaction profile, suggesting that mechanical compaction dominates diagenesis for controlling porosity at this site. Similar patterns were observed at Sites 814, 817, and 819 (see "Site 814," "Site 817," and "Site 819" chapters, this volume). Within the open-hole logged interval, velocities are somewhat greater, and densities are similar to those normally observed in terrigenous sediments of comparable depths. Average velocity increases from 1.75 km/s at 110 mbsf to 2.5 to 2.9 km/s at 900 to 986 mbsf, compared to typical values for these depths of 1.65 and 2.3 km/s (Hamilton, 1979). Density increases from 1.8 g/cm<sup>3</sup> at 110 mbsf to 2.2 g/cm<sup>3</sup> at 950 mbsf, compared to typical values for these depths of about 1.68 and 2.3 g/cm<sup>3</sup> (Hamilton, 1976).

The density log has many intervals above 450 mbsf that may have been affected by poor pad contact. We chose not to use the neutron log to evaluate the extent of density log problems and to determine porosity (see "Site 820" chapter,

this volume). Instead, we calculated the Archie (1942) component,  $m$  (Fig. 53), which can be used to indicate cementation in log intervals of good density, as well as used to flag quality-control for the density log. Swings to values of  $m$  larger than 3 probably indicate horizons where the density log was unreliably low because of poor pad contact. Such intervals are common above 450 mbsf.

For intervals that have not been washed out, the Archie component,  $m$ , can be used to assess possible changes in style of pore structure (see "Site 817" chapter, this volume). Although the Archie (1942) relationship may not be applicable in this lithology, it can identify a trend for further study. The dominant feature of a plot of  $m$  (Fig. 53) is a gradual decrease from 2.6 at 110 to 150 mbsf to 1.9 at 950 to 980 mbsf. Similarly, velocity and resistivity ratios are useful for identifying changes in pore morphology; a gradual change in "A/B ratio" from 0.25 at 110 to 150 mbsf to 0.15 below 950 mbsf is evident in Figure 54.

The velocity log has been converted to an integrated traveltime log (Fig. 55) to facilitate depth-to-time conversion for comparing Site 823 data with seismic facies. For the unlogged interval between the seafloor and 107.8 mbsf, we used a simple linear interpolation between water velocity at the seafloor and the first log value at 107.8 mbsf. We subjectively estimated an error of less than 7 ms associated with uncertainties of velocities in the top 107.8 mbsf.

### Log-Based Units

Lithology at Site 823 is dominated by variations in concentration of the two principal components: calcite (either nanofossils or micrite) and clay minerals. We base this conclusion on smear-slide descriptions (see "Lithostratigraphy" section, this chapter); it is independently demonstrated by the geochemical logs. Figure 56 shows a strong correlation among logs obtained using three different tools. The elements potassium, aluminum, and silicon (all abundant in the clay minerals illite and kaolinite) correlate positively with each other and correlate inversely with the abundance of calcium. Thus, these geochemical logs are semiquantitative indicators of relative abundance of calcite and clay minerals.

The porosity-sensitive logs in Figure 51 correlate moderately well with the gamma-ray log (SGR in Fig. 56), while gamma-ray maxima correspond to velocity, resistivity, and density minima. Furthermore, the other geochemical logs, potassium, aluminum and silicon, correlate moderately with the porosity logs. This pattern is not as strong as the correlation among porosity logs or the correlation among geochemical logs, but it does imply a substantial effect of mineralogy on porosity. This pattern is typical in ODP holes having clay-mineral variation. Higher concentrations of clay minerals are evidenced by higher gamma-ray counts, particularly if illite (3%–8% potassium; Serra, 1986) is a significant constituent of the clays, and clay minerals substantially increase the porosity of uncompacted (<2 km overburden) sediments. The inverse correlation between clay-indicator element logs and both velocity and resistivity, as well as the positive correlation between the calcium log and velocity and resistivity, is particularly strong below 800 mbsf.

Spectral gamma-ray values at Site 823 are similar to those at the Great Barrier Reef transect (Sites 819–822), but are substantially higher than sites on Queensland and Marion plateaus. Potassium in particular has increased by more than a factor of 10, to values ranging from 0.5% to 1.0%. Thorium increased by a factor of three, and the total SGR count is nearly double that at Site 817 (see "Site 817" chapter, this volume), having values that range from 30 to 50 API units. These patterns are attributable to the much higher contents of

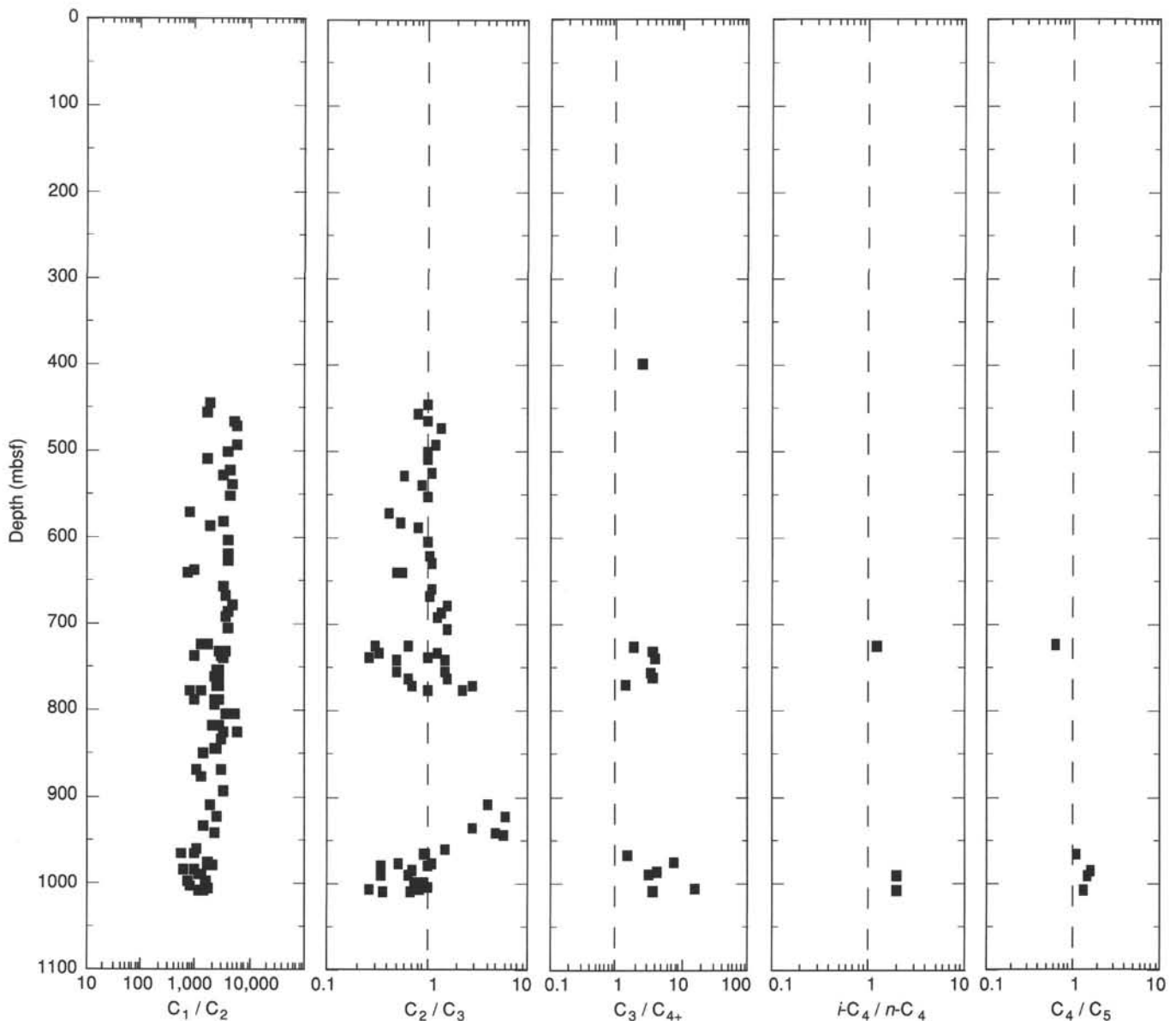


Figure 42. Evolution with depth of hydrocarbon gas ratios at Site 823.

clay and proportionately lower contents of carbonate at Sites 819 through 823, in comparison to earlier Leg 133 sites.

Based on log responses, the openhole logged interval of Site 823 can be divided into seven units: log Unit 1 from the base of the pipe (69 mbsf) to 370 mbsf, log Unit 2 from 370 to 453 mbsf, log Unit 3 from 453 to 650 mbsf, log Unit 4 from 650 to 745 mbsf, log Unit 5 from 745 to 870 mbsf, log Unit 6 from 870 to 900 mbsf, and log Unit 7 from 900 mbsf to the bottom of the logged interval at 978 mbsf.

Log Unit 1 is characterized by a smooth compaction profile for the velocity and resistivity logs, as shown in Figure 51. One can see a small number of thin layers of higher resistivity and velocity that probably resulted from density changes within similar lithologies.

Log Unit 2 is characterized by a change in character and amplitude of the geochemical logs (Fig. 56). The aluminum log response is extremely variable and is the highest recorded so far during Leg 133 (8%), which suggests the presence of thin layers having a clay mineral composition that is not typical of

the sites investigated during Leg 133. Slumps can be seen in those cores in log Unit 2 (see "Lithostratigraphy" section, this chapter), which suggests that material may have come from a different source than so far encountered during the leg.

Log Unit 3 has a character similar to log Unit 1 and similar geochemical log values, except for aluminum, which increases from 2% to 2.5%. A rhythmic cycle of increasing calcium with depth occurs from 450 to 490 mbsf that also affects the velocity log (Fig. 51).

Log unit 4 is bounded at the top by a decrease in spectral gamma-ray response and an increase in calcium. This log boundary was seen at 650 mbsf, which is within lithologic Unit IV (see "Lithostratigraphy" section, this chapter); this depth coincides with a change in age from early Pliocene to late Miocene. This depth corresponds to the base of a rhythmic unit in the velocity log (Fig. 51) in which velocity increases upward, which might indicate an upward-coarsening sequence.

Log Unit 4 exhibits variable character in the geochemical logs (Fig. 56) without general rhythmic trends. The interface

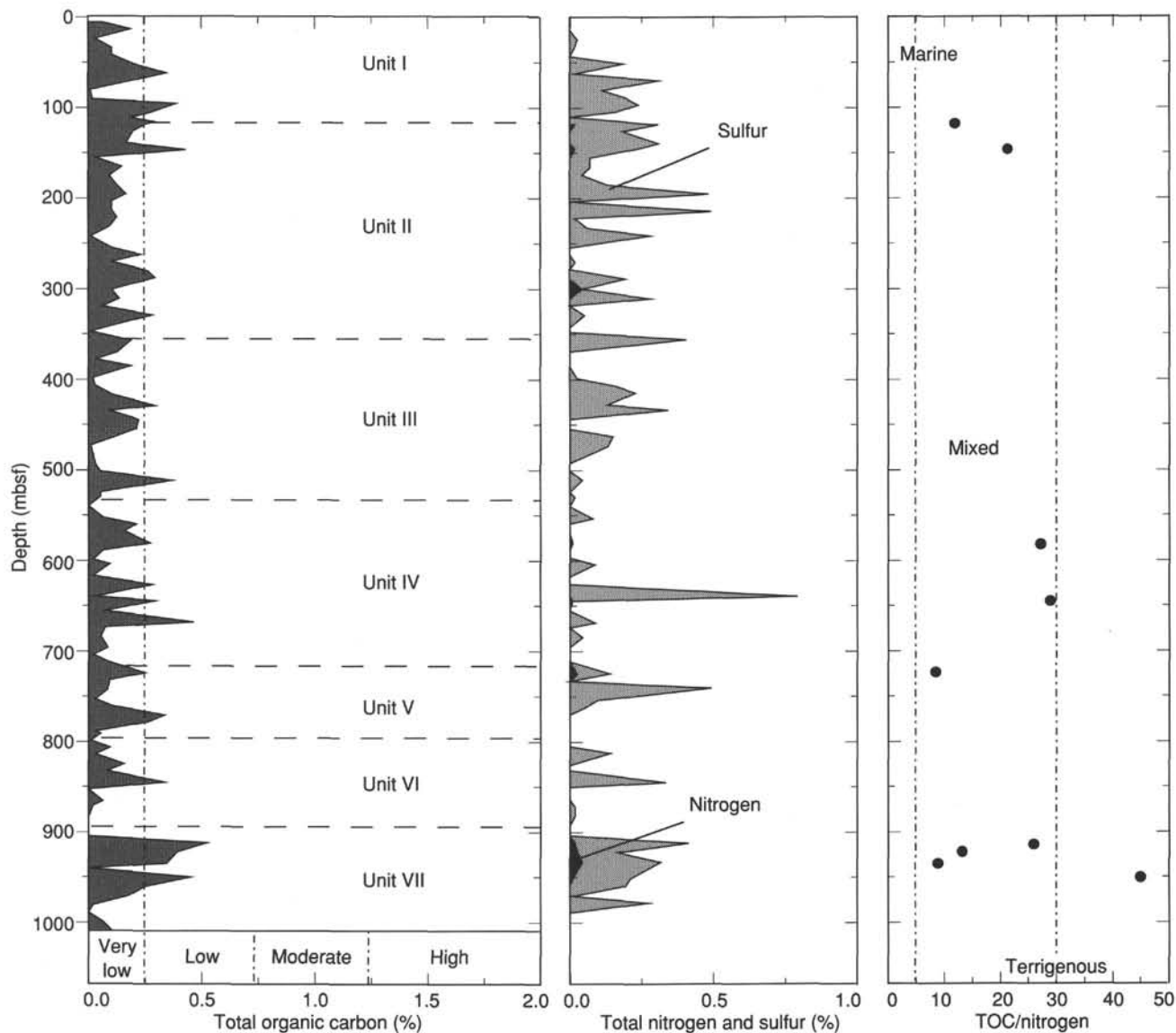


Figure 43. Distribution with depth of concentrations of total organic carbon, nitrogen, sulfur, and TOC/nitrogen ratio at Site 823.

between lithologic Units IV and V (715 mbsf; see “Lithostratigraphy” section, this chapter) can be seen in the logs (Fig. 56) as the top of an 8-m-thick layer at 711 mbsf probably rich in clay minerals.

Log Unit 5 has a rhythmic geochemical response of gradually increasing and then decreasing calcium, and the reverse response in SGR, potassium, aluminum, and silicon logs. The lithologic Unit V/VI interface (798 mbsf; see “Lithostratigraphy” section, this chapter) was not detected in the geochemical logs (Fig. 56), but was evident in resistivity and velocity logs (Fig. 51) as a thin, high-porosity layer from 797 to 800 mbsf.

Log Unit 6 corresponds to the lower 30 m of Unit VI (see “Lithostratigraphy” section, this chapter) and is a rhythmic sequence having calcium and velocity that decrease upward and the reverse for clay mineral indicators. This is consistent with an upward-fining sequence.

Log Unit 7 (900–950 mbsf) is the reverse of log Unit 6 and is consistent with grain size, which coarsens upward. The change from log Unit 6 to log Unit 7 at 900 mbsf is also the

Unit VI/Unit VII interface (see “Lithostratigraphy” section, this chapter).

### Temperature

We ran the Lamont-Doherty Geological Observatory (L-DGO) temperature tool at the bottom of the seismic stratigraphic and geochemical tool strings. Because hole temperatures were reduced by circulation during coring and by hole conditioning immediately prior to logging, we were unable to infer an equilibrium thermal profile from the two deep-temperature logging runs. Our recorded maximum temperatures of 37.0° and 41.1°C thus are minimum estimates of equilibrium temperature.

We ran the temperature tool not to estimate heat flow, but in case fluid flow was present. In Figure 57, we plot measured temperature as a function of pressure recorded simultaneously by the tool. Depths shown are approximate and may be revised by up to 10 m during post-cruise merging of Schlumberger time/depth data with temperature-tool time/pressure data.

**Table 7. Concentrations of total organic carbon, inorganic carbon, total carbon, total nitrogen, and sulfur in X-ray diffraction and physical properties samples from Site 823.**

Core, section, interval (cm)	Depth (mbsf)	Sample	Total organic carbon (%)	Total inorganic carbon (%)	Total carbon (%)	Total nitrogen (%)	Total sulfur (%)	TOC/ nitrogen	TOC/ sulfur
133-823A-									
1H-3, 145-150	4.45	XRD	0.06	8.08	8.14	0.00	0.00		
2H-5, 145-150	13.25	XRD	0.19	5.65	5.84	0.00	0.00		
3H-5, 145-150	22.75	XRD	0.03	8.30	8.33	0.00	0.03		1
4H-5, 145-150	32.25	XRD	0.10	8.03	8.13	0.00	0.02		5
5H-5, 145-150	41.75	XRD	0.10	9.74	9.84	0.00	0.00		
6H-5, 145-150	51.25	XRD	0.20	7.62	7.82	0.00	0.18		1
7H-5, 145-150	60.75	XRD	0.35	9.29	9.64	0.00	0.02		17
8H-5, 145-150	70.25	XRD	0.20	7.87	8.07	0.00	0.31		1
9H-5, 145-150	79.75	XRD	0.01	7.26	7.27	0.00	0.11		0
10H-5, 145-150	89.25	XRD	0.02	6.01	6.03	0.00	0.19		0
11H-3, 91-94	95.21	PP	0.39	4.82	5.21	0.00	0.24		2
12H-3, 90-93	104.7	PP	0.27	7.64	7.91	0.00	0.16		2
823B-12H-5, 140-150	110.7	XRD	0.19	9.36	9.55	0.00	0.00		
823B-13X-3, 86-89	116.66	PP	0.29	3.63	3.92	0.00	0.29		1
823A-13H-5, 145-150	117.75	XRD	0.25	2.44	2.69	0.02	0.29	12	1
133-823B-									
14X-3, 90-93	126.3	PP	0.20	6.85	7.05	0.00	0.18		1
15X-5, 140-150	139.5	XRD	0.17	6.24	6.41	0.00	0.31		1
16X-3, 90-92	145.6	PP	0.43	6.74	7.17	0.02	0.22	21	2
17X-3, 90-93	155.3	PP	0.03	4.59	4.62	0.00	0.07		0
18X-3, 140-150	165.5	XRD	0.15	7.05	7.20	0.00	0.07		2
19X-3, 90-93	174.7	PP	0.09	5.54	5.63	0.00	0.04		2
20X-3, 90-93	184.4	PP	0.13	6.77	6.90	0.00	0.13		1
21X-3, 140-150	194.6	XRD	0.17	7.63	7.80	0.00	0.48		0
22X-3, 90-93	203.7	PP	0.10	8.26	8.36	0.00	0.00		
23X-3, 90-93	213	PP	0.10	7.48	7.58	0.00	0.49		0
24X-2, 140-150	221.6	XRD	0.13	7.54	7.67	0.00	0.02		7
25X-3, 90-93	231.9	PP	0.09	4.42	4.51	0.00	0.06		1
26X-3, 90-92	241.6	PP	0.01	7.45	7.46	0.00	0.28		0
27X-6, 140-150	255.42	XRD	0.11	8.10	8.21	0.00	0.00		
28X-4, 90-92	262.4	PP	0.23	7.39	7.62	0.00	0.00		
29X-3, 90-92	270.6	PP	0.11	6.98	7.09	0.00	0.02		6
30X-2, 140-150	279.2	XRD	0.26	6.78	7.04	0.00	0.00		
31X-3, 91-92	288.97	PP	0.30	5.51	5.81	0.00	0.19		2
32X-3, 90-93	299.5	PP	0.11	6.20	6.31	0.04	0.00		
33X-4, 140-150	311.2	XRD	0.14	6.00	6.14	0.00	0.28		1
34X-3, 90-93	318.8	PP	0.06	5.99	6.05	0.00	0.00		
35X-3, 100-102	328.6	PP	0.28	8.09	8.37	0.00	0.05		6
36X-5, 140-150	341.6	XRD	0.08	7.78	7.86	0.00	0.00		
37X-3, 90-93	347.8	PP	0.01	8.44	8.45	0.00	0.00		
38X-3, 97-99	356.79	PP	0.19	6.81	7.00	0.00	0.40		0
39X-5, 140-150	370.4	XRD	0.13	8.85	8.98	0.00	0.00		
40X-3, 100-103	376.7	PP	0.03	5.86	5.89	0.00	0.00		
41X-3, 100-103	386.4	PP	0.19	6.18	6.37	0.00	0.00		
42X-4, 140-150	397.9	XRD	0.02	3.15	3.17	0.00	0.03		1
43X-3, 100-102	405.6	PP	0.03	5.64	5.67	0.00	0.16		0
44X-3, 97-99	415.27	PP	0.10	7.64	7.74	0.00	0.23		0
45X-5, 140-150	428.3	XRD	0.29	8.11	8.40	0.00	0.13		2
46X-3, 100-102	434.6	PP	0.09	5.41	5.50	0.00	0.34		0
47X-3, 100-102	444.3	PP	0.22	8.17	8.39	0.00	0.00		
48X-4, 140-150	455.8	XRD	0.21	8.11	8.32	0.00	0.00		
49X-3, 100-103	463.6	PP	0.13	7.52	7.65	0.00	0.15		1
50X-3, 100-103	473.2	PP	0.01	7.03	7.04	0.00	0.13		0
52X-4, 140-150	493.7	XRD	0.03	9.80	9.83	0.00	0.00		
53X-3, 100-102	501.5	PP	0.05	7.09	7.14	0.00	0.00		
54X-3, 100-103	511.1	PP	0.37	7.64	8.01	0.00	0.04		9
55X-5, 140-150	524.2	XRD	0.05	8.76	8.81	0.00	0.00		
56X-3, 105-107	530.45	PP	0.05	7.61	7.66	0.00	0.02		2
57X-3, 132-133	540.02	PP	0.00	8.62	8.62	0.00	0.00		
58X-5, 140-150	552.8	XRD	0.06	6.50	6.56	0.00	0.08		1
59X-3, 104-106	559.04	PP	0.21	7.77	7.98	0.00	0.00		
60X-3, 134-135	569.04	PP	0.16	7.21	7.37	0.00	0.00		
61X-5, 140-150	581.7	XRD	0.27	6.45	6.72	0.01	0.00	27	
62X-3, 146-149	588.36	PP	0.06	6.05	6.11	0.00	0.00		
63X-3, 144-149	598.04	PP	0.02	9.30	9.32	0.00	0.00		
64X-1, 135-150	604.55	XRD	0.09	7.92	8.01	0.00	0.09		1
65X-3, 144-147	617.24	PP	0.02	8.37	8.39	0.00	0.00		
66X-3, 100-102	626.5	PP	0.28	8.04	8.32	0.00	0.00		
67X-5, 135-150	639.55	XRD	0.03	7.27	7.30	0.00	0.79		0
68X-3, 63-66	645.23	PP	0.29	6.19	6.48	0.01	0.00	29	
69X-3, 109-111	654.99	PP	0.07	9.62	9.69	0.00	0.00		
70X-5, 135-150	668	XRD	0.46	6.74	7.20	0.00	0.09		5
71X-3, 86-89	674.16	PP	0.07	9.65	9.72	0.00	0.00		
72X-3, 114-116	684.04	PP	0.05	6.34	6.39	0.00	0.04		1
73X-4, 135-150	695.45	XRD	0.08	7.00	7.08	0.00	0.00		
74X-3, 82-84	703.12	PP	0.02	6.53	6.55	0.00	0.00		

Table 7 (continued).

Core, section, interval (cm)	Depth (mbsf)	Sample	Total organic carbon (%)	Total inorganic carbon (%)	Total carbon (%)	Total nitrogen (%)	Total sulfur (%)	TOC/nitrogen	TOC/sulfur
75X-3, 80-83	712.7	PP	0.08	7.69	7.77	0.00	0.00		
76X-4, 135-150	724.45	XRD	0.25	4.11	4.36	0.03	0.11	8	2
77X-3, 133-135	732.53	PP	0.09	5.55	5.64	0.00	0.00		
78X-3, 129-131	742.19	PP	0.08	5.96	6.04	0.00	0.49		0
79X-4, 135-150	753.45	XRD	0.03	5.71	5.74	0.00	0.10		0
80X-3, 142-144	761.72	PP	0.11	3.94	4.05	0.00	0.05		2
81X-3, 146-149	771.46	PP	0.34	4.21	4.55	0.00	0.00		
82X-1, 135-150	778.05	XRD	0.26	7.45	7.71	0.00	0.00		
823C-1R-3, 130-150	788.3	XRD	0.03	8.47	8.50	0.00	0.00		
823B-83X-3, 130-132	790.7	PP	0.05	4.64	4.69	0.00	0.00		
133-823C-									
2R-3, 149-150	798.09	PP	0.01	11.03	11.04	0.00	0.00		
3R-3, 14-16	806.04	PP	0.09	11.60	11.69	0.00	0.00		
4R-1, 130-150	813.9	XRD	0.03	7.76	7.79	0.00	0.14		0
5R-3, 97-99	826.27	PP	0.16	9.47	9.63	0.00	0.00		
6R-1, 127-128	833.27	XRD	0.08	7.73	7.81	0.00	0.00		
7R-2, 130-150	844.5	XRD	0.34	5.44	5.78	0.00	0.33		1
8R-1, 75-77	852.15	PP	0.00	10.92	10.92	0.00	0.00		
9R-3, 124-127	865.34	PP	0.06	7.92	7.98	0.00	0.00		
10R-1, 130-150	872.1	XRD	0.02	8.45	8.47	0.00	0.02		1
11R-3, 83-85	884.23	PP	0.00	8.71	8.71	0.00	0.02		0
12R-3, 121-123	894.31	PP	0.00	10.11	10.11	0.00	0.00		
13R-4, 130-150	904.99	XRD	0.00	7.48	7.48	0.00	0.00		
14R-3, 103-105	913.43	PP	0.53	6.79	7.32	0.02	0.39	26	1
15R-3, 9-10	922.19	PP	0.39	5.79	6.18	0.03	0.14	13	3
16R-4, 130-150	934.6	XRD	0.35	3.34	3.69	0.04	0.28	9	1
17R-3, 40-42	941.8	PP	0.00	7.15	7.15				
18R-3, 79-81	951.79	PP	0.45	3.72	4.17	0.01	0.20	45	2
19R-3, 130-150	961.6	XRD	0.25	3.43	3.68	0.00	0.19		1
20R-3, 57-58	970.47	PP	0.18	5.50	5.68	0.00	0.01		18
21R-3, 94-95	980.54	PP	0.02	7.98	8.00	0.00	0.27		0
22R-3, 120-136	990.4	XRD	0.00	3.63	3.63	0.00	0.00		
23R-3, 58-60	999.48	PP	0.06	5.74	5.80	0.00	0.00		
24R-3, 38-39	1008.98	PP	0.10	3.80	3.90	0.00	0.00		

PP = physical properties sample; XRD = X-ray diffraction sample.

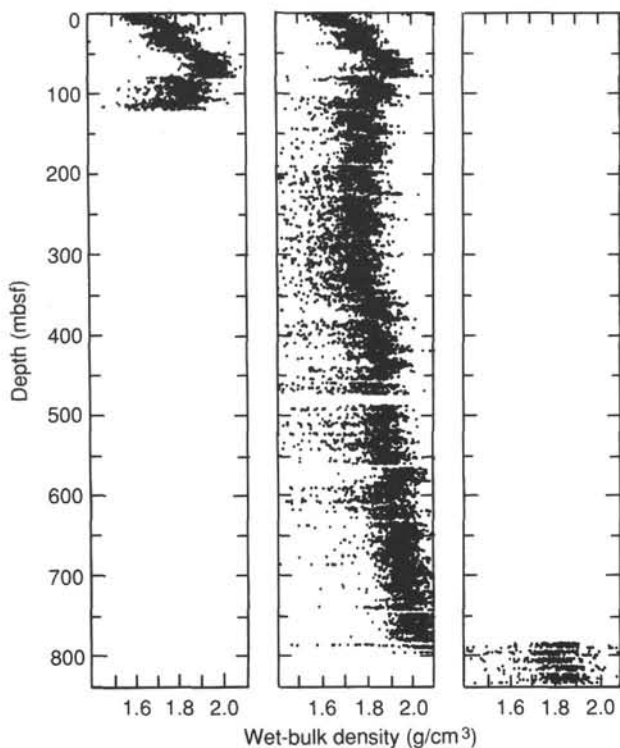


Figure 44. GRAPE bulk-density measurements for Site 823. Data values have been averaged at 5-cm intervals.

The temperature pattern in Figure 57 exhibits evidence of slight thermal lags from a mud-clogged end sub. Clogging of mud can occur when the temperature tool, which is the bottom tool of the tool string, hits the bottom of a hole containing sticky clay. The effect on the log is a higher temperature for the upcoming log than for the downgoing log, and a maximum temperature recording, not at the deepest point in the hole, but somewhat shallower than the deepest point on the upcoming log. When rigged down after logging, the temperature tool did suffer a mud-clogged end sub.

Upcoming, and particularly downgoing, logs for the interval from 0 to 780 mbsf were strongly affected by recent pipe motion and circulation associated with logging while pipe was pulled. Below 780 mbsf, the formation was unaffected by pipe motion, and an approach to equilibrium linear temperature gradient is evident.

#### Hole Deviation

At Hole 823C, hole deviation (measured using the FMS) was a relatively constant  $0.5^\circ$  to  $1.0^\circ$  to the north (Fig. 58). Somewhat surprisingly, in view of the large amounts of high-dip sediments cored and the deep penetration, this deviation was small.

#### SEISMIC STRATIGRAPHY

The BMR water-gun seismic profile collected during a 1987 site survey (Symonds and Davies, 1988; Feary et al., 1990) on an east-west line across Site 823 shows that the site area has a uniform seismic geometry (Fig. 59). The site is located in a basin near the center of Queensland Trough, between two fault-bounded basement blocks (Fig. 1). The section about 1.0 s

Table 8. Index properties data, Site 823.

Core, section, interval, (cm)	Depth (mbsf)	Bulk density (g/cm <sup>3</sup> )	Grain density (g/cm <sup>3</sup> )	Porosity (%)	Water content (%)	Void ratio
133-823A-						
1H-1, 43-46	0.43	1.53	2.86	74.0	97.6	2.85
1H-2, 77-77	2.27	1.54	2.82	73.7	96.7	2.81
1H-3, 90-93	3.90	1.57	2.86	72.4	89.2	2.63
1H-4, 90-93	5.40	1.59	2.93	73.0	88.6	2.70
2H-1, 90-93	6.70	1.63	2.57	67.0	72.7	2.03
2H-2, 90-93	8.20	1.60	3.18	69.2	79.6	2.25
2H-3, 90-93	9.70	1.58	2.76	71.6	87.1	2.53
2H-4, 90-93	11.20	1.63	2.83	70.1	78.9	2.34
2H-5, 90-93	12.70	1.60	2.88	70.8	83.3	2.42
2H-6, 90-93	14.20	1.61	2.85	69.3	78.7	2.25
3H-1, 90-93	16.20	1.70	2.78	62.7	60.6	1.68
3H-2, 90-93	17.70	1.73	2.81	63.2	59.7	1.72
3H-3, 90-93	19.20	1.76	2.89	63.4	58.4	1.73
3H-4, 90-93	20.70	1.79	2.80	60.5	53.1	1.53
3H-5, 90-93	22.20	1.74	2.72	62.2	57.8	1.65
3H-6, 90-93	23.70	1.71	2.74	65.2	63.8	1.87
4H-1, 90-93	25.70	1.68	2.84	67.7	70.7	2.10
4H-2, 90-93	27.20	1.67	2.70	62.6	62.4	1.67
4H-3, 90-93	28.70	1.66	2.72	65.6	68.1	1.91
4H-4, 90-93	30.20	1.66	2.88	68.2	72.4	2.14
4H-5, 90-93	31.70	1.71	2.79	67.4	68.1	2.07
4H-6, 90-93	33.20	1.70	2.83	65.7	65.5	1.92
5H-1, 90-93	35.20	1.76	2.71	60.2	53.8	1.51
5H-2, 90-93	36.70	1.81	2.75	57.8	48.6	1.37
5H-3, 90-93	38.20	1.75	2.77	61.1	55.5	1.57
5H-4, 90-93	39.70	1.82	2.86	62.2	53.9	1.65
5H-5, 90-93	41.20	1.74	2.80	61.9	57.5	1.63
5H-6, 90-93	42.70	1.91	2.84	60.2	47.7	1.51
6H-1, 90-93	44.70	1.74	2.81	62.4	58.0	1.66
6H-2, 90-93	46.20	1.75	2.75	62.6	57.8	1.68
6H-3, 90-93	47.70	1.72	2.76	63.7	61.2	1.75
6H-4, 90-93	49.20	1.78	2.81	53.0	43.9	1.13
6H-5, 90-93	50.70	1.87	2.81	55.6	43.8	1.25
6H-6, 90-93	52.20	1.87	2.94	54.9	43.1	1.22
7H-1, 90-93	54.20	1.84	2.76	56.3	45.5	1.29
7H-2, 90-93	55.70	1.86	2.83	53.9	42.1	1.17
7H-3, 90-93	57.20	1.87	2.95	55.9	44.1	1.27
7H-4, 90-93	58.70	1.97	2.89	55.7	40.7	1.26
7H-5, 90-93	60.20	1.90	2.62	53.0	40.2	1.13
7H-6, 90-93	61.70	1.91	2.76	52.0	38.6	1.09
8H-1, 90-93	63.70	1.96	2.65	51.2	36.6	1.05
8H-2, 90-93	65.20	1.95	2.88	50.3	35.8	1.01
8H-3, 90-93	66.70	1.86	2.88	56.2	44.8	1.28
8H-4, 90-93	68.20	1.95	2.80	49.7	35.4	0.99
8H-5, 90-93	69.70	1.95	2.86	51.1	36.6	1.04
8H-6, 90-93	71.20	1.93	2.79	52.3	38.5	1.10
9H-1, 90-93	73.20	1.98	2.80	48.6	33.6	0.95
9H-2, 90-93	74.70	1.92	2.93	51.1	37.4	1.05
9H-3, 90-93	76.20	1.93	2.91	51.1	37.2	1.05
9H-4, 90-93	77.70	2.00	2.75	48.0	32.6	0.92
9H-5, 90-93	79.20	1.96	2.75	49.4	34.7	0.98
9H-6, 90-93	80.70	1.94	2.78	51.7	37.7	1.07
10H-1, 90-93	82.70	1.77	2.74	59.9	53.3	1.50
10H-2, 90-93	84.20	1.78	2.99	55.9	47.3	1.27
10H-3, 90-93	85.70	1.88	2.82	52.8	40.3	1.12
10H-4, 90-93	87.20	1.84	2.74	54.6	43.8	1.20
10H-5, 90-93	88.70	1.85	2.77	55.7	44.4	1.26
10H-6, 90-93	90.20	1.87	2.78	56.0	44.5	1.27
11H-1, 90-93	92.20	1.78	2.81	51.6	42.2	1.07
11H-2, 90-93	93.70	1.89	2.74	53.2	40.6	1.14
11H-3, 90-93	95.20	1.83	2.79	56.0	45.5	1.27
11H-4, 90-93	96.70	1.94	2.78	54.0	40.1	1.18
11H-5, 90-93	98.20	1.91	2.78	54.9	41.7	1.22
11H-6, 90-93	99.70	1.79	2.76	53.1	43.8	1.13
12H-1, 90-93	101.70	1.82	2.61	57.4	47.6	1.35
12H-2, 90-93	103.20	1.88	2.76	54.5	42.4	1.20
12H-3, 90-93	104.70	1.76	2.53	57.1	49.7	1.33
12H-4, 90-93	106.20	1.87	2.80	52.2	40.0	1.09
12H-5, 90-93	107.70	2.04	2.78	44.9	29.1	0.82
12H-6, 90-93	109.20	1.81	2.74	57.7	48.5	1.36
13H-1, 90-93	111.20	1.81	2.76	55.6	45.8	1.25
13H-2, 90-93	112.70	1.82	2.77	54.2	43.8	1.19
13H-3, 90-93	114.20	1.67	2.92	68.1	72.0	2.13
13H-4, 90-93	115.70	1.83	2.73	56.5	46.1	1.30
13H-5, 90-93	117.20	1.84	2.78	53.5	42.4	1.15

Table 8 (continued).

Core, section, interval, (cm)	Depth (mbsf)	Bulk density (g/cm <sup>3</sup> )	Grain density (g/cm <sup>3</sup> )	Porosity (%)	Water content (%)	Void ratio
133-823B-						
13H-6, 90-93	118.70	1.87	2.74	52.0	39.9	1.09
12H-1, 90-93	104.20	1.81	2.78	56.7	47.4	1.31
12H-2, 90-93	105.70	1.88	2.79	53.4	41.0	1.15
12H-3, 90-93	107.20	1.90	2.76	52.5	39.5	1.10
12H-4, 90-93	108.73	1.87	2.80	57.3	45.7	1.34
12H-5, 90-93	110.23	1.89	2.83	55.5	43.1	1.25
12H-6, 90-93	111.70	1.88	2.76	53.9	41.5	1.17
12H-7, 70-73	113.00	1.85	2.74	59.4	49.2	1.47
13X-1, 90-93	113.70	1.85	2.76	56.1	45.2	1.28
13X-2, 90-93	115.20	1.85	2.76	55.7	44.6	1.26
13X-3, 86-89	116.66	1.82	2.77	56.5	46.5	1.30
13X-4, 90-93	118.20	1.79	2.74	60.0	52.2	1.50
13X-5, 90-93	119.70	1.80	2.73	58.9	50.5	1.44
14X-1, 90-93	123.30	1.76	2.87	58.3	51.5	1.40
14X-2, 90-93	124.80	1.74	2.77	58.5	52.5	1.41
14X-3, 90-93	126.30	1.80	2.78	60.0	52.1	1.50
14X-4, 90-93	127.80	1.86	2.74	55.4	44.1	1.24
14X-5, 90-93	129.30	1.86	2.67	56.3	45.1	1.29
14X-6, 90-93	130.80	1.82	2.76	58.6	49.2	1.41
15X-1, 90-93	133.00	1.91	2.85	57.5	44.5	1.35
15X-2, 90-93	134.50	1.88	2.64	53.4	41.0	1.15
15X-3, 90-93	136.00	1.83	2.81	55.0	44.4	1.22
15X-4, 90-93	137.50	1.89	2.72	54.8	42.3	1.21
15X-5, 90-93	139.00	1.80	2.81	58.6	50.0	1.42
15X-6, 90-93	140.50	1.93	2.76	55.1	41.4	1.23
16X-1, 90-93	142.60	1.97	2.70	57.8	43.1	1.37
16X-2, 90-93	144.10	1.91	2.73	52.6	39.4	1.11
16X-3, 90-93	145.60	1.96	2.74	53.7	38.9	1.16
16X-4, 90-93	147.10	1.88	2.77	52.7	40.4	1.11
16X-5, 90-93	148.60	1.87	2.75	52.9	40.7	1.12
16X-6, 90-93	150.10	1.95	2.73	50.2	35.9	1.01
17X-1, 90-93	152.30	1.88	2.79	55.9	43.9	1.27
17X-2, 90-93	153.80	1.84	2.76	54.6	43.9	1.20
17X-3, 90-93	155.30	1.81	2.75	50.6	40.2	1.02
17X-4, 90-93	156.80	1.89	2.75	54.4	41.7	1.19
17X-5, 90-93	158.30	1.88	2.91	59.7	48.0	1.48
18X-1, 90-93	162.00	1.79	2.78	52.5	42.8	1.11
18X-2, 90-93	163.50	1.82	2.76	50.1	39.2	1.00
18X-3, 90-93	165.00	1.93	2.72	51.3	37.3	1.05
18X-4, 90-93	166.50	1.89	2.76	55.4	42.8	1.24
18X-5, 90-93	168.00	1.82	2.76	57.9	48.3	1.38
18X-6, 90-93	169.50	1.81	2.72	55.4	45.8	1.24
19X-1, 90-93	171.70	1.93	2.85	54.4	40.7	1.19
19X-2, 90-93	173.20	1.81	2.76	58.4	49.3	1.40
19X-3, 90-93	174.70	1.85	2.80	55.0	43.9	1.22
19X-4, 90-93	176.20	1.86	2.76	53.7	42.2	1.16
19X-5, 90-93	177.70	1.87	2.71	53.6	41.7	1.16
19X-6, 90-93	179.20	1.91	2.75	55.1	42.0	1.23
20X-1, 90-93	181.40	1.76	2.77	59.8	53.2	1.49
20X-2, 90-93	182.90	1.80	2.74	59.3	50.8	1.46
20X-3, 90-93	184.40	1.90	2.73	53.2	40.2	1.14
20X-4, 90-93	185.90	1.96	2.72	50.3	35.6	1.01
21X-1, 90-93	191.10	1.83	2.82	57.7	47.8	1.36
21X-2, 90-93	192.60	1.73	2.75	64.0	61.1	1.78
21X-3, 90-93	194.10	1.81	2.87	63.0	55.6	1.71
21X-4, 90-93	195.60	1.86	2.80	62.6	52.8	1.68
21X-5, 90-93	197.10	1.88	2.76	55.6	43.5	1.25
21X-6, 90-93	198.60	1.81	2.75	57.5	48.2	1.35
22X-1, 90-93	200.70	1.90	2.77	53.2	40.1	1.14
22X-2, 90-93	202.20	1.92	2.76	55.1	41.6	1.23
22X-3, 90-93	203.70	1.72	2.82	62.3	59.1	1.65
22X-4, 90-93	205.20	1.81	2.80	58.1	49.1	1.39
22X-5, 90-93	206.70	1.74	2.79	61.8	57.0	1.62
22X-6, 90-93	208.20	1.87	2.82	55.8	44.0	1.26
23X-1, 90-93	210.00	1.86	2.73	53.5	41.8	1.15
23X-2, 90-93	211.50	1.83	2.74	55.5	45.0	1.25
23X-3, 90-93	213.00	1.86	2.75	54.2	42.6	1.18
23X-4, 90-93	214.50	1.94	2.81	51.7	37.7	1.07
23X-5, 90-93	216.00	1.83	2.73	55.5	45.3	1.25
23X-6, 90-93	217.50	1.78	2.74	57.6	49.4	1.36
24X-1, 90-93	219.60	1.81	2.63	55.6	46.0	1.25
24X-2, 90-93	221.10	1.91	2.79	49.8	36.5	0.99
24X-3, 90-93	222.60	1.90	2.79	51.2	38.1	1.05
24X-4, 90-93	224.10	1.94	2.84	50.6	36.4	1.03
24X-5, 90-93	225.60	1.95	2.74	48.7	34.4	0.95

Table 8 (continued).

Core, section, interval, (cm)	Depth (mbsf)	Bulk density (g/cm <sup>3</sup> )	Grain density (g/cm <sup>3</sup> )	Porosity (%)	Water content (%)	Void ratio
25X-1, 90-93	228.90	1.78	2.76	57.1	48.9	1.33
25X-2, 90-93	230.40	1.71	2.81	61.2	57.8	1.58
25X-3, 90-93	231.90	1.87	2.73	52.3	40.0	1.10
25X-4, 90-93	233.40	1.75	2.72	60.8	55.4	1.55
25X-5, 90-93	234.90	1.87	2.77	52.1	39.9	1.09
25X-6, 90-93	236.40	1.86	2.78	54.6	43.0	1.20
26X-1, 90-93	238.60	1.79	2.70	56.6	48.0	1.31
26X-2, 90-93	240.10	1.75	2.68	61.3	55.7	1.58
26X-3, 90-93	241.60	1.81	2.77	57.1	47.7	1.33
26X-4, 90-93	243.10	1.74	2.78	61.2	56.4	1.58
26X-5, 90-93	244.60	1.71	2.73	61.1	57.7	1.57
26X-6, 90-93	246.10	1.81	2.72	55.1	45.3	1.23
27X-1, 90-93	248.92	1.87	2.78	53.4	41.4	1.14
27X-3, 90-93	250.42	1.88	2.86	54.6	42.4	1.20
27X-4, 90-93	251.92	1.88	2.78	54.6	42.3	1.20
27X-5, 90-93	253.42	1.87	2.45	55.4	43.5	1.24
27X-6, 90-93	254.92	1.84	2.75	55.6	44.8	1.25
27X-7, 90-93	256.42	1.92	2.83	52.9	39.4	1.13
28X-1, 90-93	257.90	1.74	2.55	59.6	54.0	1.47
28X-2, 90-93	259.40	1.82	2.75	56.5	46.6	1.30
28X-3, 90-93	260.90	1.86	2.91	55.0	43.4	1.22
28X-4, 90-93	262.40	1.83	2.76	57.0	46.8	1.33
28X-5, 90-93	263.90	1.81	2.76	55.1	45.2	1.23
28X-6, 90-93	265.40	1.85	2.77	55.2	44.0	1.23
29X-1, 90-93	267.60	1.82	2.76	54.1	43.6	1.18
29X-2, 90-93	269.10	1.81	2.80	57.4	48.1	1.35
29X-3, 90-93	270.60	1.83	2.81	56.7	46.4	1.31
29X-4, 90-93	272.10	1.82	2.85	57.0	47.2	1.33
29X-5, 90-93	273.60	1.73	2.76	60.1	55.0	1.51
29X-6, 90-93	275.10	1.80	2.76	58.6	49.9	1.41
30X-1, 90-93	277.20	1.74	2.79	61.8	57.1	1.62
30X-2, 90-93	278.70	1.83	2.94	56.8	46.5	1.32
30X-3, 90-93	280.20	1.73	2.82	50.0	42.1	1.00
30X-4, 90-93	281.70	1.84	2.75	56.4	45.9	1.29
30X-5, 90-93	283.20	1.84	2.77	56.1	45.4	1.28
31X-2, 90-93	287.46	1.80	2.97	56.2	46.9	1.28
31X-3, 90-93	288.96	1.91	2.75	50.8	37.5	1.03
31X-4, 90-93	290.46	1.83	2.74	57.6	47.6	1.36
31X-5, 90-93	291.96	1.82	2.75	57.4	47.6	1.35
31X-6, 90-93	293.46	1.76	2.83	58.2	51.3	1.40
31X-7, 90-93	294.96	1.85	2.75	54.6	43.3	1.20
32X-1, 90-93	296.50	1.89	2.78	54.2	41.6	1.18
32X-2, 90-93	298.00	1.92	2.79	55.4	41.9	1.24
32X-3, 90-93	299.50	1.94	2.86	54.0	40.0	1.17
32X-4, 90-93	301.00	1.87	2.74	56.3	44.7	1.29
32X-5, 90-93	302.50	1.81	2.84	57.2	48.1	1.34
32X-6, 90-93	304.00	1.96	2.62	50.2	35.5	1.01
33X-1, 90-93	306.20	1.96	2.76	53.2	38.4	1.14
33X-2, 90-93	307.70	1.83	2.47	53.9	43.2	1.17
33X-3, 90-93	309.20	1.86	2.80	52.2	40.3	1.09
34X-1, 90-93	315.80	1.77	2.71	57.9	50.3	1.38
34X-2, 90-93	317.30	1.93	2.75	52.2	38.4	1.09
34X-3, 90-93	318.80	1.87	2.74	55.0	43.3	1.22
34X-4, 90-93	320.30	1.83	2.78	54.3	43.7	1.19
34X-5, 93-96	321.83	1.79	2.77	56.4	47.7	1.30
34X-6, 90-93	323.30	1.82	2.77	56.4	46.6	1.29
35X-1, 100-102	325.60	1.99	2.82	54.9	39.4	1.22
35X-2, 100-102	327.10	1.83	2.77	55.7	45.2	1.26
35X-3, 100-102	328.60	1.75	2.78	62.6	58.0	1.68
35X-4, 100-102	330.10	1.95	2.81	53.5	39.1	1.15
35X-5, 100-102	331.60	1.84	2.71	58.6	48.5	1.42
35X-6, 100-102	333.10	1.92	2.47	51.9	38.3	1.08
36X-1, 100-104	335.20	2.01	2.96	51.9	36.0	1.08
36X-2, 100-103	336.70	1.89	2.96	55.9	43.6	1.27
36X-3, 96-100	338.16	1.84	2.74	60.3	50.7	1.52
36X-4, 98-101	339.68	1.68	2.74	64.5	64.9	1.82
36X-5, 96-99	341.16	1.82	2.50	56.5	46.7	1.30
36X-6, 97-99	342.67	1.89	2.82	64.4	53.7	1.81
37X-1, 90-93	344.80	1.87	2.79	57.9	46.4	1.38
37X-2, 90-93	346.30	1.83	2.79	55.3	44.7	1.24
37X-3, 90-93	347.80	1.91	2.76	54.2	40.9	1.18
37X-4, 90-93	349.30	1.85	2.76	55.1	43.8	1.23
37X-5, 90-93	350.80	1.86	2.76	57.1	45.8	1.33
37X-6, 90-93	352.30	1.86	2.82	57.1	45.8	1.33
38X-2, 97-99	355.29	1.95	2.76	49.5	35.1	0.98
38X-3, 97-99	356.79	2.09	2.73	51.3	33.7	1.06
38X-4, 97-99	358.29	1.87	2.79	57.3	45.6	1.34

Table 8 (continued).

Core, section, interval, (cm)	Depth (mbsf)	Bulk density (g/cm <sup>3</sup> )	Grain density (g/cm <sup>3</sup> )	Porosity (%)	Water content (%)	Void ratio
38X-5, 97-99	359.79	1.94	2.81	51.8	37.8	1.08
38X-6, 97-99	361.29	2.00	2.74	52.4	36.6	1.10
38X-7, 98-100	362.80	1.94	2.73	50.5	36.4	1.02
39X-1, 72-75	363.72	1.96	2.79	55.4	40.8	1.24
39X-2, 72-75	365.22	2.00	2.86	55.3	39.4	1.24
39X-3, 72-75	366.72	1.90	2.83	56.6	43.8	1.30
39X-4, 72-75	368.22	1.98	2.84	52.9	37.7	1.12
39X-5, 72-75	369.72	1.87	2.91	58.8	47.6	1.43
39X-6, 72-75	371.22	1.96	2.79	49.8	35.1	0.99
40X-1, 100-103	373.70	1.93	2.78	51.4	37.4	1.06
40X-2, 100-103	375.20	2.00	2.83	51.8	36.0	1.07
40X-3, 100-103	376.70	1.95	2.88	52.2	37.8	1.09
40X-4, 100-103	378.20	2.02	2.90	47.7	31.9	0.91
40X-5, 100-103	379.70	2.03	2.80	48.2	32.1	0.93
40X-6, 100-103	381.20	2.02	2.85	47.1	31.4	0.89
41X-1, 100-103	383.40	1.88	2.78	61.4	50.3	1.59
41X-2, 100-103	384.90	1.91	2.85	56.9	44.1	1.32
41X-3, 100-103	386.40	1.91	2.68	53.7	40.4	1.16
41X-4, 100-103	387.90	1.89	2.84	57.8	45.7	1.37
41X-5, 100-103	389.40	1.93	2.80	54.1	40.3	1.18
41X-6, 100-103	390.90	1.92	2.80	52.7	39.1	1.11
42X-1, 100-103	393.00	1.88	2.73	54.2	42.0	1.19
42X-2, 100-103	394.50	1.90	2.78	53.7	40.7	1.16
42X-3, 100-103	396.00	2.05	2.78	48.3	31.9	0.94
42X-4, 100-103	397.50	1.90	2.86	53.2	40.2	1.14
42X-5, 100-103	399.00	1.99	2.91	48.9	33.7	0.96
42X-6, 100-103	400.50	1.88	2.74	53.8	41.5	1.16
43X-1, 100-102	402.60	1.97	2.82	50.4	35.5	1.02
43X-2, 100-102	404.10	1.95	2.86	55.4	41.1	1.24
43X-3, 100-102	405.60	1.92	2.78	53.8	40.3	1.16
43X-4, 100-102	407.10	2.01	2.75	47.4	31.8	0.90
43X-5, 100-102	408.60	1.91	2.73	52.4	39.1	1.10
43X-6, 100-102	410.10	1.88	2.80	54.0	41.6	1.17
44X-1, 100-102	412.30	1.98	2.74	48.2	33.2	0.93
44X-3, 97-99	415.27	2.01	2.81	49.6	33.9	0.98
45X-1, 100-102	421.90	1.84	2.73	54.3	43.2	1.19
45X-3, 100-102	424.90	1.85	2.67	52.0	40.3	1.08
45X-5, 100-102	427.90	1.90	2.72	57.0	44.4	1.32
46X-1, 100-102	431.60	2.00	2.73	47.8	32.4	0.91
46X-3, 100-102	434.60	2.02	2.74	47.0	31.2	0.89
46X-5, 100-102	437.60	2.02	2.66	45.5	30.0	0.84
47X-1, 100-102	441.30	1.99	2.68	44.6	29.8	0.81
47X-3, 100-102	444.30	1.98	2.69	45.6	30.9	0.84
47X-5, 100-102	447.30	2.02	2.83	46.4	30.7	0.87
48X-1, 100-102	450.90	1.88	2.69	56.7	44.6	1.31
48X-3, 100-102	453.90	1.86	2.73	54.7	43.1	1.21
48X-5, 8-10	455.98	1.91	2.75	52.3	39.1	1.10
49X-1, 100-102	460.60	1.83	2.72	57.4	47.5	1.35
49X-3, 100-102	463.60	1.87	2.69	52.5	40.3	1.11
49X-5, 100-102	466.60	1.90	2.74	52.5	39.5	1.10
49X-6, 100-102	468.10	1.94	2.71	50.2	36.0	1.01
50X-1, 100-102	470.20	1.87	2.63	53.6	41.6	1.15
50X-3, 100-102	473.20	1.89	2.63	49.1	36.4	0.97
52X-1, 100-103	488.80	1.96	2.76	49.4	34.8	0.98
52X-3, 102-103	491.82	1.99	2.69	46.7	31.6	0.88
52X-5, 90-93	494.70	1.94	2.73	50.1	35.9	1.00
53X-1, 107-109	498.57	1.99	2.67	45.7	30.8	0.84
53X-3, 100-102	501.50	1.97	2.73	47.6	32.8	0.91
53X-5, 56-57	503.60	2.00	2.66	46.4	31.2	0.87
53X-7, 5-6	506.09	2.00	2.72	49.4	33.9	0.98
54X-1, 100-103	508.10	1.95	2.64	47.8	33.5	0.92
54X-3, 100-103	511.10	1.87	2.73	46.2	33.8	0.86
54X-5, 94-96	514.04	1.90	2.69	50.6	37.5	1.03
55X-1, 100-103	517.80	1.90	2.70	49.1	36.0	0.97
55X-3, 100-103	520.80	1.97	2.64	46.7	32.0	0.88
55X-5, 95-97	523.75	1.84	2.70	55.7	45.1	1.26
56X-1, 112-114	527.52	1.98	2.66	47.7	32.7	0.91
56X-3, 104-107	530.44	1.98	2.72	47.1	32.2	0.89
56X-5, 59-61	532.99	1.93	2.64	50.2	36.5	1.01
57X-1, 120-122	536.90	1.91	2.72	48.3	35.1	0.94
57X-3, 132-133	540.02	2.01	2.66	51.3	35.4	1.05
57X-5, 134-135	543.04	2.00	2.67	50.7	35.1	1.03
58X-1, 105-107	546.45	2.04	2.63	46.7	30.6	0.88
58X-2, 107-108	547.97	2.02	2.71	46.5	30.9	0.87
58X-3, 107-108	549.47	2.05	2.70	50.4	33.7	1.02
58X						

Table 8 (continued).

Core, section, interval, (cm)	Depth (mbsf)	Bulk density (g/cm <sup>3</sup> )	Grain density (g/cm <sup>3</sup> )	Porosity (%)	Water content (%)	Void ratio
58X-6, 106-108	553.96	2.05	2.66	47.5	31.1	0.91
59X-1, 104-106	556.04	1.95	2.68	52.1	37.7	1.09
59X-2, 108-110	557.58	2.04	2.69	53.1	36.4	1.13
59X-3, 104-106	559.04	2.04	2.64	45.9	30.0	0.85
59X-4, 102-104	560.52	2.02	2.70	49.1	33.2	0.97
59X-5, 101-103	562.01	2.01	2.79	45.3	30.0	0.83
60X-1, 126-128	565.96	2.14	2.71	47.3	29.2	0.90
60X-2, 134-135	567.54	2.00	2.66	45.1	30.0	0.82
60X-3, 134-135	569.04	2.07	2.70	43.8	27.7	0.78
60X-4, 145-146	570.65	2.07	2.67	45.8	29.3	0.85
60X-5, 119-120	571.89	2.05	2.75	42.7	27.2	0.75
61X-1, 149-150	575.79	2.14	2.63	50.6	32.0	1.03
61X-2, 143-145	577.23	2.07	2.70	46.2	29.7	0.86
61X-3, 143-145	578.73	2.09	2.69	43.3	26.9	0.77
61X-4, 149-150	580.29	2.13	2.67	45.5	28.0	0.83
61X-5, 149-150	581.79	2.05	2.65	42.7	27.1	0.74
61X-6, 146-149	583.26	2.06	2.72	43.7	27.9	0.78
62X-1, 146-149	585.36	2.11	2.74	39.7	23.8	0.66
62X-2, 146-149	586.86	2.09	2.70	42.6	26.4	0.74
62X-3, 146-149	588.36	2.08	2.66	43.9	27.6	0.78
62X-4, 146-149	589.86	2.00	2.72	45.0	29.9	0.82
62X-5, 146-149	591.36	1.99	2.66	48.1	32.8	0.93
62X-6, 146-149	592.86	2.10	2.72	45.1	28.2	0.82
63X-1, 138-140	594.98	2.04	2.69	47.6	31.5	0.91
63X-2, 138-140	596.48	2.02	2.68	47.6	31.9	0.91
63X-3, 138-140	597.98	2.07	2.70	40.3	24.9	0.67
63X-4, 138-140	599.48	2.02	2.65	47.5	31.8	0.91
63X-5, 138-140	600.98	2.04	2.73	45.0	29.2	0.82
63X-6, 138-140	602.48	2.06	2.70	44.7	28.7	0.81
64X-2, 138-140	606.08	2.08	2.67	44.2	27.8	0.79
64X-3, 138-140	607.58	2.01	2.76	48.3	32.7	0.94
64X-4, 138-140	609.08	1.97	2.67	49.1	34.2	0.96
65X-1, 138-140	614.18	2.08	2.72	43.6	27.4	0.77
65X-2, 138-140	615.68	2.03	2.69	45.2	29.6	0.82
65X-3, 138-140	617.18	2.03	2.63	47.3	31.3	0.90
65X-4, 138-140	618.68	2.03	2.69	45.2	29.6	0.83
65X-5, 138-140	620.18	2.09	2.70	41.7	25.8	0.72
66X-1, 100-102	623.50	1.99	2.69	46.5	31.4	0.87
66X-2, 100-102	625.00	2.20	2.65	41.0	23.6	0.69
66X-3, 100-102	626.50	2.01	2.68	38.9	24.8	0.64
66X-4, 100-102	628.00	2.00	2.70	43.7	28.8	0.78
66X-5, 100-102	629.50	2.10	2.72	44.0	27.3	0.79
66X-6, 100-102	631.00	2.01	2.78	43.9	28.9	0.78
67X-1, 115-118	633.35	2.01	2.71	46.9	31.5	0.88
67X-2, 57-59	634.27	2.03	2.71	41.6	26.5	0.71
67X-3, 54-56	635.74	2.02	2.73	43.3	28.1	0.76
67X-4, 95-97	637.65	2.13	2.68	40.2	24.0	0.67
67X-5, 57-59	638.77	2.06	2.89	44.4	28.3	0.80
67X-6, 14-17	639.84	2.09	2.72	46.6	29.7	0.87
68X-1, 49-52	642.09	2.05	2.53	40.2	25.1	0.67
68X-2, 99-102	644.09	2.04	2.66	39.6	24.9	0.66
68X-3, 63-66	645.23	2.10	2.71	42.7	26.4	0.74
68X-4, 117-120	647.27	2.13	2.70	44.0	26.8	0.79
68X-5, 81-84	648.41	2.08	2.72	41.7	25.8	0.72
68X-6, 111-114	650.21	2.04	2.65	40.7	25.6	0.69
69X-1, 57-59	651.47	2.10	2.69	37.7	22.6	0.60
69X-2, 13-15	652.53	2.09	2.97	41.6	25.6	0.71
69X-3, 109-111	654.99	2.18	2.71	44.5	26.5	0.80
69X-4, 106-108	656.46	2.09	2.68	41.6	25.6	0.71
69X-5, 72-75	657.62	2.07	2.67	45.2	28.9	0.83
69X-6, 78-80	659.18	2.03	2.90	45.2	29.6	0.83
70X-1, 144-146	662.04	2.12	2.64	40.4	24.3	0.68
70X-2, 144-146	663.59	2.20	2.74	37.0	20.9	0.59
70X-3, 144-146	665.09	1.98	2.70	40.1	26.2	0.67
70X-4, 144-146	666.59	2.10	2.65	41.1	25.1	0.70
70X-6, 144-146	669.59	1.98	2.65	40.7	26.6	0.69
71X-1, 84-86	671.14	2.10	2.69	39.4	23.8	0.65
71X-2, 105-108	672.85	2.08	2.66	44.1	27.8	0.79
71X-3, 86-89	674.16	2.04	2.71	45.3	29.4	0.83
71X-4, 70-73	675.50	2.10	2.72	42.5	26.2	0.74
71X-5, 81-84	677.11	2.11	2.71	38.6	23.1	0.63
71X-6, 54-57	678.34	2.13	2.67	41.2	24.8	0.70
72X-1, 87-90	680.77	2.02	2.73	43.3	28.2	0.77
72X-2, 136-138	682.76	2.10	2.66	41.3	25.2	0.70
72X-3, 114-116	684.04	2.15	2.77	39.5	23.2	0.65
72X-4, 102-104	685.42	2.09	2.68	43.5	27.1	0.77
72X-5, 79-81	686.69	2.09	2.71	41.1	25.2	0.70

Table 8 (continued).

Core, section, interval, (cm)	Depth (mbsf)	Bulk density (g/cm <sup>3</sup> )	Grain density (g/cm <sup>3</sup> )	Porosity (%)	Water content (%)	Void ratio
72X-6, 100-103	688.40	2.10	2.69	38.5	23.1	0.63
73X-1, 124-125	690.84	2.09	2.70	39.3	23.9	0.65
73X-2, 124-125	692.34	2.12	2.77	41.3	24.9	0.70
73X-3, 70-71	693.30	2.13	2.63	38.3	22.6	0.62
73X-4, 44-46	694.54	2.19	2.72	37.0	20.9	0.59
73X-5, 53-55	696.13	2.15	2.71	35.8	20.6	0.56
73X-6, 81-83	697.91	2.14	2.70	39.4	23.2	0.65
74X-1, 93-94	700.23	2.10	2.67	38.4	23.0	0.62
74X-2, 86-88	701.66	2.12	2.70	39.2	23.3	0.65
74X-3, 82-84	703.12	2.12	2.75	37.4	22.0	0.60
74X-4, 134-136	705.14	2.14	2.69	40.1	23.8	0.67
74X-5, 59-60	705.89	2.12	2.65	37.0	21.8	0.59
74X-6, 123-125	708.03	2.15	2.73	38.2	22.2	0.62
75X-1, 80-83	709.70	2.05	2.71	42.0	26.6	0.73
75X-2, 80-83	711.20	2.08	2.76	42.0	26.0	0.72
75X-3, 80-83	712.70	2.14	2.67	40.7	24.2	0.69
75X-4, 80-83	714.20	2.09	2.71	43.8	27.3	0.78
75X-5, 80-83	715.70	1.97	2.67	41.0	27.0	0.69
75X-6, 80-83	717.20	2.03	2.68	48.1	32.0	0.93
76X-1, 140-142	720.00	2.15	2.65	40.1	23.6	0.67
76X-2, 124-126	721.34	2.16	2.67	38.7	22.5	0.63
76X-3, 103-105	722.63	2.11	2.70	40.7	24.6	0.69
76X-5, 133-135	725.93	2.20	2.78	40.5	23.2	0.68
76X-6, 142-144	727.52	2.12	2.86	41.8	25.3	0.72
77X-1, 141-143	729.61	2.09	2.79	46.8	29.8	0.88
77X-3, 134-136	732.54	2.08	2.73	45.5	28.8	0.84
77X-5, 140-142	735.60	2.13	2.72	42.5	25.7	0.74
78X-1, 127-129	739.17	2.10	2.66	42.6	26.2	0.74
78X-2, 127-129	740.67	2.07	2.69	42.6	26.7	0.74
78X-3, 127-129	742.17	2.10	2.72	42.3	25.9	0.73
79X-1, 141-143	749.01	1.99	2.74	39.7	25.6	0.66
79X-2, 141-143	750.51	2.14	2.68	41.9	25.1	0.72
79X-3, 141-143	752.01	2.09	2.82	43.7	27.3	0.78
79X-5, 141-143	755.01	2.11	2.72	43.2	26.5	0.76
79X-6, 141-143	756.51	2.12	2.74	40.5	24.3	0.68
80X-1, 141-143	758.71	2.13	2.73	39.2	23.2	0.64
80X-2, 144-146	760.24	2.04	2.74	37.8	23.4	0.61
80X-3, 143-145	761.73	2.13	2.71	39.0	23.1	0.64
80X-4, 147-149	763.27	2.16	2.78	39.4	23.0	0.65
80X-5, 147-149	764.77	2.14	2.73	42.3	25.4	0.73
80X-6, 139-141	766.19	2.04	2.75	44.0	28.4	0.79
81X-1, 147-149	768.47	2.17	2.75	39.0	22.6	0.64
81X-3, 147-149	771.47	2.19	2.74	39.6	22.8	0.66
81X-5, 147-149	774.47	2.13	2.67	38.6	22.9	0.63
82X-1, 144-146	778.14	2.26	2.72	32.5	17.3	0.48
82X-2, 134-135	779.54	2.33	2.73	30.6	15.6	0.44
82X-3, 134-135	781.04	2.02	2.67	37.8	23.8	0.61
83X-1, 144-146	787.84	2.17	2.61	36.2	20.5	0.57
83X-2, 119-121	789.09	2.12	2.71	43.0	26.2	0.76
83X-3, 128-130	790.68	2.15	2.63	41.5	24.6	0.71
133-823C-						
1R-1, 101-102	785.01	2.10	2.72	37.2	22.2	0.59
1R-2, 71-72	786.21	2.12	2.71	36.2	21.2	0.57
1R-3, 22-23	787.22	2.24	2.65	37.2	20.5	0.59
1R-4, 30-31	788.80	2.15	2.64	38.1	22.2	0.62
1R-5, 29-31	790.29	2.27	2.75	30.6	16.0	0.44
2R-1, 85-87	794.45	2.26	2.68	32.4	17.2	0.48
2R-2, 51-53	795.61	2.34	2.63	26.0	12.9	0.35
2R-3, 149-150	798.09	2.04	2.71	39.4	24.7	0.65
24-4, 113-115	799.23	2.01	2.76	46.3	30.9	0.86
3R-1, 121-123	804.11	2.12	2.70	33.7	19.5	0.51
3R-2, 117-119	805.57	2.13	2.67	35.4	20.6	0.55
3R-3, 14-16	806.04	2.19	2.67	33.5	18.6	0.51
3R-4, 24-26	807.64	2.26	2.73	31.7	16.8	0.47
4R-1, 28-30	812.88	2.22	2.71	31.6	17.1	0.46
4R-2, 110-112	815.20	2.20	2.63	30.6	16.7	0.44
4R-3, 100-102	816.60	2.13	2.70	36.2	21.0	0.57
4R-4, 94-96	818.04	2.25	2.74	30.6	16.2	0.44
5R-1, 8-10	822.38	2.21	2.70	30.3	16.4	0.44
5R-2, 4-5	823.84	2.20	2.67	31.8	17.4	0.47
5R-3, 97-99	826.27	2.27	2.72	28.3	14.7	0.39
5R-4, 52-54	827.32	2.23	2.72	32.5	17.5	0.48
5R-5, 109-110	829.39	2.20	2.74	32.8	18.0	0.49
5R-6, 33-34	830.13	2.22	2.61	30.9	16.6	0.45
6R-1, 36-38	832.36	2.30	2.74	29.5	15.2	0.42

Table 8 (continued).

Core, section, interval, (cm)	Depth (mbsf)	Bulk density (g/cm <sup>3</sup> )	Grain density (g/cm <sup>3</sup> )	Porosity (%)	Water content (%)	Void ratio
7R-1, 7-9	841.77	2.26	2.69	30.1	15.8	0.43
7R-2, 65-66	843.85	2.14	2.69	35.9	20.8	0.56
7R-3, 10-11	844.80	2.38	2.73	26.3	12.8	0.36
7R-4, 18-20	846.38	2.32	2.70	28.0	14.1	0.39
7R-5, 120-122	848.90	2.27	2.67	30.9	16.2	0.45
7R-6, 9-11	849.29	2.09	2.64	35.9	21.3	0.56
8R-1, 75-77	852.15	2.68	2.69	37.7	16.8	0.61
9R-1, 73-74	861.83	2.09	2.89	42.8	26.5	0.75
9R-2, 45-47	863.05	2.10	2.65	37.9	22.6	0.61
9R-3, 124-127	865.34	2.25	2.67	33.7	18.1	0.51
9R-4, 110-113	866.70	2.23	2.45	38.3	21.4	0.62
9R-5, 118-119	868.28	2.03	2.73	42.6	27.4	0.74
10R-1, 38-40	871.18	2.04	2.68	43.2	27.7	0.76
10R-2, 140-142	873.70	2.32	2.66	31.0	15.8	0.45
10R-3, 50-52	874.30	2.09	2.72	45.4	28.6	0.83
10R-4, 106-108	876.36	1.99	2.78	46.7	31.7	0.87
10R-5, 140-143	878.20	1.92	2.69	54.2	40.7	1.18
10R-6, 65-67	878.95	1.99	2.70	49.6	34.2	0.98
11R-1, 80-82	881.20	2.22	2.70	36.9	20.6	0.59
11R-2, 138-140	883.28	2.24	2.58	34.3	18.6	0.52
11R-3, 82-84	884.22	2.19	2.71	36.0	20.2	0.56
11R-4, 68-70	885.58	2.19	2.66	38.4	21.8	0.62
11R-5, 80-82	887.20	1.93	2.74	51.9	38.0	1.08
12R-1, 95-97	891.05	2.05	2.77	44.8	29.0	0.81
12R-2, 138-140	892.98	2.15	2.68	43.4	26.1	0.77
12R-3, 121-123	894.31	2.19	2.68	34.6	19.3	0.53
12R-4, 71-72	895.31	2.14	2.72	40.0	23.6	0.67
12R-5, 55-56	896.65	2.29	2.72	33.3	17.5	0.50
12R-6, 25-26	897.85	2.30	2.69	30.1	15.5	0.43
13R-1, 60-62	900.30	2.11	2.69	45.6	28.5	0.84
13R-2, 138-140	902.07	2.26	2.72	32.2	17.1	0.47
13R-3, 61-63	902.80	2.10	2.69	39.6	24.0	0.66
13R-4, 45-47	904.14	2.34	2.70	26.0	12.9	0.35
13R-5, 41-43	905.60	2.06	2.75	41.6	26.1	0.71
13R-6, 27-29	906.96	2.15	2.74	37.7	21.9	0.60
14R-1, 108-110	910.48	2.09	2.74	41.9	25.8	0.72
14R-2, 135-137	912.25	1.99	2.70	46.4	31.3	0.86
14R-3, 103-105	913.43	2.05	2.69	44.7	28.7	0.81
14R-4, 53-55	914.43	2.02	2.74	46.9	31.2	0.88
14R-5, 132-134	916.72	2.29	2.86	42.7	23.6	0.75
15R-1, 19-21	919.29	2.22	2.75	33.4	18.2	0.50
15R-2, 13-15	920.73	2.19	2.66	3.97	22.8	0.66
15R-3, 12-14	922.22	2.05	2.75	42.9	27.3	0.75
15R-4, 24-26	923.84	2.21	2.81	34.4	19.0	0.52
15R-5, 41-43	925.51	2.10	2.61	39.7	24.1	0.66
15R-6, 74-76	927.34	2.35	2.68	27.1	13.4	0.37
16R-1, 52-54	929.32	2.26	2.74	31.6	16.7	0.46
16R-2, 97-99	931.27	2.21	2.83	31.5	17.1	0.46
16R-3, 86-88	932.66	2.24	2.70	31.0	16.5	0.45
16R-4, 55-56	933.85	2.10	2.65	37.5	22.4	0.60
16R-5, 123-124	936.03	2.12	2.73	34.8	20.2	0.53
17R-1, 62-64	939.02	2.20	2.75	32.3	17.7	0.48
17R-2, 121-122	941.11	2.13	2.71	34.4	19.8	0.53
17R-3, 40-42	941.80	2.20	2.69	33.6	18.6	0.51
17R-4, 112-113	944.02	1.97	2.72	41.4	27.4	0.71
17R-5, 5-6	944.45	2.29	2.73	29.3	15.1	0.41
17R-6, 27-28	946.17	2.38	2.65	33.0	16.5	0.49
17R-7, 20-22	947.60	2.29	2.67	26.8	13.6	0.37
18R-1, 96-98	948.96	2.30	2.70	28.7	14.6	0.40
18R-2, 20-21	949.70	2.31	2.72	25.6	12.8	0.34
18R-3, 79-81	951.79	2.20	2.73	33.8	18.7	0.51
18R-4, 111-112	953.61	2.19	2.68	32.2	17.7	0.48
18R-5, 111-113	955.11	2.34	2.74	26.1	12.9	0.35
18R-6, 17-19	955.67	2.11	2.76	36.2	21.3	0.57
19R-1, 113-115	958.43	2.34	2.76	28.5	14.3	0.40
19R-2, 70-72	959.50	2.23	2.71	32.7	17.6	0.49
19R-3, 110-111	961.40	2.25	2.71	32.8	17.6	0.49
19R-4, 96-98	962.76	2.15	2.79	38.2	22.3	0.62
19R-5, 33-34	963.63	2.35	2.67	26.9	13.3	0.37
20R-1, 80-81	967.70	2.15	2.73	38.2	22.2	0.62
20R-2, 10-11	968.50	2.46	2.68	19.8	9.0	0.25
20R-3, 57-58	970.47	2.43	2.58	27.6	13.2	0.38
20R-4, 84-85	972.24	2.23	2.79	31.9	17.2	0.47
20R-5, 69-70	973.59	2.27	2.75	30.6	16.0	0.44
20R-6, 45-46	974.85	2.45	2.62	25.5	11.9	0.34
21R-1, 134-136	977.94	2.21	2.74	33.3	18.2	0.50
21R-2, 107-108	979.17	2.21	2.76	33.3	18.2	0.50

Table 8 (continued).

Core, section, interval, (cm)	Depth (mbsf)	Bulk density (g/cm <sup>3</sup> )	Grain density (g/cm <sup>3</sup> )	Porosity (%)	Water content (%)	Void ratio
21R-3, 94-95	980.54	2.60	2.75	12.9	5.4	0.15
21R-4, 120-121	982.30	2.26	2.72	34.4	18.5	0.52
21R-5, 20-21	982.80	2.13	2.72	37.8	22.2	0.61
21R-6, 50-52	984.60	2.31	2.75	29.5	15.1	0.42
22R-1, 85-86	987.05	2.20	2.70	35.2	19.6	0.54
22R-2, 38-39	988.08	2.29	2.70	30.2	15.6	0.43
22R-3, 1-3	989.21	2.32	2.70	29.0	14.7	0.41
22R-4, 65-66	991.35	2.20	2.78	39.4	22.5	0.65
22R-5, 83-84	993.03	2.16	2.72	37.9	21.9	0.61
22R-6, 30-31	994.00	2.16	2.68	34.5	19.6	0.53
23R-1, 93-94	996.83	2.11	2.71	35.7	21.0	0.56
23R-2, 24-26	997.64	2.30	2.74	25.8	13.0	0.35
23R-3, 57-59	999.47	2.60	2.69	12.0	5.0	0.14
23R-4, 32-34	1000.72	2.41	2.68	22.6	10.6	0.29
23R-5, 117-119	1003.07	2.31	2.85	28.9	14.7	0.41
24R-1, 118-120	1006.78	2.20	2.69	29.1	15.7	0.41
24R-2, 102-104	1008.12	2.17	2.70	37.6	21.6	0.60
24R-3, 37-39	1008.97	2.09	2.74	41.2	25.2	0.70

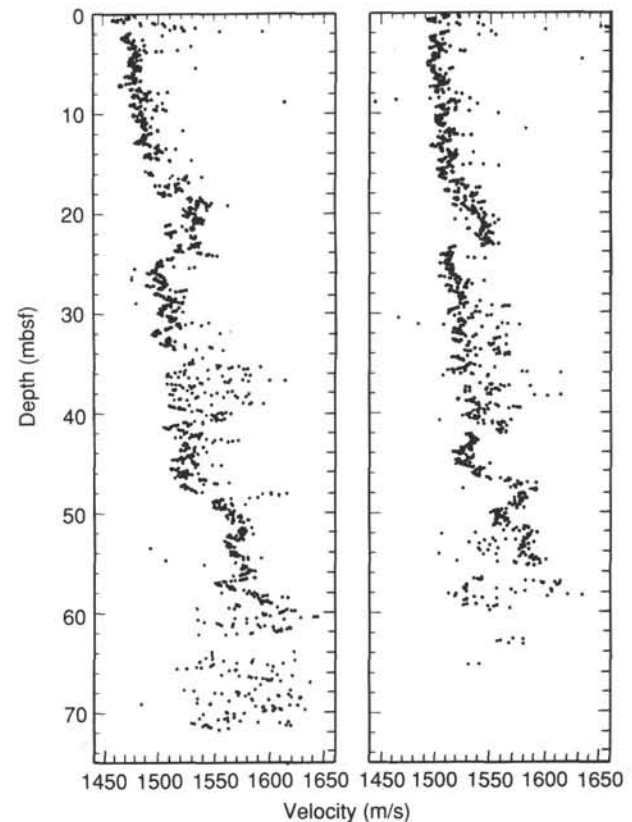


Figure 45. MST sonic velocity data Site 823. Raw data values with amplitudes greater than 30 have been averaged in 5-cm intervals.

TWT below the seafloor, which is just below TD, was subdivided into 11 sequences on the basis of standard seismic stratigraphic procedures. Because this is a basinal site, many of the sequence boundaries do not display disconformable relationships in the site-survey data, and in many cases, boundaries were based primarily on changes in reflection amplitude, reflection continuity, and on changes in seismic character. We are not certain at this stage which of the sequence boundaries have regional significance; however, it is apparent from the site-survey data and the associated seismic transit line across Queensland Trough (Fig. 1) that one should

Table 9. Compressional-wave velocity data, Site 823.

Core, section, interval (cm)	Depth (mbsf)	Distance (mm)	Traveltime ( $\mu$ s)	Velocity (m/s)
133-823A-				
1H-1, 43-46	0.43	30.12	22.44	1503
1H-2, 77-80	2.27	29.07	21.78	1500
1H-3, 90-93	3.90	29.46	21.89	1512
1H-4, 90-93	5.40	28.13	21.02	1511
2H-1, 90-93	6.70	29.98	21.97	1534
2H-2, 90-93	8.20	28.34	21.14	1513
2H-3, 90-93	9.70	28.02	20.90	1515
2H-4, 90-93	11.20	29.90	22.14	1516
2H-5, 90-93	12.70	29.97	22.20	1514
2H-6, 90-93	14.20	29.31	21.77	1514
3H-1, 90-93	16.20	30.86	22.32	1552
3H-2, 90-93	17.70	30.55	22.21	1545
3H-3, 90-93	19.20	29.77	21.53	1560
3H-4, 90-93	20.70	29.99	21.58	1567
3H-5, 90-93	22.20	30.25	22.03	1544
3H-6, 90-93	23.70	28.22	20.61	1552
4H-1, 90-93	25.70	30.08	22.14	1525
4H-2, 90-93	27.20	30.16	21.83	1555
4H-3, 90-93	28.70	30.60	22.41	1531
4H-4, 90-93	30.20	29.37	21.55	1536
4H-5, 90-93	31.70	30.15	22.12	1531
4H-6, 90-93	33.20	30.12	22.10	1531
5H-1, 90-93	35.20	29.12	20.48	1617
5H-2, 90-93	36.70	29.22	20.25	1645
5H-3, 90-93	38.20	29.94	21.41	1580
5H-5, 90-93	41.20	28.37	20.69	1554
5H-6, 90-93	42.70	29.59	22.65	1459
6H-1, 90-93	44.70	30.16	21.87	1552
6H-2, 90-93	46.20	29.51	21.52	1546
6H-3, 90-93	47.70	29.33	21.35	1551
6H-4, 90-93	49.20	30.03	21.29	1595
6H-5, 90-93	50.70	30.47	21.36	1614
6H-6, 90-93	52.20	30.24	21.15	1620
7H-1, 90-93	54.20	29.68	21.09	1593
7H-2, 90-93	55.70	29.33	22.18	1482
7H-6, 90-93	61.70	31.16	23.81	1453
8H-1, 90-93	63.70	30.42	20.79	1664
9H-1, 90-93	73.20	30.12	22.94	1464
9H-2, 90-93	74.70	30.73	21.00	1662
10H-1, 90-93	82.70	30.29	21.22	1616
10H-3, 90-93	85.70	29.59	20.88	1607

be able to trace many of these sequences throughout the trough. We briefly describe these seismic sequences below, as interpreted from BMR water-gun data (Fig. 59); all time depths and thicknesses are two-way traveltimes in seconds below the seafloor, as measured at the site.

Sequence 1 extends from the seafloor down approximately 0.09 s, and its thickness varies within the site area. The character of its upper part has been largely disguised by interference with the seafloor reflection. However, beyond this event, the sequence is characterized by high-amplitude, flat-lying, parallel reflections, which become lower in amplitude toward its base (Fig. 59). The lower boundary of the sequence is one of the most irregular in the section and is overlapped above and conformable with reflectors below. Sequence 1 may be a basin-fill facies that has smoothed out the underlying irregular topography.

Sequence 2 is approximately 0.03 s thick and is characterized by a low-amplitude, discontinuous to chaotic reflection configuration. Its lower boundary is slightly irregular and appears to be gently overlapped and downlapped from above, conformable with reflectors below.

As Sequences 3 to 7 generally have similar internal configurations (i.e., low-amplitude, discontinuous to chaotic reflections, reflection-free in some instances), only their thicknesses, boundaries, and special features are described here.

Sequence 3 is 0.15 s thick and contains strong, discontinuous reflectors toward its top. Its lower boundary has been

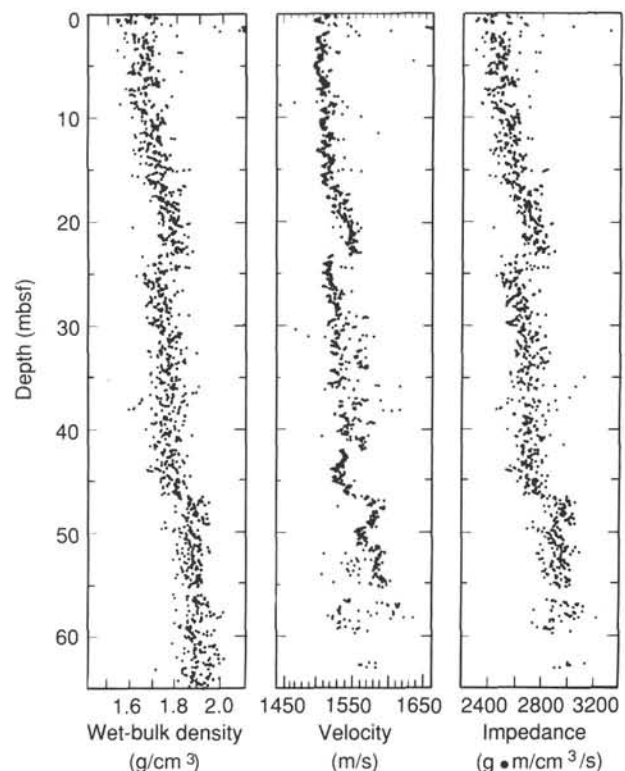


Figure 46. GRAPE wet-bulk density, MST sonic velocity, and impedance calculated as a product of sonic velocity and bulk density.

gently overlapped from above and, in places, exhibits subtle truncation of reflectors below.

Sequence 4 is 0.15 s thick and contains a thin band of strong reflectors near its top and a thicker band near its base. Its lower boundary is gently overlapped from above and may be rough, but on a small scale.

Sequence 5 is 0.12 s thick and is characterized as a reflection-free zone. Its lower boundary may be gently overlapped from above and is conformable with reflectors below.

Sequence 6 is 0.16 s thick and contains a thin band of high-amplitude reflectors near its top. Much of the rest of the sequence is reflection-free, except for vague, low-amplitude reflections near its base to the east of the site (Fig. 59). Its lower boundary is a strong, gently undulating reflector.

Sequence 7 is 0.11 s thick and is characterized by chaotic reflections toward its base. Its lower boundary marks a dramatic change in character of seismic profile to higher amplitude reflections that vary much more in thickness and configuration.

Sequence 8 is only 0.03 s thick and consists of one or two continuous, variable amplitude reflectors.

Sequence 9 is 0.04 s thick and is characterized by variable amplitude reflectors that overlap its lower boundary.

Sequence 10 is 0.09 s thick, but thickens to more than 0.17 s to the west of the site. The sequence is characterized by wavy to subparallel, variable amplitude, continuous reflections. Its lower boundary commonly is downlapped, and reflectors below have been truncated. Total depth at the site lies within this sequence.

Sequence 11 lies below TD and consists of variable amplitude, discontinuous reflections. It exhibits small-throw faulting in places, and both this sequence and Sequence 10 above are gently folded. This faulting and folding seems to intensify in the section below.

Table 10. Vane shear strength data, Hole 823B.

Core, section, interval (cm)	Depth (mbsf)	Spring number	Torque (degrees)	Strain (degrees)	Shear strength (kPa)
133-823B-					
1H-1, 98-99	0.98	4	9	19	10.7
1H-2, 98-99	2.48	4	11	17	13.1
1H-3, 98-99	3.98	4	9	11	10.7
1H-4, 98-99	5.48	4	7	16	8.3
1H-5, 98-99	6.98	4	10	16	11.9
1H-6, 38-39	7.88	4	7	11	8.3
2H-1, 98-99	9.28	2	19	23	8.9
2H-2, 98-99	10.78	2	21	19	9.9
2H-3, 98-99	12.28	2	24	24	11.3
2H-4, 98-99	13.78	2	23	19	10.8
2H-5, 98-99	15.28	2	32	24	15.1
2H-6, 98-99	16.78	2	29	18	13.6
2H-7, 38-39	17.68	2	21	18	9.9
3H-1, 98-99	18.78	2	22	17	10.4
3H-2, 98-99	20.28	2	19	16	8.9
3H-3, 98-99	21.78	2	26	19	12.2
3H-4, 98-99	23.28	2	51	22	24.0
3H-5, 98-99	24.78	2	33	22	15.5
3H-6, 98-99	26.28	2	16	22	7.5
3H-7, 38-39	27.18	2	27	21	12.7
4H-1, 98-99	28.28	2	34	22	16.0
4H-2, 92-93	29.72	2	28	23	13.2
4H-3, 92-93	31.22	2	35	20	16.5
4H-4, 92-93	32.72	2	35	22	16.5
4H-5, 98-99	34.28	2	34	22	16.0
4H-6, 85-86	35.65	2	31	20	14.6
4H-7, 65-66	36.95	2	64	20	30.1
5H-1, 98-99	37.78	2	56	22	26.3
5H-2, 85-86	39.15	2	70	20	32.9
5H-3, 98-99	40.78	2	59	18	27.8
5H-4, 98-99	42.28	2	43	20	20.2
5H-5, 98-99	43.78	2	30	22	14.1
5H-6, 88-89	45.18	2	51	23	24.0
5H-7, 28-29	46.08	2	65	24	30.6
6H-1, 91-92	47.21	2	47	22	22.1
6H-2, 98-99	48.78	2	97	24	45.6
6H-3, 98-99	50.28	2	82	24	38.6
6H-4, 93-94	51.73	2	60	22	28.2
6H-5, 98-99	53.28	2	37	22	17.4
6H-6, 104-105	54.84	2	85	18	40.0
6H-7, 54-55	55.84	2	51	24	24.0
7H-1, 98-99	56.78	2	65	28	30.6
7H-2, 98-99	58.28	2	68	23	32.0
7H-3, 110-111	59.90	2	51	19	24.0
7H-4, 88-89	61.18	2	78	18	36.7
7H-5, 118-119	62.98	2	70	23	32.9
7H-6, 87-88	64.17	2	66	18	31.1
7H-7, 21-22	65.01	2	53	20	24.9
8H-1, 98-99	66.28	2	116	19	54.6
8H-2, 96-97	67.76	2	51	20	24.0
8H-3, 98-99	69.28	2	47	19	22.1
8H-4, 97-98	70.77	2	62	25	29.2
8H-5, 118-119	72.48	2	106	30	49.9
8H-6, 92-93	73.72	2	71	20	33.4
8H-7, 22-23	74.52	2	157	25	73.9
9H-1, 85-86	75.65	4	52	18	61.8
9H-2, 98-99	77.28	4	65	20	77.3
9H-3, 80-81	78.60	4	51	22	60.7
9H-4, 98-99	80.28	4	12	12	14.3

The sequences described above form the uppermost part (1.0 s) of the sedimentary section in this area. Basement was not seen in water-gun data, but may be about 2.3 s below seafloor on normal resolution air-gun data near the site area.

#### Correlation With Site 823 Lithostratigraphy

Correlation with Site 823 was based mainly on a depth match with the synthetic seismogram that was computed using *in-situ* velocity derived from a sonic log obtained from downhole logging. Because of doubts concerning some of the density log data, a constant density was used to calculate acoustic impedance for the synthetic seismogram (see "Explanatory Notes" chapter, "Downhole Measurements" section, this volume, and "Downhole Logging" section, this

Table 10 (continued).

Core, section, interval (cm)	Depth (mbsf)	Spring number	Torque (degrees)	Strain (degrees)	Shear strength (kPa)
9H-5, 94-95	81.74	4	27	16	32.1
9H-6, 86-87	83.16	4	19	16	22.6
9H-7, 49-50	84.29	4	33	14	39.2
10H-1, 86-87	85.16	4	40	13	47.6
10H-2, 86-87	86.66	4	36	11	42.8
10H-3, 86-87	88.16	4	39	8	46.4
10H-4, 86-87	89.66	4	28	17	33.3
10H-5, 86-87	91.16	4	40	14	47.6
10H-6, 86-87	92.66	4	38	14	45.2
11H-1, 86-87	94.66	4	53	13	63.0
11H-2, 86-87	96.16	4	50	16	59.5
11H-3, 86-87	97.66	4	46	15	54.7
11H-4, 86-87	99.16	4	43	13	51.1
11H-5, 86-87	100.66	4	55	20	65.4
11H-6, 86-87	102.16	4	60	23	71.4
12H-1, 86-87	104.16	4	57	15	67.8
12H-2, 91-92	105.71	4	46	17	54.7
12H-3, 91-92	107.21	4	42	23	50.0
12H-4, 91-92	108.71	4	46	19	54.7
12H-5, 53-54	109.83	4	8	11	9.5
12H-6, 99-100	111.79	4	10	11	11.9
13X-2, 99-100	115.29	4	35	10	41.6
13X-3, 98-99	116.78	4	51	10	60.7
13X-4, 97-98	118.27	4	18	11	21.4
13X-5, 97-98	119.77	4	38	13	45.2
14X-1, 97-98	123.37	4	23	10	27.4
14X-2, 90-91	124.80	4	25	10	29.7
14X-3, 94-95	126.34	4	22	11	26.2
14X-4, 95-96	127.85	4	43	12	51.1
14X-5, 95-96	129.35	4	67	12	79.7
14X-6, 95-96	130.85	4	24	10	28.5
15X-1, 96-97	133.06	4	18	11	21.4
15X-2, 94-95	134.54	4	34	12	40.4
15X-3, 94-95	136.04	4	57	15	67.8
15X-4, 94-95	137.54	4	38	14	45.2
15X-5, 94-95	139.04	4	48	15	57.1
15X-6, 90-91	140.50	4	38	12	45.2
17X-1, 109-110	152.49	4	43	13	51.1
17X-2, 109-110	153.99	4	45	13	53.5
17X-3, 109-110	155.49	4	49	15	58.3
17X-4, 109-110	156.99	4	19	7	22.6
17X-5, 109-110	158.49	4	22	14	26.2
18X-1, 102-103	162.12	4	22	17	26.2
18X-2, 102-103	163.62	4	64	16	76.1
18X-3, 102-103	165.12	4	34	15	40.4
18X-4, 97-98	166.57	4	28	20	33.3
18X-5, 97-98	168.07	4	26	12	30.9
18X-6, 83-84	169.43	4	56	13	66.6
19X-1, 107-108	171.87	4	38	11	45.2
19X-2, 108-109	173.38	4	24	10	28.5
19X-3, 82-83	174.62	4	33	10	39.2
19X-4, 82-83	176.12	4	24	11	28.5
19X-5, 87-88	177.67	4	43	18	51.1
19X-6, 87-88	179.17	4	63	16	74.9
20X-1, 106-107	181.56	4	13	15	15.5
20X-2, 106-107	183.06	4	47	15	55.9
20X-3, 106-107	184.56	4	33	13	39.2
20X-4, 106-107	186.06	4	81	14	96.3
21X-2, 106-107	192.76	4	19	13	22.6
21X-3, 74-75	193.94	4	30	13	35.7
21X-4, 73-74	195.43	4	24	12	28.5

chapter, for details of how synthetic seismograms were produced and descriptions of relevant logs). In Figure 60, we summarize this correlation by showing site seismic data, the synthetic seismogram, and acoustic impedance (basically the filtered velocity log) with its related depth scale, next to the Site 823 lithostratigraphic summary. No unambiguous match is seen between the seismic section and the synthetic seismogram; however, most strong reflections and sequence boundaries do correlate with reflectors in the synthetic seismogram. The absence of strong reflections throughout most of the synthetic seismogram may imply that only the consistency of changes in physical properties along the section, and thus the coherency of the reflectors, that is causing them to stand out as significant seismic events.

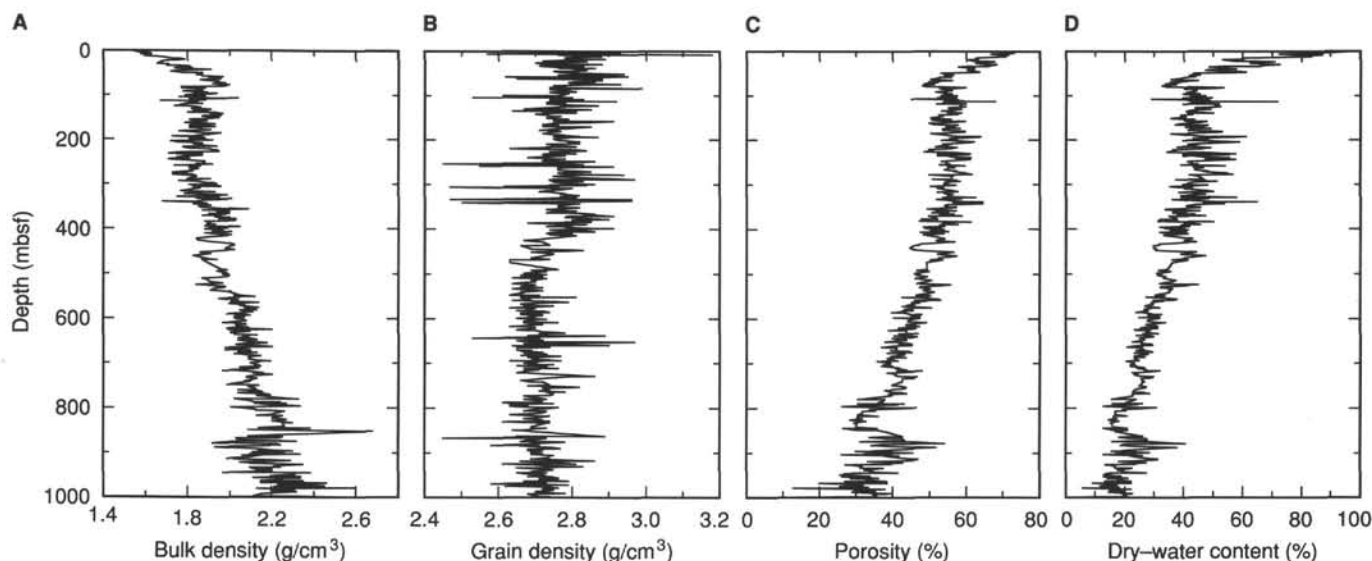


Figure 47. Plot of physical properties vs. depth, Site 823. A. Bulk density; data were obtained from mass and volume measurements of samples taken from split cores. B. Grain density. C. Porosity; data were obtained from mass and volume measurements of samples taken from split cores. D. Dry-water content; data were obtained from mass and volume measurements of samples taken from split cores.

Sequences 1 and 2 are approximately 80 and 40 m thick, respectively, and correlate with lithologic Unit I. This is a hemipelagic unit consisting of nanofossil ooze and mixed sediments of Pleistocene age (<1.27 Ma; nanofossil Zones CN13b to CN15). Sequence 1 corresponds mainly with Subunit IA and Sequence 2 mainly with Subunit IB, while the latter unit is more terrigenous and contains thick turbidite beds. These subunits have been interpreted as having been deposited by a combination of pelagic background sedimentation that was supplemented with debris flows and turbidites.

Sequences 3 and 4 are 100 and 140 m thick, respectively, and together correspond with Unit II, which is a hemipelagic to pelagic ooze and chalk of late Pliocene age (1.27–3.5 Ma; nanofossil Zones CN12a to CN13b). The band of strong reflectors that separates Sequences 3 and 4 may be related to debris flows. The strong reflector within Sequence 4 at 2.57 s below sea level may correlate with the ooze/chalk transition at this site (approximately 310 mbsf).

Sequence 5 is approximately 145 m thick and correlates with Subunits IIIA and IIIB, which are early Pliocene in age (3.5–4.2 Ma; nanofossil Zones CN11a and CN11b). The boundary between these two subunits cannot be seen in the seismic profile. Subunit IIIA consists of lithoclastic rudstone, conglomerate, and mixed sediments that were deposited by large debris flows and slumps, whereas Subunit IIIB consists of hemipelagic sediments and nanofossil chalks to mixed sediments with turbidites, but no debris flows.

Sequence 6 is 200 m thick and correlates with Subunit IIIC and Unit IV, which are of early Pliocene to late Miocene age (4.24–>5.28 Ma; nanofossil Zones CN9 to CN10c). The zone of strong reflectors at the top of this sequence corresponds to the two large debris flows in Subunit IIIC. The remainder of the sequence relates to Unit IV, which consists of nanofossil chalk, mixed sediments, and claystones that were largely deposited by slumping, with a decrease in the number of debris flows and turbidites.

Sequence 7 is approximately 140 m thick and largely correlates with Unit V, which is composed of nanofossil mixed sediments to nanofossil claystones of late Miocene age (nanofossil Zone CN9), and perhaps the top part of Unit VI.

Sequence 8 is approximately 80 m thick and corresponds with the basal part of Unit VI, which is a late Miocene clay-rich chalk and skeletal packstone with nanofossil chalk. This unit has been interpreted as having been deposited by turbidity currents and debris flows.

Sequence 9 is 60 m thick and correlates with the upper part of Unit VII, which has a late Miocene age (CN9). This unit comprises nanofossil chalks and claystones containing large amounts of lithoclastic rudstone (debris flows) and bioclastic packstone (turbidites). It contains the first occurrence of shallow-water, platform-derived clasts, probably shed from the build-up on the basement high to the east. The top of Sequence 9 can be traced east, where it may form the upper boundary of the slope and debris facies related to this build-up.

Sequence 10 is about 150 m thick and only its upper part lies above TD. It corresponds to the basal part of Unit VI, which has a middle Miocene age (CN6–CN7).

Sequences 10 and 11 and the underlying section are gently folded and faulted in the site area, and the top of Sequence 10 has been overlapped by upper Miocene sediments. This indicates that Queensland Trough experienced significant structural reactivation and enhanced basin formation toward the end of the middle Miocene and probably into the early late Miocene. These processes may have been responsible for more rapid infill of the trough because of increased turbidite, debris-flow, and slump activity related to slope changes that resulted from the reactivation.

In general, the seismic character of seismic sequences at Site 823 agrees well with the lithologic interpretation of their depositional processes (see “Lithostratigraphy” section, this chapter). However, several sequence boundaries are not clearly defined within the lithostratigraphic subdivision and, in some cases, may be reflecting facies and diagenetic changes.

## SUMMARY AND CONCLUSIONS

### Overview

Site 823 is located in the central-western Queensland Trough, toward the deepest part of the basin. In addition to collecting pelagic sediments produced in overlying surface

Table 11. Thermal conductivity data, Site 823.

Core, section, interval (cm)	Depth (mbsf)	Probe number	Thermal conductivity (W/m-K)	Standard error (W/m-K)	Calculated drift (W/m-K)
133-823B-					
1H-2, 51-51	2.01	32	0.9000	0.00730	-0.01438
1H-3, 50-50	3.50	14	0.9352	0.00712	0.02189
1H-5, 51-51	6.51	5	1.0071	0.00781	0.05451
1H-6, 51-51	8.01	150	0.9525	0.00414	0.01014
2H-2, 60-60	10.40	32	0.9194	0.00472	-0.03089
2H-3, 60-60	11.90	14	0.9818	0.00696	0.00422
2H-5, 60-60	14.90	5	1.0401	0.00476	0.03195
2H-6, 60-60	16.40	150	1.0296	0.00390	0.00711
3H-2, 60-60	19.90	32	1.0171	0.00521	-0.02618
3H-3, 60-60	21.40	14	1.0897	0.00618	0.01701
3H-5, 60-60	24.40	5	1.0291	0.00701	0.01477
3H-6, 60-60	25.90	150	0.9767	0.00424	-0.01111
4H-2, 90-90	29.70	32	1.0067	0.00448	-0.01265
4H-3, 90-90	31.20	14	1.0995	0.00780	0.01979
4H-5, 90-90	34.20	5	1.1563	0.00884	0.03908
4H-6, 90-90	35.70	150	1.0600	0.00718	-0.01603
5H-2, 60-60	38.90	32	1.0177	0.00689	-0.01061
5H-3, 60-60	40.40	14	1.1168	0.00624	0.02430
5H-5, 60-60	43.40	5	1.0746	0.00661	0.01650
5H-6, 60-60	44.90	150	1.0222	0.00448	-0.00742
6H-2, 60-60	48.40	32	1.0248	0.00596	-0.01220
6H-3, 60-60	49.90	14	1.1368	0.00397	0.01889
6H-5, 60-60	52.90	5	1.3016	0.00641	0.07859
6H-6, 60-60	54.40	150	1.1260	0.00560	0.01933
7H-2, 84-84	58.14	32	1.0715	0.00462	-0.02345
7H-3, 61-61	59.41	14	1.1409	0.00589	0.02359
7H-5, 32-32	62.12	5	1.2373	0.00808	0.05063
7H-6, 55-55	63.85	150	1.1048	0.00556	-0.00693
8H-2, 45-45	67.25	32	1.1243	0.00479	-0.00357
8H-3, 58-58	68.88	14	0.8457	0.00702	-0.02141
8H-4, 100-100	70.80	5	1.1103	0.00613	0.02574
8H-5, 90-90	72.20	150	1.0318	0.00690	-0.01497
9H-2, 103-103	77.33	32	1.1207	0.00532	-0.00709
9H-3, 97-97	78.77	14	1.2986	0.00662	0.02539
9H-5, 103-103	81.83	5	1.0862	0.00544	0.04095
9H-6, 50-50	82.80	150	0.9440	0.00591	0.01258
10H-2, 41-41	86.21	32	1.0051	0.00602	-0.00838
10H-3, 122-122	88.52	14	1.0516	0.00594	-0.00703
10H-5, 103-103	91.33	5	1.0315	0.00543	0.01814
10H-6, 74-74	92.54	150	1.0617	0.00365	-0.00242
11H-2, 68-68	95.98	32	1.0722	0.00425	-0.01495
11H-3, 53-53	97.33	14	1.0456	0.00717	0.00314
11H-5, 71-71	100.51	5	1.0952	0.00415	0.03735
11H-6, 99-99	102.29	150	1.1110	0.00354	-0.00340
12H-2, 50-50	105.30	32	1.1300	0.00379	-0.02509
12H-3, 80-80	107.10	14	1.1418	0.00546	0.01773
12H-5, 28-28	109.58	5	1.0562	0.00506	0.02706
12H-6, 93-93	111.73	150	0.9906	0.00430	0.01821
13X-2, 82-82	115.12	32	0.7868	0.01282	-0.09174
13X-3, 67-67	116.47	14	1.0531	0.00535	0.03484
13X-4, 52-52	117.82	5	1.1992	0.00400	0.05689
13X-5, 66-66	119.46	150	1.1337	0.00680	0.00605
14X-3, 67-67	126.07	32	1.0766	0.00446	-0.00167
14X-4, 67-67	127.57	14	1.1071	0.00675	0.02406
14X-5, 67-67	129.07	5	1.0953	0.00484	0.03512
14X-6, 67-67	130.57	150	0.9984	0.00313	-0.00459
15X-2, 54-54	134.14	32	1.1163	0.00678	0.00007
15X-3, 53-53	135.63	14	1.1049	0.00773	0.02458
15X-4, 52-52	137.12	5	1.1165	0.00586	0.04469
15X-5, 51-51	138.61	150	1.1346	0.00579	-0.00361
16X-2, 37-37	143.57	32	1.0085	0.00553	-0.01380
16X-3, 31-31	145.01	14	1.0733	0.00703	0.02078
16X-4, 31-31	146.51	5	1.1555	0.00601	0.03492
16X-5, 31-31	148.01	150	1.0627	0.00563	0.00532
17X-2, 62-62	153.52	32	1.0240	0.00299	-0.01907
17X-3, 62-62	155.02	14	1.1558	0.00484	0.02080

waters, the site receives redeposited material with a strong terrigenous component from the Australian continental margin, as well as shallow-water carbonate material produced on carbonate platforms that border the trough. The redeposited material is transported to the depositional site in suspension as fine-grained clays or micrite or in gravity flows, to be redeposited as turbidites, debris flows, or slumps. Evaluation of the type, number, and composition of this redeposited material reaching the basal setting as a function of time provides

Table 11 (continued).

Core, section, interval (cm)	Depth (mbsf)	Probe number	Thermal conductivity (W/m-K)	Standard error (W/m-K)	Calculated drift (W/m-K)
17X-4, 53-53	156.43	5	1.1016	0.00661	0.02680
17X-5, 53-53	157.93	150	1.0620	0.00842	-0.00856
18X-2, 52-52	163.12	32	1.0447	0.00491	-0.01574
18X-3, 52-52	164.62	14	1.1999	0.00623	0.02875
18X-4, 52-52	166.12	5	1.1124	0.00296	0.03360
18X-5, 52-52	167.62	150	1.1662	0.00676	0.02943
19X-2, 61-61	172.91	32	0.9937	0.00557	-0.03517
19X-3, 61-61	174.41	14	1.7222	0.07891	0.13952
19X-4, 61-61	175.91	5	1.0940	0.00587	0.00079
19X-5, 61-61	177.41	150	0.9546	0.00774	-0.03551
20X-1, 86-86	181.36	32	1.1049	0.00678	-0.00168
20X-2, 86-86	182.86	14	1.0945	0.00566	0.02079
20X-3, 86-86	184.36	5	1.1394	0.00528	0.02951
20X-4, 86-86	185.86	150	1.2136	0.00441	0.02308
21X-2, 60-60	192.30	32	1.1023	0.00332	-0.00063
21X-3, 60-60	193.80	14	1.0236	0.00386	-0.00570
21X-4, 60-60	195.30	5	1.1014	0.00568	0.01451
21X-5, 60-60	196.80	150	1.1261	0.00523	0.00324
22X-2, 90-90	202.20	32	1.0906	0.00568	-0.01291
22X-3, 68-68	203.48	14	1.0242	0.00624	0.00538
22X-4, 90-90	205.20	5	1.1244	0.00378	0.02152
22X-5, 50-50	206.30	150	1.1190	0.00539	-0.00492
23X-2, 32-32	210.92	32	0.9312	0.00486	-0.03219
23X-3, 70-70	212.80	14	0.9554	0.00331	0.02126
23X-5, 77-77	215.87	5	0.6104	0.00807	-0.00649
23X-6, 67-67	217.27	150	1.2140	0.00544	0.01719
24X-2, 58-58	220.78	32	1.1422	0.00829	0.02034
24X-3, 58-58	222.28	14	0.9406	0.00782	-0.03361
24X-4, 58-58	223.78	5	1.2597	0.00451	0.03873
24X-5, 58-58	225.28	150	1.0974	0.00483	-0.00059
25X-2, 62-62	230.12	32	1.1155	0.00576	-0.00701
25X-3, 51-51	231.51	14	1.1391	0.00775	0.03266
25X-5, 79-79	234.79	5	1.3426	0.00443	0.05250
25X-6, 75-75	236.25	150	1.1361	0.00735	0.01537
26X-2, 59-59	239.79	32	1.0118	0.00510	-0.01895
26X-3, 73-73	241.43	14	1.1298	0.00673	0.01557
26X-5, 73-73	244.43	5	1.0929	0.00504	0.02619
26X-6, 73-73	245.93	150	1.0380	0.00355	-0.01775
27X-2, 71-71	248.73	32	0.9752	0.00623	-0.03253
27X-3, 71-71	250.23	14	0.9017	0.00633	-0.02603
27X-5, 71-71	253.23	5	1.0569	0.00610	-0.01165
27X-6, 71-71	254.73	150	1.1650	0.00629	0.00959
28X-2, 61-61	259.11	32	1.0603	0.00498	-0.01391
28X-3, 61-61	260.61	14	1.1232	0.00492	0.01499
28X-5, 61-61	263.61	5	1.1121	0.00579	0.02123
28X-6, 58-58	265.08	150	1.1318	0.00679	0.01202
29X-2, 53-53	268.73	32	1.0683	0.00693	-0.00192
29X-3, 53-53	270.23	14	1.0307	0.00578	-0.00492
29X-5, 45-45	273.15	5	1.1206	0.00346	0.02573
29X-6, 53-53	274.73	150	1.1136	0.00549	-0.00272
30X-2, 3-3	277.83	150	1.0008	0.00618	-0.02032
30X-3, 62-62	279.92	32	1.0331	0.00558	-0.01631
30X-5, 135-135	283.65	14	1.0374	0.00565	-0.01745
30X-6, 53-53	284.33	5	1.0612	0.00468	0.00870
31X-2, 120-120	287.76	32	1.0140	0.00605	-0.01836
31X-3, 66-66	288.72	14	1.0408	0.00558	0.00269
31X-5, 92-92	291.98	5	1.0476	0.00324	0.01765
31X-6, 138-138	293.94	150	0.9310	0.00584	-0.01401
32X-2, 19-19	297.29	32	1.1275	0.00565	-0.01084
32X-3, 90-90	299.50	14	1.2063	0.00650	0.02266
32X-5, 22-22	301.82	5	1.0896	0.00556	0.02098
32X-6, 82-82	303.92	150	1.2311	0.00506	0.01313
33X-2, 50-50	307.30	32	1.1851	0.00454	0.00603
33X-3, 40-40	308.70	14	0.8323	0.00402	-0.02183
33X-5, 50-50	311.80	5	0.9650	0.00640	0.01139
33X-6, 40-40	313.20	150	0.9928	0.00569	0.00015

information concerning environmental changes affecting the shallower-water surroundings.

The Site 823 location was selected to recover a basal section that would provide a record of basin-fill sediments as well as material for paleoceanographic studies. Drilling yielded a record of background hemipelagic to pelagic sedimentation intermixed with gravity-flow deposits spanning from the late Miocene to the Pleistocene. In conjunction with shore-based studies, this record promises to provide detailed information

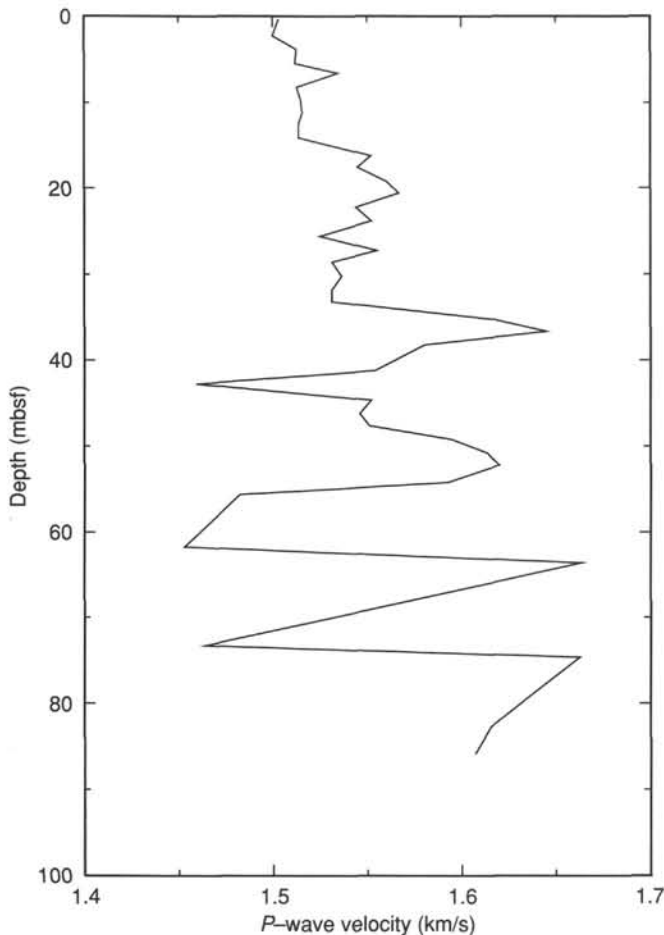


Figure 48. *P*-wave velocity at Site 823. Data were obtained from samples taken from split cores using the Hamilton frame.

about causes and consequences of regional stratigraphic events. Initial shipboard results reveal a preliminary sedimentation history that is consistent with data gathered at other Leg 133 drill sites on the northeastern Australian margin.

#### Sedimentation History

The distribution of gravity-flow deposits with time in the basal sequence at Site 823 provides a record of erosional processes occurring on the adjacent continental shelf and slope, as well as on the neighboring carbonate platforms. These sediments have good biostratigraphic control and chronologic integrity, considering the high number of redeposited layers. This indicates that little erosion of background sediment or reworking of older material took place, and the sequence can provide a high-resolution record of late Neogene events. We subdivided the late Neogene sedimentation history into seven periods that coincided with the seven lithologic units, as these were defined by type, number, and composition of redeposited material, as well as from the variable amount of detrital material flux to the pelagic ooze.

#### Late Miocene (Approximately 10.4–7.5 Ma)

Sediments deposited during this period contain a comparatively high number of debris-flow and turbidite deposits. Their compositions indicate strong sources from both the continental shelf, with high clay and quartz contents, and the carbonate platforms and shelf, with coral debris and large

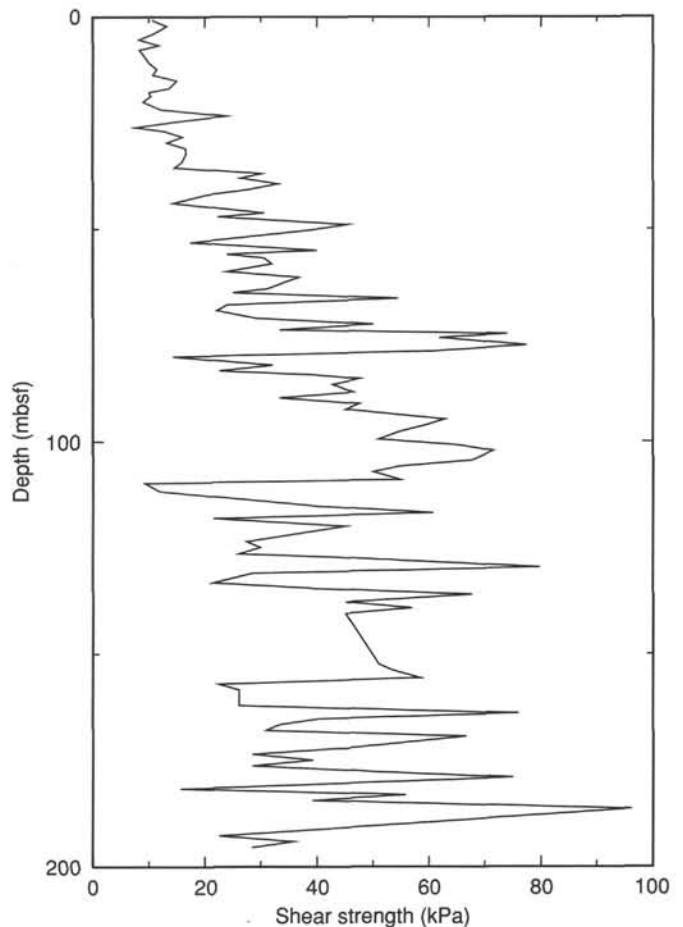


Figure 49. Shear strength at Site 823. Data were obtained from split cores using the Wykeham-Farrance motorized vane apparatus on the split cores.

benthic foraminifers. The medium-to-coarse sand-size of the redeposited material enriched in quartz implies that source areas were near the depositional site. Another possibility is that reworking of continental and platform-derived sediments from submarine highs to the east and west of Site 823 occurred. We propose that major declines in sea level, such as that at about 10.4 Ma, caused slope sediments on the sides of the trough to become unstable, leading to an increased number of gravity-flow deposits.

#### Late Miocene (Approximately 7.5–6.3 M)

Comparatively fewer gravity-flow deposits occurred during this period. This indicates that the slopes were more stable (i.e., less material was brought to these slopes for later removal downslope to the basal site). In addition, a decreased amount of fine-grained terrigenous influx to the hemipelagic component was matched by an increased amount of micrite, the shallow-water, carbonate bank-derived component. The alternation between clay-rich sediment gravity flows and light-colored nannofossil chalk indicates cyclic terrigenous influx. However, the diminished thickness of turbidites and the presence of debris flows imply a relatively higher sea level during this period than in the preceding period. As terrigenous influx was not continuous, but apparently cyclic, terrigenous material must have reached the outer shelf or slope regions only during certain intervals.

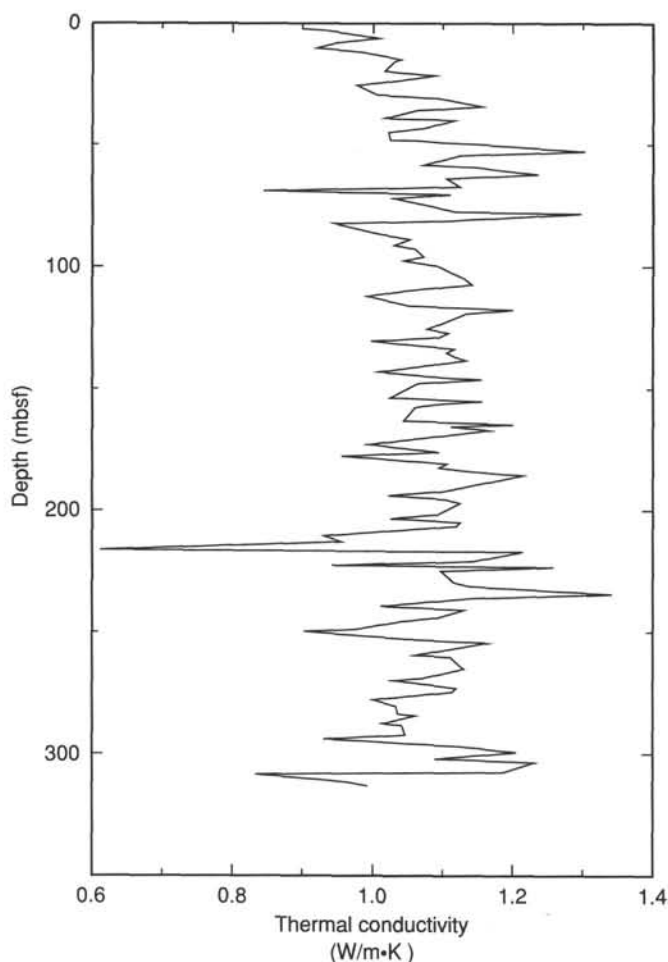


Figure 50. Thermal conductivity at Site 823. Data were obtained from split cores using a needle probe apparatus.

#### *Late Miocene (Approximately 6.3–5.5 Ma)*

This period of time is characterized by the least amount of coarse-grained (sand-sized) gravity-flow deposits (turbidites or debris flows), but an increased occurrence of slump deposits. This indicates that redeposition is a local phenomenon. High clay contents of predominantly hemipelagic sediments indicate steady dilution of the pelagic sedimentary component by terrigenous influx. The presence of claystone with dispersed iron sulfides is greater in the lower part of this time interval. No micrite occurs in the sediments, implying that carbonate banks were not supplying material to the basin. This period of diminished carbonate-bank productivity was recognized at all Queensland Plateau sites.

#### *Latest Miocene to Earliest Pliocene (Approximately 5.6–4.2 Ma)*

Long-term variations between clay-rich and more carbonate intervals characterize the sediments of this period. The high abundance of slump deposits, increasing amount of turbidites, and the presence of clay-rich intervals indicate a renewed redeposition of coarser-grained material from the surrounding slopes. These events might be related to variations in sea level. Micrite continues to be absent from the hemipelagic sediments, indicating that diminished carbonate-bank productivity persisted throughout the latest Miocene into the early Pliocene, as recognized at all Queensland Plateau sites.

#### *Late to Early Pliocene (Approximately 4.2–3.5 Ma)*

Micrite again reappears as a hemipelagic component, which is consistent with the rejuvenation of the carbonate banks, as recognized at Queensland Plateau sites. This period also was marked by a huge increase in numbers and thicknesses of debris-flow and slump deposits. This observation may be associated with a major decline in sea level at 3.9 Ma.

#### *Late Pliocene to Early Pleistocene (Approximately 3.5–1.25 Ma)*

Sediments deposited during this period exhibit regular variations between claystone and nannofossil chalk with micrite, indicating large-scale fluctuations in the dominant source for the fine-grained flux. In addition, these sediments contain the highest number of thin turbidites occurring at regular intervals. The frequency of these turbidites implies a steady flux of terrigenous sediments to the shelf for transport periodically into the basin.

#### *Early to Late Pleistocene (Approximately 1.25 Ma to Present)*

In these sediments, regular variations continue to exist between claystone and chalk, but clay contents were greater in the earliest Pleistocene, while nannofossil chalk was greater during the late Pleistocene. In addition, the amount of hemipelagic sediment decreased with respect to the number of gravity-flow deposits. During this period, numerous debris flows, turbidites, and slumps occurred. Major debris-flow events may correspond to decreased sea levels at 1.0 and 0.8 Ma.

### Conclusions

In summary, the Neogene record of redeposited events recovered at Site 823 contains a unique documentation of changes in paleoenvironment and sea level occurring in shallower waters surrounding Queensland Trough. From the record of gravity-flow deposits, a good correlation exists between falling sea level and destabilization of slope deposits, producing mass wasting. In addition to changes in sea level, changes in climate can alter the flux of terrigenous material to the shelf and slope, where it can be transported as gravity flows to the basin once the sediment pile has been destabilized.

Changes in climate also can impact ocean circulation and, in turn, influence the sorting and transport of detrital material. Intensified bottom-water currents during cooler intervals might have transported the finer-grained material into the basin, whereas the coarser-grained sediments remained behind to be transported to the trough as discrete gravity-flow deposits. This differentiation of grain size might explain the observed variable addition of clay to the pelagic sediments as a climatically induced process.

Our interpretation of these initial results (based on ship-board studies) is preliminary and is only a first attempt to extract information about climate and sea levels stored in this sequence. Shore-based studies promise to provide more detailed information about frequency and composition of the redeposited material and the environmental factors that initiated slope instability and redeposition.

### REFERENCES

- Archie, G. E., 1942. The electrical resistivity log as an aid in determining some reservoir characteristics, *J. Pet. Tech.*, 5:1–8.
- Burns, R. E., Andrews, J. E., et al., 1973. *Init. Repts. DSDP*, 21: Washington (U.S. Govt. Printing Office).
- Feary, D. A., Pigram, C. J., Davies, P. J., Symonds, P. A., Droxler, A. W., and Peerdeman, F., 1990. Ocean Drilling Program—Leg 133 safety package. *Bur. Miner. Res. Aust. Rec.*, 1990/6.
- Hamilton, E. L., 1976. Variation of density and porosity with depth in deep-sea sediments. *J. Sediment. Petrol.*, 46:280–300.
- , 1979. Sound velocity gradients in marine sediments. *J. Acoust. Soc. Am.*, 65:909–922.

- Klein, G. deV., 1985. The frequency and periodicity of preserved turbidites in submarine fans as a quantitative record of tectonic uplift in collision zones. *Tectonophysics*, 119:181–193.
- Quadfasel, D., Kudrass, H., and Frische, A., 1990. Deep-water renewal by turbidity currents in the Sulu Sea. *Nature*, 348:320–322.
- Richards, J. P., Chappell, B. W., and McCulloch, M. T., 1990. Intra-plate-type magmatism in a continent-island-arc collision zone: Pongera intrusive complex, Papua New Guinea. *Geology*, 18:958–961.
- Serra, O., 1986. *Fundamentals of Well-log Interpretation 2. The Interpretation of Logging Data*: Amsterdam (Elsevier).
- Symonds, P. A., and Davies, P. J., 1988. Structure, stratigraphy, evolution and regional framework of the Townsville Trough and Marion Plateau region—research cruise proposal, project 9131.11. *Bur. Miner. Res. Aust. Record*, 1988/48.
- van Morkhoven, F.P.C.M., Berggren, W. A., Edwards, A. S., et al., 1986. Cenozoic cosmopolitan deep-water benthic foraminifera. *Bull. Cent. Rech. Explor.-Prod. Elf-Aquitaine*, Mem. 11.
- Weaver, P.P.E., and Kuijpers, A., 1983. Climatic control of turbidite deposition on the Madeira Abyssal Plain. *Nature*, 306:360–363.
- Winterer, E. L., 1970. Submarine valley systems around the Coral Sea Basin (Australia). *Mar. Geol.*, 8:229–244.

Ms 133-116

**NOTE: All core description forms (“barrel sheets”) and core photographs have been printed on coated paper and bound separately as Part 2 of this volume, beginning on page 813.**

**Formation microscanner images for this site are presented on microfiche in the back of Part 2.**

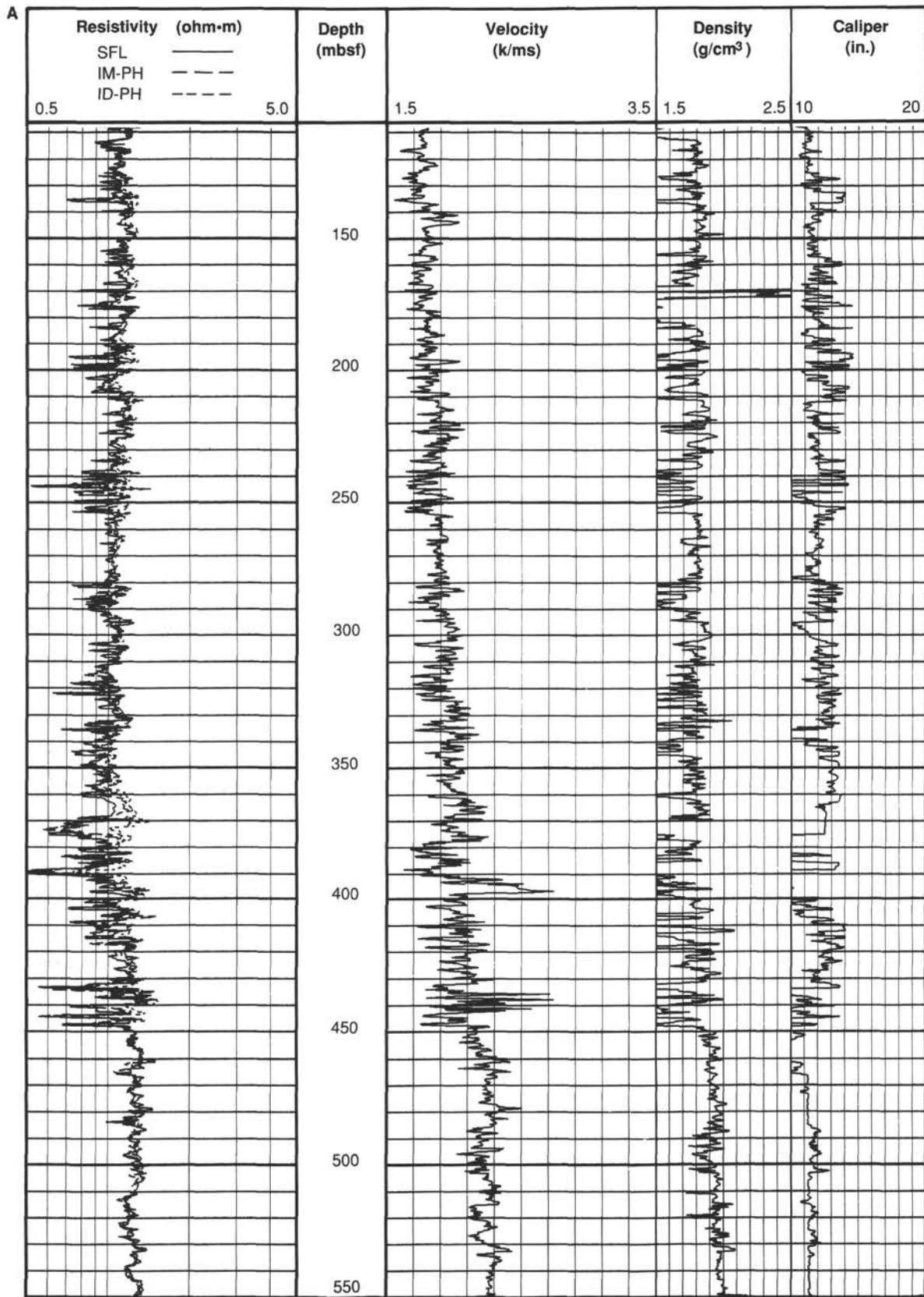


Figure 51. Porosity-sensitive logs obtained by seismic stratigraphic tool string at Hole 823C. A. At 108–550 mbsf. B. At 550–986 mbsf.

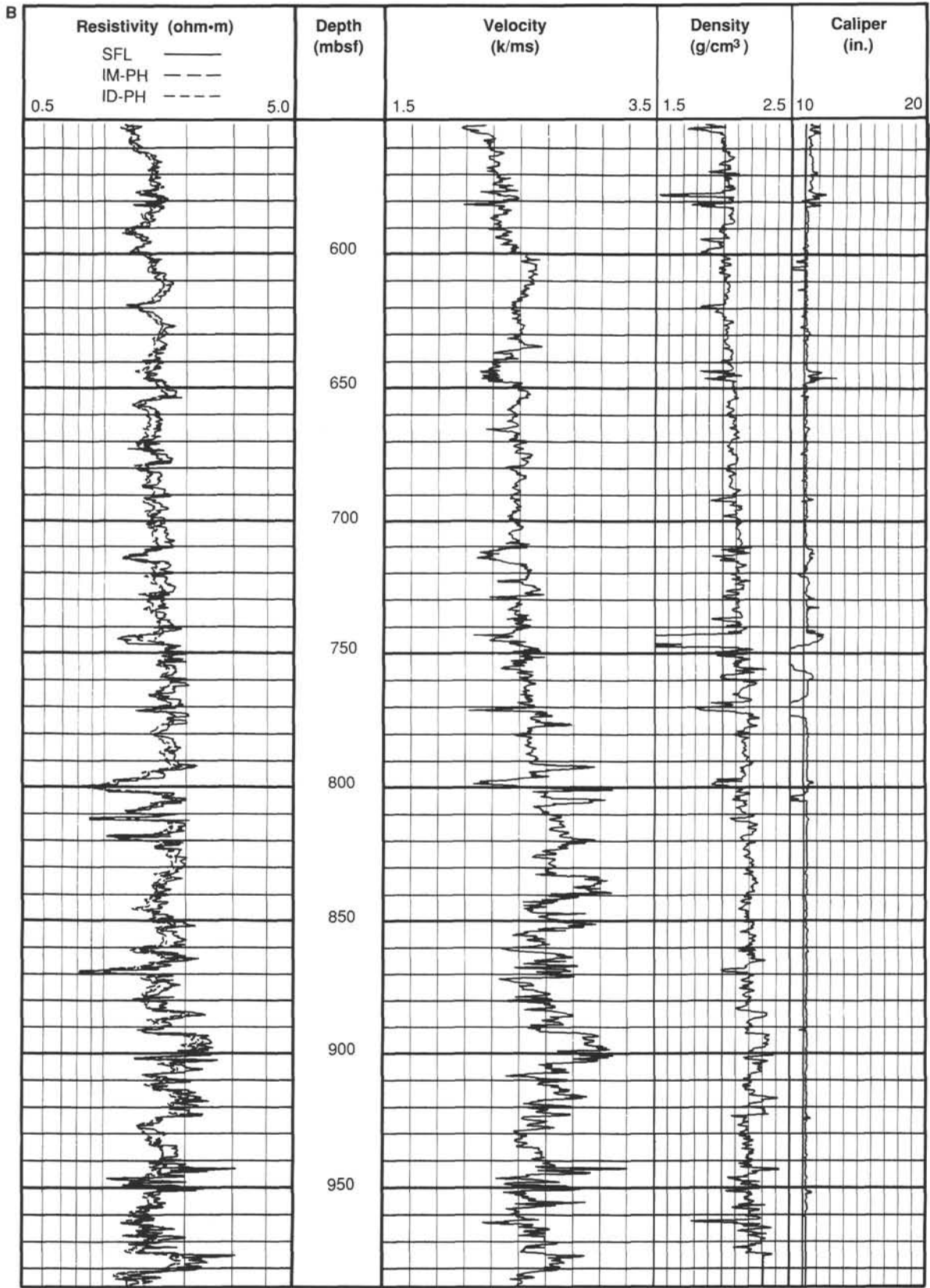


Figure 51 (continued).

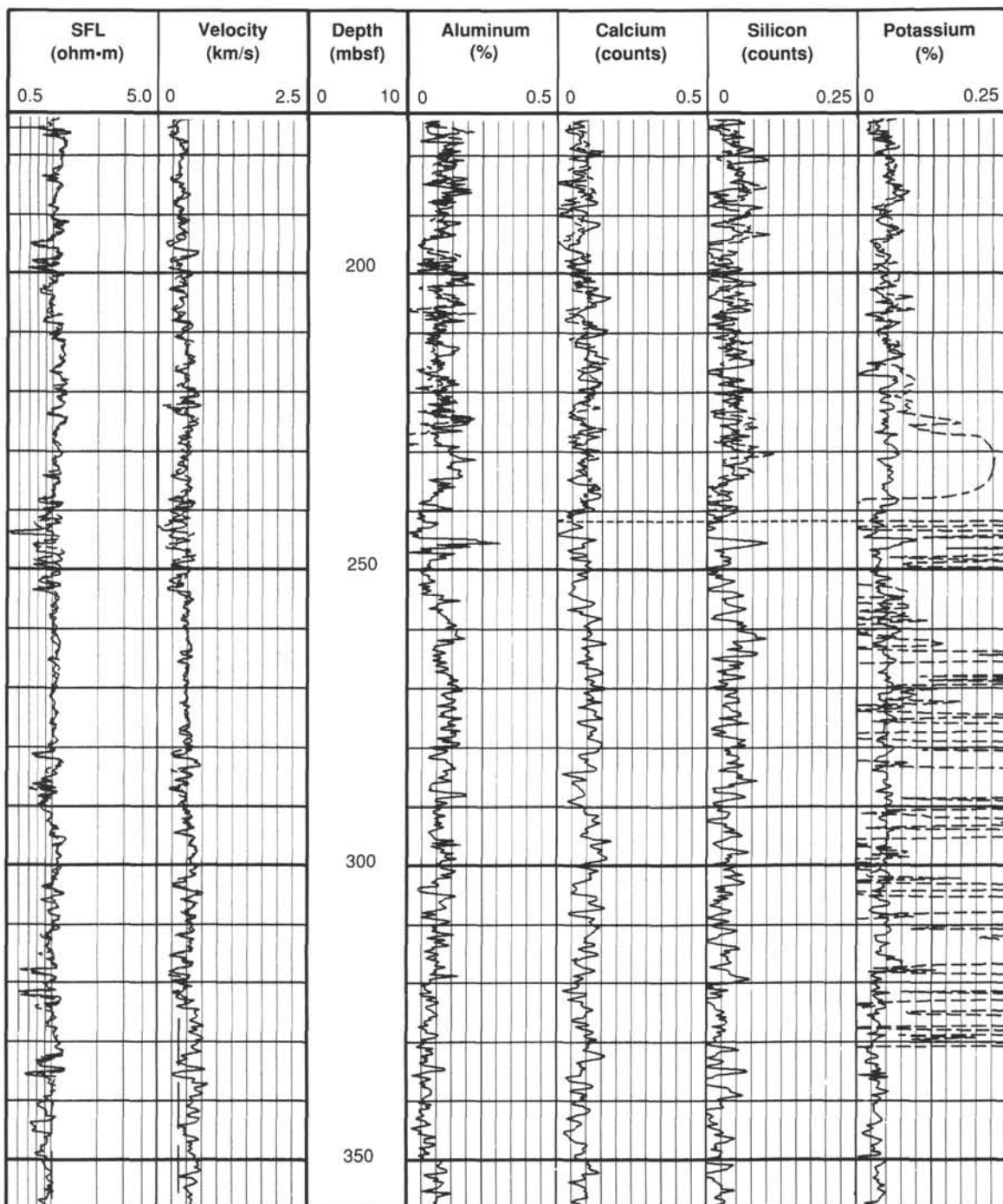


Figure 52. Logs for interval from 174 to 358 mbsf at Site 823, showing replicability of two logging passes over portions of this interval.

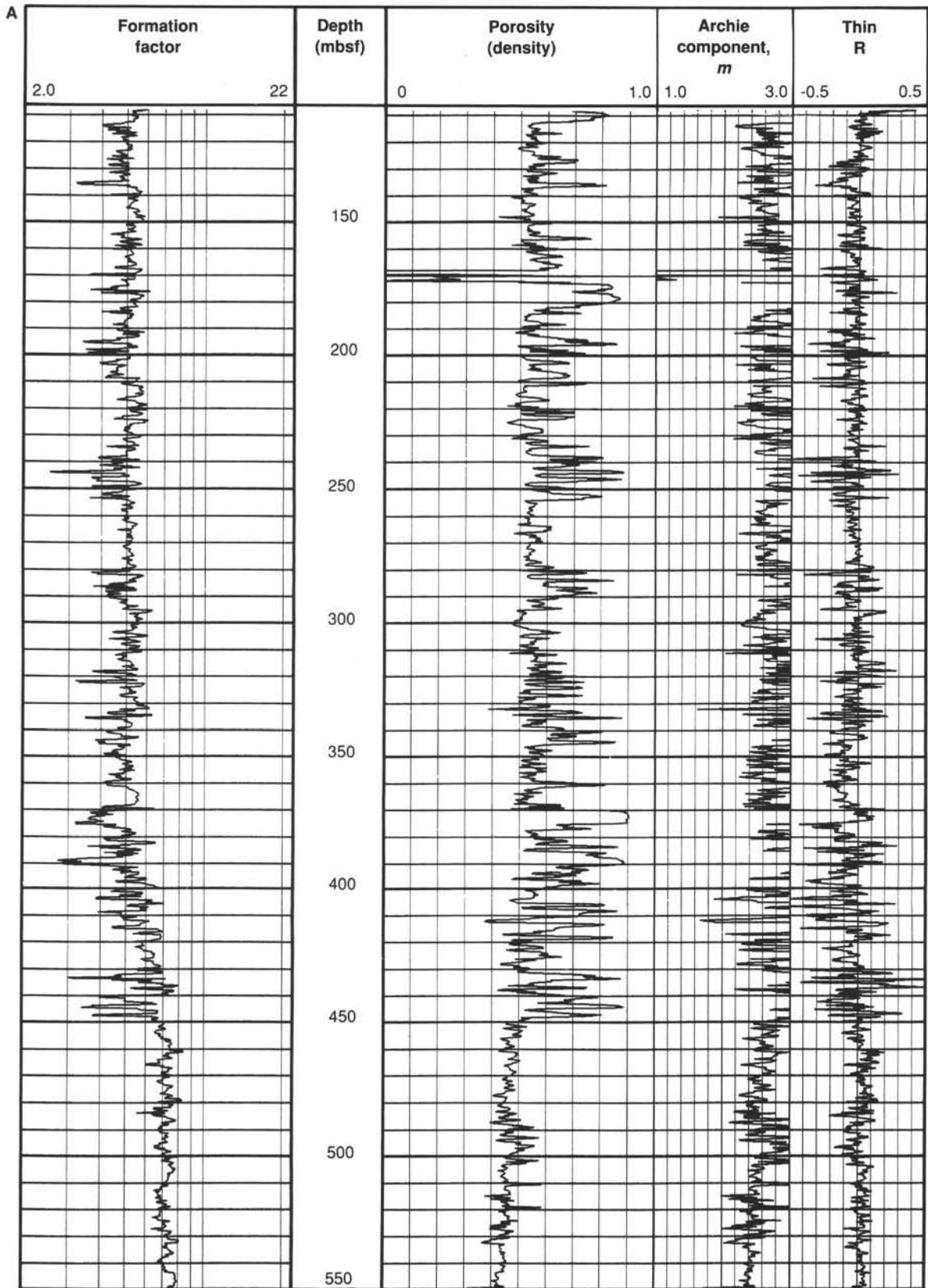


Figure 53. Site 823 logs of electrical resistivity formation factor (from ratio of formation resistivity to fluid resistivity), porosity (from density log), the Archie component  $m$  that relates formation factor to porosity, and the parameter "Thin R," which responds to thin-bed effects. A. At 108–550 mbsf. B. At 550–988 mbsf.

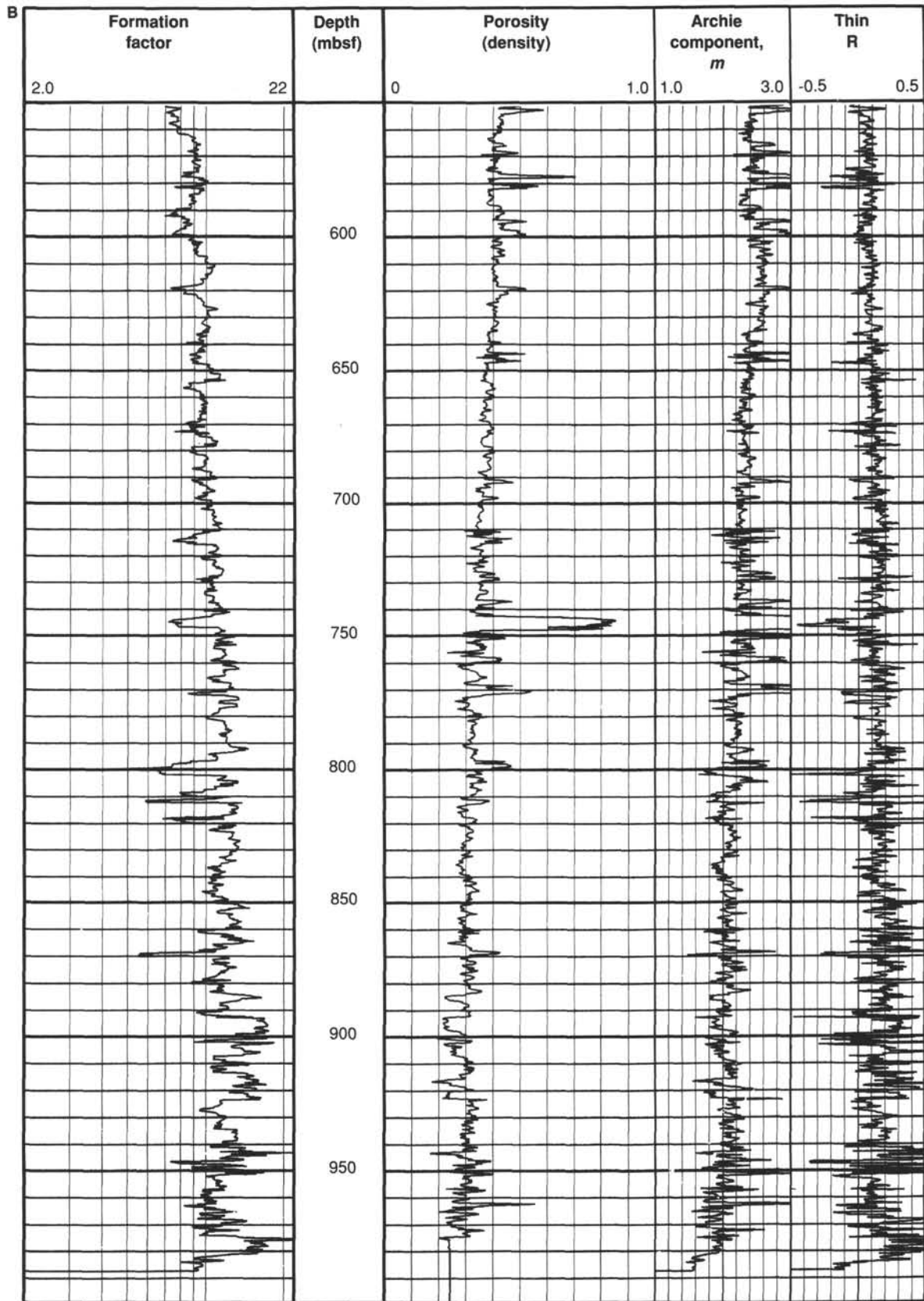


Figure 53 (continued).

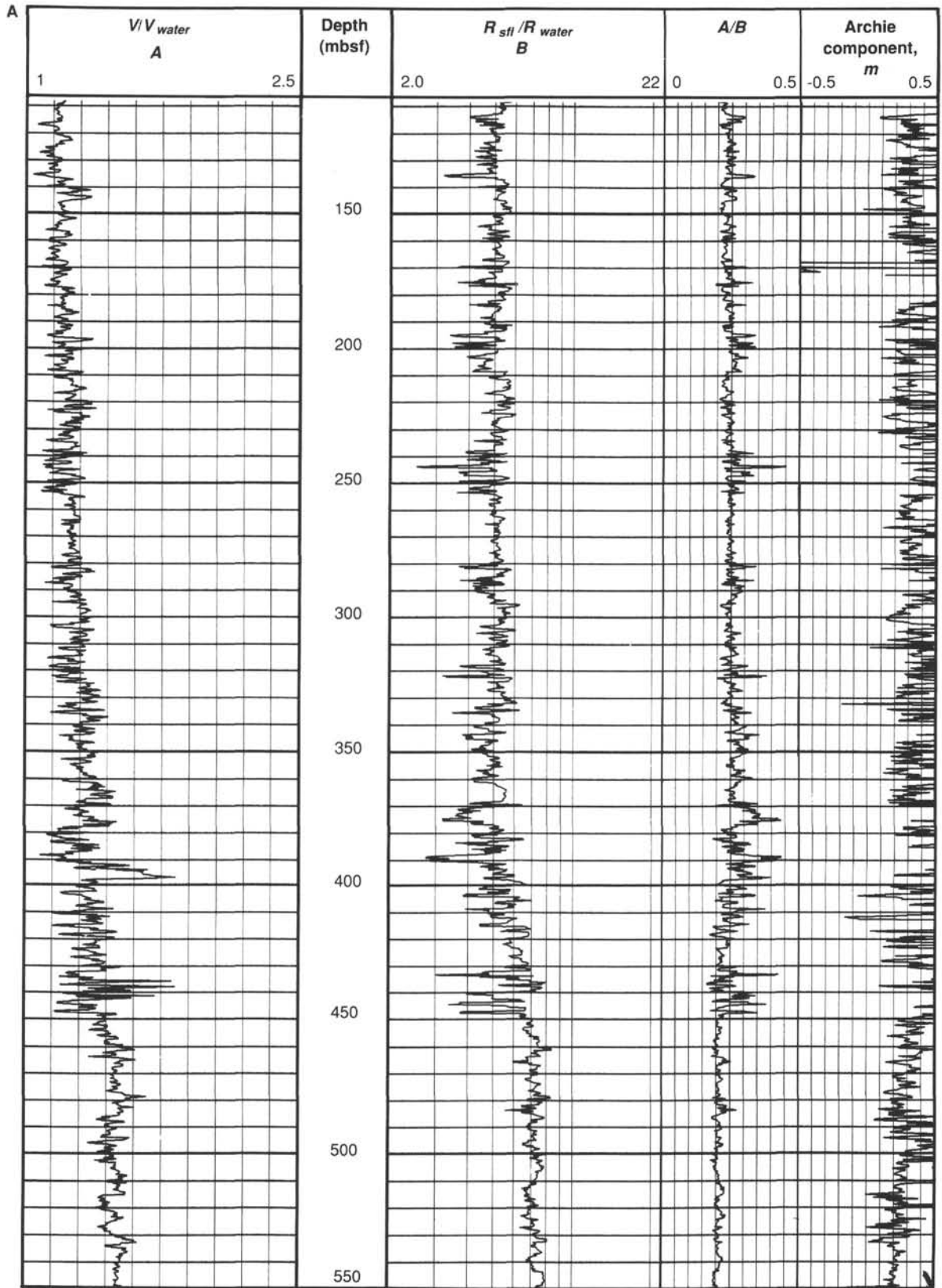


Figure 54. Velocity and resistivity logs for Site 823, plotted as ratios to each other and to water to highlight changes in pore geometry. A. At 108–550 mbsf. B. At 550–986 mbsf.

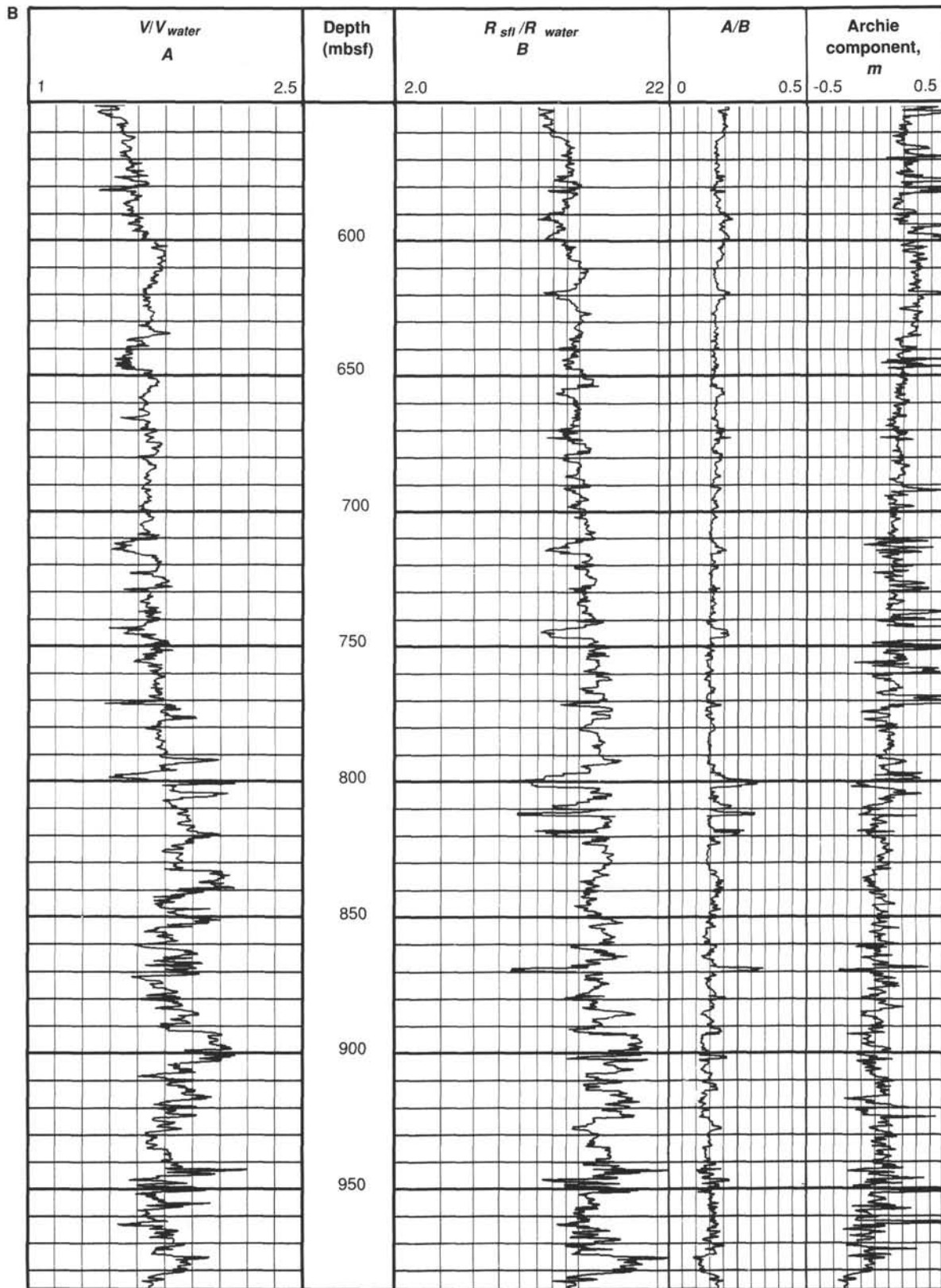


Figure 54 (continued).

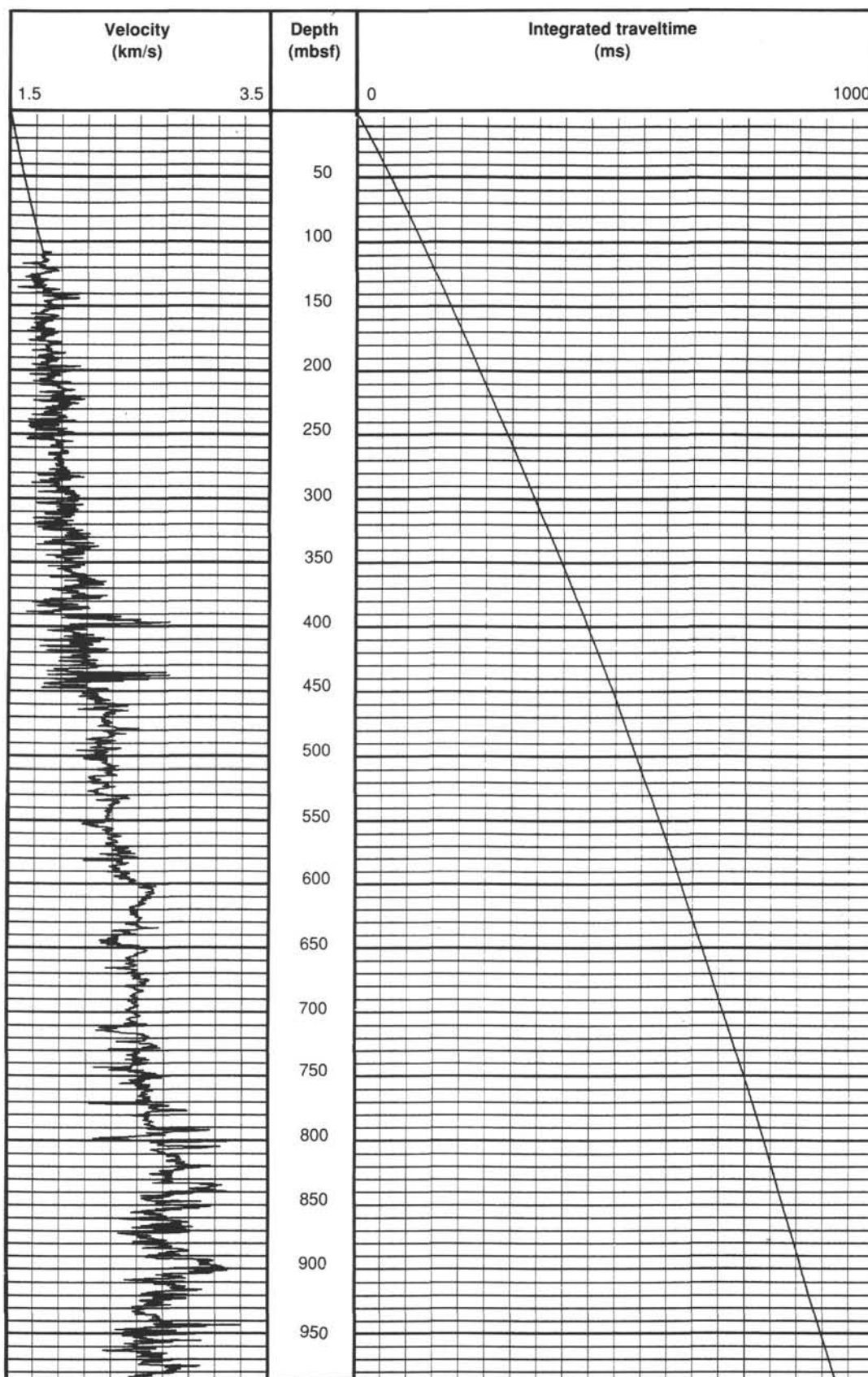


Figure 55. Velocity log and integrated two-way traveltime function that it implies for matching core-based information from Site 823 with seismic sections across the site.

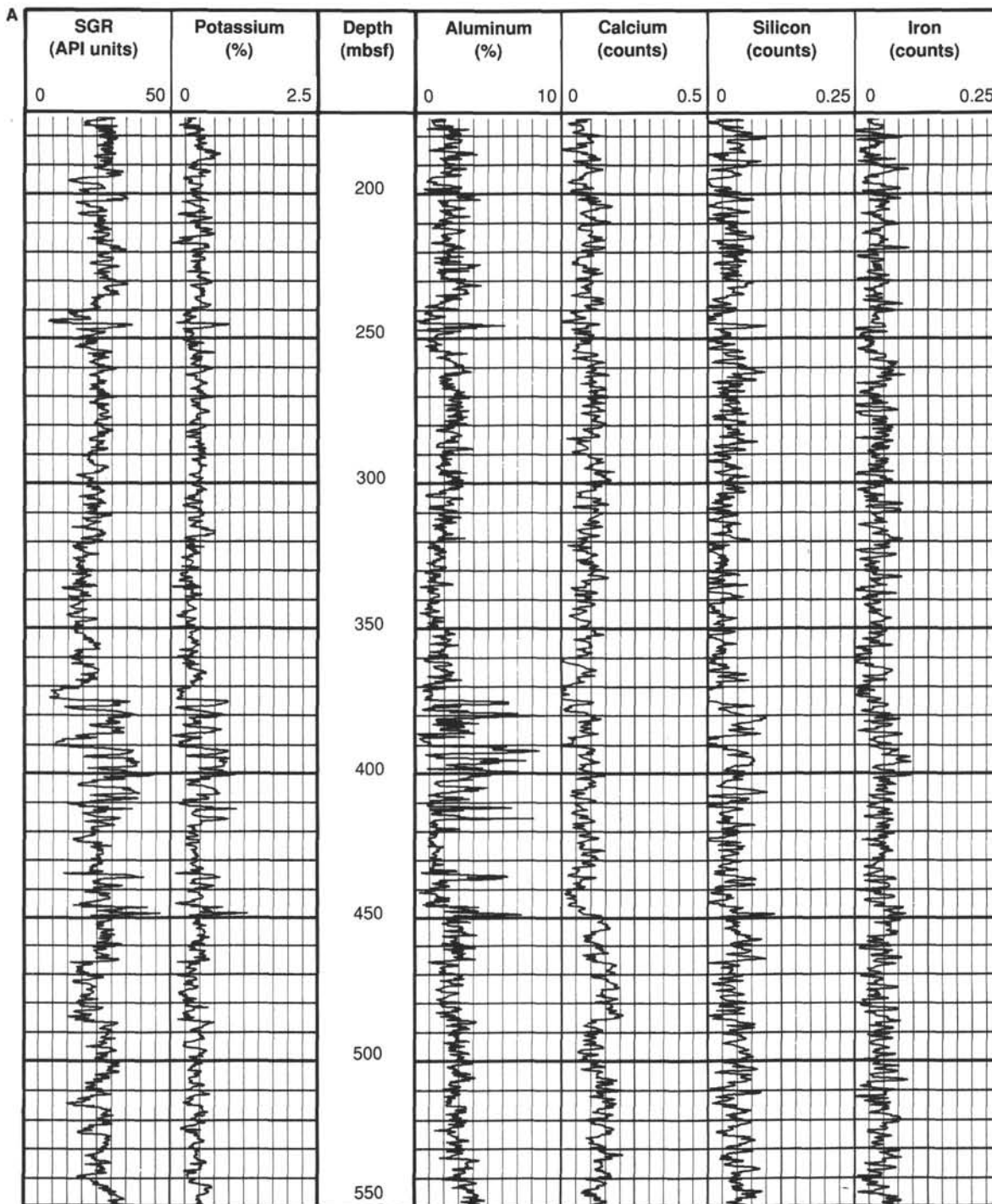


Figure 56. Geochemical logs from portion of Site 823 for which openhole logs were obtained. Note that elements abundant in clay minerals (potassium, aluminum, and silicon) correlate with each other, but are inversely correlated with calcium (predominantly in calcite). A. At 174–550 mbsf. B. At 550–978 mbsf.

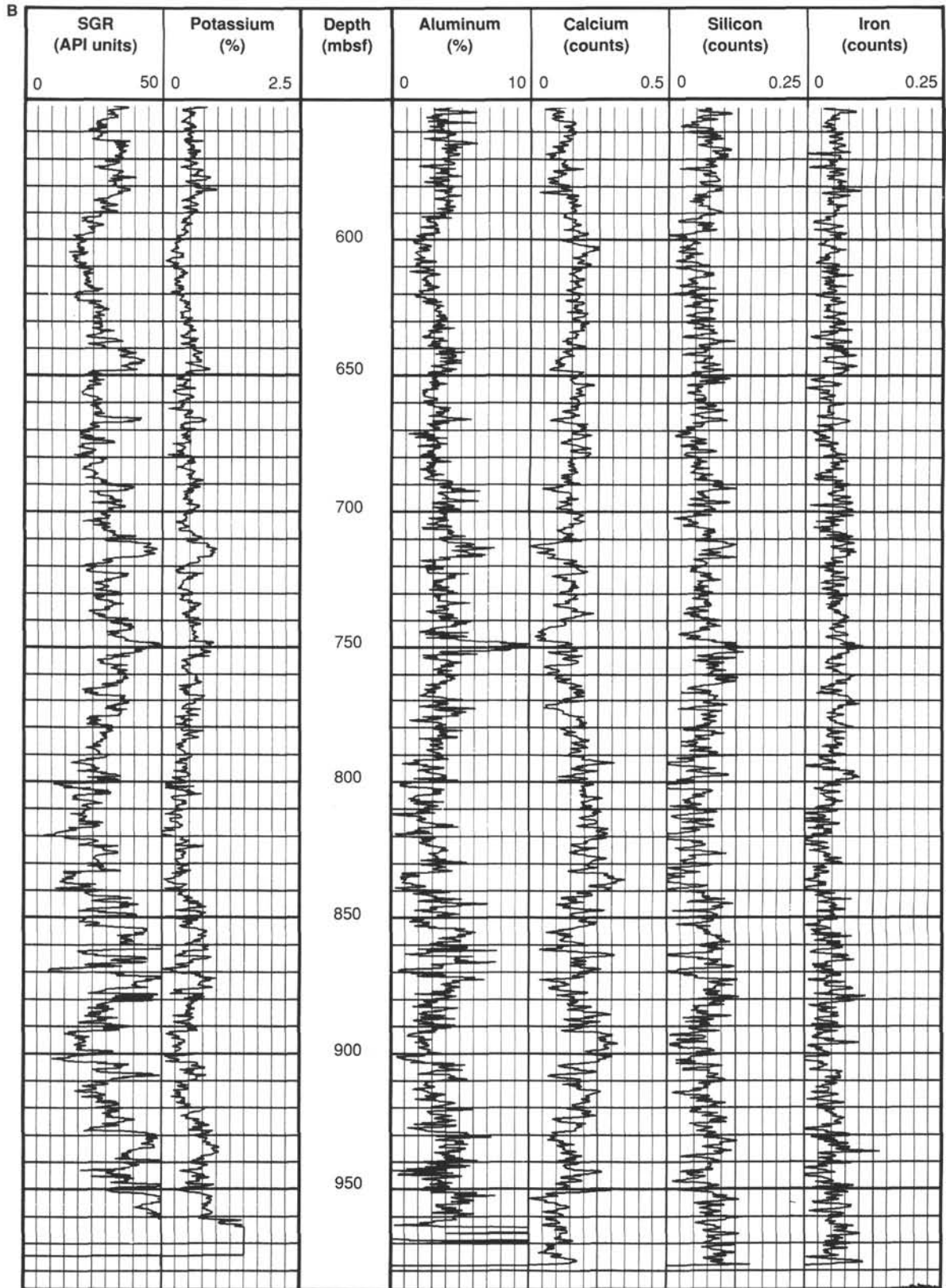


Figure S6 (continued).

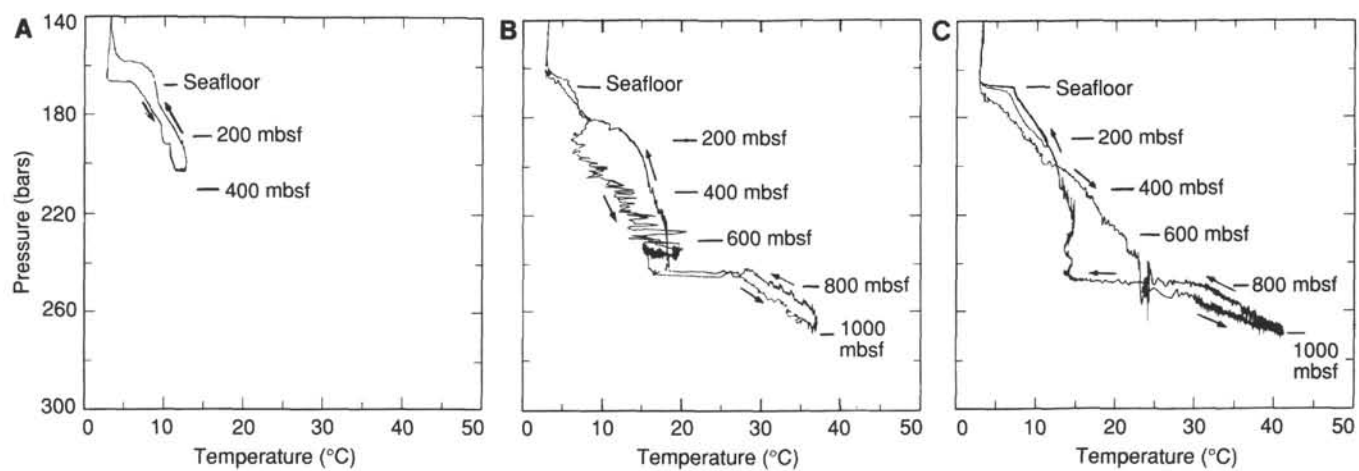


Figure 57. Temperature logs as a function of pressure (or depth) for first three logging runs at Site 823. **A.** First seismic stratigraphic run. **B.** Second seismic stratigraphic run. **C.** Geochemical run.

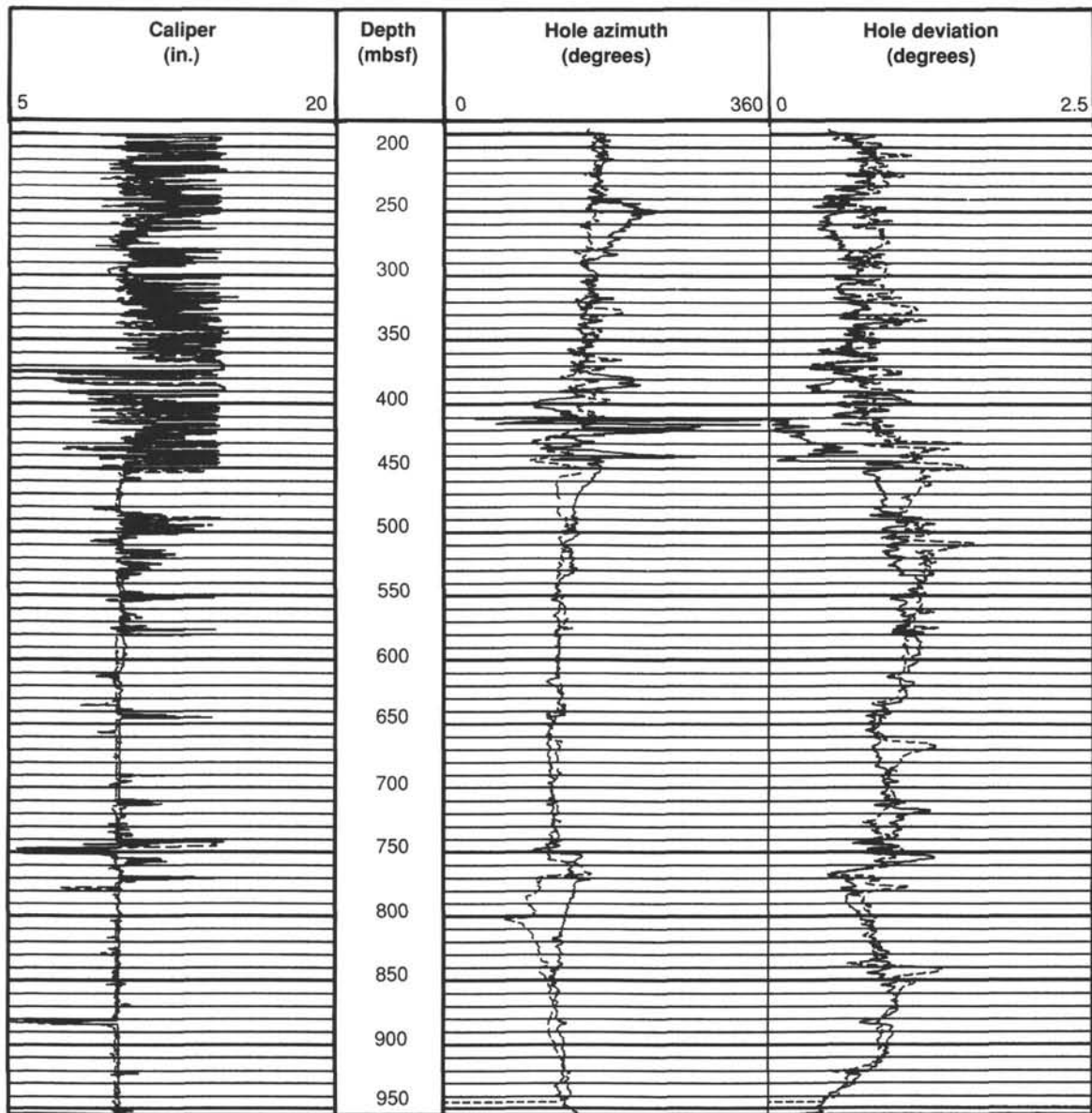


Figure 58. Hole deviation and its azimuth (Hole 823A).

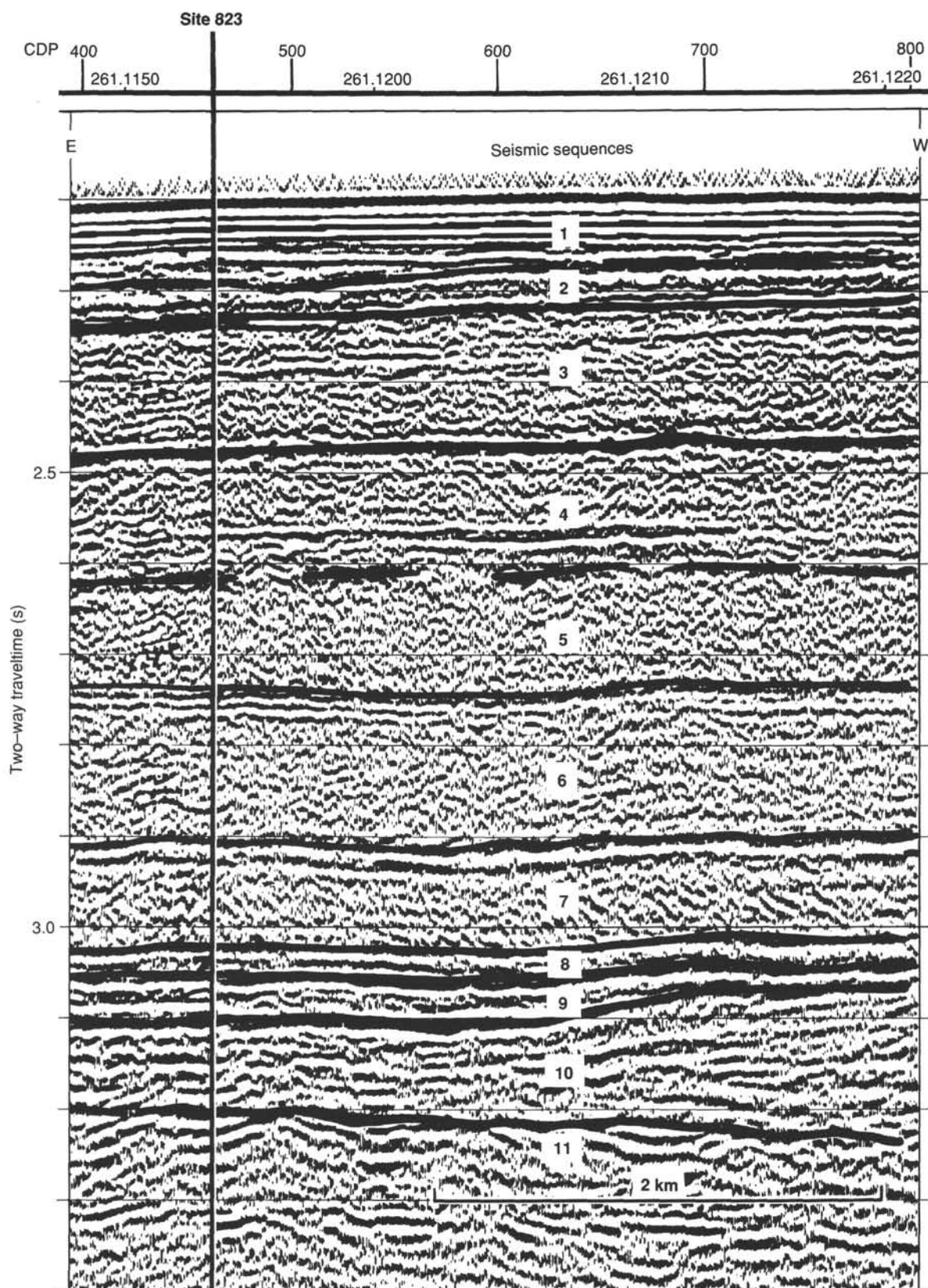


Figure 59. Portion of BMR multifold, water-gun seismic profile (Line 75/41, Part A) across Site 823. Characteristics of preliminary seismic sequences I through 11 are shown, as identified within site area. Profile location is shown in Figure 4 (see "Site Geophysics" section, this chapter).

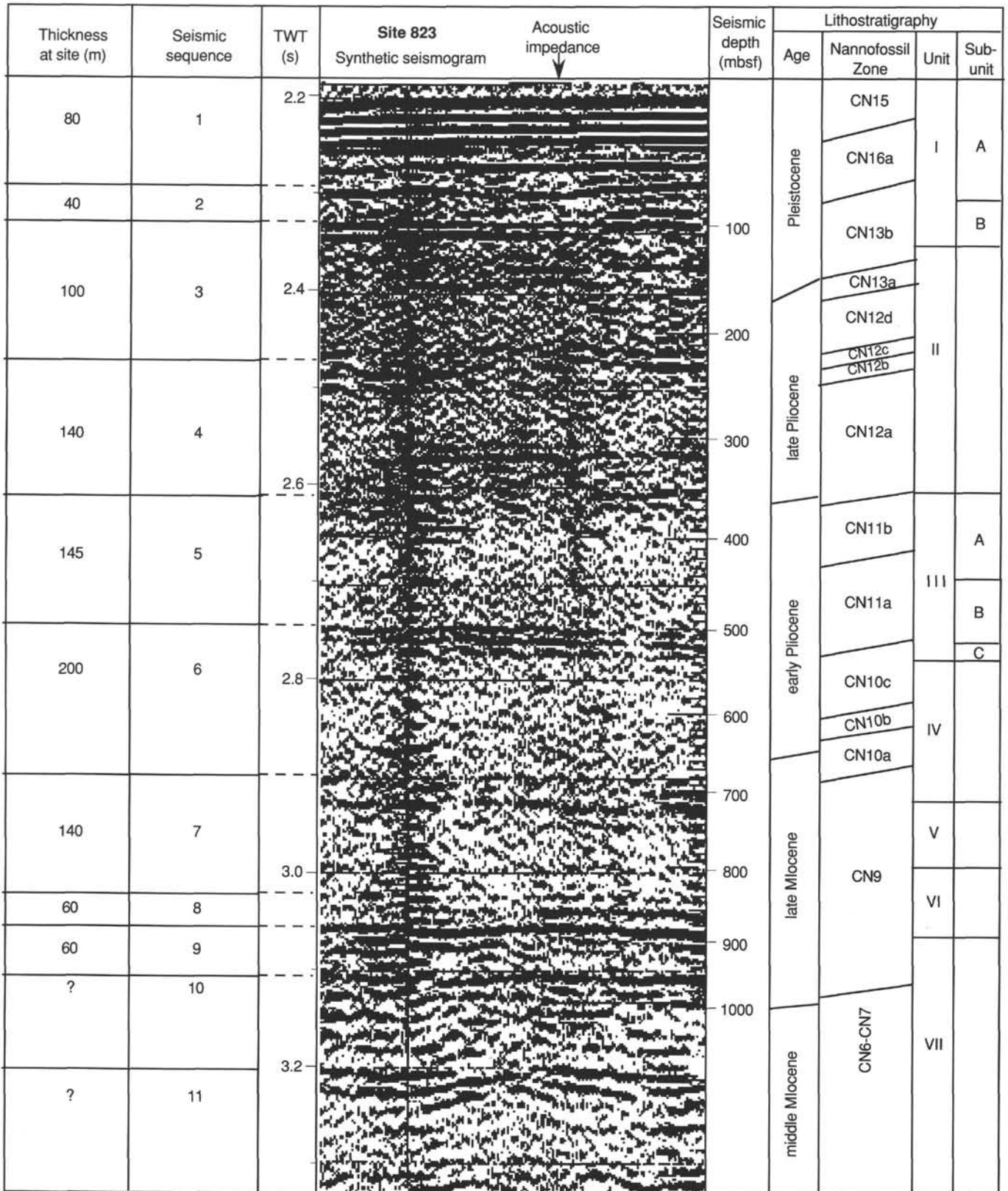


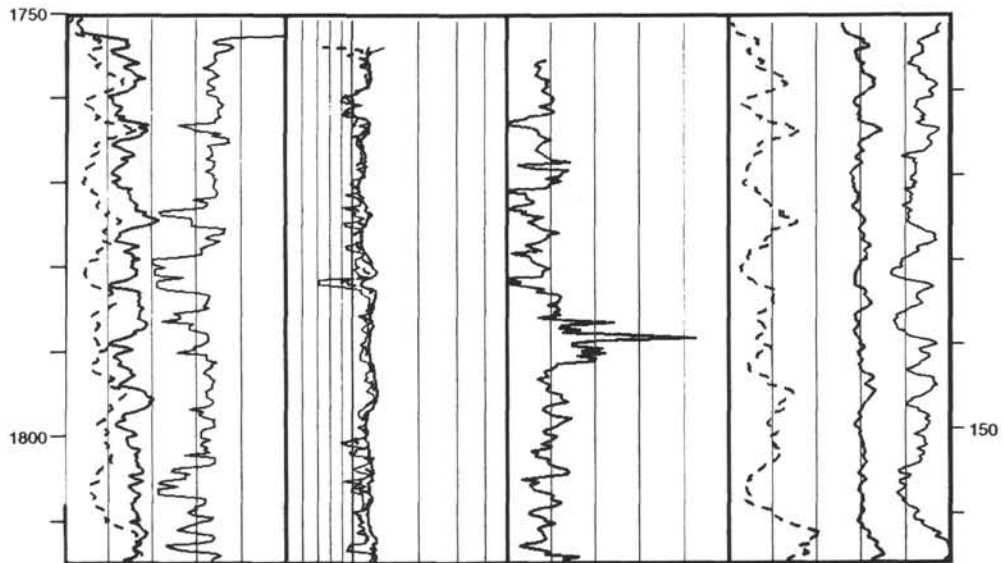
Figure 60. Preliminary correlation of seismic sequences at Site 823 with drilling results. Synthetic seismogram and acoustic impedance (filtered velocity log) were derived from downhole logging and from simplified lithostratigraphy of site.

Hole 823C: Resistivity-Sonic-Natural Gamma Ray Log Summary

CORE RECOVERY	SPECTRAL GAMMA RAY			RESISTIVITY			TRANSIT TIME			URANIUM		THORIUM		POTASSIUM	
	TOTAL			FOCUSED											
	0	API units	100	0.5	ohm-m	5	190	$\mu$ s/ft	90	10	ppm	0	0	15	2.5
	COMPUTED			SHALLOW											
	0	API units	100	0.5	ohm-m	5						0		15	
	CALIPER			DEEP											
	18	in.	8	0.5	ohm-m	5	190	$\mu$ s/ft	90	-2.5	ppm	2.5			

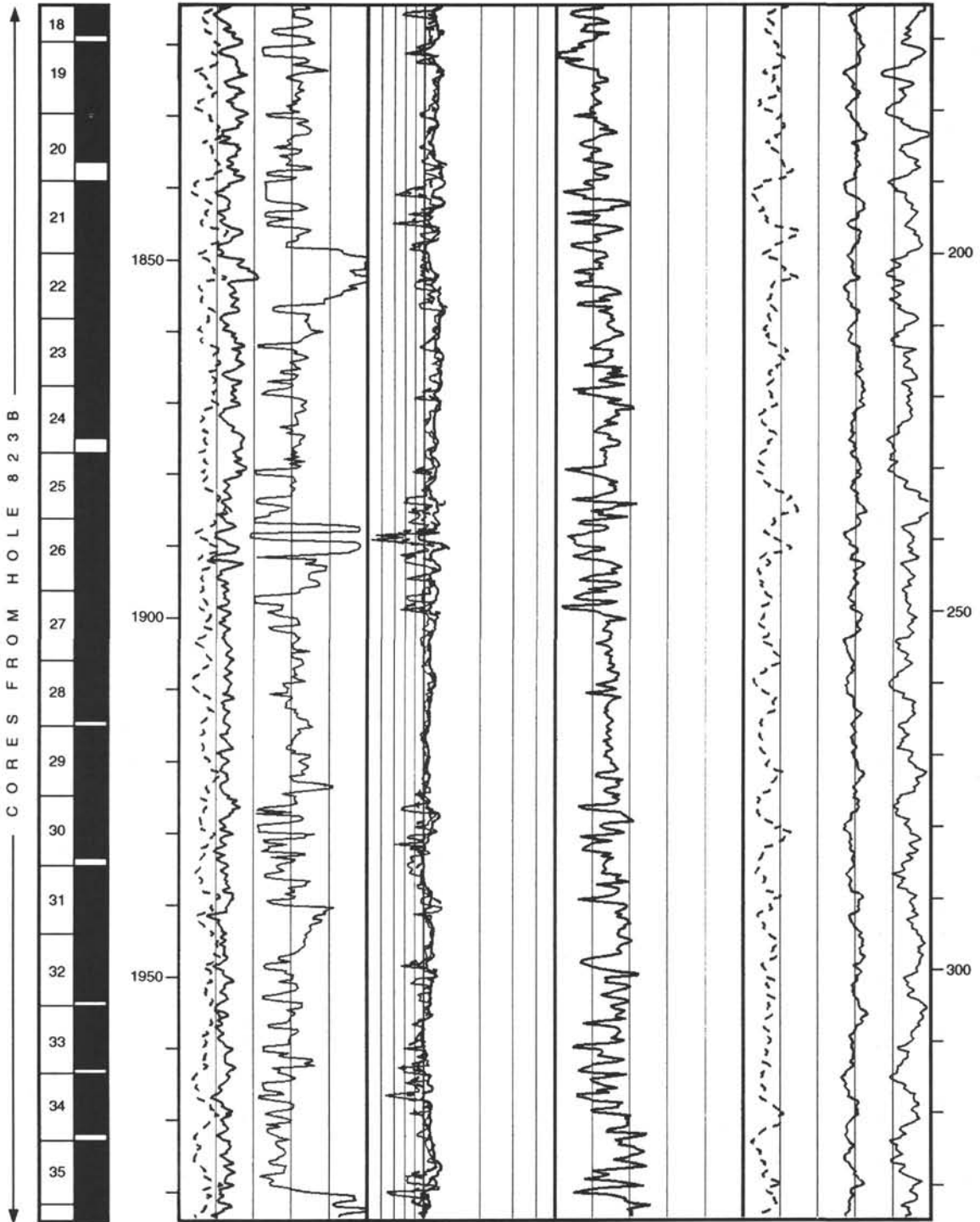


DATA RECORDED OPEN HOLE

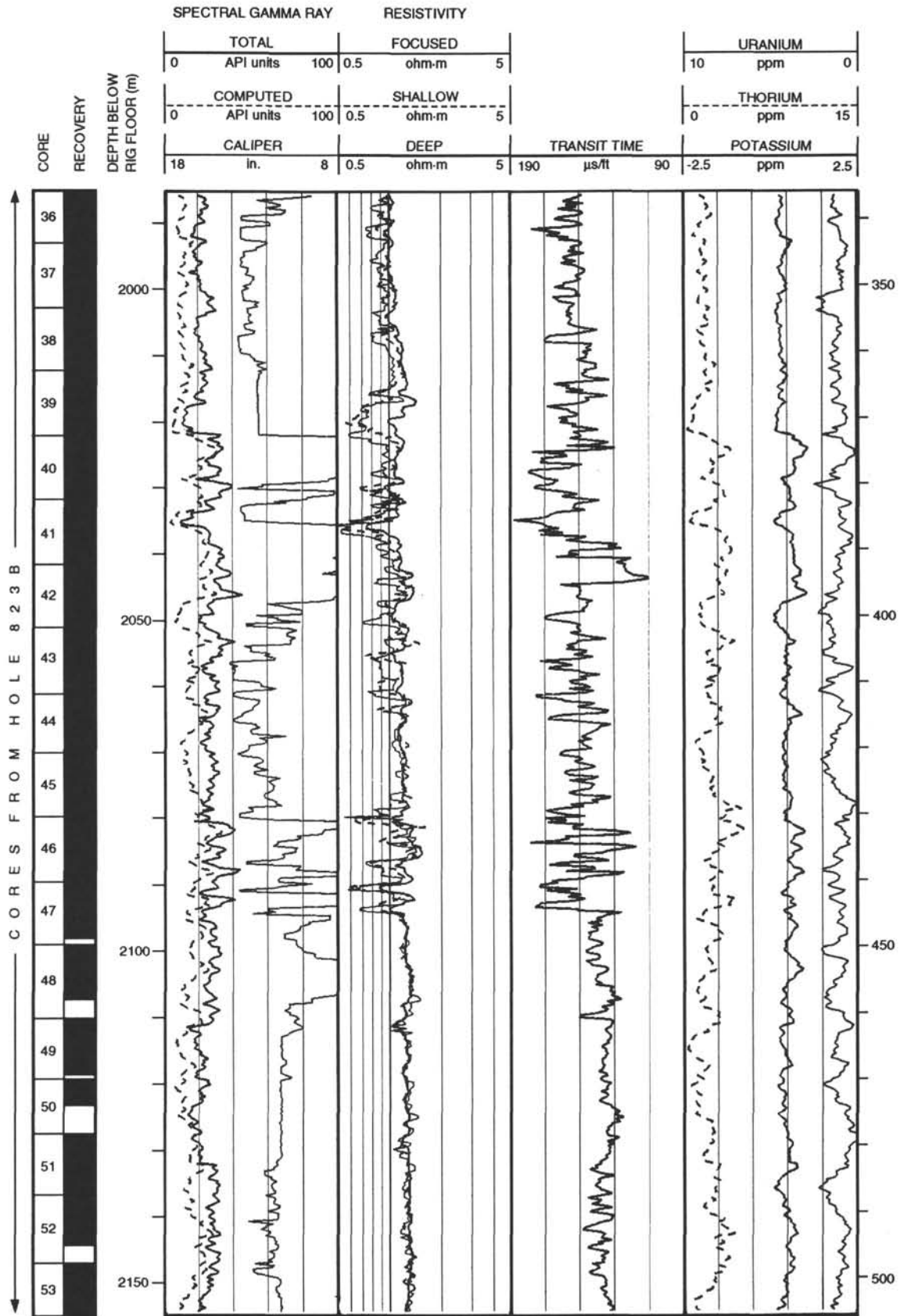


Hole 823C: Resistivity-Sonic-Natural Gamma Ray Log Summary (continued)

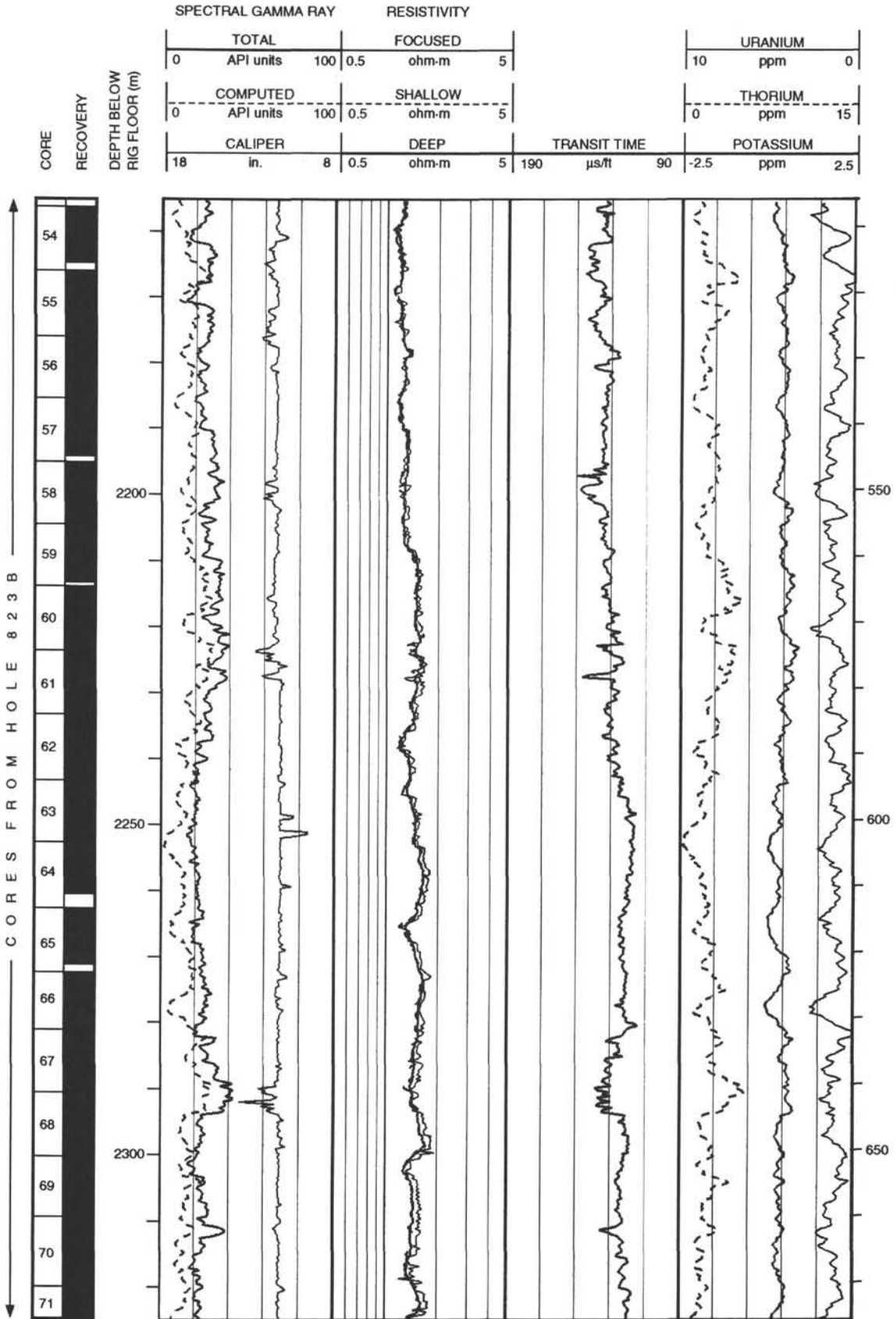
CORE RECOVERY	DEPTH BELOW RIG FLOOR (m)	SPECTRAL GAMMA RAY			RESISTIVITY			TRANSIT TIME			URANIUM		THORIUM		POTASSIUM	
		TOTAL			FOCUSED											
		0	API units	100	0.5	ohm-m	5	10	ppm	0	0	ppm	15	-2.5	ppm	2.5
		0	COMPUTED	API units	100	0.5	ohm-m	5	0	THORIUM	ppm	15				
18	CALIPER	in.	8	0.5	ohm-m	5	190	μs/ft	90	-2.5	ppm	2.5				



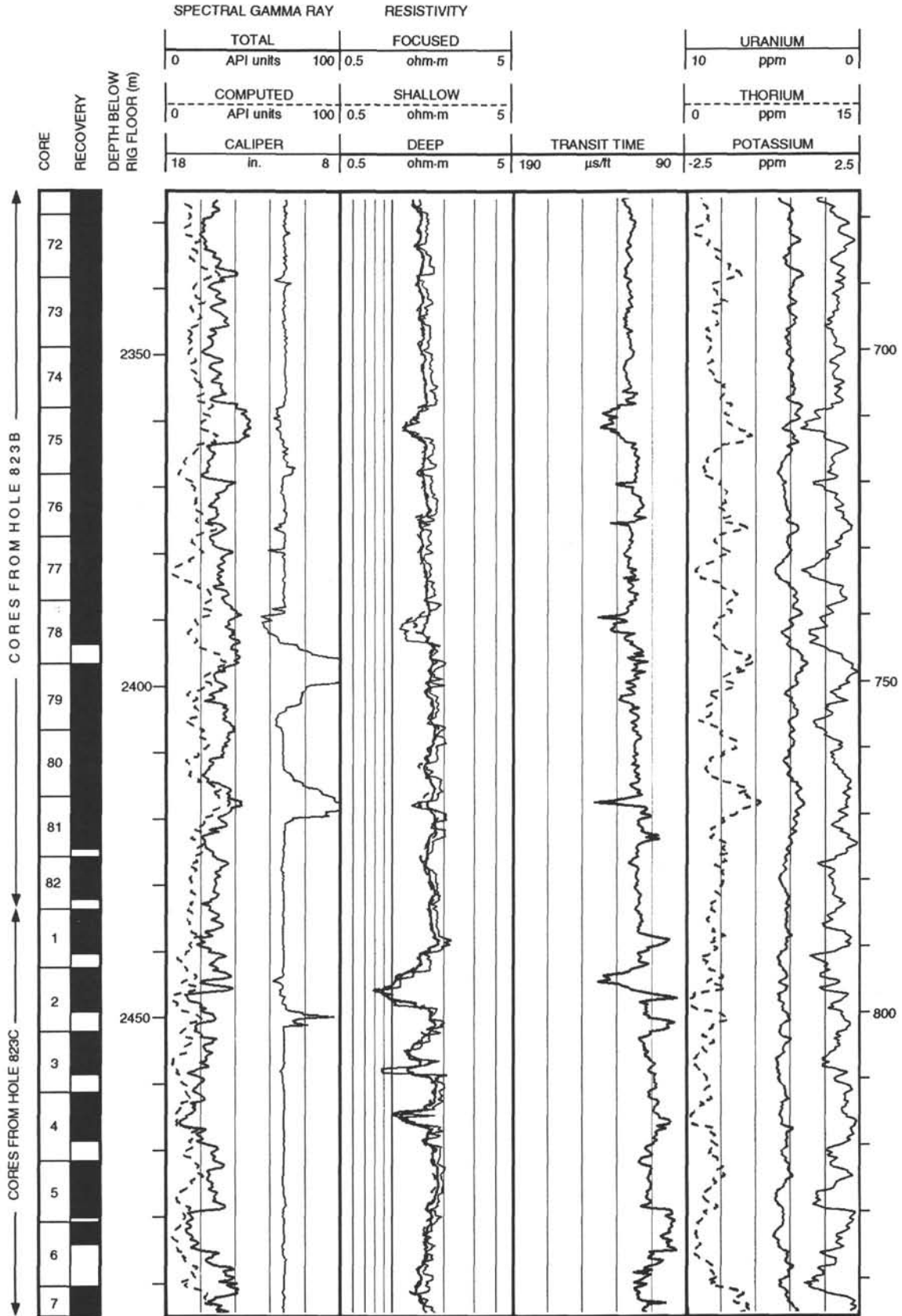
Hole 823C: Resistivity-Sonic-Natural Gamma Ray Log Summary (continued)



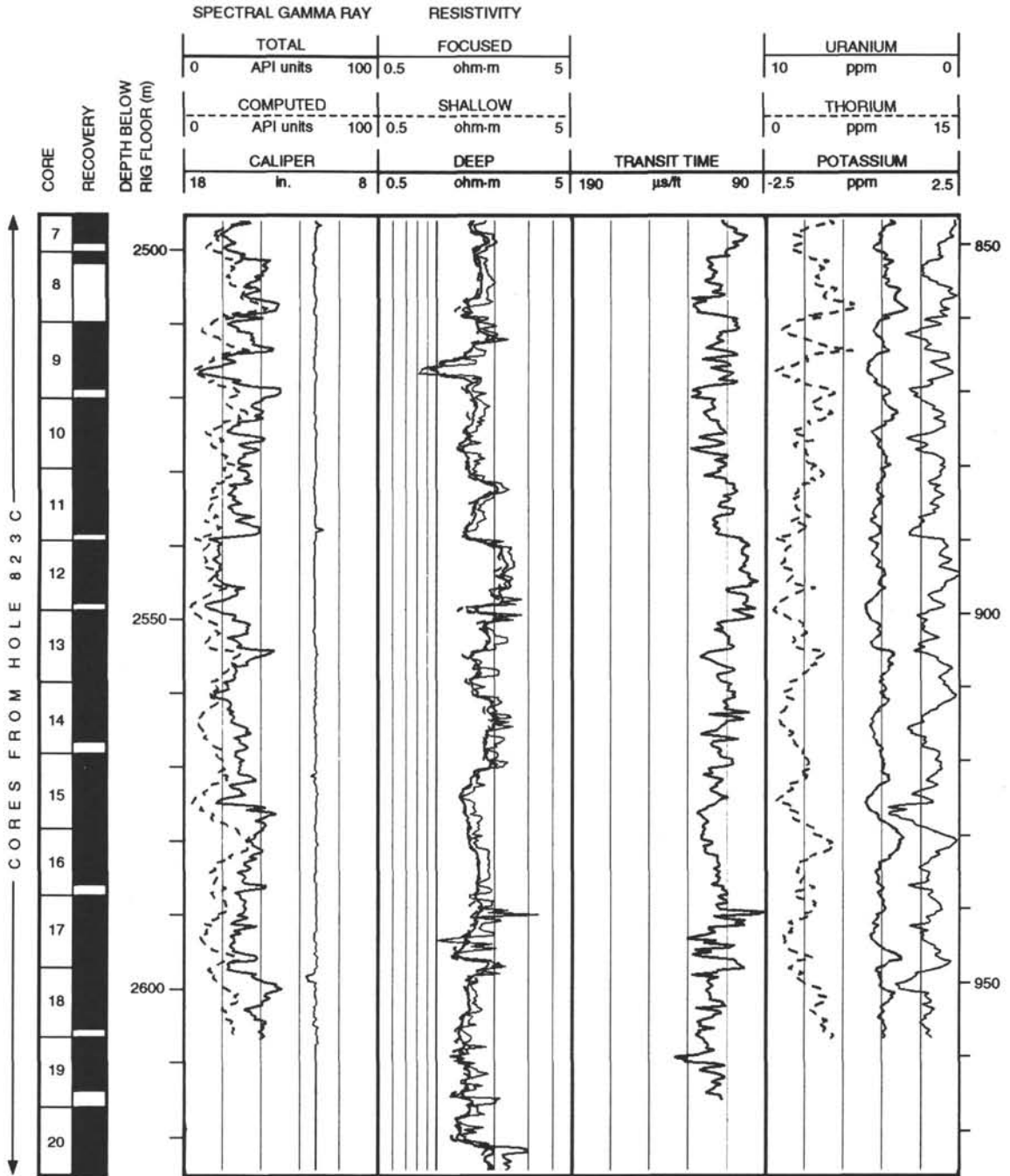
Hole 823C: Resistivity-Sonic-Natural Gamma Ray Log Summary (continued)



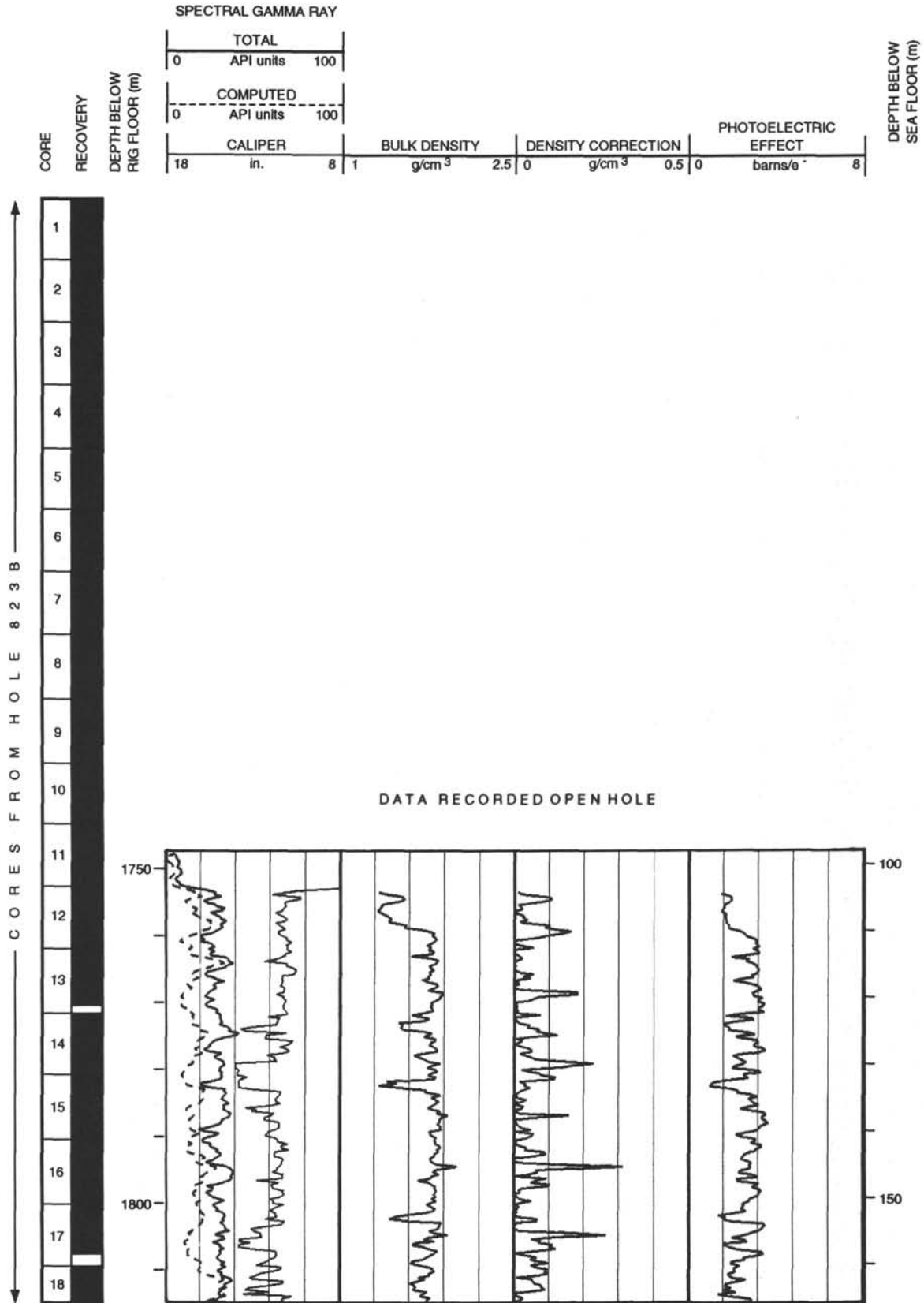
Hole 823C: Resistivity-Sonic-Natural Gamma Ray Log Summary (continued)



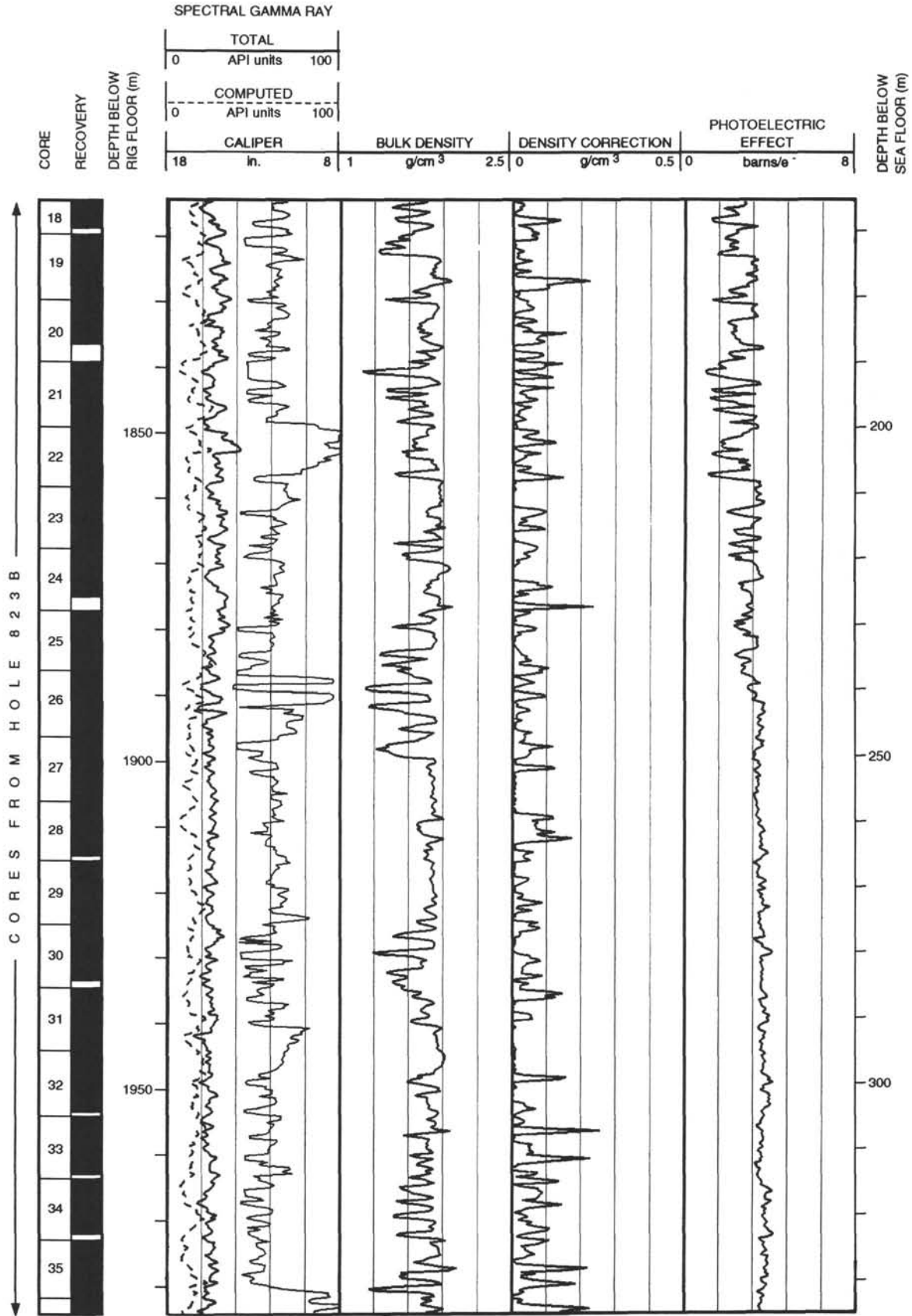
Hole 823C: Resistivity-Sonic-Natural Gamma Ray Log Summary (continued)



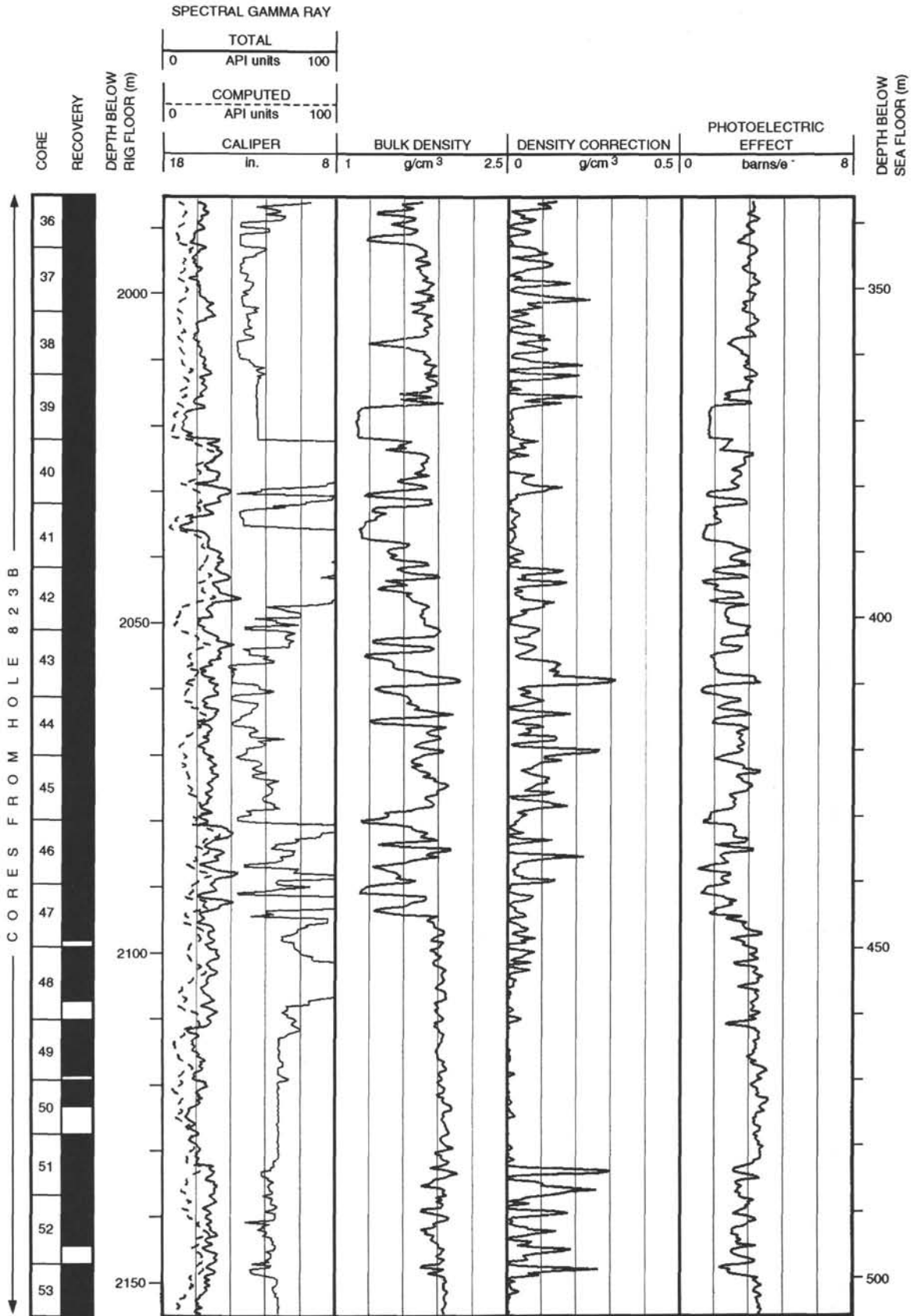
Hole 823C: Density-Natural Gamma Ray Log Summary



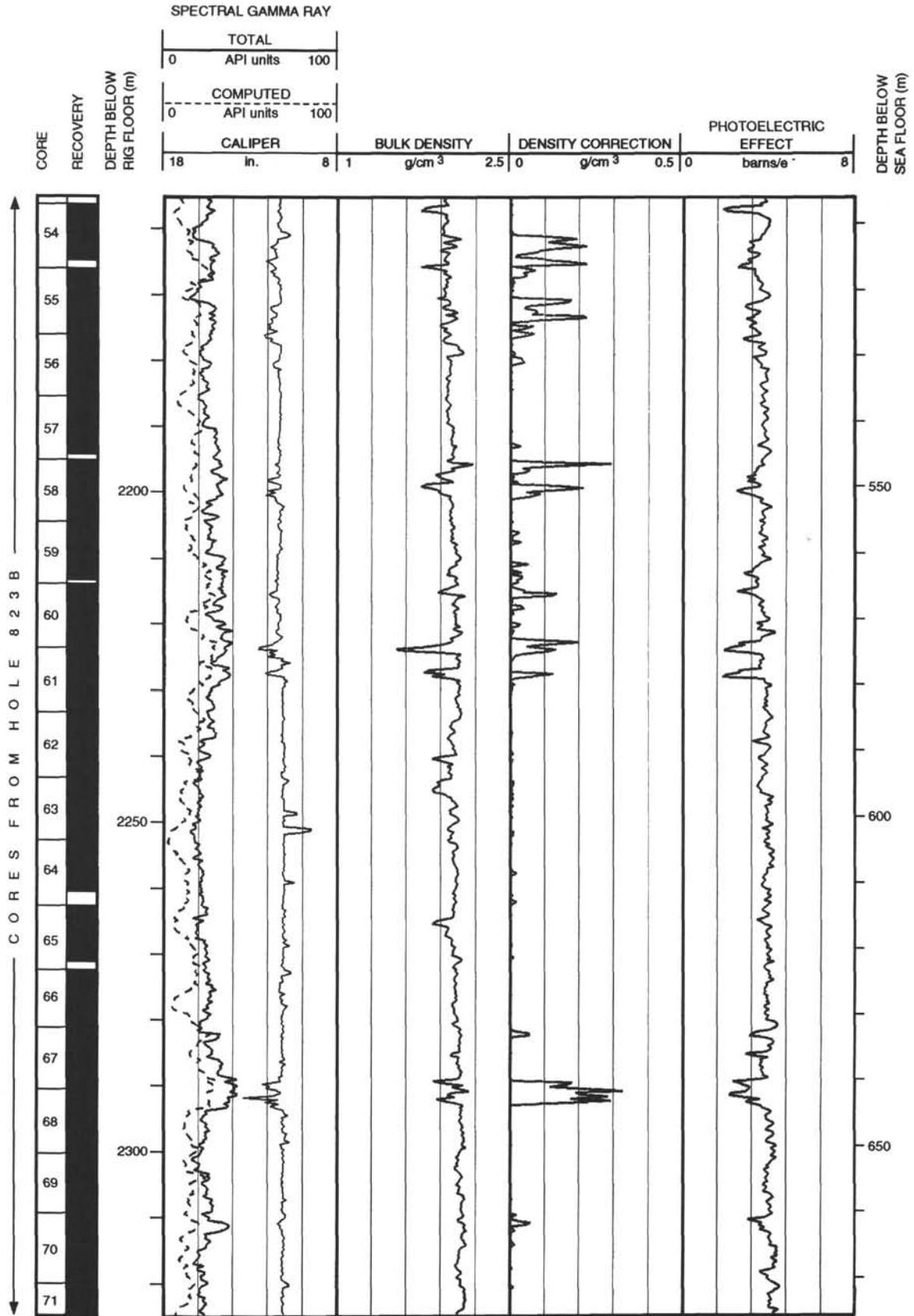
Hole 823C: Density-Natural Gamma Ray Log Summary (continued)



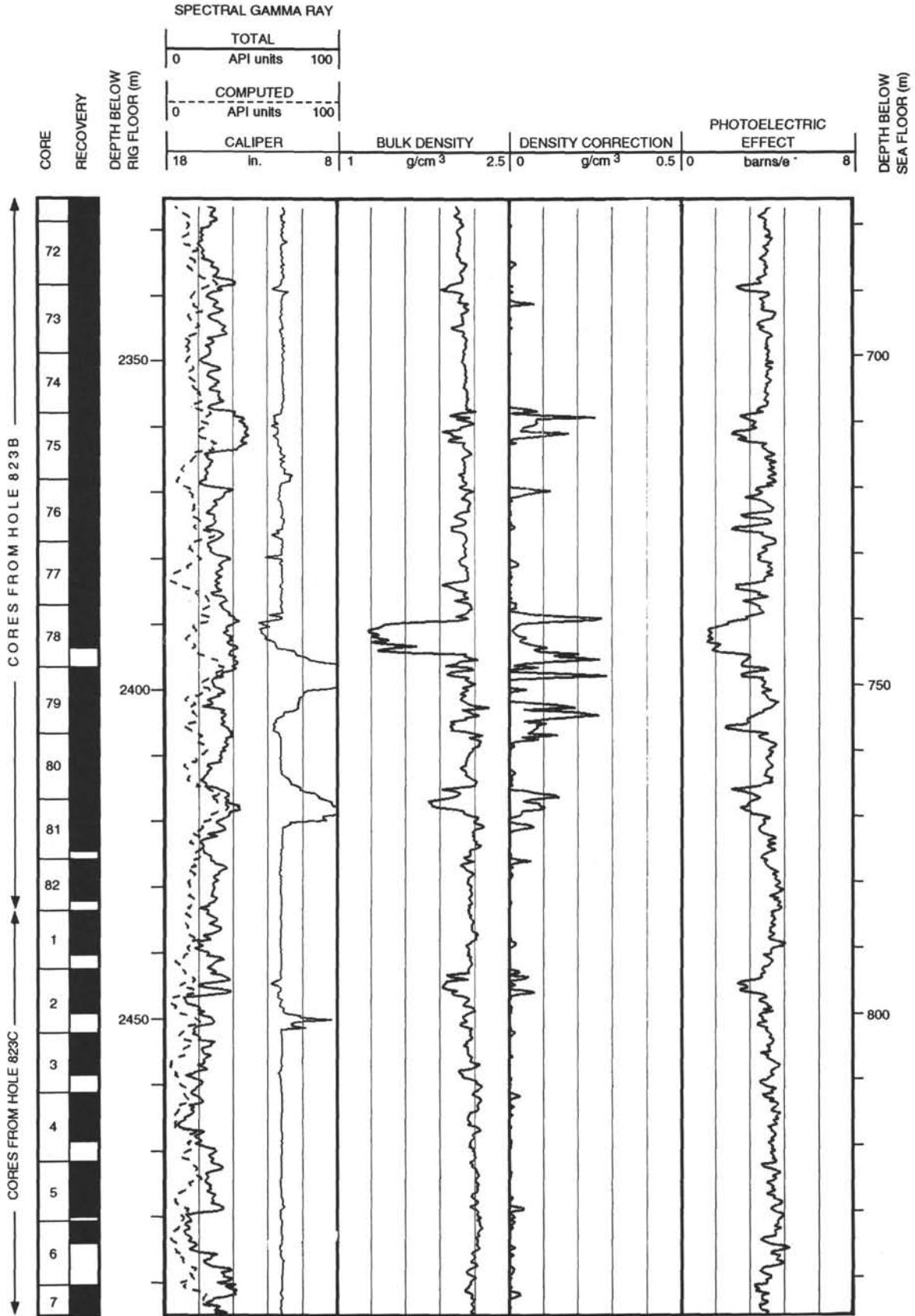
Hole 823C: Density-Natural Gamma Ray Log Summary (continued)



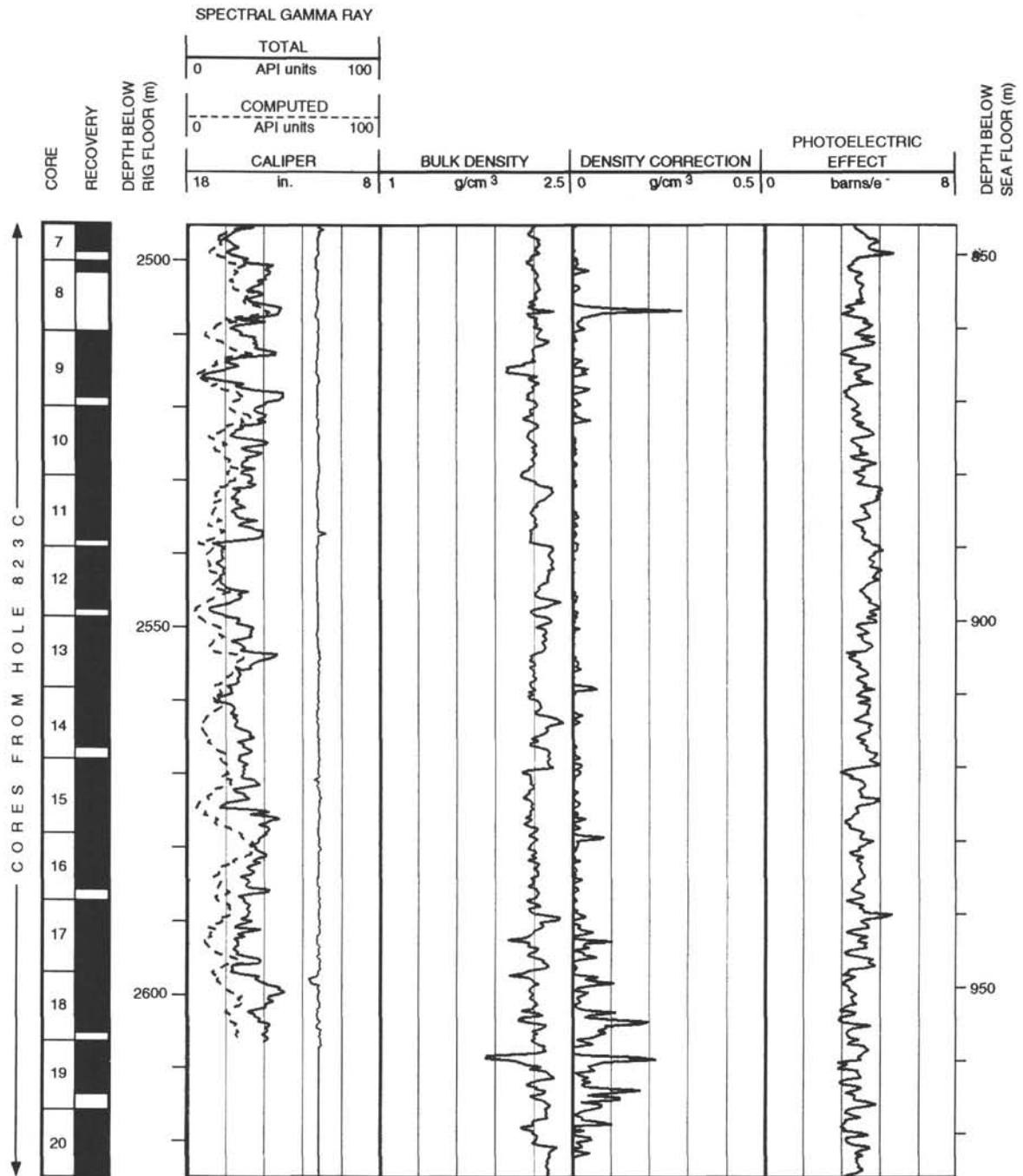
Hole 823C: Density-Natural Gamma Ray Log Summary (continued)



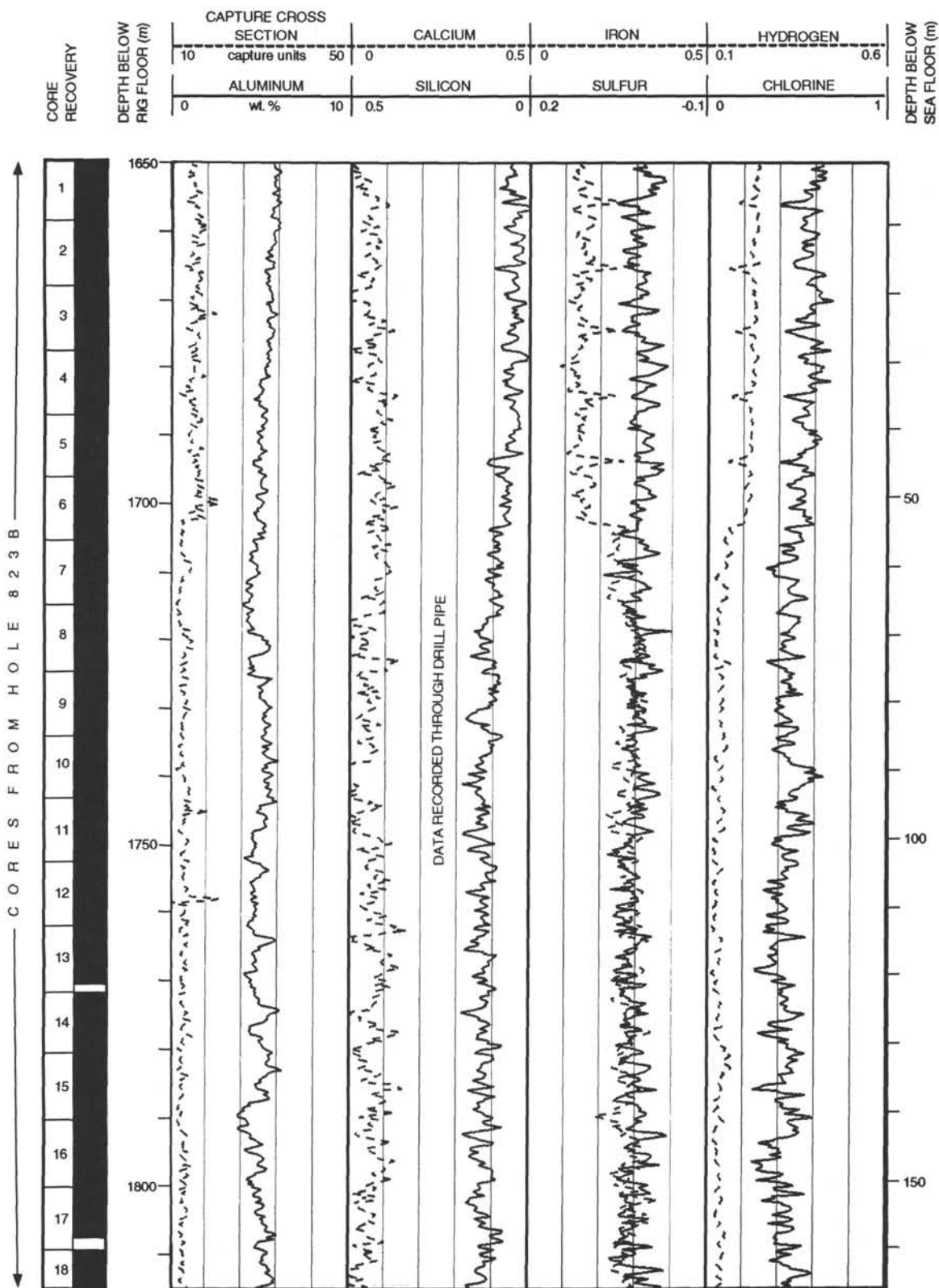
Hole 823C: Density-Natural Gamma Ray Log Summary (continued)



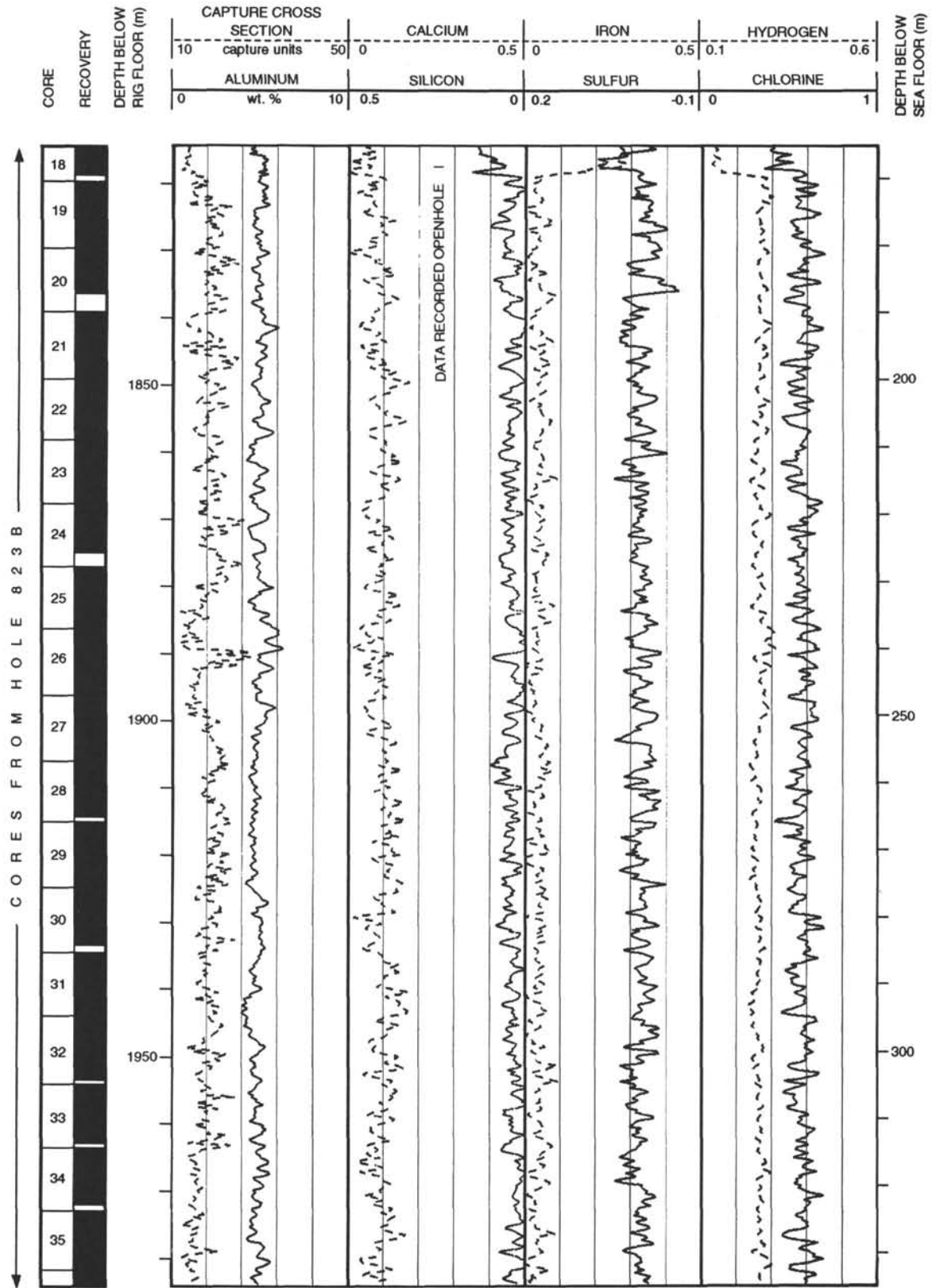
Hole 823C: Density-Natural Gamma Ray Log Summary (continued)



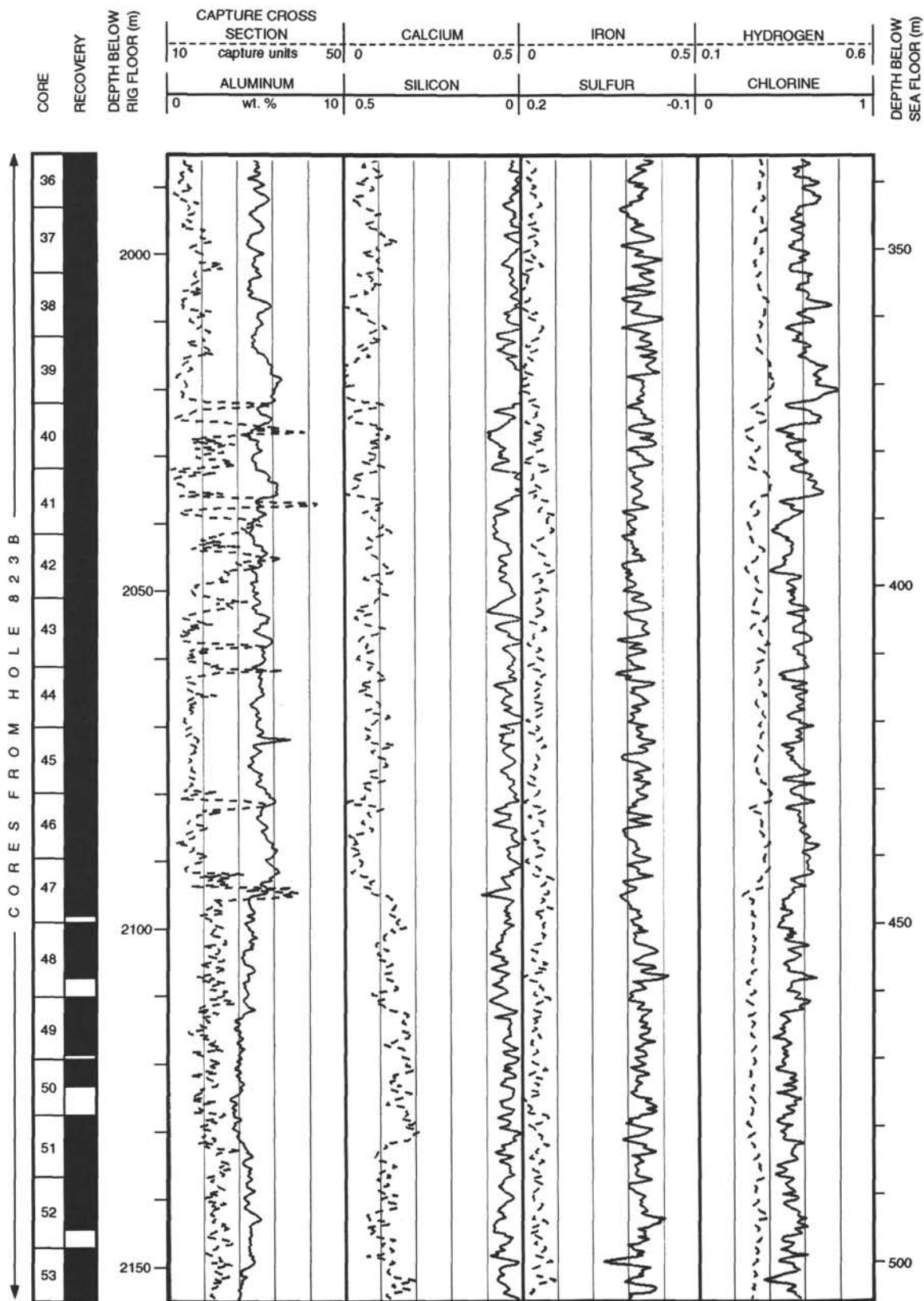
Hole 823C: Geochemical Log Summary



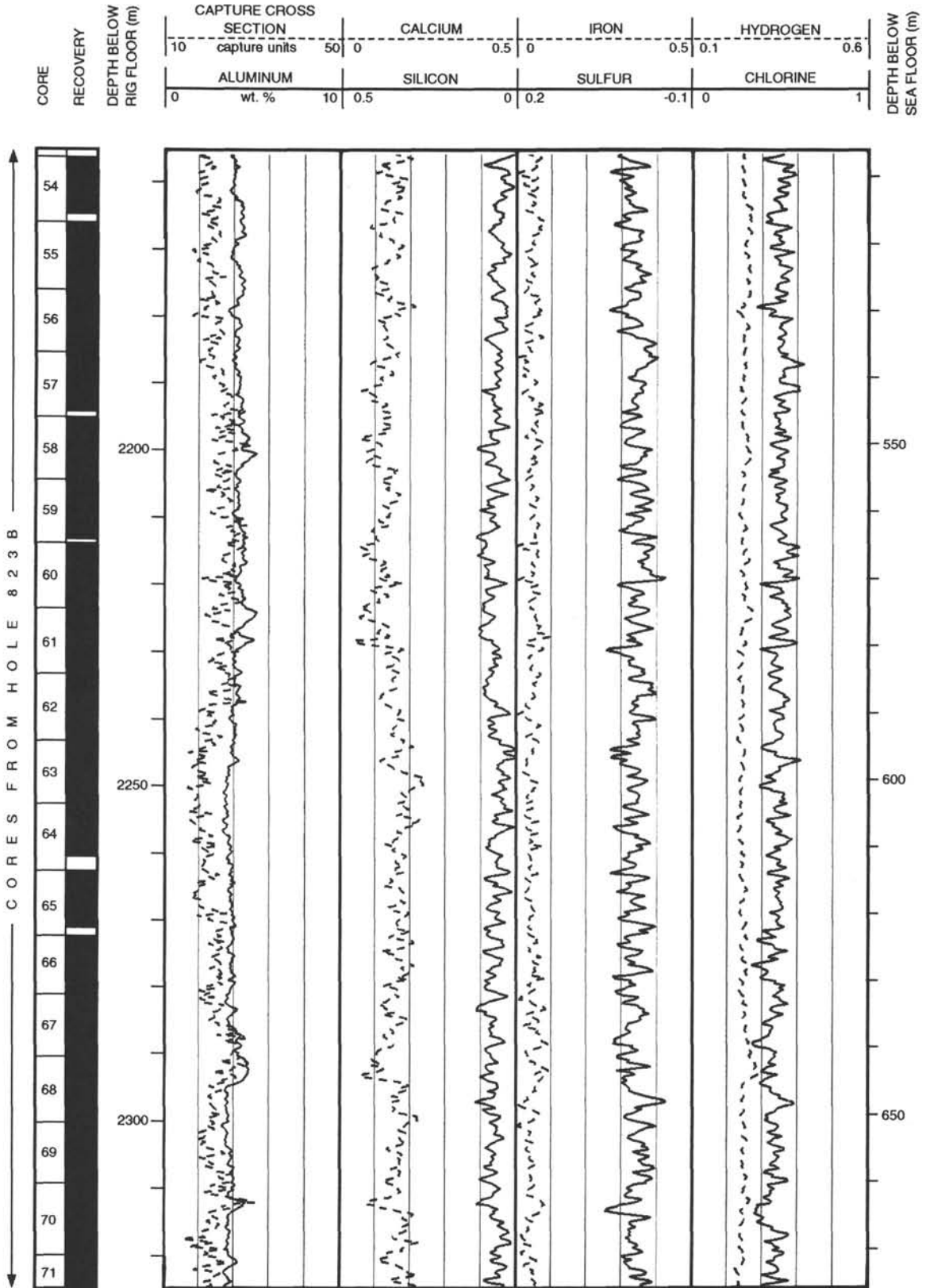
Hole 823C: Geochemical Log Summary (continued)



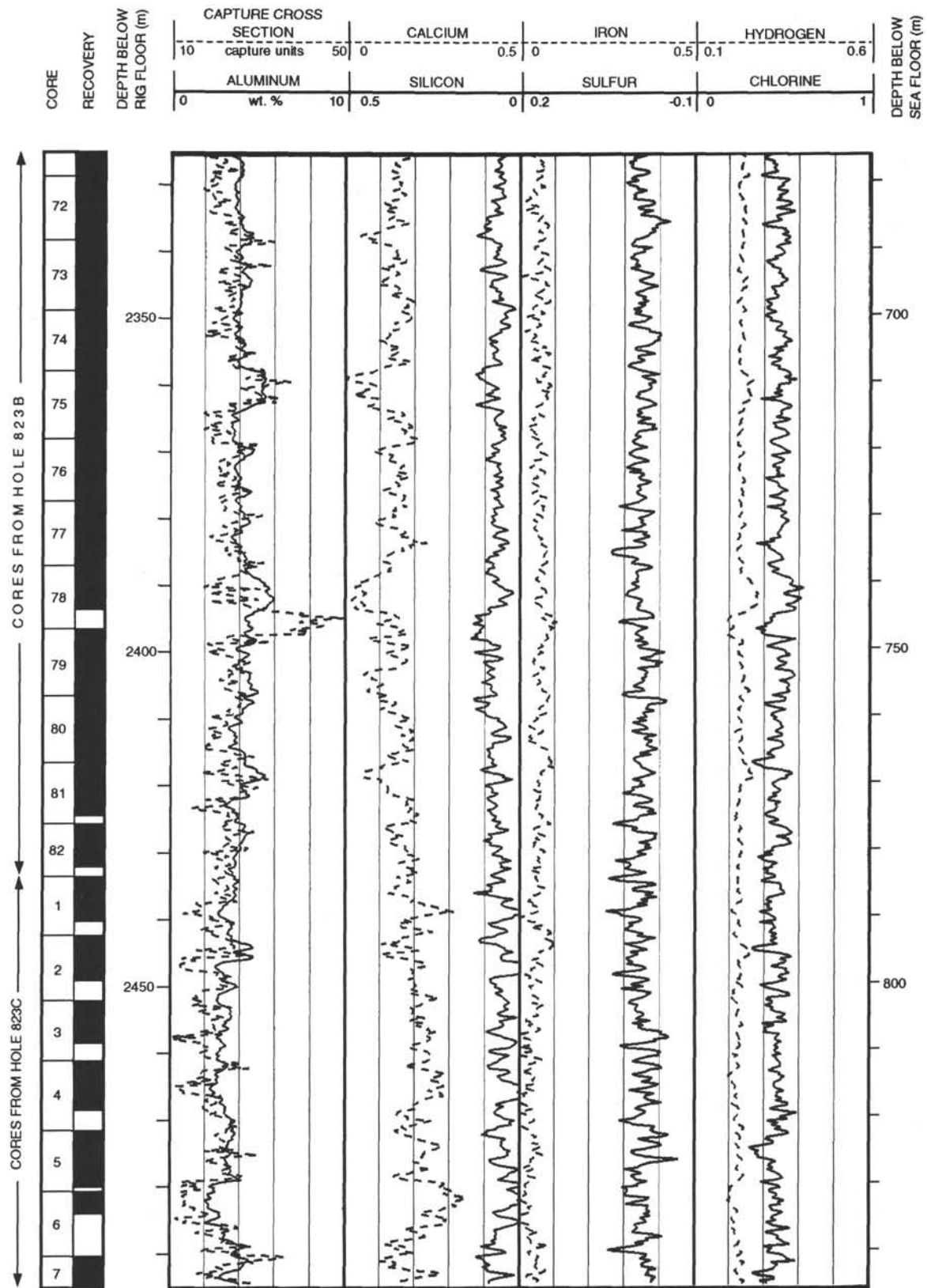
Hole 823C: Geochemical Log Summary (continued)



Hole 823C: Geochemical Log Summary (continued)



Hole 823C: Geochemical Log Summary (continued)



Hole 823C: Geochemical Log Summary (continued)

